Acta Universitatis Szegediensis

Acta Biologica Szegediensis

Volume 54, Number 2, 2010

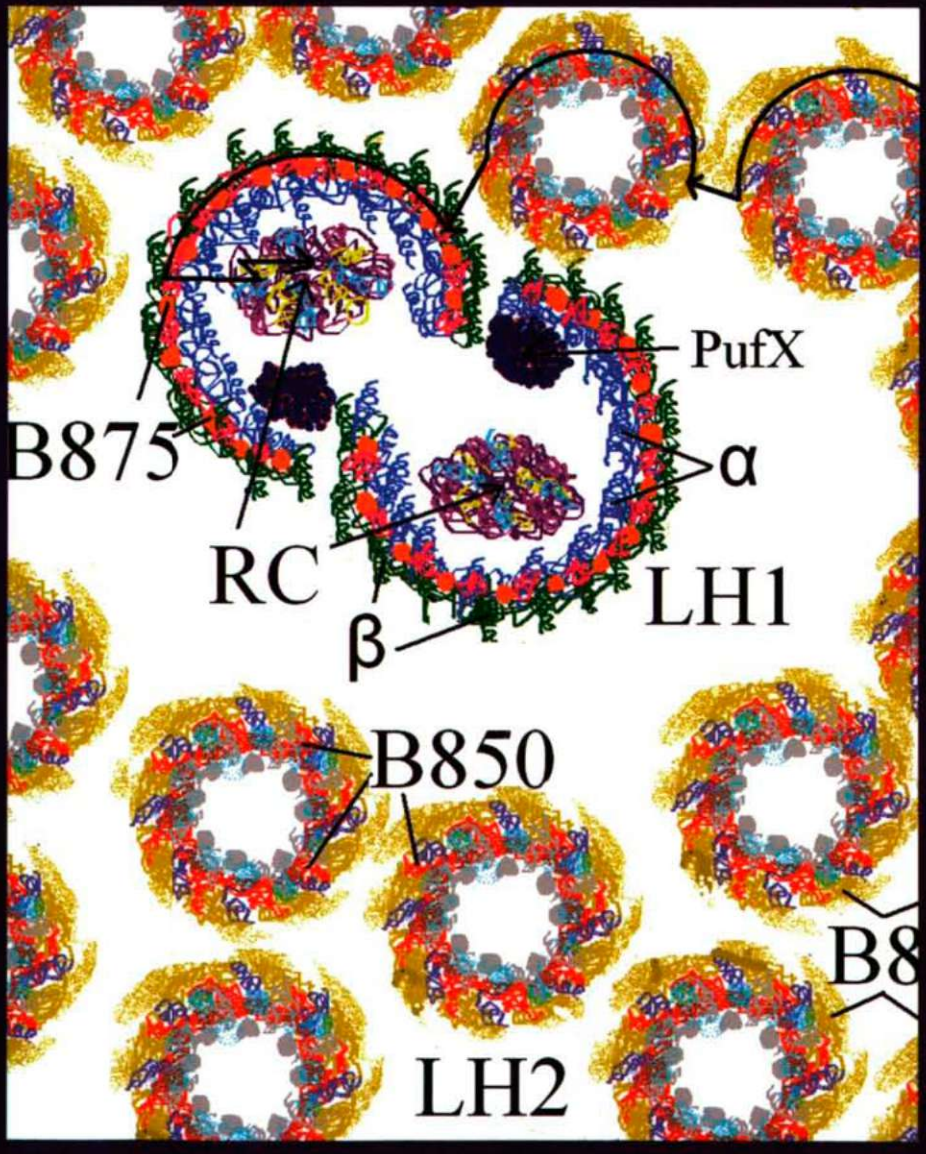

University of Szeged, Szeged, Hungary

Acta Biologica Szegediensis

Acta Biologica Szegediensis (ISSN 1588-385X print form; ISSN 1588-4082 online form), a member of the Acta Universitatis Szegediensis family of scientific journals (ISSN 0563-0592), is published yearly by the University of Szeged. Acta Biologica Szegediensis covers the growth areas of modern biology and publishes original research articles and reviews, involving, but not restricted to, the fields of anatomy, embryology and histology, anthropology, biochemistry, biophysics, biotechnology, botany and plant physiology, all areas of clinical sciences, conservation biology, ecology, genetics, microbiology, molecular biology, neurosciences, paleontology, pharmacology, physiology and pathophysiology, and zoology. Occasionally, Acta Biologica Szegediensis will publish symposium materials. Acta Biologica Szegediensis particularly encourages young investigators and clinicians to submit novel results of interest.

Submission of manuscripts

Manuscripts should be prepared in accordance with the Instructions to Authors published in each issue, also available at http://www.sci.u-szeged.hu/ABS, and submitted to:

Károly Gulya
Acta Biologica Szegediensis, Editorial Office
Department of Cell Biology and Molecular Medicine
University of Szeged
4 Somogyi u., H-6720 Szeged, Hungary
Phone: 36 (62) 544-570, fax: 36 (62) 544-569
E-mail: gulyak@bio.u-szeged.hu

Correspondence relating to the status of the manuscripts, proofs, publication, reprints and advertising should be sent to:

Tamás Mikola
Acta Biologica Szegediensis, Editorial Office
Department of Cell Biology and Molecular Medicine
University of Szeged
4 Somogyi u., H-6720 Szeged, Hungary
Phone: 36 (62) 544-569, fax: 36 (62) 544-569
E-mail: zool@bio.u-szeged.hu

Subscriptions

Acta Biologica Szegediensis is published yearly in two issues per volume. All subscriptions relate to the calendar year and must be pre-paid. The annual subscription rate is currently 100 USD and includes air mail delivery and handling.

Acta Biologica Szegediensis is indexed in BIOSIS Database, EMBASE, Excerpta Medica, Elsevier BIOBASE (Current Awareness in Biological Sciences) and Zoological Record.

The Table of Contents for the current issue and those for previous issues can be found at http://www.sci.u-szeged.hu/ABS.

ACTA BIOLOGICA SZEGEDIENSIS VOLUME 54(2), 2010

Table of Contents

Articles

On the cover: Artistic visualization of a photosynthetic light harvesting apparatus. (See Asztalos et al. in this issue)

Volume 54(2):75-81, 2010
Acta Biologica Szegediensis
http://www.sci.u-szeged.hu/ABS

ARTICLE

Diffuse idiopathic skeletal hyperostosis – appearance and diagnostics in Hungarian osteoarcheological materials

László Paja[1,2]*, Erika Molnár[1], Brigitta Ősz[1,2], László Tiszlavicz[3], András Palkó[4], Hélène Coqueugniot[5], Olivier Dutour[6,7], György Pálfi[1]

[1]Department of Biological Anthropology, University of Szeged, Szeged, Hungary, [2]Hungarian National Museum, Centre for National Heritage, Szeged, Hungary, [3]Department of Pathology, University of Szeged, Szeged, Hungary, [4]Department of Radiology, University of Szeged, Szeged, Hungary, [5]Laboratoire d'Anthropologie des Populations du Passé, CNRS, UMR 5199 - PACEA, Université de Bordeaux 1, Bordeaux, France, [6]Laboratoire de Paléoanthropologie, École Pratique des Hautes Études, Bordeaux, France, [7]Department of Anthropology, University of Toronto, Toronto, Canada

ABSTRACT Diffuse idiopathic skeletal hyperostosis (DISH) or Forestier's disease appears in different skeletal elements, and usually characterized by the calcification of the right side anterior longitudinal ligament of the spine and by the ossification of entheses and ligaments at extra-spinal sites. Although the etiology of DISH is still unknown, but the presence of it seems to be connected with some metabolic diseases, like type II diabetes or obesity. On the basis of Resnick's criteria, the recognition of DISH is not difficult, but in paleopathology, the osteoarcheological series' different state of preservation may result in diagnostical uncertanity. This paper summarizes the results of the physical anthropological examinations carried out seven osteoacheological series from the Great Hungarian Plain, and points to those osseous alterations, which may be helpful in the diagnosis of DISH. **Acta Biol Szeged 54(2): 75-81 (2010)**

KEY WORDS

diagnostic criteria
diffuse idiopathic skeletal hyperostosis (DISH)
Hungary
hyperostosis
osteoarcheology
paleopathology

Diffuse idiopathic skeletal hyperostosis (DISH) or Forestier's disease is one of the metabolic disorders that recognisable in the connective and supportive tissues. Pathophysiologically it is characterized by calcification and ossification of soft tissues, especially ligaments and entheses, and it was first described by Forestier and Rotes-Querol in 1950 (Forestier and Rotes-Querol 1950). Later Resnick and his colleagues investigated the correlation between the spinal alterations related to DISH and extraspinal ossification and calcification findings, and in 1976 published their results (Resnick et al. 1976; Resnick and Niwayama 1976). In the second publication Resnick and Niwayama postulated three criteria for the diagnosis of DISH, these are now widely used in literature, and they may help in differentiation of this disease from other spinal disorders, such as ankylosing spondylitis or spondylosis deformans.

The spine has two anatomopathologic spinal types (Cammisa et al. 1998), Type I is related to DISH. It is characterized by irregular ligament calcification, particularly the anterior longitudinal ligament of the spine. The entire spinal column may be involved, but the most typical sites are the mid-low cervical and the mid-low thoracic vertebral segments, bony ankylosis may develop. Radiologically a special view can be seen, as a result of the non-homogenous calcification a radiotransparent band is visible between the vertebral body and the outer layer of the ligament. The calcification appears usually on the right side of the spine. The left side is typically spared or less involved, which is probably attributable to the pulsating aorta. We have to note that zygapophyseal joint gaps and intervertebral spaces are not affected, the original width of these elements are not usually decreased (Olivieri et al. 2009).

Concerning extra-spinal alterations, bony spurs develop at entheses, the most affected sites are the patellae, calcanei and the ulna's olecranon. Ligament ossification, such as sacro-iliac ligament ossification may results in sacro-iliac fusion. DISH appears more often in males than females, and the frequency increases in individuals over 40 years of age (Olivieri et al. 2009).

Although the etiology of DISH is not clear, but several conditions seems to be associated with the disease. These include obesity, hyperlipidemia, hyperuricemia, hyperinsulinemia and late onset (Type II) diabetes (Burner and Rosenthal 2009). Not only recent population studies or case reports show correlation between obesity and DISH, but paleopathological studies also reported some association between the two diseases. A high prevelance of DISH cases has been recognized in ancient clergymen, and it has been hypothesised that the „monastic way of life" might be a predisposing factor of DISH (Rogers and Waldron 2001; Verlaan et al. 2007). Other paleopathological studies point out that development of DISH has a correlation with higher social status (Jankauskas

Accepted Dec 16, 2010
*Corresponding author. E-mail: pajalac2000@yahoo.com

Table 1. List of the examined osteoarcheological series.

Cemetery (abbreviation)	Datation	No. of individuals	References of basic data
Homokmégy - Székes (HSZ)	10-11th c. AD	186	Paja et al. 2007
Magyarhomorog - Kónyadomb MHK)	10-11th c. AD	368	Szigeti 2001
Ópusztaszer - Monostor (OPM)	11-18th c. AD	1089	Farkas (ed.) 1998
Bátmonostor - Pusztafalu (BMP)	12-16th c. AD	3782	Farkas et al. 2004
Óföldeák (OF)	12-18th c. AD	419	Paja 2000
Szeged - Vár (SZV)	14-15th c. AD	641	Ősz et al. 2009
Bácsalmás - Óalmás (BA)	16-17th c. AD	481	Békei 1995, Lovász 2005

Table 2. Osseous alterations of the skeletons diagnosed with DISH and early-stage DISH (eDISH) (+: alteration is present, -: alteration is not present, n: anatomic element is missing, alteration is not recognisable).

		HSZ-47	MHK-217	OPM-9268	OPM-R6	BMP-46	OF-16996	SZV-290	MHK-80	OPM-644	SZV-303	BA-159	BA-173
		male Senium	male Maturus	male Adultus	undet. adult	male Senium	male Adultus	male Ad-Mat.	male Maturus	male Senium	male Mat.	male Senium	male Maturus
right anterior spinal ligament ossification		+	+	+	+	+	+	+	+	+	+	+	+
- complete (no. of vertebrae)		5	7+2	4	4	9	9	5	2+2	2+2	2+2	2	3+2
- not complete (no. of intervertebral gaps)		0	4	0	0	1	0	0	1	2	4	8	6
- number of affected vertebrae		5	13	4	4	10	9	5	5	5	6	10	11
narrowed intervertebral disc space		-	-	-	-	-	-	-	-	-	n	-	-
narrowed zygapophyseal joint space		-	+	-	-	+	+	-	-	-	-	-	-
ossification at vertebral foramen		+	+	+	+	+	+	+	+	+	n	+	+
calcification on vertebral disc surface		-	-	-	+	+	+	+	+	+	-	+	+
enthesopathy	upper limb and girdle	+	+	-	n	+	n	+	-	+	+	-	+
	lower limb and girdle	+	+	+	n	+	n	+	+	+	+	+	+
other ossification	spinal	-	-	-	n	-	+	-	-	-	n	+	-
	extra-spinal	-	+	-	n	-	n	+	-	+	-	+	+
sacroileitis		-	+	-	-	-	n	-	-	-	-	-	-
diagnosis		DISH							eDISH				

2003; Giuffra et al. 2010). In recent populations dysphagia is also found in correlation with DISH in several cases (Oppenlander et al. 2009; Seidler et al. 2009; Miyamoto et al. 2009; Masiero et al. 2010), and increased affinity to fracture of the fusioned spine is also mentioned in the recent medical literature (Westerveld et al. 2009).

Concerning the most frequently used methods in recent populations, the diagnosis of DISH is generally based on radiologic analyses. The widely used diagnostic criteria of Resnick and Niwayama (Resnick and Niwayama 1976) are at least four vertebral bodies' fusion, the preservation of the intervertebral disc, the absence of zygapophyseal and sacroiliac joint changes. According to Arlet and Mazières three involved contiguous vertebrae at the lower thoracic spine is sufficient for the diagnosis (Arlet and Mazières 1985). In the opinion of Julkunen et al. bony bridges between two vertebral bodies in at least two sites of the spine have to be characteristic for DISH (Julkunen et al. 1975). However, another set of criteria, defined by Utsinger as probable DISH, lowered the threshold for spinal alterations to the fusion of three adjacent vertebral bodies, but added the presence of extra-spinal enthesopathies to the diagnostic measures (Utsinger 1985).

In Waldron's opinion the operational definition for DISH in paleopathological analysis means the presence of the ossification and fusion of four adjacent vertebral bodies, which are associated with the ossification of extraspinal entheses and ligaments (Waldron 2008).

Biochemical analyses also carried out to make a proper diagnosis for DISH. Denko et al. demonstrated a significant increase in serum growth hormone, insulin-like growth factor –I and insulin in Caucasoid females diagnosed with DISH. In males only growth hormone and insulin were higher than normal controls (Denko and Malemud 2005; Denko et al. 1996).

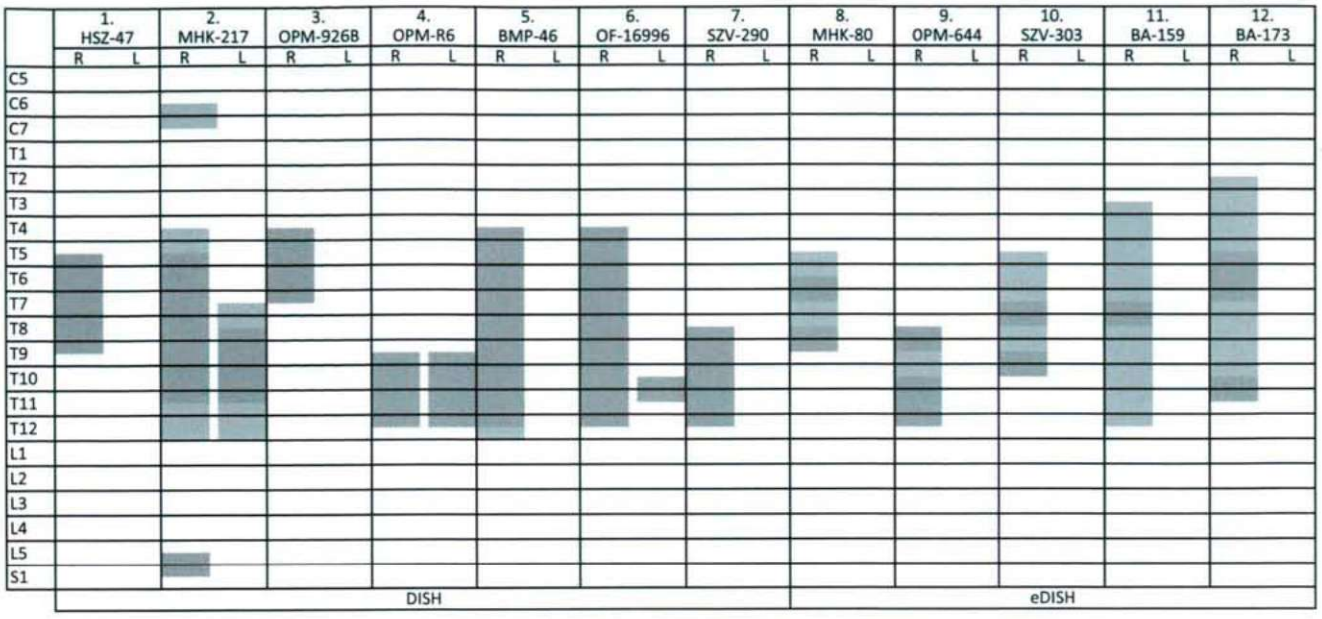

Figure 1. Localization of the complete (orange) and not complete (blue) ossification of the anterior longitudinal ligament in the DISH and early-stage DISH cases (R-right side, L-left side).

Materials and Methods

During our analysis, osteoarcheological remains of seven cemeteries (skeletal remains of 6966 individuals) from the Great Hungarian Plain were examined (Table 1).

During the previously made basic anthropological examinations, determination of sex, estimation of age at death, metric analyses and differenent paleopathological analyses also were done (Table 1).

In our recent study paleopathological anomalies were diagnosed on the basis of macromorphological observations, additionally CT scan was taken and histological examinations also were conducted to support diagnoses.

As for morphological analysis we used a record sheet, on which all of the vertebral and extra-spinal alterations have been recorded. We examined the ligament ossification (size, position, number of completely and not completely fusioned segments), the statement of vertebral articulational surfaces (costal and zygapophyseal facets), the presence and laterality of vertebral bodies' marginal osteophytosis, the statement of intervertebral disc surfaces and any other alterations that might be associated with the development of DISH.

We used the criteria of Resnick and Niwayama (1976); if the intervertebral disc spaces and zygapophyseal joint gaps were close to the original situation, narrowing of these spaces were not visible and at least four vertebral body were completely fused by the calcification of the anterior longitudinal ligament, our diagnosis was DISH. If fewer than four adjacent vertebrae were fused, our diagnosis was early-stage DISH (eDISH). The diagnosis was eDISH also in those cases, where the number of the completely fused vertebrae reached the expected four, but they were separated by intact vertebra(e), or vertebra(e) with calcified, but not completely fused ligament elements.

Concerning radiological examinations, the specimens have been scanned on a GE Lightspeed VCT scan (tube voltage: 120 kV, current: 50 mA) with a 512x512 matrix leading to a voxel size of 0,61 mm x 0,61 mm and a slice thickness of 0,62 mm. Original CT-data were adjusted, and 2D and 3D reconstructions were carried out.

At three specimens from the grave OPM-644 histological analyses were done. The samples from the calcified right-side anterior longitudinal ligament, calcified thyroid cartilage and bony spurs of the anterior patella were partly decalcified (trichloroacetic acid, 5%, 4°C, 2-3 days) and embedded in paraffin resin. Thin sections (4um) were prepared for histological analysis, hematoxylin and eosin stain was used.

Results

In the material of the examined osteoarcheological series, 7 cases of diffuse idiopathic skeletal hyperostosis (DISH) and 5 cases of early-stage DISH were found, the osseous changes of the affected skeletons can be seen in the Table 2 and Figure 1.

In the first group at least 4 contiguous segments were fused by the ossificationed and calcified anterior longitudinal ligament, the bony bridges were localized on the right side at the anterio-lateral surface of the vertebral bodies (Fig. 1, Fig. 2). Beside this pathognomic phenomenon – except of

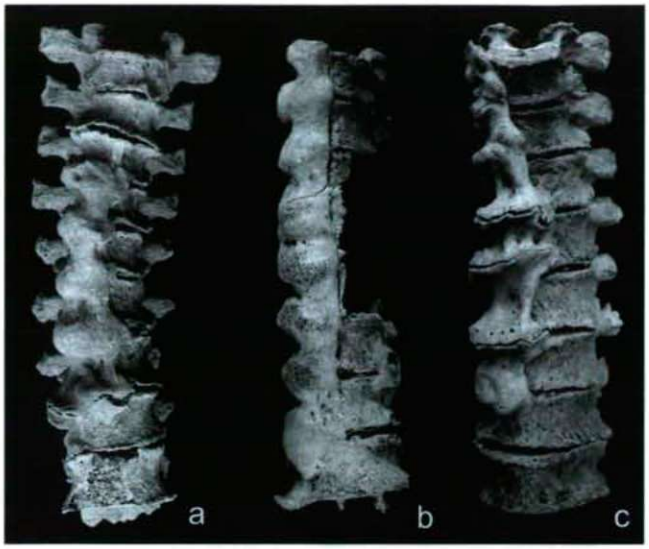

Figure 2. The right side ossification of the anterior longitudinal ligament is pathognomic to diffuse idiopathic skeletal hyperostosis; a: sample of HSZ-47 (male, aged over 60), diagnosis: DISH; b: sample of OF-16996 (male, aged 40-60), diagnosis: DISH; c: sample of BA-173 (male, aged 40-60), diagnosis: early-stage DISH.

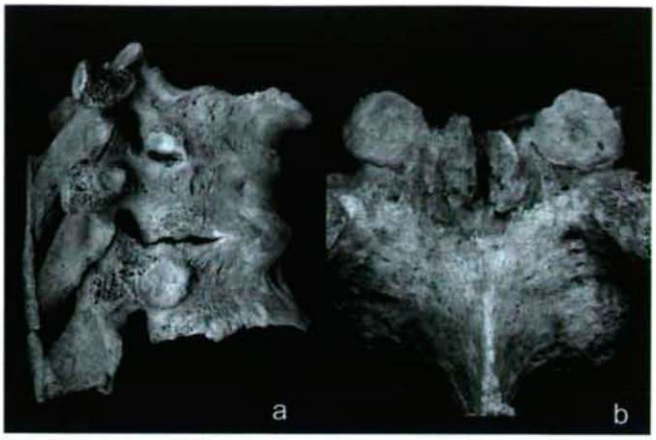

Figure 3. Ossification of the spinal ligaments in the sample of BMP-46 (male, aged over 60), a: ossification of the supraspinous ligament; b: bony elements between the two upper facet joints may be caused by the ossification of the ligamentum flavum.

those samples, where the vertebral bodies, as a result of post-mortem changes were not recognisable –the intervertebral spaces were intact in all cases, narrowing or fusions of the intervertebral spaces were not visible. Zygapophyseal joint gaps were also not involved (Fig. 3a), but at the samples of MHK-217, OF-16996 and BMP-46 we found ossified elements of the zygapophyseal joint capsules, these phenomenon confirm our diagnosis for DISH.

In the first group enthesopathies were found at the lower limbs and girdles in all cases, the most frequent sites are the Achilles-tendon insertion of calcanei, and the enthesopathies of the hip bone. The upper extremitties' entheses did not give us such a clear results, in two cases these areas were missing, in one case enthesopathy was not seen at these sites. Calcification of the vertebral disc surfaces appears in four skeletons, at three cases these alterations are not visible. Ossified elements inside the vertebral foramen and between the superior and inferior articular facets of the vertebrae are seen in all of the definite DISH cases (Fig. 3b).

Sacro-iliac ligament fusion can be seen only one case (MHK-217), the post-mortem destroyed unilateral (right side) fusion is associated with unilateral (left side) sacroileitis. In this case, beside the right side vertebral ligament ossification (T4-T12, L5-S1) left side anterior ligament ossification (T7-T12) and complete fusion of the zygapophyseal joint between the L5-S1 segments are also visible. On the basis of the osseous lesions (Olivieri et al. 2009; Olivieri et al. 2007) two different diseases arises in the etiological background, the co-existance of DISH and early-stage ankylosing spondylitis is not disclosed either (Jordana et al. 2009; Paja et al. 2010).

The diagnosis of DISH cases is confirmed by CT analysis as well. The anterior side ligament ossification shows the 'coating phenomenon', the outer part of the ligament appears as a dense layer, the inner part of the ligament is more radiolucent, the shape of the vertebral body did not became squared (Fig. 4c). The vertebral disc spaces and the zygapophyseal joint spaces remained opened, the width of these sites did not became narrow (Fig. 4a, Fig. 4b).

The second group, where the diagnosis is eDISH, includes five cases, bony changes of the affected skeletons can be seen in the Table 2 and Figure1. Although the number of completely fused contiguous vertebrae did not reach the expected four in these cases, special patterns of eDISH are still found (Fig. 1). In four of these cases the number of fused vertebral bodies is at least four, but they are not all adjacent to each other. The other special characteristic is in this group is that the ossification of anterior longitudinal ligament affected at least five vertebrae in all eDISH cases in an incomplete form; in the individuals of BA-159 and BA-173 this number reached ten and eleven, respectively.

Beside anterior ligament ossifications intervertebral disc and zygapophyseal joint gaps with original width are seen in all cases. Lower limbs and girdles' enthesopathies developed in all skeletal remains, in case of upper limbs and girdles, enthesopathies appeared only in one skeleton, in other one case these skeletal parts are missing. Extra-spinal ossification, such as sternal alterations or supraspinous ligament ossification was found in three cases, changes associated with sacroileitis were not seen. Similarly to DISH cases, vertebral foramen changes appeared in all cases, flame-like new bone-formations developed.

The MHK-80 individual's skeletal remains showed some alterations, which may not associated with DISH. Multiple healed fractures can be seen in five ribs, the right clavicle, the

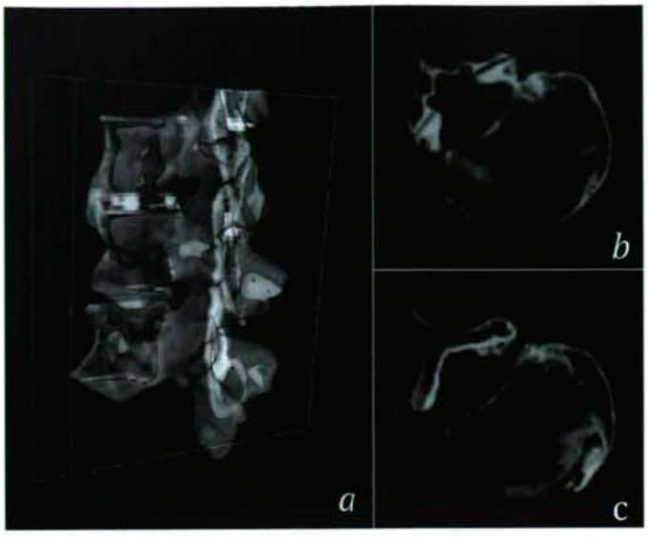

Figure 4. CT reconstructions of the thoracic spine (T9-T11) diagnosed with DISH (sample of OF-16996 - male, aged 40-60,). a: 2D-3D recontstruction of thoracic vertebrae shows unaffected interververtebral disc spaces; b: the zygapophyseal joint spaces are not involved, the vertebral body is not distorted in its shape; c: the ossification of the ligamentum flavum results in exuberant bony spur in the vertebral foramen, the anterior longitudinal ligamentum ossification appears on the right side of the vertebral body.

Figure 5. The light microscopic picture of the anterior longitudinal ligament (sample of OPM-644, male, aged over 60) shows normal mature bone structure, but increased accumulation of calcium is seen (hematoxylin and eosin stain, original magnification 10x).

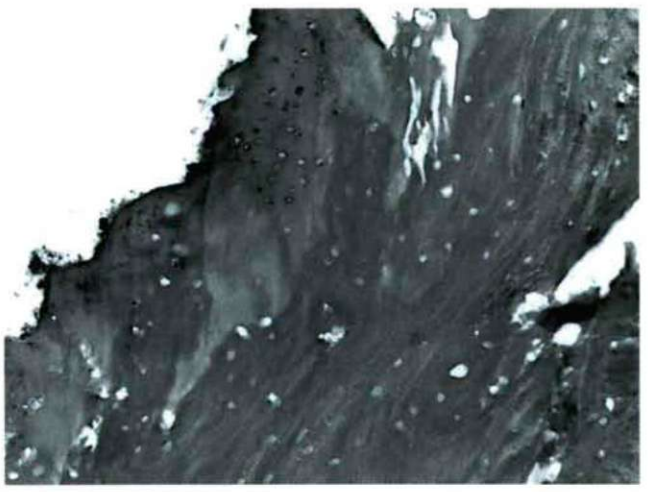

Figure 6. The microscopic picture of the section from anterior patellar spur (sample of OPM-644, male, aged over 60) reveals normal bony structure as well, in some parts, as sign of chondrogen ossification – cartilaginous lacunae are also visible (hematoxylin and eosin stain, original magnification 20x).

right fibula and the left tigh bone. The fracture of the femoral diaphysis healed with disclocation, the cloacal openings and periostal reactions refer to the presence of non-specific infection (periostitis, osteomyelytis). This infection may caused the complete ankylosis of the knee, bony bridges between the femoral and tibial condyles, lytic alterations and proliferative new bone formations are present surrounding the original articulation. However, bony ankylosis of the knee may caused tuberculosis (*Mycobacterium tuberculosis, Mycobacterium bovis*) as well (Blondiaux et al. 1999; Kósa and Tiszlavicz 1999; Thomson and Miles 1921). Although traumatic alterations – especially opened wounds or fractures – favor the pyogenic etiology, but traumatic changes may also reactivate earlier tuberculotic infection (Sauer et al. 2009). Beside lower extremity's alterations lytic lesions can be seen in the first lumbar vertebral arch, the spinous process disappeared, a round-shape, abscess-like lesion of the right lateral process is also visible. These alterations may be caused by pyogenic infection (Carragee 1997; Garcia and Grantham 1960; Nather 2005), but tuberculosis in the background is not disclosed either (Anderson 1940; Moore 1922; Nasser et al. 2002). Summarizing the phenomena, the etiology of these multiple alterations is not clear, further molecular examinations need to carried out.

During our examination, microscopic analyses also were done, samples of the OPM-644 skeleton were examined. The light microscopic picture of the anterior longitudinal ligament (Fig. 5) and thyroid cartilage shows normal mature bone structure, but increased accumulation of calcium is seen. The microscopic picture of the section from anterior patellar spur reveals normal bony structure as well, in some parts, as sign of chondrogen ossification – cartilaginous lacunae are also visible (Fig. 6).

Histological analysis reveals a long-term ossification and calcification process, these data fit to diffuse idiopathic skeletal hyperostosis, where a slowly developing hyperostotic process is present.

Discussion and Perspectives

As a result of our analysis, material of seven osteoarcheological series was investigated. The sample contains remains of 6966 individuals, the fact that the state of preservation of the material greatly varies made some difficulties during the analysis. As DISH is a diffuse disease involving almost the whole skeleton, the presence of lots of skeletal elements is necessary for a more precise diagnosis. In that case, when taphonomic processes results in fragmentary state of preservation, or results in the lack of any part of skeletal remains, the number of definite cases decreases. As a result of the above mentioned facts, statistical analysis was not calculated, prevelance of DISH is not countable in this sample. Connection between DISH and social status of the individuals diagnosed with DISH is not known, detailed archeological data are not present, so association between DISH and higher social status is not examinable.

Concerning Resnick and Niwayama criteria, the differentiation and separation of DISH and early-stage DISH cases seems to be very artificial, the very thin line between the two categories is based on the difference of only one alteration. In those cases, where fusion at least four adjacent vertebral bodies is present, the diagnosis is DISH, while if less than four contiguous vertebrae are fused, the diagnosis is eDISH. Concerning other spinal and extra-spinal alterations there's no difference between the two categories, diffuse ossification and calcification processes are found in all cases of the two categories. Interestingly enthesopathies were not seen in all cases, but ossification in the vertebral foramen (possibly as a result of ligamentum flavum ossification) is visible in all of them. Although the little number of cases does not let to draw unequivocal conclusions, on the basis of these facts diagnostic criteria for DISH and eDISH may need to be reconsidered in the future. In our previous opinion, the diagnosic criteria of DISH in osteoarcheological samples possibly need to be expanded, and some pathologic features (e.g. ligamentum flavum ossification) and patterns (number and relation of vertebrae with complete and not complete fusions) should be taken into account.

Future studies, possibly together with more precise histological, medical imaging and biochemical analyses, needs to be done to investigate the diffuse idiopathic skeletal hyperostosis on three axes:

analyses of the typical lesions, developmental stages, morphological variations and paleodemographical attribute of the definite and early-stage DISH cases;

the co-existance of DISH and other diseases with ligament ossification (ossification of ligamentum flavum and ossification of posterior longitudinal ligament) are present in both medical (Ehara et al. 1998; Epstein 2000) and paleopathological literature (Pálfi et al. 2009). Paleopathological analyses of the associations among these diseases may be helpful in the understanding of these diseases;

paleopathological differential diagnosis of DISH and other diseases (e.g. ankylosing spondylitis, degenerative spinal alterations, infections) can be difficult for many reasons. If more than one disease develop in the same skeleton, differential diagnosis is more complicated, so the more precise differentiation of diseases would be very important.

Concerning these axes, different methods and collaborations need to be used; this pluridisciplinar approach may provide helpful new informations for equally paleopathology, osteology and researchers, who would like to get more information about past populations' health status.

Acknowledgements

The support of the Hungarian Scientific Research Fund (OTKA Grant No. 78555), the Euromedic Diagnostics Szeged Kft (medical director dr. István Horváth) and Zsolt Bereczki is greatly acknowledged.

References

Anderson RL (1940) Isolated tuberculosis of the spinal process of a vertebra: Report of a case. J Bone Joint Surg 22:741-744.

Arlet J, Mazières B (1985) Hyperostotic disease. Rev Med Interne 6:553-564.

Békei G (1995) A gerincoszlop és a sternum fejlődési rendellenességeinek tanulmányozása a Bácsalmás – Homokbánya temető embertani anyagán. Diploma work. József Attila University, Department of Biological Anthropology, Szeged.

Blondiaux J, Hedouin V, Chastanet P, Pavaut M, Moyart V, Flipo RM (1999) Epidemiology of tuberculosis: A 4th to 12th c. AD picture in a 2498-skeleton series from northern France. In: Pálfi Gy, Dutour O, Deák J, Hutás I eds., Tuberculosis Past and Present. Golden Book Publisher Ltd., Tuberculosis Foundation. Budapest-Szeged. pp. 403-409.

Burner TW, Rosenthal AK (2009) Diabetes and rheumatic diseases. Curr Opin Rheumatol 21:50-54.

Cammisa M, De Serio A, Gugliemi G (1998) Diffuse idiopathic skeletal hyperostosis. Eur J Radiol 27, Supplement 1:7-11.

Carragee EJ (1997) Pyogenic vertebral osteomyelitis. J Bone Joint Surg Am 79:874-880.

Denko CW, Malemud CJ (2005) Role of the growth hormone/insulin-like growth factor-1 paracrine axis in rheumatic diseases. Semin Arthritis Rheum 35:24-34.

Denko CW, Boja B, Moskovitz RW (1996) Growth factors, insulin-like growth factor –I and growth hormone, in synovial fluid and serum of patients with rheumatic disorders. Osteorthritis Cartilage 4:245-249.

Ehara S, Shimamura T, Nakamura R, Yamazaki K (1998) Paravertebral ligamentous ossification: DISH, OPLL and OLF. Eur J Radiol 27:196-205.

Epstein, NE (2000) Simultaneous cervical diffuse idiopathic skeletal hyperostosis and ossification of the posterior longitudinal ligament resulting in dysphagia or myelopathy in two geriatric North Americans. Surg Neurol 53:427-431.

Farkas Gy (szerk.) (1998) Ópusztaszer-Monostor lelőhely antropológiai leletei. AGAPE Kft. Ferences Nyomda és Könyvkiadó, Szeged.

Farkas Gy, Józsa L, Paja L (2004) Developmental anomalies and other pathological lesions of the sternum in a medieval osteological sample. Acta Biol Szeged 48:39-42.

Forestier J, Rotes-Querol J (1950) Senile ankylosing hyperostosis of the spine. Ann Rheum Dis 9:321-330.

Garcia A, Grantham SA (1960) Hematogenous Pyogenic Vertebral Osteomyelytis. J Bone Joint Surg Am 42:429-436,520.

Giuffra V, Giusiani S, Fornaciari A, Villari N, Vitiello A, Fornaciari G (2010)

Diffuse idiopathic skeletal hyperostosis in the Medici, Grand Dukes of Florence (XVI century). Eur Spine J 19:S103-S107.

Jankauskas R (2003) The incidence of diffuse idiopathic skeletal hyperostosis and social status correlations in Lithuania. Int J Osteoarchaeol 13:289–293.

Jordana X, Galtés I, Couto AR, Gales L, Damas M, Lima M, Bruges-Armas J (2009) The coexistence of ankylosing spondylitis and DISH - a post-mortem diagnosis. Clin Rheumatol 28:353-356.

Julkunen H, Heinonen OP, Knekt P, Maatela J (1975) The epidemiology of hyperostosis of the spine together with its symptoms and related mortality in a general population. Scand J Rheumatol 4:23-27.

Kósa F, Tiszlavicz L (1999) Demographic interpretations of bone tuberculosis in historical anthropological material and in living populations. In Pálfi Gy, Dutour O, Deák J, Hutás I, eds., Tuberculosis Past and Present. Golden Book Publisher Ltd., Tuberculosis Foundation. Budapest-Szeged. pp. 403-409.

Lovász G (2005) Bácsalmás-Óalmás 16-17. századi temető általános embertani feldolgozása (2001-2003-as feltárás). University of Szeged, Department of Biological Anthropology, Szeged.

Mader R (2002) Clinical manifestations of diffuse idiopathic skeletak hyperostosis of the cervical spine. Seminars in Arthritis and Rheumatism 32:130-135.

Masiero S, Padoan E, Bazzi M, Ponzoni A (2001) Dysphagia due to diffuse idiopathic skeletal hyperostosis: an analysis of five cases. Rheumatol Int 30:681–685.

Miyamoto K, Sugiyama S, Hosoe H, Iinuma N, Suzuki Y, Shimizu K (2009) Postsurgical recurrence of osteophytes causing dysphagia in patients with diffuse idiopathic skeletal hyperostosis. Eur Spine J 18:1652-1658.

Moore BH (1922) A case of spontaneous fracture of the transverse process of a lumbar vertebra – due to tuberculosis. The Journal of Bone & Joint Surgery 4:322-324.

Nasser I, Mahi M, Semlali S, Kacemi L, El Quessar A, Chakir N, El Hassani MR, Jiddane M (2002) Tuberculosis of the posterior vertebral arch:A case report. J Neuroradiol 29:204-207.

Nather A, David V, Hee HT, Thambiah J (2005) Pyogenic vertebral osteomyelytis: a review of 14 cases. J Orthop Surg 13:240-244.

Olivieri I, D'Angelo S, Palazzi C, Padula A, Mader R, Khan MA (2009) Diffuse idiopathic skeletal hyperostosis: Differentiation from ankylosing spondylitis. Curr Rheumatol Rep 11:321-328.

Olivieri I, D'Angelo S, Cutro MS, Padula A, Peruz G, Montaruli M, Scarano E, Giasi V, Palazzi C, Khan MA (2007) Diffuse idiopathic skeletal hyperostosis may give the typical postural abnormalities of advanced ankylosing spondylitis. Rheumatology 46:1709-1711.

Oppenlander ME, Orringer DA, La Marca F, McGillicuddy JE, Sullivan SE, Chandler WF, Park P (2009) Dysphagia due to anterior cervical hyperosteophytosis. Surg Neurol 72:266-271.

Ősz B, Hajnal K, Marcsik A, Fogas O, Horváth F, Zádori P, Kelemen K, Vandulek Cs, Schultz M, Márk L, Molnár E, Pálfi Gy (2009) Preliminary report on the paleopathological research of the skeletal material from the Szeged medieval castle excavation. Acta Biol Szeged 53:125-138.

Paja L, Márk L, Zádori P, Vandulek Cs, Ősz B (2010) Well-developed spinal ossifications: cases of ankylosing spondylitis from Hungarian skeletal materials – Imaging and protein diagnostics. 18th European Meeting of the Paleopathology Association, 23th – 26th Aug, 2010, Vienna, Austria, Abstracts and Program, 192.

Paja L (2000) Patológiás elváltozások vizsgálata az óföldeáki erődtemplom XII-XVIII. századi temetőjének embertani anyagában. Diploma work. University of Szeged, Department of Biological Anthropology, Szeged.

Paja L, Molnár E, Marcsik A (2007) Homokmégy - Székes (10-11. század) lelőhely embertani anyagának ismertetése (előzetes eredmények). Folia, Anthropologica 5:93-96.

Pálfi Gy, Molnár E, Kristóf L, Cuvigny H, Brun JP, Donoghue HD, Spigelman M, Szikossy I, Pap I (2009) Paleopathological study of two partially mummified bodies. GPLF - Meeting of the French-speaking paleopathologists, Szeged, Hungary, 30th April -3rd May 2009, 'From Past Lesions to modern Diagnostics' Abstract Book and Program, pp. 99-100.

Resnick D, Niwayama G (1976) Radiographic and pathologic features of spinal involvement in diffuse idiopathic skeletal hyperostosis (DISH). Radiology 119:559-568.

Resnick D, Shaul SR, Robins JM (1976) Diffuse Idiopathic Skeletal Hyperostosis (DISH): Forestier's Disease with Extraspinal Manifestations. Radiology 115:513-524.

Rogers J, Waldron T (2001) DISH and the Monastic Way of Life. Int J Osteoarcheol 11:357-365.

Rogers J, Waldron T (1995) A Field Guide to Joint Disease in Archeology. John Wiley and Sons. Chichester, West Sussex. England.

Sauer B, Hofmann GO, Tiemann A (2009) Acute exacerbation of tuberculous osteoarthritis of the knee caused by trauma: clinical management. Z Orthop Unfall 147:734-739.

Seidler TO, Pèrez Àlvarez JC, Wonneberger K, Hacki T (2009) Dysphagia caused by ventral osteophytes of the cervical spine: clinical and radiographic findings. Eur Arch Otorhinolaryngol 266:285-291.

Szigeti T (2001) A Magyarhomorog-Kónyadomb 10-11. századi temető vázcsontjainak metrikus és paleopatológiai feldolgozása. Diploma work. University of Szeged, Department of Biological Anthropology, Szeged.

Thomson A, Miles A (eds) (1921) Manual of surgery – Oxford Medical Publications, Vol. 1, General surgery. Henry Frowde and Hodder & Stoughton, London, p. 345.

Utsinger PD (1985) Diffuse idiopathic skeletal hyperostosis. Clin Rheum Dis 11:325-351.

Verlaan JJ, Oner FC, Maat GJR (2007) Diffuse idiopathic skeletal hyperostosis in ancient clergymen. Eur Spine J 16:1129-1135.

Waldron T (2008) Paleopathology. Cambridge Manuals in Archeology. Cambridge University Press, Cambridge, pp. 72-77.

Westerveld LA, Verlaan JJ, Oner FC (2009) Spinal fractures in patients with ankylosing spinal disorders: a systematic review of the literature on treatment, neurological status and complications. Eur Spine J 18:145–156.

Volume 54(2):83-91, 2010
Acta Biologica Szegediensis
http://www.sci.u-szeged.hu/ABS

ARTICLE

Skeletal manifestation of tuberculosis in a late medieval anthropological series from Serbia

Gabriella Lovász[1,2]*, György Pálfi[1], Antónia Marcsik[1], Annamária Pósa[1,3], Endre Neparáczky[1,3], Erika Molnár[1]

[1]Department of Biological Anthropology, University of Szeged, Szeged, Hungary, [2]Municipal Museum of Subotica, Subotica, Serbia, [3]Department of Genetics, University of Szeged, Szeged, Hungary

ABSTRACT The aim of this study is to present the results of the paleopathological investigation of tuberculosis (TB) in the late medieval (16th-17th c. AD) anthropological series of the Zombor-Repülőtér site from Serbia. The paleopathological analysis of TB was carried out in two phases during which macromorphological methods were used. The first phase of the investigation focused on classical/advanced stage skeletal TB alterations. In the second phase the atypical/early-stage TB lesions and 3 stress factors were also taken into consideration. The first phase of the investigation revealed two cases of tuberculosis in the series. However, in the second phase of the investigation additional 32 probable TB cases were recognized. The association of different tuberculous lesions (both classical and atypical/early stage alterations) as well as stress indicators were found in most of these cases, which rises the probability of the diagnosis of tuberculosis. The remarkable difference between the prevalence in the two phases of the investigation shows that the detection of diagnostic criteria related to atypical/early-stage tuberculosis raises the possibility of identifying TB cases. **Acta Biol Szeged 54(2): 83-91 (2010)**

KEY WORDS

tuberculosis
Pott's disease
early-stage TB lesions
paleopathology
Zombor
Serbia

Human tuberculosis is an infectious disease affecting a number of organs, especially the lungs. It is caused by pathogens of the *Mycobacterium tuberculosis* complex, most often the *Mycobacterium tuberculosis* and the *Mycobacterium bovis*. The manifestation of symptoms depends on several factors, such as the type of the pathogen, the infected individual's age and the condition of the immune system (Bloom 1994; Madkour 2004). The pathogens might spread from the place of the primary infection (e. g. lungs) either by haematogenous route or in a direct way to other organs and tissues where they may trigger inflammatory reactions. The bones can also be affected, though only 3% of all the tuberculous infectious cases occur in the skeletal involvement (Resnick and Niwayama 1988; Aufderheide and Rodríguez-Martin 1998; Ortner 2003).

In the case of anthropological findings, usually only dry bones are available, thus we can observe only skeletal TB. Classically, the lesions used to identify tuberculosis in skeletal material are characteristic lytic lesions, with little reactive bone formation. These alterations occur particularly in areas of cancellous bone, especially in vertebrae, as well as metaphysis and epiphysis of long bones, but virtually any bone can be affected (Resnick and Niwayama 1988; Ortner 2003).

The most common "classic" representation of skeletal tuberculosis affects the vertebral column (tuberculous spondylitis, Pott's disease), causing cavitation in the vertebra as well as sharply angulated kyphosis of the spine or rarely "cold abcess" on the ventral surface of the vertebrae (Resnick and Niwayama 1988; Aufderheide and Rodríguez-Martin 1998; Ortner 2003). Tuberculosis of the hip joint (tuberculous coxitis) is the second most frequent skeletal lesion after vertebral involvement, but the knee (tuberculous gonitis) or other joints (e. g. elbow, wrist, ankle) can also be affected with the consequences of the erosion of the articular surface, subluxation and bony ankylosis (Resnick and Niwayama 1988; Aufderheide and Rodríguez-Martin 1998; Ortner 2003). Beside these lesions tuberculous osteomyelitis in the diaphysis of the long bones and the short tubular bones of the hands and feet (spina ventosa), lytic, rounded lesions in the skull and pulmonary calcifications might also occur, but these conditions are relatively rare (Resnick and Niwayama 1988; Molnár and Pálfi 1994; Pálfi et al. 1999; Haas et al. 2000; Ortner 2003).

However, the classical skeletal TB changes indicate a more or less developed stage of tuberculosis. Early-stage TB is not recognizable on the basis of the previously listed lesions and this causes the underestimation of the prevalence of tuberculosis in the examined historical populations. Since the recognition of the importance of establishing diagnostic criteria for early-stage TB a number of studies have been focusing on searching for atypical/non classical bone alterations linked to tuberculous infection. These researches are mainly

Accepted Dec 14, 2010
*Corresponding author. E-mail: lovaszg@bio.u-szeged.hu

based on the study of skeletal collections with known causes of death. As the result of these surveys 3 different groups of alterations seem very likely to be linked with TB:

a) rib lesions: sharply circumscribed lytic lesions and/or diffuse periostitis on the visceral surface of ribs, particularly in pulmonary tuberculosis (e. g. Kelley and Micozzi 1984; Roberts et al. 1994; Santos and Roberts 2001, 2006; Pálfi 2002; Maczel 2003; Matos and Santos 2006; Raff et al. 2006);

b) superficial vertebral alterations: irregular pitting and holes especially on the ventral surface of the vertebral bodies, but with no cavitation and collapse of the bodies (e. g. Baker 1999, Haas et al. 1999, 2000; Pálfi 2002; Maczel 2003; Molnár et al. 2005; Zink et al. 2007; Nerlich and Lösch 2009);

c) endocranial lesions: small granular impressions or abnormal blood vessel impressions with branched or reticulated course as well as plates of new bone in the inner surface of the skull vault found in the cases of tuberculous meningitis (Schultz 1999, 2001; Hershkovitz et al. 2002; Pálfi 2002; Maczel 2003; Lewis 2004).

The analyses of ancient microbial DNA in samples showing any of these alterations confirmed the presence of MTB complex organisms in a significant number of the examined cases (e.g. Spigelman and Lemma 1993; Haas et al. 1999; 2000; Maczel 2003; Molnár et al. 2005; Raff et al. 2006; Zink et al. 2007; Nerlich and Lösch 2009). On the basis of these examinations, these minor pathological conditions are suggested to be indicative of early stage of tuberculosis, and are named Minor Osseous Lesions Attributable to Tuberculosis – "MOLAT" (Maczel 2003).

Apart from the above mentioned changes, the correlation between tuberculosis and stress indicators, such as porotic hyperostosis, linear enamel hypoplasia and long bone periostitis, were also recognized in some studies (Stuart-Macadam 1989; Santos and Roberts 2001; Pálfi 2002; Maczel 2003).

Although several studies showed correlation between TB and the above mentioned alterations, it should be noted that these lesions are not always TB specific. Other conditions, such as infections, malnutrition, neoplastic conditions or traumas might also cause similar changes; therefore these new criteria should be used cautiously. Nevertheless, based on the association of these lesions we can presume the tuberculous origin in a higher probability. In order to justify the diagnosis of TB, biomolecular examinations (DNA, protein and mycolic acid analyses) are also required (Fletcher et al. 2003; Maczel 2003. Hershkovitz et al. 2008; Donoghue 2009; Redman et al. 2009; Boros-Major et al. 2010).

The aim of this study is to present the results of the paleopathological investigation of TB in the late medieval (16th-17th c. AD) anthropological series of the Zombor-Repülőtér site from Serbia. The examinations were carried out in two phases. Focusing on classical TB lesions, the first phase of the investigation revealed only two cases of tuberculosis (Lovász et al. 2008). However, the examination of the Bácsalmás-Óalmás anthropological series originating from a similar geographic region and the same historical period showed a number of tuberculous cases based on atypical/early-stage TB lesions (e. g. Pálfi and Ardagna 2002; Maczel 2003; Marcsik et al. 2006, 2007; Pálfi and Molnár 2009). Ancient DNA analyses also confirmed the presence of MTB complex organisms in a significant number of these cases (Molnár et al. 2005; Zink et al. 2007; Nerlich and Lösch 2009). Considering these results and paying special attention to the lesions attributed to early-stage tuberculosis, in the second phase of the pathological investigation we re-examined the skeletal material of Zombor-Repülőtér. On the one hand, we wanted to know whether the prevalence of TB had changed in the second phase of the investigation. On the other hand, we wanted to find out if there was any association among TB related lesions and which alterations appeared together the most frequently. With the results of our research we wish to provide a basis for further paleoproteomic and mycolic acid analyses and especially ancient DNA examinations, in order to find more evidence of the connection between these alterations and TB infection.

Materials and Methods

The graveyard of Zombor-Repülőtér near the Northern-Serbian town of Sombor was excavated during World War II. The excavation was led by László Wollner with the help of the Anthropological Institution (today: Department of Biological Anthropology) of the University of Szeged, Hungary. The series consists of 196 skeletons, and after the time of the excavation it was stored in Szeged, where the archaeological and basic anthropological examinations were carried out. The archaeological findings of the graveyard suggest that this population emigrated from the southern part of Serbia or Montenegro during the Turkish occupation. After the war, the material from this site was moved back to Serbia, first to the Museum of Vojvodina (Novi Sad), later to the Municipal Museum of Sombor (Bartucz 1960; Korek 1994). Unfortunately the data of the anthropological investigations had been lost therefore the reinvestigation of the material became essential.

During the palaeopathological investigation 130 adults (60 males, 66 females, 4 individuals with undetermined sex) and 66 subadults were examined (Lovász et al. 2008). The pathological analysis of TB was carried out in two phases during which macromorphological methods were used. The first phase of the investigation focused on classical/advanced stage skeletal TB alterations (tuberculous spondylitis, tuberculous arthritis). In the second phase the atypical/early-stage TB lesions (rib lesions, superficial vertebral changes, endocranial alterations, early-stage spondylodiscitis) were also taken into consideration. In addition, the association of tuberculosis related lesions and 3 stress factors (long bone periostitis, cribra

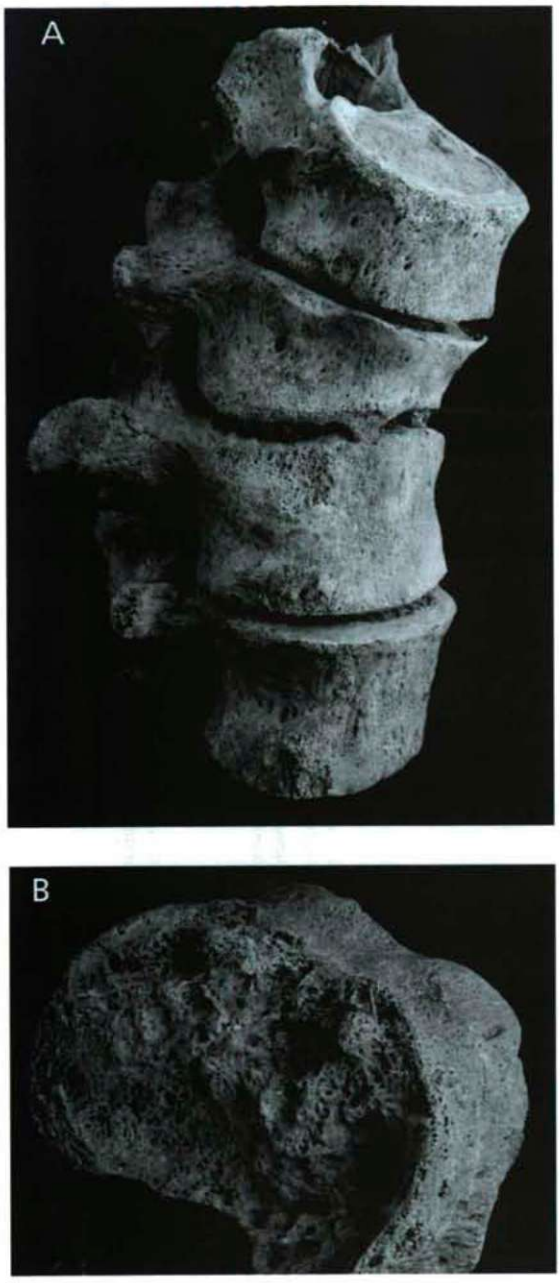

Figure 1. Tuberculous spondylitis: a) kyphotic angulation of the lumbar region (T12-L3); b) lytic focus in the body of the L1 vertebra (Grave no. 84, 23-25 year-old male).

orbitalia, cribra cranii) were also detected.

Results

The first phase of the investigation revealed two cases in the series showing alterations of an advanced stage of TB.

The skeletal remains of a young male adult (Grave no. 84) revealed severe pathological lesions on the 1st and 2nd lumbar vertebrae (Fig. 1). In the lower part of the body of the first lumbar vertebra lytic focus and some reactive bone formation were seen. In addition, on the ventral surface of the body periosteal reactions were observed too. The second lumbar vertebra also showed deep cavitation in the upper part of the body accompanied by reactive bone formation as well as periostitis on the ventral surface. As a consequence of these lesions, the angulation of the spine was also recognizable. These changes correspond to the diagnostic criteria of tuberculous spondylitis. Beside these alterations, the anterior surface of the bodies of the lower thoracic and third lumbar vertebrae revealed superficial inflammatory alterations. Moreover, periostitis on the right tibia and both fibula was found (Lovász et al. 2008).

Figure 2. Healed lumbo-sacral tuberculosis with L5-sacrum fusion and cold abscess (Grave no. 51, 45-50 year-old male).

The mature male individual of Grave no. 51 also showed serious alterations on the vertebral column: the 5th lumbar vertebra fused to the sacrum (Fig. 2). On the body of L5 vertebra remodelled bone formation and osteophyts were also seen. In addition, the ventral surface of the sacrum showed lytic lesions accompanied by extensive but also remodelled reactive bone formation probably in response to an overlying abscess. Moreover, inflammatory changes were observed in both sacroiliac joints as well. These alterations refer to healed lumbo-sacral tuberculosis accompanied by bilateral

Table 1. Skeletal manifestations of advanced and potential early-stage TB in the anthropological material of Zombor-Repülőtér site – individual data.

Grave No.	Reg. No.	Age at death	Sex	Classical TB alterations		Potential TB lesions (atypical or eraly-stage alterations)				Associated stress indicators			Other inflammatory lesions
				Tuberculous spondylitis	Tuberculous arthritis	Rib lesions	Superficial vertebral changes	Endocranial alterations	Early stage spondylodiscitis	Long bone periostitis	Cribra orbitalia	Cribra cranii	
5	191	35-40	Male	-	-	-	Thoracic region	Blood vessel impressions	-	2 tibiae	-	-	2 clavicles: periostitis
7	180	16-18	-	-	-	-	-	Blood vessel impressions	-	-	-	-	-
8	194/a	23-25	Female	-	-	-	-	Blood vessel impressions	-	2 femora, 2 tibiae, 2 fibulae	-	-	-
10	196	50-55	Male	-	-	Rough texture	-	-	-	-	-	-	T12-L5: disc lesions not related to TB
11	197	23-25	Male	-	-	-	Thoracic and lumbar region	-	-	-	-	-	Manubrium of sternum: porous appearance of the dorsal surface
13	199	45-50	Male	-	-	Rough texture	-	-	-	2 femora, 2 tibiae	-	-	-
24	211	30-35	Female	-	-	Rough texture, blood vessel impressions	-	-	-	2 tibiae	-	-	L2-L3: disc lesions not related to TB
25	212	12-14	-	-	-	-	-	Blood vessel impressions	-	-	-	-	2 rami of mandible: periotitis
26	215	18-20	-	-	-	-	Thoracic and lumbar region	-	T12: shallow cavitation in the distal disc	-	porotic	-	Manubrium of sternum: porous appearance of the dorsal surface
28	217	55-60	Male	-	-	Rough texture	-	-	-	2 tibiae, 2 fibulae	-	-	L4: disc lesions not related to TB
29	218	4-6	-	-	-	-	-	Blood vessel impressions	-	2 femora	trabecular	-	-
33	222	25-30	Female	-	-	-	-	Blood vessel impressions	-	-	porotic	-	-
40	229	23-25	Female	-	-	-	Thoracic and lumbar region	Blood vessel impressions	-	2 femora, 2 tibiae, 2 fibulae	-	-	-
46	235	16-18	-	-	-	Periosteal appositions	-	-	-	2 tibiae, 2 fibulae	-	-	-
48	237	23-25	Male	-	-	Periosteal appositions	Lumbar region	Blood vessel impressions	-	2 femora, 2 tibiae, 2 fibulae	-	-	-
51	240	45-50	Male	L5-sacrum fusion, cold abcess	-	-	-	-	-	-	-	-	sacroiliac joint (bilateral): athritis; left metatarsals: periostitis, possibly caused by malleolus medialis fracture

Table 1. continued

55	244	23-25	Female	-	-	Periosteal appositions	Thoracic region	-	-	2 tibiae, 2 fibulae	-	-	-
58	247	18-19	-	-	-	-	Thoracic and lumbar region	-	-	2 femora, 2 tibiae	porotic	-	-
69	265	23-25	Female	-	-	Rough texture, blood vessel impressions	Thoracic region	-	-	-	-	-	-
70	266	2-3	-	-	-	-	-	Blood vessel impressions	-	-	porotic	-	-
84	280	23-25	Male	L1-L2: cavitation of the bodies	-	-	Thoracic and lumbar region	-	-	right tibia, 2 fibulae	-	-	-
95	394	2-3	-	-	-	-	-	Blood vessel impressions	-	-	trabecular	-	-
97	294	23-25	Female	-	-	-	Thoracic region	Granular impressions and blood vessel impressions	-	2 femora, 2 tibiae	-	-	Manubrium of sternum: porous appearance of the dorsal surface
98	295	25-30	Female	-	-	-	Thoracic and lumbar region	-	-	2 tibiae	-	-	-
100	297	25-30	Male	-	-	Rough texture	-	-	-	2 femora, 2 tibiae	porotic	-	-
102	299	45-55	Male	-	-	Rough texture	-	-	-	2 tibiae	-	-	L1-L2: disc lesions not related to TB
108	406	0,5-1,5	-	-	-	-	-	Periosteal appositions	-	-	-	-	-
113	411	9-10	-	-		-	-	Blood vessel impressions	-	-	cribrotic	porotic	-
118	327	1-3	-	-	-	-	-	Blood vessel impressions	-	-	trabecular	-	-
szórvány	250	9-10	-	-	-	-	-	Blood vessel impressions	-	-	porotic	-	-
szórvány	252	5-6	-	-	-	-	-	Blood vessel impressions	-	-	porotic	-	-
szórvány	310	23-25	Male	-	-	-	Thoracic and lumbar region	-	-	2 femora, 2 tibiae	-	-	-
szórvány	341	Infant	-	-	-	-	-	Periosteal appositions	-	-	porotic	-	-
szórvány	349	45-50	Female	-	-	-	Lumbar region	-	-	2 femora, 2 humeri	-	-	-

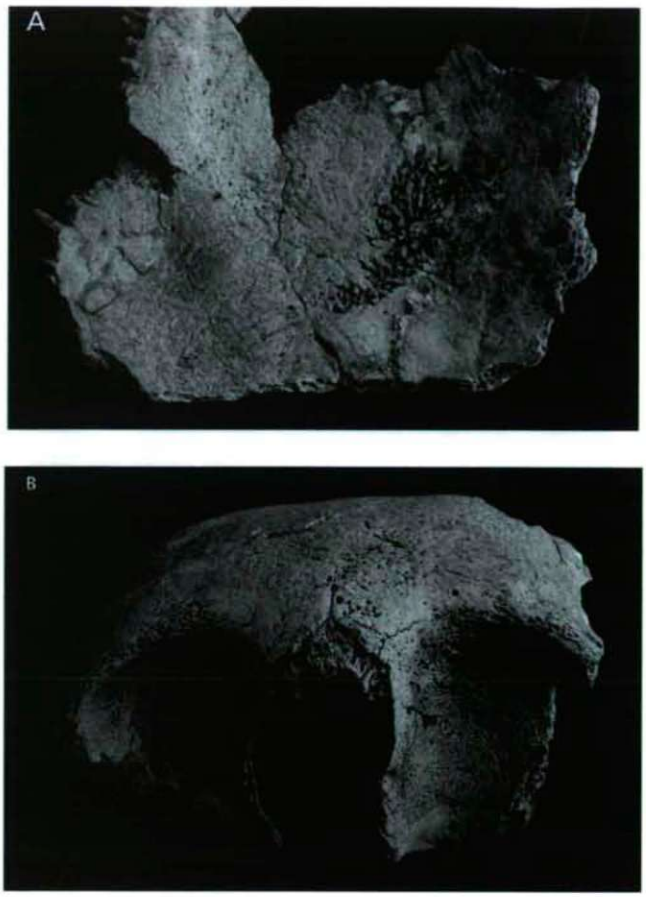

Figure 3. Potential early-stage TB showing association of: a) blood vessel impressions on the internal surface of the left parietal bone; b) bilateral trabecular cribra orbitalia (Grave no. 29, 4-6 year-old infant).

sacroileitis (Lovász et al. 2008).

The second phase of the investigation revealed 32 other probable TB cases, thus their total number rose up to 34 (see Table 1). Among these individuals 14 belong to subadults and 14 to young adults (6 males, 8 females), furthermore 6 mature individuals (5 males, 1 female) were also affected. As far as early-stage TB lesions are concerned, except for Grave no. 51, every individual showed at least one type of the alterations mentioned above.

In most of the cases (17 cases) endocranial lesions were seen. The majority of the alterations appeared in subadults (11 cases), but 6 young adults were also affected (2 males and 4 females). Abnormal blood vessel impressions on the internal surface of the skull vault were seen in the largest number (15 cases), and in one of the cases these lesions were accompanied by granular impressions as well. Two other individuals showed only periosteal appositions on the endocranium.

Superficial vertebral alterations were recognized in a smaller number of individuals (13 cases). The lesions were found mainly in young adults (5 males and 5 females), though

Table 2. Number of cases showing association of classical and atypical/early stage tuberculous lesions as well as stress indicators (TS: Tuberculous spondylitis, RL: Rib lesions, SVCh: Superficial vertebral changes, EA: Endocranial alterations, ESS: Early stage spondylodiscitis, LBP: Long bone periostitis, CO: Cribra orbitalia, CC: Cribra cranii).

	TS	RL	SVCh	EA	ESS	LBP	CO	CC
TS								
RL	0							
SVCh	1	3						
EA	0	1	4					
ESS	0	0	1	0				
LBP	1	8	10	6	0			
CO	0	1	2	9	1	3		
CC	0	0	0	1	0	0	1	

a mature female and two juvenile individuals also showed changes on the vertebral bodies. As mentioned before, one of the individuals showing tuberculous spondylitis (Grave no. 84) also belonged to this group.

As for rib lesions, alterations were found in 10 cases. A juvenile and two young adults (1 male and 1 female) showed signs of periosteal appositions on the visceral surfaces of the ribs, indicating an active inflammatory process. In seven other cases rough texture of the visceral surfaces of the ribs was detected, which was probably due to healed and remodelled periosteal bone formation. This alteration was found mainly on mature male skeletons: 4 mature and 1 young male adults as well as 2 young female adults were affected.

Beside these atypical alterations, in one of the juvenile cases (Grave no. 26) spondylodiscitis was found: shallow cavitation and inflammatory reactions were observed in the body of the 12th thoracic vertebra. This lesion is probably due to TB infection, and might be the sign of an early stage of tuberculous spondylitis. In addition, superficial vertebral lesions and cribra orbitalia were also detected in this case.

Potential early-stage TB lesions were accompanied by stress factors in a number of cases. Long bone periostitis was found in most of the cases (18 cases), mainly in young adults: 3 subadults, 5 young male adults, 6 young female adults, 3 mature male and 1 mature female individuals were affected. The lesions appeared only on the lower extremities (mostly on tibiae and femora) except for one case, where the humerus also showed periostitis. Porotic hyperostosis was also frequently seen in association with tuberculous changes. The orbital roof (cribra orbitalia) was affected in 12 cases (10 subadults, 1 young female adult and 1 young male adult) and mainly the porotic form was detected. However, cribra cranii was found in the case of one subadult.

As for the prevalence of TB cases in the skeletal material of the Zombor-Repülőtér site, we could state that it was quite different in the two phases of the examination. In the first phase the prevalence was P1=2/196*100%=1,02%, and in the sec-

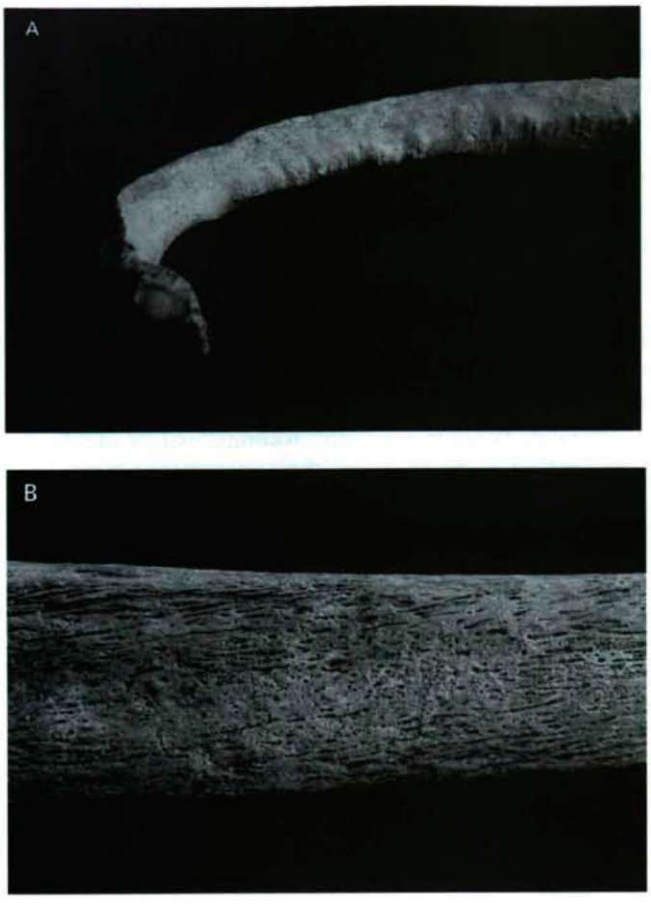

Figure 4. Potential early-stage TB showing association of: a) remodelled lesions on the visceral surface of the right 8th rib; b) remodelled periosteal reactions on the left tibia (Grave no 28, 55-60 year-old male).

ond phase this value rose up to P2=34/196*100%=17,35%.

Concerning the association of different tuberculous lesions (both classical and atypical/early-stage alterations) as well as stress indicators, we found that these changes occurred together in 28 cases (82,35% of all tuberculous cases). The majority of the cases showed two types of these lesions (19 cases). Moreover, in 8 cases we found the association of three lesions and in one case we recognized as many as four of these changes.

The most frequent association was the co-occurrence of a potential early-stage TB lesion and one of the stress indicators (Table 2). Superficial vertebral alterations and long bone periostitis association were observed in the highest number of the cases (10 cases). Furthermore, the combinations of endocranial alterations and cribra orbitalia (9 cases; Fig. 3) as well as rib lesions and long bone periostitis (8 cases; Fig. 4) were often found. The co-occurrence of potential early-stage TB lesions were also recognized, but in a relatively low number. Superficial vertebral changes and endocranial alterations were found together in 4 cases, the association

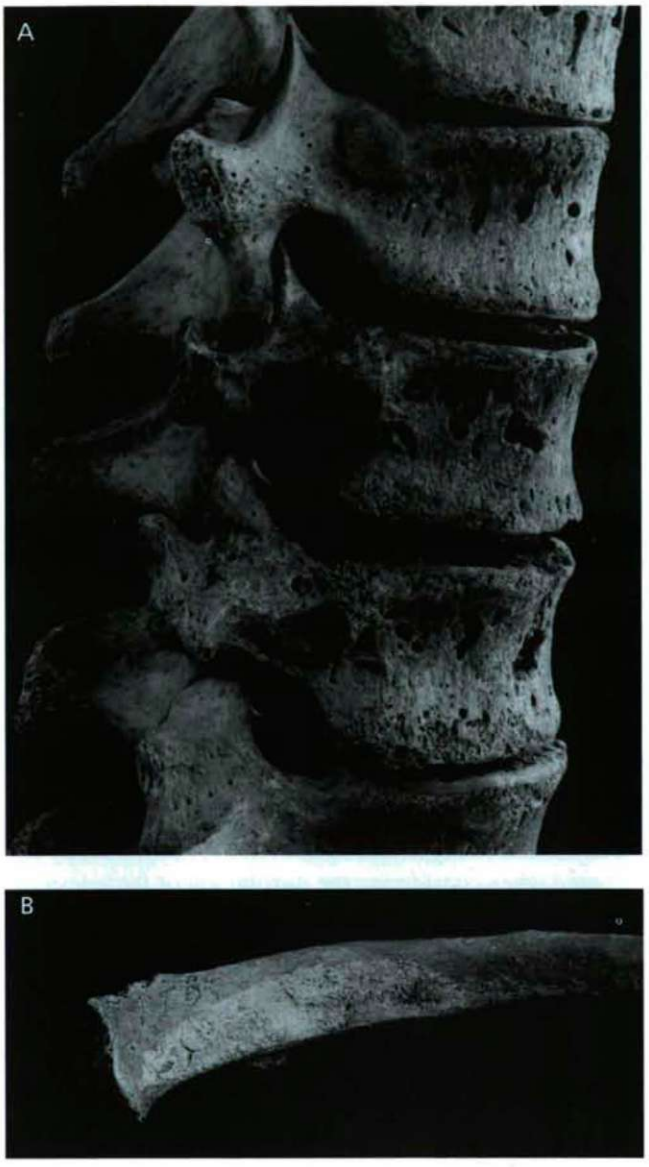

Figure 5. Potential early-stage TB showing association of: a) superficial vertebral changes on the T10-12 vertebrae; b) periosteal apposition on the visceral surface of the left 9th rib (Grave no. 55, 23-25 year-old female).

of rib lesions and superficial vertebral changes occurred in 3 cases (Fig. 5). Endocranial alterations accompanied by rib lesions were detected in a single case.

Discussion

Regarding the results of the first phase of the investigation, we could state that in the Zombor-Repülőtér skeletal material the characteristic, advanced-stage tuberculous alterations (e. g. tuberculous spondylitis), on which diagnosis was mainly based even some years ago, were present only in 2 cases.

However, taking into consideration the atypical/early-stage TB changes beside the classical alterations, the second phase of the examination revealed additional 32 potential tuberculous cases. Among all TB related cases, 33 showed at least one type of early-stage TB lesions, even in the case where an advanced-stage bone lesion was also present. The remarkable difference between the prevalence in the two phases of the investigation shows that the detection of diagnostic criteria related to atypical/early-stage tuberculosis raises the possibility of identifying TB cases. Therefore, it could also be concluded that for a more appropriate estimation of TB frequency, the application of new criteria and detection methods is inevitable.

Although there are many evidences about the connection of these atypical/early-stage lesions and tuberculosis, it is important to note that these alterations are not always TB specific. Thus, in the cases where the diagnosis was based on these atypical lesions, the tuberculous origin is only presumed, although the association of these changes raises the probability of the diagnosis. However, in addition to the frequent and simultaneous appearance of the supposed tuberculous changes, biomolecular confirmation (*i.e.* DNA, mycolic acid) of TB infection might justify the tuberculous aetiology of the lesions.

The TB related atypical bone changes appeared in almost all age groups (except for elderly individuals), particularly in subadults and young adults. Moreover, a certain tendency can be noted when considering the distribution of these lesions. The endocranial alterations appeared especially in subadults – this result corresponds with medical data from the pre-antibiotic era, which reports that a relatively high number of tuberculous children suffered and died from meningitis (Datta and Swaminathan 2001). Superficial vertebral changes were found mainly in young adults. These data might suggest particular, age-specific skeletal responses to the infection. However, in the case of rib lesions this tendency is not as clear as in the case of other atypical changes: the active form was observed in young (juvenile and young adults) individuals, but the remodelled, probably healed form was found in similar numbers, both in young adult and mature skeletons.

The activity of the tuberculous infection at the time of death was also recognizable in most of the cases. Endocranial lesions, superficial vertebral changes, as well as periosteal appositions on the ribs are suggested to be signs of active inflammation. These lesions were observed in 26 cases indicating an active tuberculous process and a possible cause of death. One of the individuals showing tuberculous spondylitis (Grave no. 84) also revealed an active form of the inflammation. The remodelled bone formations found in the other case of classical TB (Grave no. 51) and 6 cases with rib lesions are suggested to be the result of recovery process. However, a young adult female individual revealed both superficial vertebral changes and remodelled rib lesions. This phenomenon might be explained by the possibly faster recovery of periosteal apposition on the ribs in comparison with the vertebral changes or by assuming that there was no connection between the healing of these lesions. We do not have any data about the precise chronology of the healing process, therefore the use of new technologies of medical imaging (e. g. micro CT) in comparative examinations between skeletal material and recent samples may be able to solve this question.

The association of the different tuberculous lesions as well as stress indicators was recognized in a great number of the cases. This association by itself raises the probability of the diagnosis of tuberculosis. In addition, our results show that the most common combination of these alterations is a potential early-stage TB lesion accompanied by one of the stress indicators. Furthermore, the co-occurrence of potential early-stage TB lesions was also detected. These results suggest a specific pattern in the occurrence of TB related lesions and draw our attention to the importance of further examinations regarding the association of these lesions. However, the investigation of collections with known causes of death can give us reliable data in this matter.

The palaeopathological investigation of TB also gave us an insight into the life of the population of the Zombor-Repülőtér site. Our results showed that tuberculosis occurred in high frequency there, which might indicate a poor state of health in the examined population. This may have several possible reasons. As we mentioned before, the population of the Zombor-Repülőtér site probably emigrated from the Southern regions of Serbia or Montenegro, and the migration in itself probably caused stress as that population had to adapt to a new environment. In addition, as in the rest of Europe, the climate of the Carpathian basin was becoming extremely cold in the 16th-17th centuries (called "small ice-age") and that climate meant adverse conditions for agriculture (Rácz 2001), therefore famine was frequent during that period. The political and military crisis due to the Turkish occupation could also have contributed to the frequent starvation of the people living in that region. All these conditions had negative effects on this population, and could have resulted in their decreased resistance against diseases.

Acknowledgements

The authors thank the Municipal Museum of Sombor (Gradski Muzej Sombor) and especially Dragan Radojević for the opportunity enabling them the thorough study of the skeletal collection of the Zombor-Repülőtér site. This research was supported by the Hungarian Scientific Research Fund (OTKA grant no. 78555).

References

Aufderheide AC, Rodríguez-Martin C (1998) The Cambridge Encyclopedia of Human Paleopathology. Cambridge University Press, Cambridge.

Baker BJ (1999) Early manifestations of tuberculosis in the skeleton. In Pálfi

Gy, Dutour O, Deák J, Hutás I, eds., Tuberculosis: Past and present. Golden Book Publisher and Tuberculosis Foundation, Budapest-Szeged, 299-307.

Bartucz L (1960) Die anthropologischen Merkmale der Bevölkerung aus der Umgebung von Zombor (Sombor) im XV-XVII. Jahrhundert. Acta Univ Sci Bud de Lor Eötvös nom Seb Biol 3:23-48.

Bloom BR (1994): Tuberculosis: pathogenesis, protection and control. American Society for Microbiology, Washington.

Boros-Major A, Bona A, Lovasz G, Molnar E, Marcsik A, Palfi Gy, Mark L (2011) New perspectives in biomolecular paleopathology of ancient tuberculosis: A proteomic approach. J Archaeol Sci 38:197-201.

Datta M, Swaminathan S (2001) Global aspects of tuberculosis in children. Paed Resp Rev 2:91-96.

Donoghue HD (2009) Human tuberculosis – an ancient disease, as elucidated by ancient microbial biomolecules. Microbes and Infection 11:1156-1162.

Fletcher HA, Donoghue HD, Holton J, Pap I, Spigelman M (2003) Widespread occurrence of Mycobacterium tuberculosis DNA from 18th–19th century Hungarians. Am J Phys Anthropol 120:144-152.

Haas CJ, Zink A, Molnár E, Szeimies U, Reischl U, Marcsik A, Ardagna Y, Dutour O, Pálfi Gy, Nerlich AG (2000) Molecular evidence for different stages of tuberculosis in Hungarian skeletal samples. Am J Phys Anthropol 113:293-304.

Haas CJ, Zink A, Molnár E, Marcsik A, Dutour O, Pálfi Gy (1999) Molecular evidence for tuberculosis in Hungarian skeletal samples. In Pálfi Gy, Dutour O, Deák J, Hutás I, eds., Tuberculosis: Past and present. Golden Book Publisher and Tuberculosis Foundation, Budapest-Szeged, 383-391.

Hershkovitz I, Donoghue HD, Minnikin DE, Besra GS, Lee OY-C, Gernaey AM, Galili E, Eshed V, Greenblatt CL, Lemma E, Bar-Gal GK, Spigelman M. (2008) Detection and Molecular Characterization of 9000-Year-Old Mycobacterium tuberculosis from a Neolithic Settlement in the Eastern Mediterranean. PLoS ONE 3(10): e3426. doi:10.1371/journal.pone.0003426

Hershkovitz I, Greenwald CM, Latimer B, Jellema LM, Wish-Baratz S, Eshed V, Dutour O, Rothschild BM (2002) Serpens Endocrania Symmetrica (SES): A new term and a possible clue for identifying intrathoracic disease in skeletal populations. Am J Phys Anthropol 118:201-216.

Kelley MA, Micozzi MS (1984) Rib lesions in chronic pulmonary tuberculosis. Am J Phys Anthropol 65:381-386.

Korek J (1994) A Zombor-bükkszállási 17. századi temető sírleletei. MFMÉ Szeged, 1989/90:181-202.

Lewis ME (2004) Endocranial lesions in non-adult skeletons: understanding their aetiology. Int J Osteoarch 14:82-97.

Lovász G, Molnár E, Marcsik A, Pálfi Gy (2008) Palaeopathology of a late medieval series from Serbia. Programme & Abstracts. 17th European Meeting of the Paleopathology Association, Copenhagen, 59.

Maczel M (2003) On the traces of tuberculosis. Diagnostic criteria of tuberculous affection of the human skeleton and their application in Hungarian and French anthropological series. Ph.D. thesis, University of La Méditerranée, Marseille, University of Szeged, Department of Anthropology, Szeged.

Madkour MM (2004) Tuberculosis. Springer, Berlin.

Marcsik A, Molnár E, Ősz B (2007) Specifikus fertőzések csontelváltozásai történeti népességek körében. JATE Press, Szeged.

Marcsik A, Molnár E, Szathmáry L (2006) The antiquity of tuberculosis in Hungary: the skeletal evidence. Mem Inst Oswaldo Cruz 101:67-71.

Matos V, Santos AL (2006) On the trail of pulmonary tuberculosis based on rib lesions: results from the Human Identified Skeletal Collection from the Museu Bocage (Lisbon, Portugal). Am J Phys Anthropol 130:190-200.

Molnár E, Maczel M, Marcsik A, Pálfi Gy, Nerlich GA, Zink A (2005) A csont-ízületi tuberkulózis molekuláris biológiai vizsgálata egy középkori temető embertani anyagában. Folia Anthropol 3:41-51.

Molnár E, Pálfi Gy (1994) Probable cases of skeletal infections in the 17th century anthropological series from Bácsalmás (Hungary). Acta Biol Szeged 40:117-132.

Nerlich AG, Lösch S (2009) Paleopathology of Human Tuberculosis and the Potential Role of Climate. Interdisciplinary Perspectives on Infectious Diseases 2009, Article ID 437187, 9 pages, 2009. doi:10.1155/2009/437187

Ortner DJ (2003) Identification of pathological conditions in human skeletal remains. Academic Press, San Diego.

Pálfi Gy (2002). Paleoepidemiological reconstruction of tuberculosis, with particular attention to Europe. In Bennike P, Susanne C, eds., Biennial Books of EAA 2:193-210.

Pálfi Gy, Ardagna Y (2002) Gerincbetegségek és tuberkulózis a török hódoltság korából. A Bácsalmás-Óalmás (Bácsalmás-Homokbánya) 16-17. századi antropológiai leletegyüttes fontosabb paleopatológiai adatai. In Gerelyes I, Kovács Gy, eds., A hódoltság régészeti kutatása. Opusula Hungarica, 3:237-244.

Pálfi Gy, Ardagna Y, Molnár E, Dutour O, Panuel M, Haas CJ, Zink A, Nerlich AG (1999) Coexistence of tuberculosis and ankylosing spondylitis in a 7-8th century specimen evidenced by molecular biology. In Pálfi Gy, Dutour O, Deák J, Hutás I, eds., Tuberculosis: Past and present. Golden Book Publisher and Tuberculosis Foundation, Budapest-Szeged, 401-410.

Pálfi Gy, Molnár E (2009) The Paleopathology of specific infectious diseases from Southeastern Hungary: a brief overview. Acta Biol Szeged 53:111-116.

Rácz L (2001) Magyarország éghajlattörténete az újkor idején. Juhász Gyula Felsőoktatási Kiadó, Szeged.

Raff J, Cook DC, Kaestle F (2006) Tuberculosis in the New World: a study of ribs from the Schild Mississippian population, West-Central Illinois. Mem Inst Oswaldo Cruz 101:25-27.

Redman JE, Shaw MJ, Mallet AI, Santos AL, Roberts CA, Gernaey AM, Minnikin DE (2009) Mycocerosic acid biomarkers for the diagnosis of tuberculosis in the Coimbra Skeletal Collection. Tuberculosis 89:267-277.

Resnick D, Niwayama G (1988) Diagnosis of bone and joint disorders. Saunders, Philadelphia.

Roberts Ch, Lucy D, Manchester K (1994) Inflammatory lesions of ribs: an analysis of the Terry Collection. Am J Phys Anthropol 95:169-182.

Santos AL, Roberts Ch (2006) Anatomy of a serial killer: differential diagnosis of tuberculosis based on rib lesions of adult individuals from the Coimbra Identified Skeletal Collection, Portugal. Am J Phys Anthropol 130:38-49.

Santos AL, Roberts Ch (2001) A picture of tuberculosis in young Portuguese people in the early 20th century: a multidisciplinary study of the skeletal and historical evidence. Am J Phys Anthropol 115:38-49.

Schultz M (2001) Paleohistology of bone: A new approach to study of ancient diseases. Yearbook of Phys Anthrop 44:106-147.

Schultz M (1999) The role of tuberculosis in infancy and childhood in prehistoric and historic populations. In Pálfi Gy, Dutour O, Deák J, Hutás I, eds., Tuberculosis: Past and present. Golden Book Publisher and Tuberculosis Foundation, Budapest-Szeged, pp. 501-507.

Spigelman M, Lemma E (1993) The use of the polymerase chain reaction (PCR) to detect Mycobacterium tuberculosis in ancient skeletons. Int J Osteoarch 3:137-143.

Stuart-Macadam PL (1989) Nutritional deficiency diseases. In Isçan MY, Kennedy KAR, eds., Reconstruction of life from the skeleton. Liss, New York, pp. 201-222.

Zink AR, Molnár E, Motamedi N. Pálfi Gy, Marcsik A, Nerlich AG (2007) Molecular history of tuberculosis from ancient mummies and skeletons. Int J Osteoarch 17:380-391.

Volume 54(2):93-98, 2010
Acta Biologica Szegediensis
http://www.sci.u-szeged.hu/ABS

ARTICLE

Evidence of surgical trephinations in infants from the 7th-9th centuries AD burial site of Kiskundorozsma-Kettőshatár

Zsolt Bereczki*, Erika Molnár, Antónia Marcsik, György Pálfi

Department of Biological Anthropology, Faculty of Sciences and Informatics, University of Szeged, Szeged, Hungary

ABSTRACT The authors found 3 infant skulls with cranial lesions in the 7th-9th centuries AD (Avar Age) burial site of Szeged-Kiskundorozsma-Kettőshatár. The remains were examined with standard macromorphological methods of bioarcheology. The most presumable diagnosis of the lesions is surgical trephination. Infants and Avar Age findings were formerly underrepresented in the otherwise abundant and internationally significant amount of paleopathological cases with cranial interventions found in Hungary. Thus, these findings may alter the assumption we formerly had of the cranial surgery of the Avars. During the search for trephined lesions, signs of severe inflammation of the meninges were found in one case and slight hydrocephalus occurred in another implying possible skeletal tuberculosis that put forward interesting questions in connection with healing practices and believes of this era. Together with other Avar Age findings formerly known from the nearby areas these results refine our knowledge of Avar Age medical practices and also the general picture of the medical history of the Carpathian Basin.
Acta Biol Szeged 54(2):93-98 (2010)

KEY WORDS

surgical trephination
infants
Avar Age
tuberculosis
paleopathology

Surgical trephination is a traditional curing and/or ritual custom of long history, during of which all three layers of the cranial vault are intentionally removed in a certain area of the human skull (Aufderheide and Rodríguez-Martín 1998; Ortner 2003). First evidences had been found in Mesolithic layers (Lillie 1998; Crubézy et al. 2001), but it was cultivated in all historical periods and it is still being used in some areas of the world. Though the signs of such lesions are scarce in the bioarcheological material, a lot of trephined skulls had been found in the today area of Hungary (Bartucz 1966; Nemeskéri et al. 1965). Comprehensive data collection in the available archeological (Grynaeus 1996; Tomka 2000) and biological data (Józsa and Fóthi 2007a) have only been performed in the recent past, but our picture of this custom is far from complete. The majority of these cases are connected to adult males among pagan and Christian Hungarians while children and some ethnic groups (and historical periods) like the Avars were underrepresented in these samples. The authors found 3 infant skulls with cranial lesions in the Avar Age (7th-9th centuries AD) burial site of Szeged-Kiskundorozsma-Kettőshatár, where the most presumable diagnosis is surgical trephination. The analysis of these lesions is extremely important and not only on a national level. The international scientific audience knows very little about the diverse spectrum of cranial interventions found in Hungary since only very little information has been made accessible for non-Hungarian scholars so far (Pálfi 1997; Aufderheide and Rodríguez-Martín 1998; Grynaeus 1999; Arnott et al. 2003; Bereczki and Marcsik 2005; Szathmáry and Marcsik 2006; Józsa and Fóthi 2007b).

Accepted Dec 14, 2010
*Corresponding author. E-mail: bereczki.zsolt@bio.u-szeged.hu

Materials and Methods

The Avar Age cemeteries of Szeged-Kiskundorozsma-Kettőshatár were excavated in 2004 by archeologists Patrícia Mészáros, Tibor Paluch and Csaba Szalontai (Mészáros et al. 2006) in a series of rescue excavations performed along the construction site of highway M5, northwest of the city of Szeged at the southern border of Hungary. The site is dated to the 7th-9th centuries AD. In that time, the flat area was divided by several smaller watercourses, temporary and permanent lakes, and was regularly affected by the flood of the river Tisza. The site is located on top of a slight, long elevation. The cemetery of Kiskundorozsma-Kettőshatár I consisting of 298 burials is dated from the end of the 7th to the beginning of the 9th century AD. Based on the chronology and the archeological observations it is very likely that the graveyard was used by the same population that used the nearby Kiskundorozsma-Daruhalom II cemetery in the former period. The graveyard is not completely excavated as some parts of it are situated further away from the path of highway M5. Kiskundorozsma-Kettőshatár II lies 60 m away from the first cemetery, consists of 43 graves and was used at the end of the 8th century AD. Though this cemetery is separated from Kiskundorozsma-Kettőshatár I, it may have been used by the same population. The site is fully excavated, most of the graves were robbed presumably in a single occasion by contemporary robbers, hardly any skeletons were recovered

Figure 1. obj. 263, 8-11 years old child, skull.

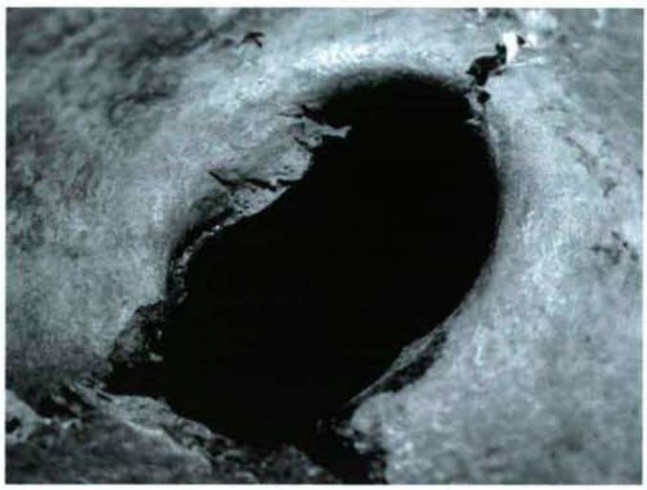

Figure 2. obj. 263, 8-11 years old child, surgical trephination.

in anatomical position. The remaining grave goods refer to an upper class burial site. The remains of altogether 360 individuals were recovered in the two cemeteries (121 subadults, 239 adults (130 males, 109 females)) (Marcsik et al. 2010). Comprehensive bioarcheological investigation of the remains is in progress at the Department of Biological Anthropology, University of Szeged. Preliminary results of these analyses have already been published (Molnar et al. 2006; Marcsik et al. 2009; Marcsik et al. 2010). During the paleopathological data collection in the Kiskundorozsma-Kettőshatár I series we came across 3 infant skulls with holes in the cranial vault that seemed to have been created *intra vitam*. Age at death was determined using standard macromorphological methods (Schour and Massler 1941; Schinz et al. 1952; Stloukal and Hanáková 1978; Knussmann 1988; Ubelaker 1989). The

Figure 3. obj. 263, 8-11 years old child, patches of trabecular new bone in the endocranial surface of the frontal bone.

skeletal material is housed in the Department of Biological Anthropology, University of Szeged, Hungary.

Results

Obj. 263 (A. P. 562), 8-11 years old child

The *post mortem* moderately deformed skull (Fig. 1) and the mandible are well-preserved, the postcranial elements are mostly missing. The elongated lesion (Fig. 2) is located in the left side of the coronal suture, 35 mm from the sphenofrontal suture. The hole is kidney-shaped, 26 mm at the biggest and 11 mm at the smallest diameter. The edges are mostly vertical and slightly rounded showing considerable healing. A secondary cortical bone layer is covering the exposed spongious part. The mid section of the anterior rim is flat inclining towards the center of the lesion with irregular edges. At the antero-inferior part some remnants of the exposed spongious bone structures are still visible. The inferior part is *post mortem* damaged.

The endocranial surface is strongly affected by different forms of new bone formation. The frontal bone is the most severely affected. The internal cortex of the upper half of the squama is thickened, the surface is irregular. Approx. 2 cm wide patches of trabecular new bone layer were formed in the middle of the squama and in the proximity of bregma (Fig. 3). The patches include small blood vessel impressions too. Similar but less severe lesions can be seen near the right side of the coronal suture both on the frontal and the right parietal bone. Near the bregma and the elongated aperture a few small tuberculi also appear in the size of 2-4 mm. The most of the parietals' internal surface is covered by fine groups of thin vessel impressions.

Some of the teeth show moderate signs of linear enamel hypoplasia (LEH) referring to a chronic stress condition of unknown origin possibly between the 3rd and 5th years of life.

Figure 4. Obj. 491, 2-3 years old child, skull.

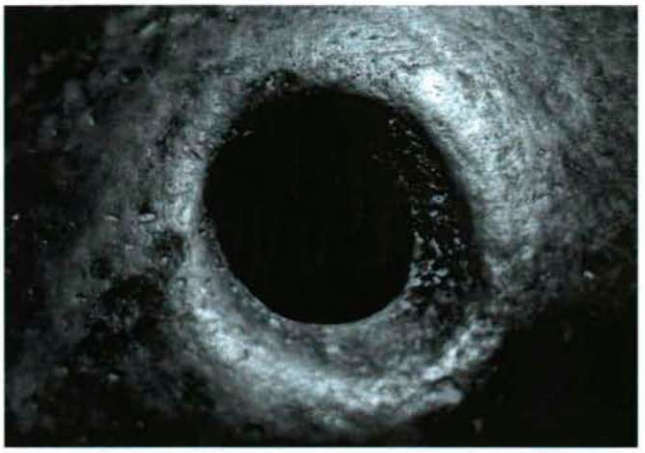

Figure 5. Obj. 491, 2-3 years old child, surgical trephination.

Obj. 491 (A. P. 654), 2-3 years old child

The skull (Fig. 4) and the mandible is well-preserved, a lot of postcranial elements are missing. A regular round hole can be seen in the anterior part of the right parietal (Fig. 5) 17 mm from the coronal suture and 35 mm from the sagittal suture. The external diameter is 11x9 mm, the internal is 7x6 mm, the aperture is getting wider towards the outer surface. The lateral edge of the lesion is almost vertical, the medial edge is somewhat less steep. Each possible section of the rim shows plain edges, with only moderate remodelling of the cortical layer, thus, the exposed spongious layer of the bone is still visible.

The shape of the head is very unusual, extremely oblong and slightly cubic. Other pathological signs are not present.

Obj. 537 (A. P. 694), 11-13 years old child

The remains of the skull (Fig. 6) are *post mortem* severely deformed and moderately preserved. Postcranial elements are present but the thorax and the distal parts of the upper extremities are mostly missing. Despite the young age, the bones show masculine characteristics, the remains may be those of a boy.

Almost in the midline of the frontal squama, slightly towards the right side, 30 mm above the right orbit a 22x16 mm ovoid hole is found (Fig. 7). The otherwise vertical edges and the surroundings of the lesion on both cortical surfaces are heavily eroded, no sign of remodelling is visible. The aperture widens towards the internal surface on the superior part.

Clear signs of a healed depressed fracture can be seen in the upper medial corner of the left orbit (Fig. 8) on the frontal sinus. The depression is 14x13 mm in size and slightly almond shaped with an 8 mm irregular, partly healed-partly damaged aperture in the middle. Most possibly connected to this trauma, a rounded bony flake protrudes from the upper medial wall of the left orbit that may have covered a blood vessel.

Figure 6. Obj. 537, 11-13 years old child, skull.

Slight bilateral porotic cribra orbitalia and LEH is also present in the skull referring to some unknown chronic stress condition in earlier life. LEH dates back to approx. the 3rd-5th years of life.

Figure 7. Obj. 537, 11-13 years old child, surgical trephination.

Figure 8. Obj. 537, 11-13 years old child, healed depressed fracture at the left orbit.

Discussion

Surgical trephinations of different state of preservation and healing can be mistaken for different forms of trauma, tumorous, infectious, inflammatory, etc. conditions, developmental defects like meningioceles and even *post mortem* alterations (Aufderheide and Rodríguez-Martín 1998; Ortner 2003; Bennike 2003). In the case of obj. 263, the clearly defined edges are mostly covered by secondary cortical bone that implies a longer period of survival of the intervention and healing. Developmental protrusion of soft tissue of any kind is not likely when the edges of the lesion are so different from each other as in this case. Meningioceles usually appear in former sites of fontanelles (Bennike 2003) and along the midline sutures (Khan et al. 2010) none of which applies for the current case. In addition, despite the moderate healing the posterior rim still shows the original plains of the cut. This hole is most probably a surgical trephination, the etiology of which becomes clearer with the interpretation of other lesions of the skull.

The endocranial lesions refer to a severe, active pathological condition that may have played a role in the death of the infant. The paleopathological occurrence of blood vessel impressions, irregular thickening and trabecular, fibrous new bone layers can be indicatives of meningitis of various origin, but lately these were observed to be frequently associated with inflammatory processes induced by mycobacterial infection too (Hershkovitz et al. 2002; Pálfi 2002; Maczel 2003). The new bone structures of this skull may be results of severe meningitis as a reaction to invasion of human pathogen mycobacteria (*Mycobacterium tuberculosis*-complex) developing symptoms of CNS TB (central nervous system tuberculosis) which have currently been reported to appear also in contemporary patients (Khoo et al. 2003; Corr 2008; Di Carlo et al. 2008) based on radiological imaging results.

Surgical trephinations are usually induced by blunt trauma, after which a need occurs for artificial smoothing of the edges of the fracture site in order to facilitate faster healing and closure of the wound (Szathmáry 1982; Aufderheide and Rodríguez-Martín 1998; Ortner 2003). In most of the cases the healed lesions do not exhibit signs of the original trauma as the damaged bony units are cut out in the course of the trephination (Szathmáry 1982; Józsa and Fóthi 2007a). This may be case for obj. 263 too. However, it is also possible that the trephination and the endocranial lesions are connected. Thick, remodelled endocranial lesions and the semi-healed rims of the trephine also take several weeks to develop. The hole may have been created within the duration of the inflammatory process because of a belief that otherwise successful surgical interventions (normally applied to heal trauma) can also help health problems that are not related to trauma. This latter phenomenon was observed among contemporary tribal populations too (Ella 1874; Bartucz 1966; Szathmáry 1982). The endocranial lesions though, may derive from a posttraumatic infection too (either the primary trauma or the correction trephination), or even a non-mycobacterial infection not connected to the trauma episode.

The aperture found on the skull of obj. 491 is the most definite case of surgical trephination among the three. The plains of the circular cut are clearly visible despite the early-stage healing. On the other hand, the cause of intervention here, however, is the least obvious among our findings. According to Józsa and Fóthi (2007a) some of the weapons used

in the Middle Ages had so thin pointed parts that may have caused severe but very little traumatic lesions on skulls. These wounds do not show signs of the inducing trauma after they were treated with a correction trephination. In our case, however, the trephination itself is so small that such an inducing trauma is unlikely. The shape of the head provides the only possible clue, resembling hydrocephalus which again, can be caused by many primary illnesses from inflammations of infectious origin to metabolic deficiencies and developmental anomalies (Aufderheide and Rodríguez-Martín 1998; Ortner 2003; Corr 2008). This almost punctured surgery may have been used to treat symptoms of this disease – either by decreasing intracranial pressure that might have caused headache because of the increased volume of subarachnoid fluid, or only because of the believes mentioned in the interpretation of obj. 263.

The most classical trauma etiology occurs in the case of the lesions of obj. 537. The skull is moderately preserved, and the hole on the frontal bone does not provide enough information on its own because of the damaged surfaces of the rim and the surrounding ecto- and endocranial areas. The healed depressed fracture on the left side of the frontal sinus, however, helps to shed light on the origins of the trephination. The depressed fracture and the wound that required correction (trephination) may have originated from the same episode of trauma. There is also a probability that the trephined area underwent a posttraumatic infection as some porosity possibly related to inflammatory hypervascularisation is clearly visible in the nearby outer surface just like in the case of the surgical trephination of Hódmezővásárhely-Nagysziget grave no. 55 mature female skull (Bereczki and Marcsik 2005). Unfortunately, this porosity cannot be undoubtedly attributed to *intra vitam* processes, and other signs of a possible septic inflammation can also not be detected because of the *post mortem* changes of the area. Cribra orbitalia and LEH observed in this case are, of course, not necessarily connected to the trauma and the possible surgical intervention, as both phenomena must started developing before the lesions of the frontal bone.

All three trephinations may have been prepared with fine cutting movements with sharp-bladed tools, as in most of the cases of the 9th-11th century AD Hungarian material (Szathmáry 1982). The method of operation, however, can only be surely identified in the case of obj. 491, since healing (obj. 263) and diagenesis (obj. 537) obstructs the observation.

The description and analyses of trephined remains do not follow a commonly accepted set of aspects and uniform way of publication of the results in the Hungarian literature as Józsa and Fóthi (2007a) pointed out. We still lack the necessary amount of information to interpret the history of cranial surgery in Hungary with accuracy. Furthermore, Avar Age trephinations are rare in the records. Tomka (2000) only cites 10 trephined skulls from the Avar Age, while Józsa and Fóthi (2007a) mention 13 surgical interventions from this era among 130 trephined skulls found in the Carpathian Basin. 10 of these Avar cases are adult males and 3 adult females. According to our assumption, two of these cases are definitely *perimortem* lesions (Kiskőrös) possibly not performed for medical but purely for ritual reasons. In the south-eastern part of Hungary Józsa and Fóthi (2007a) only cite 5 Avar Age skulls with surgical trephination (Szeged-Fehértó, Szeged-Kundomb, Szőreg, Nagykamarás, Vedresháza) all of which belonged to adult males. In their total sum of 130 skulls they only found 11 cases with unidentified sex. As no differentiation is available between infants and adults with undetermined age at death within this number, we can only presume that currently there are less than 11 cases of surgical trephinations known in subadult subjects, and Avar Age infants are definitely not part of the sample.

Thus, our findings considerably increase the number of surgical trephinations from the Avar Age and they have no parallels so far within this era in the sense of age at death of the subject. In the case of obj. 491 the size of the lesion is also unique. We can only compare our data to results of the nearby Avar Age excavations in the north of Serbia. Czékus (2007) found a lesion on the skull of Stara Moravica grave no. 90 (approx. 65 yrs male, moderate healing) similar in size (9 mm) to that of obj. 491. Lovász (personal communication) found a trephined skull fragment belonging to an approx. 2.5 years old child in grave no. 51 of Bački Sokolac (moderate healing). Further Avar Age cases in the surroundings are found in the Bélmegyer-Csömöki-domb cemetery (grave no. 27, 40-50 yrs male, minor healing (Józsa 1990) and in the Maroslele 24 site (KÖH 38672) (grave no. 1, 18-22 yrs female, no healing (Paja and Pópity personal communication). The number of Avar Age surgical trephination has virtually doubled with the new findings (five to ten) in the southeastern part of the Great Hungarian Plain. Based on these data have to assume that the Avar Age population of the area was more familiar with the practice of surgical trephination than we thought it before. It is possible that all the mentioned cases belong to the heritage of a distinct local trepanning tradition.

In order to see how frequent surgically trephined remains are in the Avar material we performed a basic inventory analysis and compared the data of the Avars with that of the early Hungarians. Our department has analyzed remains of 8109 Avar Age (6th-9th century AD) individuals and among them 10 trephined skulls were found (0.12%). Conquering Hungarians (9th-10th century AD) are represented with 1430 individuals and 12 trephined skulls among them (0.84%). Árpád Age findings sum up to 3883 individuals where 11 trephined skulls can be recorded (0.28%). The early Hungarians still provide the overwhelming majority of the trephination cases in the southeastern part of the Great Hungarian Plain as it was already mentioned by other scholars (Grynaeus 1996; Tomka 2000; Józsa and Fóthi 2007a). With the new Avar findings

the advantage of the Hungarian skulls is not bigger by one order any more, especially when Avar data are compared to the Árpád Age series.

Concluding we can say that the new findings considerable increased the number of known cases with surgical trephination from the Avar Age both on the local and on the national level. Young age at death for trephined individuals is a formerly unknown phenomenon from this historical period. The possible association of TB and other health damaging conditions in these cases require further aDNA and biomarker analyses. On the whole, the remains of these three deceased children open a new window to the medical history of the Avar people.

Acknowledgement

The authors wish to express their gratitude to Gabriella Lovász (Municipal Museum of Subotica, Serbia) for information on archeological sites in Serbia and also Dániel Pópity and László Paja (Center for National Heritage, Hungarian National Museum) for the information on the Maroslele skull. This study was supported by the Hungarian National Research Fund OTKA no. 78555.

References

Arnott R, Finger S, Smith C (2003) Trepanation: History, Discovery, Theory. Swets & Zeitlinger, Lisse, The Netherlands.

Aufderheide AC, Rodríguez-Martín C (1998) The Cambridge Encyclopedia of Human Paleopathology. Cambridge University Press.

Bartucz L (1966) A praehistorikus trepanáció és orvostörténeti vonatkozású sírleletek. Palaeopathologia III, Országos Orvostörténeti Könyvtár, Budapest.

Bennike P (2003) Ancient trepanations and differential diagnoses: a re-evaluation of skeletal remains from Denmark. In Arnott R, Finger S, Smith C (2003) eds. Trepanation: History, Discovery, Theory. Swets & Zeitlinger, Lisse, The Netherlands, pp. 95-115.

Bereczki Zs, Marcsik A (2005) Trephined skulls from ancient populations in Hungary. Acta Medica Lituanica 12:65-69. http://www.ebiblioteka.lt/resursai/LMA/Acta%20medica%20Lituanica/ActM_065_069.pdf

Corr PD (2008) Imaging in CNS Tuberculosis. http://emedicine.medscape.com/article/344862-imaging

Crubézy É, Bruzek J, Guilaine J, Cunha E, Rougé D, Jelinek J (2001) The antiquity of cranial surgery in Europe and in the Mediterranean basin. Comptes Rendus de l'Académie des Sciences – Series IIA – Earth and Planetary Sciences 332:417-423.

Czékus G (2007) Az ómoravicai (Stara Moravica) avar temető csontvázmaradványainak embertani jellemzése. Oral communication – Az MBT Szegedi csoportjának ünnepi ülése Prof. Dr. Farkas L. Gyula tiszteletére 75. születésnapja alkalmából, Szeged. 2007. jún. 29.

Di Carlo P, Cabibi D, Casuccio A, Mazzola A, Romano A, Titone L (2008) Features in Tubercular Meningoencephalitis Diagnosis: 18 Childhood Cases. Am J Inf Dis 4:187-192.

Ella S (1874) Native medicine and surgery in the South Sea island. The Medical Times and Gazette.

Grynaeus T (1996) Isa, por... A honfoglalás és az Árpád-kori magyarság betegségei és gyógyításuk. Fekete Sas Kiadó, Budapest.

Grynaeus T (1999) Skull Trephination In the Carpathian Basin. Mankind Quarterly 40:131.

Hershkovitz I, Greenwald CM, Latimer B, Jellema LM, Wish-Baratz S, Eshed V, Dutour O, Rothschild BM (2002) Serpens Endocrania Symmetrica (SES): A new term and a possible clue for identifying intrathoratic disease in skeletal populations. Am J Phys Anthropol 118:201-216.

Józsa L, Fóthi E (2007a) Trepanált koponyák a Kárpát-medencében. Folia Anthropologica 6:5-18.

Józsa L, Fóthi E (2007b) Trepanált koponyák Magyarországon – 115 eset összesítése. Orvostörténeti Közlemények 198-199:15-30., http://www.ncbi.nlm.nih.gov/pubmed/18175532

Józsa V (1990) Pathologiás elváltozások egy avar kori széria (Bélmegyer-Csömöki-domb) embertani anyagában. Diploma work, József Attila University, Department of Biological Anthropology, Szeged, supervisor: Antónia Marcsik.

Khan AN, Turnbull I, MacDonald S, Sabih D (2010) Encephalocele imaging. http://emedicine.medscape.com/article/403308-overview

Khoo JLS, Lau KY, Cheung CM, Tsoi TH (2003) Central Nervous System Tuberculosis. J HK Coll Radiol 6:217-228.

Knussmann R (1988) Anthropologie; Gustav Fischer, Stuttgart-New York.

Lillie MC (1998) Cranial surgery dates back to Mesolithic. Nature 391:854.

Maczel M (2003) On the traces of tuberculosis – Diagnostic criteria of tuberculous affection of the human skeleton and their application in Hungarian and French anthropological series. PhD dissertation, UMR 6578 CNRS-University of La Méditerranée, Marseilles – Department of Biological Anthropology, University of Szeged, Szeged, supervisors: Olivier Dutour, Antónia Marcsik.

Marcsik A, Molnár E, Ősz B, Donoghue HD, Zink A, Pálfi Gy (2009) Adatok a lepra, tuberculosis és syphilis magyarországi paleopatológiájához. Folia Anthropologica 8:5-34.

Marcsik A, Pálfi Gy, Márk L, Molnár E (2010) Cases of leproy and tuberculosis in an 8th-9th century cemetery from Hungary. 18th European Meeting of the Paleopathology Association, Program and Abstracts, 23th-26th Aug 2010, 156.

Mészáros P, Paluch T, Szalontai Cs (2006) Avar kori temetők Kiskundorzsma határában. Tatabányai Múzeum Tudományos Füzetek 8:97-109.

Molnár E, Marcsik A, Bereczki Zs, Donoghue HD (2006) Pathological cases from the 7th century in Hungary. 16th European Meeting of Paleopathology Association, Program-Abstracts, 28th Aug-1st Sept 2006, Santorini, Greece.

Nemeskéri J, Kralovánszky A, Harsányi I (1965) Trephined skulls from the tenth century. Acta Arch Hung 17:343-367.

Ortner DJ (2003) Identification of Pathological Conditions in Human Skeletal Remains. Academic Press, San Diego.

Pálfi Gy (1997) Maladies dans l'Antiquité et au Moyen-Âge. Paléopathologie comparée des anciens Gallo-Romains et Hongrois. Bulletins et Mémoires de la Société d'anthropologie de Paris, Nouvelle Séri 9:1-205. http://www.persee.fr/web/revues/home/prescript/article/bmsap_0037-8984_1997_num_9_1_2472

Pálfi Gy (2002) Paleoepidemiological reconstruction of tuberculosis, with particular attention to Europe. In Bennike P, Susanne C eds., Biennial Books EAA 2:193-210.

Schinz HR, Baensch WE, Friedl E, Uehlinger, E (1952) Ossifikationstablelle. In Schinz [et al.] eds., Lehrbuch der Röntgendiagnostik, 5. Auflage Stuttgart, Thieme.

Schour J, Massler M (1941) The development of the human dentition. J Am Dent Assoc 28:1153-1160.

Stloukal, M, Hanáková, H (1978) Die Länge der Langsknochen altslawischer Bewölkerungen unter besonderer Berücksichtigung von Wachstumsfragen. Homo 29:53-69.

Szathmáry L (1982) A bihardancsházi trepanált koponya. BMÉ 3:21-41.

Szathmáry L, Marcsik A (2006) Symbolic trephinations and population structure. Mem. Inst. Oswaldo Cruz 101, suppl.2:129-132. http://memorias.ioc.fiocruz.br/p17.pdf, http://www.ncbi.nlm.nih.gov/pubmed/17308819

Tomka P (2000) Régészeti kommentár a Lébény-Kaszás 10-11. századi temető 44. sírjának trepanált koponyaleletéhez. Arrabona 38:63-89.

Ubelaker, DH (1989) Human skeletal remains: excavation, analysis, interpretation. Taraxacum, Washington, 3rd edition.

Volume 54(2):99-101, 2010
Acta Biologica Szegediensis
http://www.sci.u-szeged.hu/ABS

ARTICLE

Studies on established *Acorus calamus* (L.) populations

Gábor Feigl[1]*, Réka Szőllősi[1], Erzsébet Mihalik[2]

[1]Department of Plant Biology, University of Szeged, Szeged, Hungary, [2]Botanic Garden of the University of Szeged, Szeged, Hungary

ABSTRACT The aim of this study was to investigate the sustainability, stress tolerance and growth parameters of an *ex situ Acorus calamus* population as well as the availability of the rhizome segments (ramets) for propagation. The main stress factors for semi aquatic plants, like *A. calamus* are the competition from dicot weeds and the severe dry conditions. We compared two experimental plots of different competition levels: low competition (moderate weeding) and high competition: without weeding. We noticed that there were differences between the competition levels only in terms of the life span of the leaves and the length of the shoots (aboveground parts). For the propagation we compared the ramets derived from the apical and lateral parts of the rhizomes as vegetative propagules. Plants derived from both types of rhizome parts showed dynamic development. We detected significantly higher leaf numbers in plants grown from lateral rhizome segments. The newly propagated plant population was kept free from weeds. However, its experimental plot was surrounded by a weedy lane. We found that the leaf number is correlated with the spatial arrangement of the individuals, namely the proximity of weeds decreased the leaf number of the plants in the periphery of the plot.
Acta Biol Szeged 54(2):99-101 (2010)

KEY WORDS

Acorus calamus
stress tolerance
vegetative parameters
survival, competition

Characteristics of *Acorus calamus*

Acorus calamus (also known as sweet flag) belonging to the family of *Araceae* is a perennial plant, living in marshlands or other aquatic habitats, with 50-100 cm or even 1.5 m-long leaves (Farkas 1999). It has a horizontal underground rhizome, which is intensively branched, with a diameter of 1-3 cm and a length of 25-50 cm. The rhizome is articulated, rich in intercellular cavities. On the top of the rhizome there are the residues of the dead leaves, which are sickle-shaped. This is an important characteristic with which to distinguish *Acorus calamus* rhizomes from other rhizomes. The roots originate from the lower surface of the rhizome, in one or two rows.

The leaves are in two rows, they are sword-shaped with a red-pigmented base. Both surfaces of the leaves are a longitudinal rib, which divides the leaves into two asymmetric sections. The mesophyll is spongy, with a special aromatic odour.

Acorus calamus is native to Central-Asia, it came to Europe in the 16th century, and nowadays it can be found on the whole Northern hemisphere. In Central Europe it propagates only asexually, with the fragmentation of the rhizomes (Farkas 1999).

Since *A. calamus* is protected in Hungary, for the successful *ex situ* conservation we have to know as much as possible about the growth parameters, the successful survival and drought and competition tolerance.

Accepted Dec 18, 2010
*Corresponding author. E-mail: feigl_gabor@lajt.hu

Materials and Methods

In the experimental area of the Botanical Garden of the University of Szeged, there was a formerly planted *ex situ* population of *Acorus calamus*. Originally it developed in monoculture, the individuals started to grow fast. Later on several competitors proliferated in the field. Although the competition level was high, there was a large calamus-density in the plot.

In order to detect the competition tolerance we separated two plots with different degrees of weed density (i.e.high and low competition levels). We counted the number of the leaves, and measured the length of the leaves and the shoots (the length of the longest leaf) using 50-50 ramets.

We selected ramets derived from the apical and lateral parts of the rhizomes (apical and lateral types) for the propagation of a novel population. The ramets were planted in the spring of 2008.

At planting we measured - the length of the rhizome of the ramets, the number of the shoots and leaves and the length of the leaves and that of the longest leaf (shoot length). We repeated the measurements of the aboveground characteristics in the autumn of 2008 and in the spring of 2009.

Statistical analyses of data were carried out using the STATISTICA 7.0 software. Since our results showed non-normal distribution, we used non-parametric ANOVA with

Table 1. Effect of the weed competition levels. Mean values of leaf number and shoot length per plant.

	Weed-competition level			
	High competition		Low competition	
	Leaf number	Shoot length (cm)	Leaf number	Shoot length (cm)
2008	-	-	2,07	35,7
2009	3,7	47,66	4,14	33,1

Table 2. Vegetative parameters of the transplanted population. Mean values of leaf number, shoot number and shoot length per plant.

	2008	2009
Shoot number	1,937	5,255
Leaf number	4,35	12,987
Shoot length (cm)	43,865	23,11

Wilcoxon's and Mann-Whitney post hoc tests. Data are given in mean ± standard deviation (SD).

Results

Effect of the weed competition

In autumn of 2008 we could not compare the vegetative characters of the two *A calamus* groups with different competition, because in the group of high competition the leaves already disappeared, indicating that the high weed competition decreases the life span of the leaves, *i.e.*, the length of the vegetation period. Individuals in the group of low weed competition had viable leaves, but numerous dead leaves were also seen.

In spring of 2009 both the leaf number and shoot length of the high competition level group were higher, than that in the low competition group. Probably the plants compensated for the shorter vegetation period with more and longer leaves (Table 1.)

Transplanted population

Vegetative parameters and survival

For planting we selected ramets with the same rhizome length. We registrated the data of the transplanted population in the autumn of 2008 and in the spring of 2009, so there were nearly one year (one vegetation period) between the two registrations.

The shoot number , leaf number and shoot length of the transplanted populations are summarized in the Table 2.

All the individuals of the transplanted population showed considerable development in one year. With the exception of the shoot length, all examined parameters were higher (Table 2.)

In 2008 all individuals survived, so we could state that the transplantation-time was ideal, and the used rhizome-fragments were suitable to survive. In spring of 2009 all ramets produced shoots except one, this means 98% survival rate. In that case we could not rule out the possibility of pest-predation.

There was a significant difference by the Mann-Whitney U-test in the leaf-number between the apical and lateral groups. (Fig. 1). The side-type rhizome, lateral rhinzome

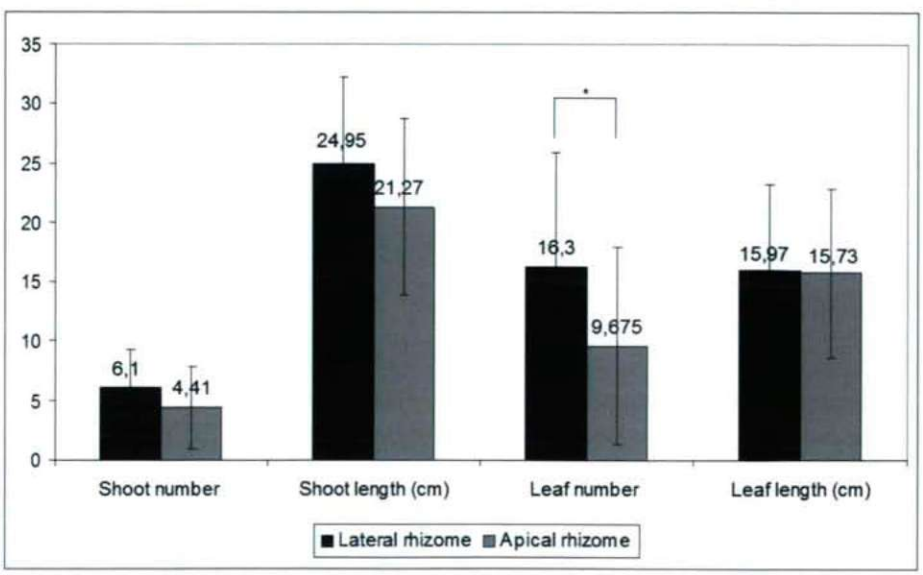

Figure 1. Comparison of the parameters of the transplanted group in spring 2009, by rhizome-type. Significant difference is marked with * at $p<0.05$.

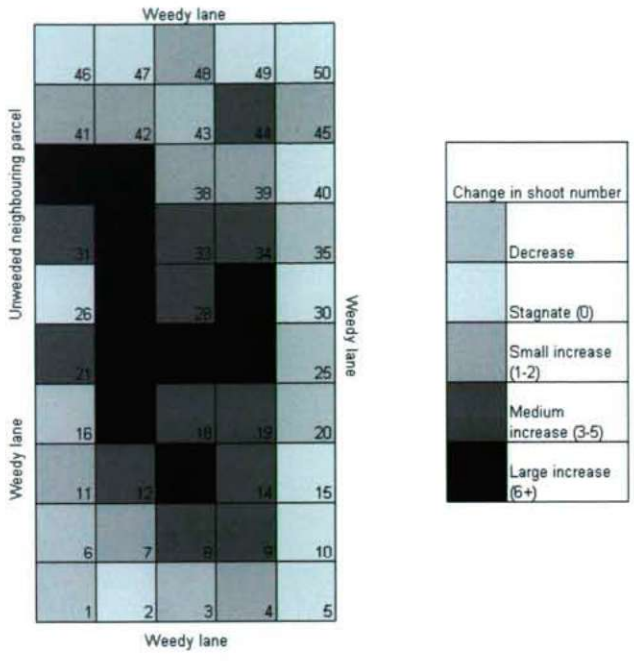

Figure 2. Shoot number changes by position in the experimental plot of competition-free population.

plants had substantially more leaves in the spring of 2009 than the end-type rhizome, apical rhinzome plants. On the other hand, there was no significant difference in the shoot- and leaf lengths and the shoot numbers between the two groups (Fig. 1).

When comparing the parameters of the individuals grown from apical and lateral rhizomes, it became clear that the lateral rhizome produced larger individuals, so for the vegetative propagation this type seems to be more suitable.

Effect of the weedy environment

On three sides of the experimental plot of the transplanted population there were weedy lanes, the plot itself was maintained without weeds. We detected that the plants near the weedy edge of the plot were smaller in the second experimental year. We compared the pattern of the shoot number between the two years. It was observed that at the edges where the individuals became closely contacted with weeds on one side, the shoot numbers decreased in 2009 as compared to the data of 2008. Individuals on the weed-free edge did not show the above-mentioned negative-edge-influence.

Inward to the centre of the plot the shoot numbers showed a rising tendency, in the middle of the non-competition area (where there were no competitors nearby) the shoot numbers increased dynamically, on one occasion we registered a nine-fold increment. Figure 2 shows the arrangement of the individuals in the plot. The numbers represent the individuals (Fig. 2).

Discussion

Our results show that *Acorus calamus* is able to tolerate the dry conditions. The weed competition has little influence on the growth characteristics of the older population, but the young plants tolerate the weeds at a lower degree, as seen on Figure 2.

For the vegetative propagation we recommend to use the side type rhizomes.

Variation of shoot numbers depends on the localisation in the experimental parcel in the case of the transplanted, competition-free group. On the edge of the parcel we noticed let-up or stagnancy in shoot numbers, while inward to the middle of the parcel, the shoot numbers showed remarkable growth.

Acknowledgements

This work was supported by the Hungarian Scientific Research Fund (T049503). Special thanks are due to G. Laskay for correcting the English of the manuscript.

References

Bagi I (2008) Zárvatermő növények adattára. Juhász Nyomda Kft., Szeged.

Farkas S (1999) Magyarország védett növényei. Mezőgazda Kiadó, Budapest.

Giovannini R, Szathmáry G (1961) Gyógynövényeink. Mezőgazdasági Kiadó, Budapest.

Haraszty Á (2004) Növényszervezettan és növényélettan. Nemzeti Tankönyvkiadó, Budapest.

Lesley Bremness (1998) Fűszer- és gyógynövények. Panemex Kft és Grafo Kft Budapest.

Mihalik E (1999) Növényanatómiai praktikum. JATEPress, Szeged.

Motley T (1994) The Ethnobotany of Sweet Flag, Acorus calamus (Araceae). Economic Botany 48(4):397-412.

Oborny B, Bartha S (1998) A közösségi ökológia frontvonalai (szerk. Fekete G.). Scientia, Budapest.

Podani J (2003) A szárazföldi növények evolúciója és rendszertana. ELTE Eötvös Kiadó, Budapest.

Soó R, Kárpáti Z (1968) Növényhatározó. Tankönyvkiadó, Budapest.

Steinbach (1996) Füvek. Mosaik Verlag GmbH, München. Ford: Horánszky (1998) Magyar Könyvklub.

Volume 54(2):103-110, 2010
Acta Biologica Szegediensis
http://www.sci.u-szeged.hu/ABS

ARTICLE

Intra-inflorescence variations in floral morphological and reproductive traits of *Iris sibirica* L.

Réka Szőllősi[1]*, Anna Medvegy[1], Anikó Németh[2], †Katalin Kálmán[1], Erzsébet Mihalik[2]

[1]Department of Plant Biology, University of Szeged, Szeged, Hungary, [2]Botanic Garden of the University of Szeged, Szeged, Hungary

ABSTRACT Within inflorescences both temporal and spatial variations can be found in aspect of either attractive traits or reproductive organs. Morphological parameters of a flower depend on several factors like intra-plant position of the flower, other extrinsic and intrinsic factors, resulting in altered intra-inflorescence flower sizes or numbers, fruit set or seed set. In our study the sexual reproductive characteristics of Siberian Iris (*Iris sibirica* L.) were investigated, with special emphasis on how the floral morphological and reproductive traits vary spatially and temporally. We found that stalks typically had 2 levels and 5 flowers, and significant differences were found among individual flowers within the inflorescences. Flower diameter, sepaloid and petaloid tepal length and length of the filament significantly decreased with blooming order but none of the parameters showed significant correlation with the number of flowers per inflorescence. Pollen viability was above 90%, and did not dicrease with flowering order, which suggests that pollen production is independent of flower position. Parameters of female reproductive success such as ovule number and seed set per fruit also declined with flowering order, which was probably due to resource limitation within stalks or plants. Values of sex allocation (P/O ratios) refer to the type of breeding system of *Iris sibirica*. **Acta Biol Szeged 54(2):103-110 (2010)**

KEY WORDS

Iris sibirica L.
cymose inflorescence
flowering order
pollen viability
female reproductive success
resource allocation

Numerous researchers have already confirmed that flowers vary in several morphological traits within inflorescences. In both racemose and cymose inflorescences, in which flowers often open sequentially, temporal and/or spatial variation can be found with respect to either attractive traits like the size of the perianth or to reproductive organs such as lenght of filaments or anthers (Brunet and Eckert 1998; Kliber and Eckert 2004; Ishii and Morinaga 2005; Zeng et al. 2008). Blooming order of racemose inflorescences generally go acropetally, from the base up to the top, and not only the flower size but also the number of pollen grains or ovules per flower, fruit set or seed set seem to decrease toward the apex (Brunet and Eckert 1998; Kudo and Molau 1999; Hiraga and Sakai 2007; Zeng et al. 2008; Zhao et al. 2008). However, plants with cymose inflorescences generally have the opposite order of anthesis, from the top downward to the base (basipetally), variation in flower size (diameter) occur to follow the same tendency like those of racemose inflorescences, *i. e.* decrease from early to late blooming flowers (Worley et al. 2000). Thus, it seems that morphological parameters of a flower depend not only on the intra-plant position of a flower, but probably on other extrinsic and intrinsic factors, as well. Intrinsic factors can be, e.g., resource allocation, competition among flowers or other architectural constraints, while pollen limitation, foliar and floral herbivory, climatic changes exert their influence externally, and these effects are often expressed as different flower sizes and numbers within an inflorescence or later as altered fruit or seed set (Wolfe 1992; Worley et al. 2000; Wesselingh and Arnold 2003; Harder and Barrett 2006; Kostrakiewicz 2006).

Although large flowers are more attractive for pollinators, higher floral display can be advantegous, too (Conner and Rush 1996; Worley et al. 2000). At the same time, if many flowers with smaller sizes are open at one time on a plant, the possibility of autogamous selfing (self-pollination) via geitonogamy increases which may reduce fitness of both flowers, individuals and the offspring, especially in the case of self-incompatible species (Eckert 2000; Worley et al. 2000; Ishii and Sakai 2001). Most of the studies conducted up to now have investigated racemose inflorescences (Kudo and Molau 1999; Mazer and Dawson 2001; Ishii and Sakai 2002; Hiraga and Sakai 2007; Zeng et al. 2008; Zhao et al. 2008), and we know relatively little about variations within cymose inflorescences. Since Siberian Iris (*Iris sibirica* L.) is protected in Hungary, and so there are not much data available about its sexual reproductive characteristics, we aimed to examine that (1) how floral morphological and reproductive traits of *Iris sibirica* L. vary among (inter-inflorescence level) and within inflorescences (intra-inflorescence level) and (2) what relationship occurs among floral traits and between these traits and the flowering sequence.

Accepted Dec 14, 2010
*Corresponding author. E-mail: szoszo@bio.u-szeged.hu

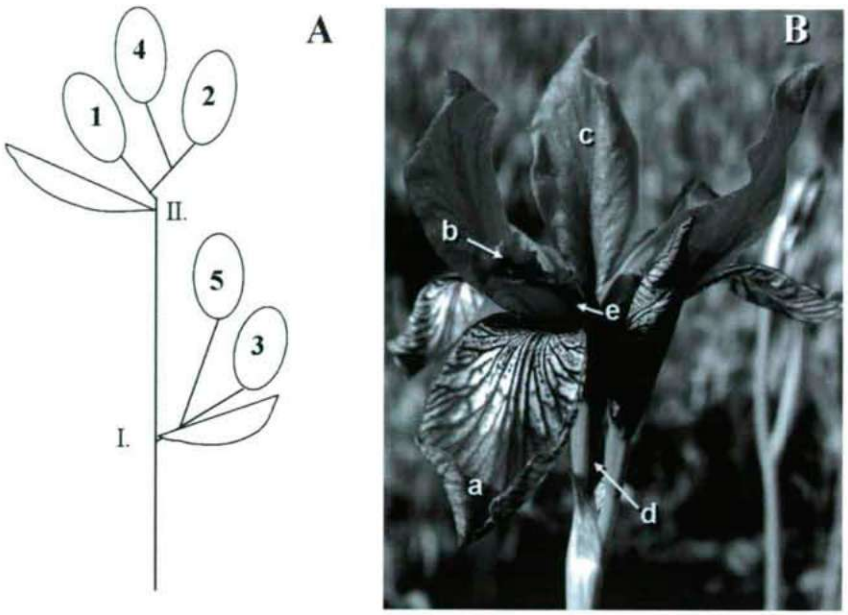

Figure 1. Schematic achitecture of a 2-level 5-flowered inflorescence (A) and a single flower (B) of *Iris sibirica* L. Roman numbers signify the levels, arabic numbers refer to flowering order within the inflorescence (A). Main parts of a flower are sepaloid tepals (a), petaloid style (b), petaloid tepals (c), ovary (d) and stamens (e).

Materials and Methods

Study species and study site

Iris sibirica L. or Siberian Iris belongs to the Iridaceae family (subfamily Iridoideae, tribe Irideae, subgenus Limniris; Goldblatt et al. 1998; Goldblatt and Manning 2008) and is native to central, eastern Europe and northern Asia. This perennial plant whose shoots grow even to 120 cm bears long narrow leaves and monochasial cymose inflorescences called rhipidium with 1-7 bluish lilac actinomorphic flowers (Goldblatt et al. 1998; Goldblatt and Manning 2008). In Hungary it is tipically found in moorlands and swamps (Molinio-Juncatea, Simon 2000) and is capable of both generative and vegetative reproduction. In its perfect flowers the tepals are arranged in 2 whorls of 3 with only 3 stamens inserted at the base of the outer tepals. The ovary is inferior positioned and is composed of 3 carpels, the short style continues in 3 petaloid style branches which are flattened and each has a rhomboid stigmatic lobe for pollen reception (Fig. 1A-B).

This stigma surface is dry with unicellular papillae (Heslop-Harrison and Shivanna 1977; Goldblatt et al. 1998) it becomes receptive within 1-2 days after flower dehiscence but only for pollen grains from other flowers. Stamens are shorter at the beginnig of blooming and anthers open distally in the buds before anthesis since the members of the *Iris* genus are protandrous. Due to temporal (protandry) and spatial separation of the anthers and the stigmatic surface (herkogamy), and having a strong self-incompatibility system, the possibility of self-pollination is excluded (Goldblatt et al. 1998).

Our investigations were carried out in an *ex situ* population of about 200 individuals in the Botanical Garden of University of Szeged, Hungary and 30 plants were randomly selected representing the population. Observations of this study group were conducted in May of 2005.

Observations on floral traits

We marked 2 flowering stalks with similar numbers and the spatial arrangement of the flowers on each individual of the 30 selected plants. We recorded the position of each flower within the inflorescence according to its blooming schedule (flowering order). Various morphological traits were measured on freshly opened flowers of one of the inflorescences, without removing them. We registered the following parameters: diameter of flowers, length and width of outer (sepaloid) tepals, length and width of inner (petaloid) tepals, length of filaments and anthers. In all, 122 flowers were involved in the measurements.

Male reproductive success variation

In order to estimate the male reproductive success, the other inflorescence was used to assess pollen yield and viability by removing only one anther from each bud and putting it into Eppendorf tubes filled with Alexander's pollen stain (Alexander 1969). Later, the anthers were chopped up within the tubes using a dissecting needle and the samples were cooked for 10 min in boiling water. Then number of aborted (green) and mature (purple red) pollen grains was determined using

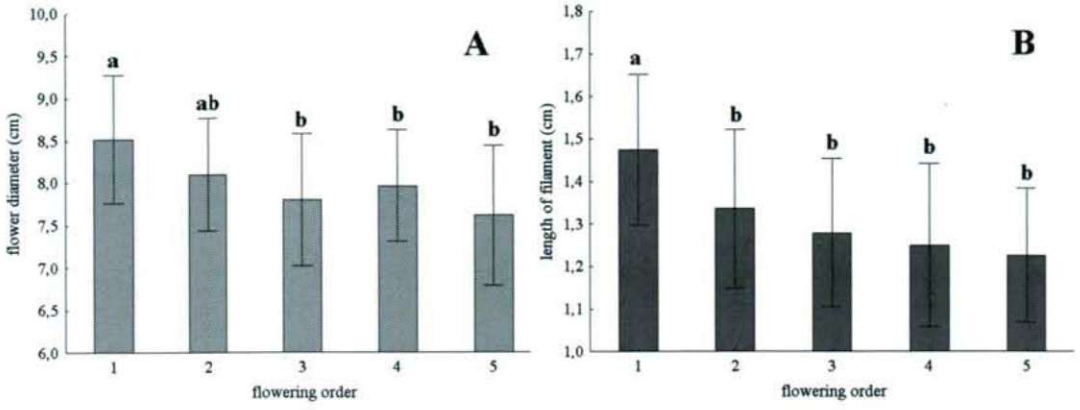

Figure 2. Flower diameter (A), filament length (B), sepaloid (C) and petaloid (D) tepal length of flowers at various positions according to flowering order within inflorescences of *Iris sibirica* L. Bars are mean values ± SD. Different letters refer to significant differences among groups at $p<0.05$.

a haemocytometer. We calculated pollen load (total pollen number) per anther and pollen viability as follows:

Total pollen number per anther= mature pollen number + aborted pollen number

Pollen viability (%) = mature pollen number / total pollen number x 100.

Female reproductive success variation

In July, all fruits of inflorescence pairs of each marked plant were collected to count the number of mature and aborted seeds. Almost 150 mature but not opened capsules were harvested. To represent the variation in female reproductive success, the number of ovules per flower and seed set per each fruit were calculated as follows:

Ovule number per flower = mature seed number + aborted seed number

Seed set per fruit = mature seed number / ovule number.

Variation in floral sex allocation

Intra-inflorescence variation of floral sex allocation was quantified by calculating pollen/ovule (P/O) ratio. We used the data (pollen load per anther and ovule number per flower) from 103 flowers. Ovule number per flower was calculated as written above.

Data analysis

Statistical analysis was carried out using STATISTICA 5.0. and 8.0 softwares. One-way ANOVA was applied to test variability of parameters, Newman-Keuls post hoc test was used to evaluate the significance of differences. To determine the relationship between flowering order and floral traits, and between fruit set and flowering order or flower position (at which level within inflorescence) a non-parametric analysis of correlation (Spearman's Rank Order Correlation) was executed. Data are given in mean values ± standard devia-

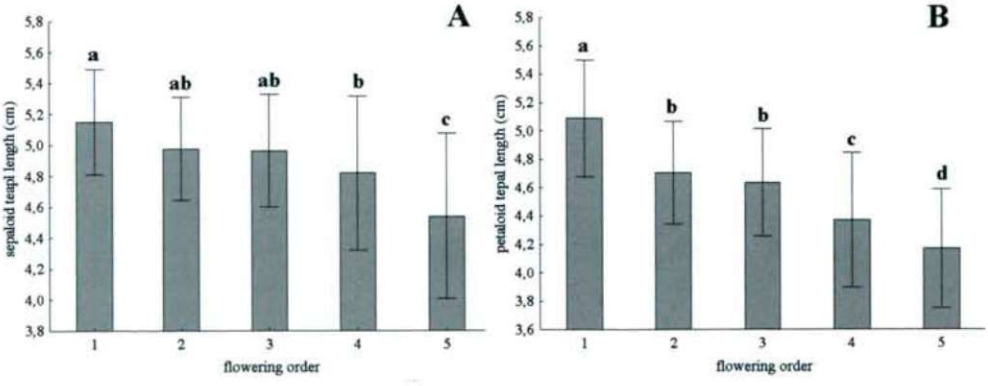

Figure 3. Sepaloid (A) and petaloid (B) tepal length of flowers at various positions according to flowering order within inflorescences of *Iris sibirica* L. Bars are mean values ± SD. Different letters refer to significant differences among groups at $p<0.05$.

Table 1. Variability of floral morphological parameters of *Iris sibirica* at inter- and intra-inflorescence levels.

Parameters	Source of variance*	F	Components of variance	Variance %
Flower diameter	inter-infl	$F_{29, 91}$= 2.206**	0.141	23
	intra-infl		0.466	77
Sepaloid tepal length	inter-infl	$F_{29, 91}$= 1.715*	0.031	15
	intra-infl		0.173	85
Sepaloid tepal width	inter-infl	$F_{29, 91}$= 3.361***	0.031	37
	intra-infl		0.054	63
Petaloid tepal length	inter-infl	$F_{29, 91}$= 1.462	0.026	10
	intra-infl		0.230	90
Petaloid tepal width	inter-infl	$F_{29, 91}$= 2.987***	0.022	33
	intra-infl		0.044	67
Length of filament	inter-infl	$F_{29, 91}$= 2.076**	0.008	21
	intra-infl		0.029	79
Length of anther	inter-infl	$F_{29, 91}$= 3.641***	0.006	40
	intra-infl		0.010	60

*inter-infl = among inflorescences, intra-infl = within inflorescences
*p<0.05; **p<0.01; ***p<0.001

Table 2. Mean ± SD, minimum and maximum values of various floral morphological parameters.

Parameters	N	Mean ± SD	Min.	Max.
Flower diameter (cm)	115	7.98 ± 0.78	5.10	10.00
Sepaloid tepal				
length (cm)	115	4.88 ± 0.46	3.10	5.70
width (cm)	115	2.32 ± 0.29	1.40	3.00
Petaloid tepal				
length (cm)	115	4.58 ± 0.50	3.20	5.80
width (cm)	115	1.59 ± 0.23	0.80	2.10
Length of filament (cm)	114	1.31 ± 0.19	0.90	1.80
Length of anther (cm)	114	1.10 ± 0.13	0.90	1.60

tion (SD). Significant differences in ANOVA analysis were established at $p<0.05$. Levels of significance were marked with * $p<0.05$, ** $p<0.01$ and *** $p<0.001$.

Results

Variations in floral morphological and reproductive traits at inter- and intra-inflorescence levels

Individuals of *Iris sibirica* produced typically 10-15 flowering shoots while two plants had extremely high number (nearly 60) of inflorescences. The inflorescences investigated bore 4-7 flowers but most of the stalks (65%) had 5 flowers (Fig. 1A). Duration of flowering of the stalks took 4-12 days, and that of 5-flowered stalks lasted for 9 days, on average.

The analysis of the results of morphological traits exhibited significant differences among stalks in flower diameter, length and width of sepaloid (outer) tepal, width of petaloid (inner) tepal, length of filament and anther (Fig. 1B; Table 1).

Table 3. Variability of floral morphological parameters of *Iris sibirica* among flower groups based on order of blooming.

Parameters	F
Flower diameter	$F_{4, 109}$= 4.863**
Sepaloid tepal length	$F_{4, 109}$= 6.032***
Sepaloid tepal width	$F_{4, 109}$= 1.725
Petaloid tepal length	$F_{4, 109}$= 15.543***
Petaloid tepal width	$F_{4, 109}$= 1.568
Length of filament	$F_{4, 109}$= 6.511***
Length of anther	$F_{4, 109}$= 2.878*

*p<0.05; **p<0.01; ***p<0.001

At the same time, 80-90% of total variance occured at intra-inflorescence level in flower diamater, sepaloid and petaloid tepal length, length of filament and anther, namely the inflorescences were more similar to each other than the flowers within the stalks. Therefore, we made groups according to flowering order. Since there was nothing but a few stalks that possessed 6 or 7 flowers, we took into account only 5-flowered inflorescences.

We took into account the data of almost 115 flowers, mean ± SD, minimum and maximum values are shown in Table 2.

After further analysis of variance significant differences were found among flowers within the stalks but only in flower diameter, sepaloid and petaloid tepal length and filament length (Table 3).

Multiple comparison of flower groups exhibited significant differences (Fig. 2. A-D). The diameter of the flowers that opened first was nealy 8 cm on average (Table 2), while the 3rd, 4th and 5th flowers were significantly smaller (Fig. 2A). Analysis of correlation also confirmed that flower diameter decreases with blooming order ($r= -0.30$, $p<0.001$; Table 4). Moreover, significantly positive correlation was found between flower diameter and the lengths of both tepals or filament length. Neither the flower diameter nor any other parameters showed significant correlation with flower number per inflorescence (Table 4). Length of filament similarly attenuated within stalks from early to late blooming flowers ($r= -0.39$, $p<0.001$; Table 4), first flowers had remarkably longer filaments than those opening later (Fig. 2B).

Both types of tepals that are considered to be the most attractive parts of the flowers, decreased in size by blooming schedule supported by the results of analysis of correlation (Table 4). Generally, second and third flowers were similar in size but there were significant differences, e.g., between the 1st and the 5th flowers (Figs. 3A and 3B.)

Male reproductive success variation

In order to determine the male reproductive success, pollen

Table 4. Relationships among various floral morphological parameters, flowering order and flower number per inflorescence. Data shown are results of Spearman's Rank Correlation, level of significance are *p<0.05; **p<0.01; ***p<0.001.

Parameters	Flower diameter	Sepaloid tepal length	Sepaloid tepal width	Petaloid tepal length	Petaloid tepal width	Length of filament	Length of anther
Flower diameter		0.56***	0.14	0.52***	0.20*	0.35***	0.16
Sepaloid tepal length			-0.02	0.53***	0.26**	0.37***	0.21*
Sepaloid tepal width				-0.04	0.32***	-0.17	-0.10
Petaloid tepal length					0.36***	0.52***	0.36***
Petaloid tepal width						0.02	0.25**
Length of filament							0.37***
Flowering order	-0.30***	-0.38***	0.18	-0.63***	-0.28**	-0.39***	-0.27**
Flower number per stalk	-0.01	0.06	-0.06	-0.09	-0.16	0.02	0.16

yield and viability was assessed by collecting anthers of 141 flowers in all, namely 25-30 flowers at each position within the stalks. We found high variability in the case of total pollen load per anther (coefficient of variance, CV= 35-40%) but there was no variation among the inflorescences ($F_{(29, 111)}$= 1.519; p= 0.063) or among the flowers within the stalks ($F_{(3, 136)}$= 0.211; p= 0.932; Fig. 4). Total pollen load per anther was 17,262 ± 6,005, and that of all flowers at various flowering positions were above 16,000, on average.

Pollen viability showed low variability (CV= 9-12%), pollen grains showed very high rate of longevity (91±9%), which did not descrease with flowering order (Fig. 5). These results suggest that polllen yield and pollen viability is not influenced by the position of the flowers in the blooming schedule, and that probably there was no pollen discount during anthesis.

Female reproductive success variation

The inflorescences observed produced generally 3±1 capsules; 60% of the 1st flowers developed to fruits, while 65% and 70% of the 2nd and 3rd flowers of the investigated stalks set fruit, respectively. Fruit to flower ratios (fruit set) of the 4th and 5th flowers were quite low with 40%. To evaluate female reproductive success nearly 150 capsules were collected and the number of mature and aborted seeds was registered, then ovule number and seed set per fruit were calculated. Remarkable differences were seen among flowers by blooming order with respect to the ovule number ($F_{(4, 143)}$= 6.431; p< 0.001). Flowers that opened first had 98 ± 27 ovules, that of the 2nd and the 3rd flowers had nearly 90, while late-opening (the 4th and the 5th) flowers had significantly lower values, namely 82 ± 19 and 70 ± 15, respectively (Fig. 6).

Capsules collected comprised of 55 ± 18 mature seeds, and mature seed/ovule ratio (seed set) was 60 ± 13%, on average. In case of both seed number per fruit ($F_{(4, 142)}$= 7.267; p< 0.001) and seed set ($F_{(4, 142)}$= 5.456; p< 0.001) we found significant differences among flower groups. Fruits developed from the 5th flowers had significantly fewer mature seeds than those from flowers that opened earlier (Fig. 7A) and the tendency was similar in seed set (Fig. 7B).

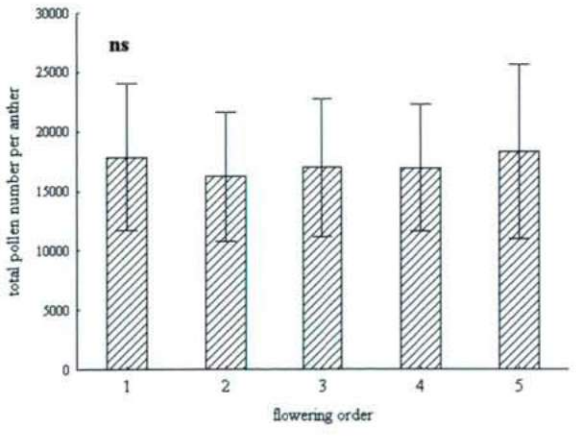

Figure 4. Total pollen number per anther at various positions within inflorescences of *Iris sibirica* L. Bars are mean values ± SD, ns= not significant differences among groups.

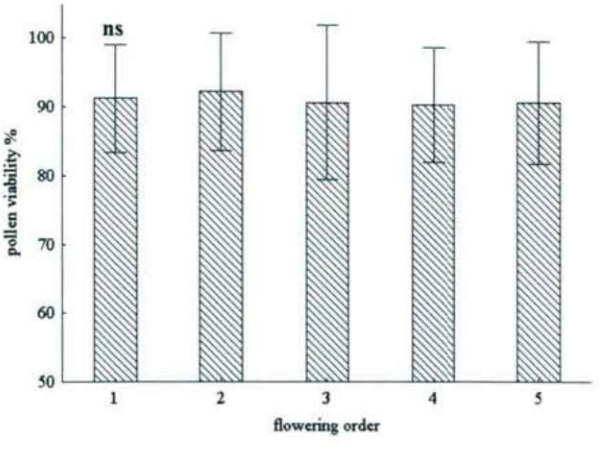

Figure 5. Pollen viability at various positions within inflorescences of *Iris sibirica* L. Bars are mean values ± SD, ns= not significant differences among groups.

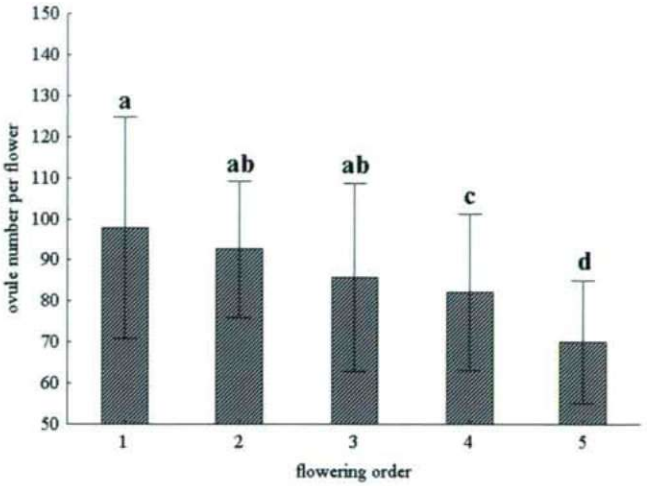

Figure 6. Ovule number per flower (mean ± SD) in flowering sequence within inflorescences of *Iris sibirica* L. Letters refer to significant differences among groups at $p < 0.05$.

Both mature seed number per fruit, ovule number per flower and seed set showed a significantly negative relationship with flowering order ($r = -0.36$, $r = -0.37$ and $r = -0.30$; $p<0.001$). At the same time, we found remarkably positive correlation between ovule number and seed set ($r = 0.65$, $p<0.001$).

Floral sex allocation

Mean values of floral sex allocation expressed as P/O ratio ranged from 580 to 960 on average, and exhibited significant differences only between the 2nd and 5th flowers (Fig. 8). This parameter seemed to be strongly variable (CV ranged from 28 to 72%) and slightly increased with blooming order ($r = 0.25$, $p<0.05$).

Discussion

Up to now most of the investigations have been conducted on reproductive characteristics and the success of racemose inflorescences, therefore, in this study we aimed to assess variations in floral morphological and reproductive parameters among and within the cymous inflorescences of a protected species, *Iris sibirica*. Since the results of ANOVA analysis showed higher dissimilarities among the flowers within the same inflorescence, we established flower groups in accordance with flowering order, as was done in former studies of species with racemose inflorescence (Ishii and Sakai 2002; Hiraga and Sakai 2007; Zeng et al. 2008; Zhao et al. 2008).

Variation in size of morphological and reproductive organs

Flowers within stalks differed from each other in terms of the diameter and length of both tepals and of the filament. These parameters declined in blooming order (Figs. 2A-B and 3A-B, Table 4), from early-opening to late-opening flowers like in the case of mass or height of perianth in acropetally opening racemose *Narthecium asiaticum* (Ishii and Sakai 2002), *Corydalis remota* var. *lineariloba* (Zeng et al. 2008), and *Aconitum gynandrum* (Zhao et al. 2008) or flower size in basipetally blooming cymose *Aquilegia caerulea* (Brunet and Eckert 1998) and *Narcissus dubius* (Worley et al. 2000). This decline of the attractive floral parts mentioned is probably due to resource limitation and/or competition within stalk and not to the architecture effects of the inflorescence, namely the distal flowers that opened first were significantly larger, while the flowers opening later were closer to the resources in photosynthetic leaves or rhizomes, but were much smaller (Zeng et al. 2008). Moreover, larger size might be more attractive and therefore an advantage for the first flowers when

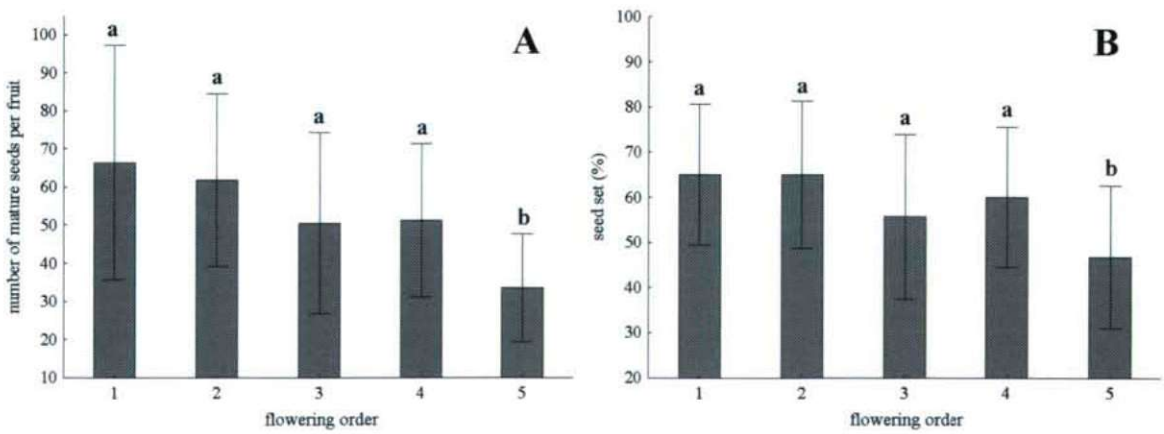

Figure 7. Mean values (±SD) of seed number per fruit (A) and seed set (B) within inflorescences of *Iris sibirica* L. in flowering order. Letters refer to significant differences among groups at $p < 0.05$.

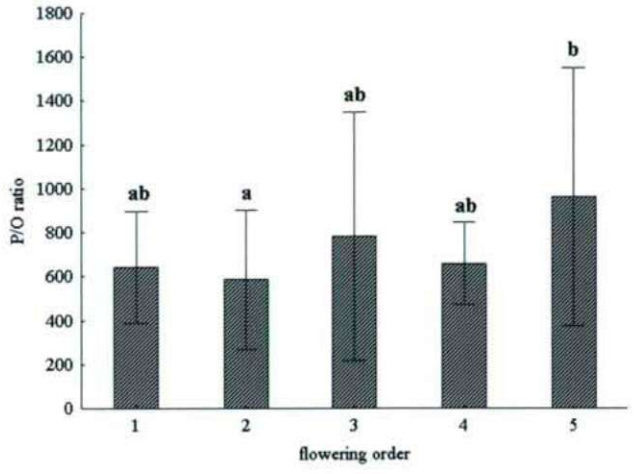

Figure 8. Mean values (±SD) of pollen/ovule ratio (P/O ratio) within inflorescences of *Iris sibirica* L. in flowering order. Different letters indicate significant differences among groups at $p< 0.05$.

a relatively few pollinators visit the plants due to low display size. Later on, when the floral display enhances and more pollinators arrive, the likelihood of successful pollination of the smaller flowers increases (Worley et al. 2000; Kennedy and Elle 2008).

Male reproductive success

Although at high variability, pollen load per anther exhibited abundance and stability during the blooming period with >90% pollen viability regardless of the position of the flower (on which level within a stalk) or of flowering order (Fig. 4 and 5), suggesting that neither pollen yield nor pollen viability might be a limiting factor in successful fruit set and seed set. Wesselingh and Arnold (2003) found that even if the amount pollen grains deposited on stigma of *Iris fulva* flowers was variable, pollen load did not affect seed production.

Variations in female reproductive success

We found a decline in fruit set according to blooming order, which was probably due to resource limitation within stalks or plants (Charlesworth and Morgan 1991; Stöcklin 1997). At the same time, Wesselingh and Arnold (2003) noticed that fruit set of *Iris fulva* with similar blooming order depended on flower position (i. e. at which level) rather than flowering order. Similarly, Buide (2004) observed a reduction in fruit set from the primary (firstly opened) flowers of cymose *Silene acutifolia* to the later flowers at secondary or tertiary positions. Nonetheless, an earlier study of Brunet (1996) showed that in the case of cymose *Aquilegia caerulea* both fruit and seed set declined significantly from the early flowers to the later ones.

Further results suggested that ovule number declined form early-opening to late-opening flowers in cymose inflorescences of *Iris sibirica* similarly to racemose inflorescences such as *Clarkia unguiculata* (Mazer and Dawson 2001), *Lobelia sessiliflora* (Hiraga and Sakai 2007) or *Corydalis remota* var. *lineariloba* (Zeng et al. 2008). Moreover, Guitián et al. (2004) found in racemose *Polygonatum odoratum* that both ovule number and pollen load per flower significantly varied with the position, *i. e.* decline of these parameters from the bottom to the top was observed. In the case of *Iris sibirica,* female function in biomass sex allocation probably depended on flower position in accordance with blooming order, while the mean number of pollen grains was constant and therefore seemed to be independent of flower position. Namely, within the stalks during anthesis plants allocated relatively fewer resources to female function in late-blooming flowers than in those opening earlier, as it had been observed in numerous protandrous but mainly racemose species, e.g. *Lobelia sessiliflora* (Hiraga and Sakai 2007), and many studies confirmed that one of the most common causes of either fruit or seed abortion might be resource limitation within plants (Charlesworth and Morgan 1991; Stöcklin 1997).

Both the mean number of seeds and seed set (mean seed/ovule ratio) also decreased with flowering sequence like in the case of protandrous and racemose *Aconitum gymnandrum* (Zhao et al. 2008), *Lobelia sessiliflora* (Hiraga and Sakai 2007) and *Corydalis ambigua* (Kudo et al. 2001), as well as those of cymose *Aquilegia canadensis* (Kliber and Eckert 2004). Three main hypotheses have been put forward to explain these intra-inflorescence variations: pollen limitation, resource limitation and architectural effect (Zeng et al. 2008). Since pollen production was abundant and pollen viability was nearly 100%, the pollen limitation hypothesis can be excluded. Nevertheless, declines of the flower size (diameter, tepals), ovule and mature seed number accross the flowering sequence suggest that female reproductive success if *Iris sibirica* L. might be limited by resources available and/or structure of the inflorescence, as it was observed in both racemous and cymose species mentioned above.

Floral sex allocation

Relatively high values of sex allocation (about 700, regardless of the flower position) refer to the type of breeding system of *Iris sibirica*, namely facultative xenogamy or obligate xenogamy, while Wang et al. (2004) reported lower P/O ratios for obligate xenogamy (betweeen 184 and 540) in various species of Zingiberaceae; therefore we may expect higher P/O ratio compared to autogamous species (Cruden 1977, Queller1984, Vasek and Weng 1988).

We found a moderate increase in P/O by flowering order due to nearly constant level of pollen yield but decreasing tendency in ovule number, which was similar to *Corydalis remota* var. *lineariloba* (Zeng et al. 2008) where flowers opened first showed lower P/O ratio compared to later ones. Mazer and Dawson (2001) also detected increasing P/O

ratios from the basal to the top flowers within racemose inflorescences of *Clarkia unguiculata*, which seemed to be significantly affected by the flower position. Moreover, in the case of the racemose *Narthecium asiaticum* the P/O ratio significantly increased from lower to upper flowers due to the approximately constant level of pollen production but a decrease in the ovule number in the order of blooming (Ishii and Sakai 2002).

At the same time, within cymose and protandrous inflorescences of *Aquilegia caerulea* the P/O ratio also increased according to flowering sequence because the ovule number per flower declined but pollen yield remained constant (Brunet 1996, revised by Zhao et al. 2008).

Conclusions

We have a relatively few data on the reproductive characteristics of Iridaceae species, especially the protected Siberian Iris. Our results show that variations in floral morphological traits and female reproductive success are probably due to intra-inflorescence rescource allocation and/or limitation. In order to find out whether other structural parameters within inflorescence (e.g. number of levels), and phenological traits such as number of opened flowers per plant affect the reproductive success of *Iris sibirica*, further investigations are needed.

Acknowledgements

This work was supported by the Hungarian Scientific Research Fund (T049503). Special thanks are due to Gábor Laskay for correcting the English of the manuscript.

References

Alexander MP (1969) Differential staining of aborted and nonaborted pollen. Biotechn Histochem 44:117-122.

Brunet J (1996) Male reproductive success and variation in fruit and seed set in *Aquilegia caerulea* (Ranunculaceae). Ecology 77:2458-2471.

Brunet J, Eckert CG (1998) Effects of floral morphology and display on outcrossing in Blue Columbine, *Aquilegia caerulea* (Ranunculaceae). Funct Ecol 12:596-606.

Buide ML (2004) Intra-inflorescence variation in floral traits and reproductive success of the hermaphrodite *Silene acutifolia*. Annals of Botany 94:441-448.

Charlesworth D, Morgan MT (1991) Allocation of resources to sex functions in flowering plants. Phil Trans R Soc Lond B 332:91-102.

Conner JK, Rush S (1996) Effects of flowers size and number on pollinator visitation to wild radish, *Raphanus raphinastrum*. Oecologia 105:509-516.

Cruden RW (1977) Pollen-ovule ratios: a conservative indicator of breeding systems in flowering plants. Evolution 31:32-46.

Eckert CG (2000) Contributions of autogamy and geitonogamy to self-fertilization in a mass-flowering, clonal plant. Ecology 81:532-542.

Goldblatt P, Manning JC, Rudall P (1998) Iridaceae. In The Families and Genera of Vascular Plants. Vol. III. Flowering Plants, Monocotyledons. Ed., Kubitzki, K. Springer-Verlag, Berlin-Heidelberg, Germany, pp. 295-325.

Goldblatt P, Manning J (2008) The Iris Family: Natural History and Classification. Published by Timber Press, pp. 49-68., 195-200.

Guitián J, Medrano M, Oti JE (2004) Variation in floral sex allocation in *Polygonatum odoratum* (Liliaceae). Annals of Botany 94:433-440.

Harder LD, Barrett SCH (2006) Ecology and evolution of flowers. Oxford University Press, New York, pp. 43., 77., 266.

Heslop-Harrison Y, Shivanna KR (1977) The receptive surface of the Angiosperm stigma. Annals of Botany 41:1233-1258.

Hiraga T, Sakai S (2007) The effects of inflorescence size and flower position on biomass and temporal sex allocation in *Lobelia sessiliflora*. Plant Ecol 188:205-214.

Ishii HS, Morinaga S-I (2005) Intra- and inter-plant level correlations among floral traits in *Iris gracilipes* (Iridaceae). Evol Ecol 19:435-448.

Ishii HS, Sakai S (2001) Implications of geitonogamous pollination for floral longevity in *Iris gracilipes*. Funct Ecol 15:633–641.

Ishii HS, Sakai S (2002) Temporal variation in floral display size and individual floral sex allocation in racemes of *Narthecium asiaticum* (Liliaceae). Am J Bot 89:441-446.

Kennedy BF, Elle E (2008) The reproductive assurance benefit of selfing: importance of flower size and population size. Oecologia 155:469-477.

Kliber A, Eckert CG (2004) Sequential decline in allocation among flowers within inflorescences: proximate mechanisms and adaptive significance. Ecology 85:1675-1687.

Kostrakiewicz K (2006). Seasonal rhythmicity of *Iris sibirica* (Iridaceae) population in the Kostrze district of Krakow (S Poland). Polish Botanical Studies 22:311-316.

Kudo G, Molau U (1999) Variations in reproductive traits at inflorescence and flower levels of an arctic legume, *Astragalus alpinus* L.: Comparisons between a subalpine and an alpine population. Plant Spec Biol 14:181-191.

Kudo G, Maeda T, Narita K (2001) Variation in floral sex allocation and reproductive success within inflorescences of *Corydalis ambigua* (Fumariaceae): Pollinatiaon efficiency or resource limitation? J Ecol 89:48-56.

Mazer SJ, Dawson KA (2001) Size-dependent sex allocation within flowers of the annual herb *Clarkia unguiculata* (Onagraceae): ontogenetic and among-plant variation. Am J Bot 88:819-831.

Queller DC (1984) Pollen-ovule ratios and hermaphordite sexual allocation strategies. Evolution 38:1148-1151.

Simon T (2000) A magyarországi edényes flóra határozója. Harasztok-virágos növények. Nemzeti Tankönyvkiadó, Budapest, pp. 696-699.

Stöcklin J (1997) Competition and the compensatory regulation of fruit and seed set in the perennial herb *Epilobium dodonaei* (Onagraceae). Am J Bot 84:763-768.

Vasek FC, Weng V (1988) Breeding systems of Clarkia sect. Phaeostoma (Onagraceae): I. Pollen-ovule ratios. Syst Bot 13:336-350.

Wang Y-G, Zhang D-X, Chen ZY (2004) Pollen histochemistry and pollen: ovule ratios in Zingiberaceae. Annals of Botany 94:583-591.

Wesselingh RA, Arnold ML (2003) A top-down hierarchy in fruit set on inflorescences in *Iris fulva* (Iridaceae). Plant Biology 5:651-660.

Wolfe LM (1992) Why does the size of reproductive structures decline through time in *Hydrophyllum appendiculatum* (Hydrophyllaceae)?: Developmental constraints vs. resource limitation. Am J Bot 79:1286-1290.

Worley AC, Baker AM, Thompson JD, Barrett SCH (2000) Floral display in *Narcissus*: Variation in flower size and number at the species, population, and individual levels. Int J Plant Sci 161:69-79.

ZengY-F, Bai W-N, Zhou Y, Zhang D-Y (2008) Variation in floral sex allocation and reproductive success in sequentially flowering inflorescence of *Corydalis remota var. linearilobа* (Fumariaceae). J Integr Plant Biol 51:299-307.

Zhao Z-G, Meng J-L, Fan B-L, Du G-Z (2008) Reproductive patterns within racemes in protandrous *Aconitum gymnandrum* (Ranunculaceae): potential mechanism and among-family variation. Plant Syst Evol 273:247-256.

Volume 54(2):111-115, 2010
Acta Biologica Szegediensis
http://www.sci.u-szeged.hu/ABS

ARTICLE

Further contribution to cytotaxonomy of the genus *Silene* L. (Sect. *Auriculatae*, Caryophyllaceae)

Abbas Gholipour[1, 2], Masoud Sheidai[1]*

[1]Shahid Beheshti University, GC., Faculty of Biological Sciences, Tehran, Iran, [2] Payame Noor University, Sari, Iran

ABSTRACT The present study reports the chromosome numbers of 18 *Silene* L. species subspecies and varieties from the sect. *Auriculatae* for the first time. *S. commelinifolia* var. *isophylla*, *S. commelinifoilia* var. *ovatifolia*, *S. araratica*, *S. meyeri* ssp. *persica*, *S. nizvana*, *S. oligophylla*, *S. persica* and *S. rhynchocarpa* showed 2n = 2x = 24 chromosome number, *S. pseudoaucheriana*, *S. gynodioica*, *S. erysimifolia*, *S. guntensis*, *S. goniocaula*, *S. lucida* *S. microphylla* showed 2n= 4x= 48 and *S. hirticalyx* had 2n=6x=72 chromosome number. The size of the chromosomes varied from 1.53 µm in Ahvan population of *S. commelinifolia* var. *commelinifolia* to 4.97 µm in *S. oligophylla*. The chromosomes were metacentric (m) and sub-metacentric (sm). The species studied differed significantly in total size of the chromosomes, size of the short arms and the long arms indicating the role of quantitative changes of chromosomes in species diversification. The *Silene* species differed in karyotype formulae and symmetry indicating qualitative changes in the chromosomes possibly due to the occurrence of structural changes. Different clustering and ordination methods showed karyotype distinctness of the species studied.
Acta Biol Szeged 54(2):111-115 (2010)

KEY WORDS

Karyotype
Silene

Silene L. is the largest genus of Caryophyllaceae with about 700 species distributed throughout the northern hemisphere; Europe, Asia and northern Africa (Greuter 1995). *Silene* includes several important weeds, very beautiful horticultural plants and some medicinal species (Swank 1932). About 110 *Silene* species grow in Iran out of which about 35 species are endemic with very limited geographical distribution (Melzheimer 1988). *Silene* species have been placed the in 44 sections (Chowdhuri 1957), but recent molecular studies do not support such sectional classifications particularly for the endemic North American taxa (Oxelman and Lidén 1995; Liden and Berglund 1997; Oxelman et al. 2001; Burleigh and Holtsford 2003). The available literature from the other parts of the world dealing with cytogenetics of *Silene* indicates the importance of such studies (Heaslip 1951; Bari 1973; Melzheimer 1978; 1980; Markova et al. 2006), while similar data is lacking for the species growing in Iran and only recently karyotype details of few *Silene* species has been reported (Sheidai et al. 2009; Gholipour and Sheidai 2010).

The basic chromosome number of *Silene* is $x = (10)\ 12$, most of the species are diploid (2n = 2x = 24), some are tetraploid (2n = 4x = 48) and hexaploid (2n = 6x = 72). Few species show higher polyploidy levels for e.g. 2n = *c.* 96, 120 and 192 (Bari 1973), while 2n = 3x = 30 is reported for *S. fortunei* (Heaslip 1951).

Accepted Oct 22, 2010
*Corresponding author. E-mail: msheidai@yahoo.com

The section *Auriculatae* (Boiss.) Schischkin is the largest section of the genus containing about 35 species in Iran, out of which 21 species are endemic with very restricted distribution in mountainous areas such as Elburz, Zagros and Azarbayejan (Melzheimer 1988). The members of this section are caespitose plants with large flowers placed at the end of short stems. Their inflorescence is unifloral or dichsial. Calyx is cylindrical–clavate, pubescent or glandular–pubescent. The petals have conspicuous auricule at the end of claw. The present study reports the chromosome number of 18 *Silene* species from the sect. *Auriculatae* growing in Iran and also provides karyotype details of 16 diploid populations of 8 *Silene* species for the first time.

Materials and Methods

Plant material

Chromosome numbers were determined in 24 populations of 18 *Silene* species, subspecies and varieties from the sect. *Auriculatae* L. growing in Iran. The species studied are: 1- *S. commelinifolia* Boiss. var. *commelinifolia*, 2- *S. commalinifolia* var. *isophylla* Bornm., 3- *S. commelinifolia* var. *ovatifolia* Melzh., 4- *S. aucheriana* Boiss., 5- *S. nizvana* Melzh., 6- *S. oligophylla* Melzh., 7- *S. meyeri* Fenzl ex Boiss. ssp. *persica* Melzh, 8- *S. rhynchocarpa* Melzh., 9- *S. persica* Boiss., 10- *S. araratica* Schisck., 11- *S. pseudoaucheriana* Melzh., 12- *S. gynodioica* Ghazanfar; 13- *S. lucida* Chowdhuri; 14- *S. erysimifolia* Stapf., 15- *S. guntensis* B. Fedtsch. 16- *S. goniocaula* Boiss., 17- *S. hirticalyx* Boiss.; and 18- *S. microphylla*

Figure 1. Representative somatic metaphase cells in *Silene* species studied. A= Metaphase cell showing 2n = 24 in *S. araratica*, B = Metaphase cell showing 2n = 48 in Bozghosh population of *S. aucheriana*, C = Metaphase cell showing 2n = 24 in Darake population of *S. commelinifolia* var. *ovatifolia*, D = Metaphase cell showing 2n = 24 in *S. gynodioica*, E = Metaphase cell showing 2n = 24 in *S. commelinifolia* var. *commelinifolia*, F = Metaphase cell showing 2n = 24 in *S. oligophylla*, G = Metaphase cell showing 2n = 24 in *S. meyeri* ssp. *Persica*, H = Metaphase cell showing 2n = 24 in Polor population of *S. persica*, I = Metaphase cell showing 2n = 24 in *S. pseudoaucheriana*, J = Metaphase cell showing 2n = 24 in *S. nizvana*, K = Metaphase cell showing 2n = 24 in *S. commelinifolia* var. *isophylla*, L = Metaphase cell showing 2n = 48 in Neor population of *S. lucida*. Scale bar = 10 μm.

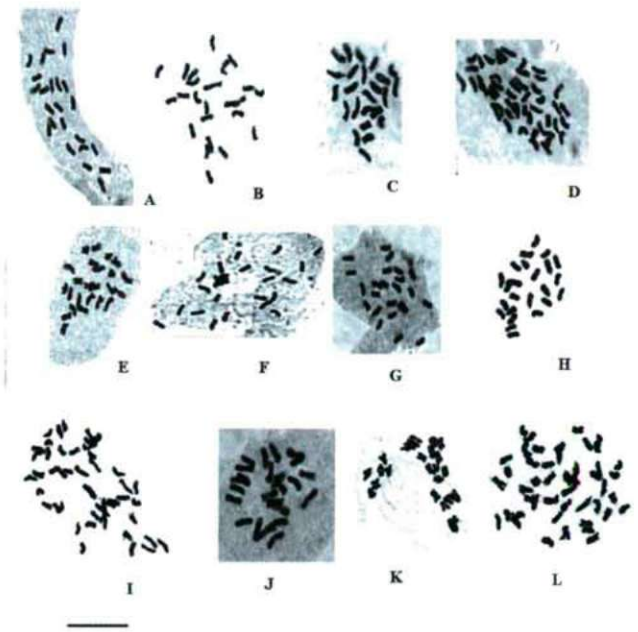

Boiss. The voucher specimens are deposited in Herbarium of Shahid Beheshti University (HSBU).

Cytological studies

For karyotypic studies freshly grown root tips were collected from the seeds of at least ten randomly selected plants in each species, pretreated with 0.002 mol 8-hydroxyquinolin (1–2 hrs.) and fixed in ethanol: acetic acid (3:1) for 24 hrs. The fixed tips were then washed thoroughly in distilled water and macerated in 60°C 1N HCl for about 5 min. Squash technique was used for cytological studies with 2% aqueous aceo-orcein as the stain. The somatic chromosome number and karyotype details were studied in at least 5 well-prepared metaphase plates. The chromosomes were photographed by digital camera and measured by Image Tools3 software (Sheidai and Rashid 2007).

The chromosomes were identified according to Levan et al. (1964), karyotype symmetry was determined according to Stebbins (1971), while other karyotype parameters like total form percentage (TF %), coefficient of variation (CV) of the chromosome size as well as A1 and A2 indices of Romero-Zarco (1986) were determined (Sheidai and Jalilian 2008).

Statistical analyses

In order to reveal significant difference, the analysis of variance (ANOVA) followed by the least significant difference test (LSD) were performed on the size of chromosomes, size of the long arms and size of the short arms as well as arms ratio among the species and populations studied (Sheidai and Jalilian 2008). Moreover, principal components analysis (PCA) was performed to identify the most variable karyotypic characters. SPSS ver. 9 (1998), NTSYS ver. 2.1 (1998) and DARwin ver. 5. (2008) was used for statistical analysis.

In order to group the species studied based on similarity in their karyotypic features, UPGMA (Unweighted Paired Group with Arithmetic Average) and Neighbor Joining (NJ) clustering methods as well as ordination based on principal components analysis (PCA) and principal coordinate analysis (PCO) were performed. NTSYS Ver. 2.02 (1998) was used for clustering and PCO analyses. Standardized karyotypic data (mean = 0, variance = 1) were used to determine taxonomic distance among the species which were used in clustering (Sheidai and Jalilian 2008). Cophenetic correlation was estimated to determine the goodness of fit of the clusters to the original data (Sheidai and Jalilian 2008).

Results

The somatic chromosome number and details of karyotypes of the *Silene* species studied are presented in Figsures 1-4. Nine species, subspecies and varieties studied showed 2n = 2x = 24 chromosome number, while the other species showed 2n = 4x = 48 and 2n = 6x = 72 chromosome number.

The size of the longest chromosome varied from 2.97 μm in Damavand population of *S. aucherianai* to 4.97 μm in *S. oligophylla*, while the size of shortest chromosomes varied from 1.53 μm in Ahvan population of *S. commelinifolia* var. *commelinifolia* to 2.75 μm in *S. oligophylla*. The chromosomes were mainly metacentric (m) and sub-metacentric (sm; Fig. 2).

The highest haploid total and mean chromosome length occurred in *S. oligophylla* (45.67 & 3.8 μm respesctively), while the lowest values of the same parameters occurred in Damavand population of *S. aucheriana* (28.95 & 2.41 μm, Table 1). The highest value of the ratio of longest to shortest chromosome occurred in Ahvan population of *S. commelinifolia* var. *commelinifolia* (2.16) while the lowest value of the same occurred in *S. nizvana* (1.53).

The highest value of coefficient of variation (CV) (33.00) for the size of chromosomes occured in Damavand population of *S. aucheriana* indicating the highest degree of size variation among its chromosomes, while the least CV value (16.00) occured in *S. rhynchocarpa*. Total form percentage value (TF%) varied from 41 in *S. commelinifolia* var. *isophylla*

Figure 2. Representative idiograms of *Silene* species studied.

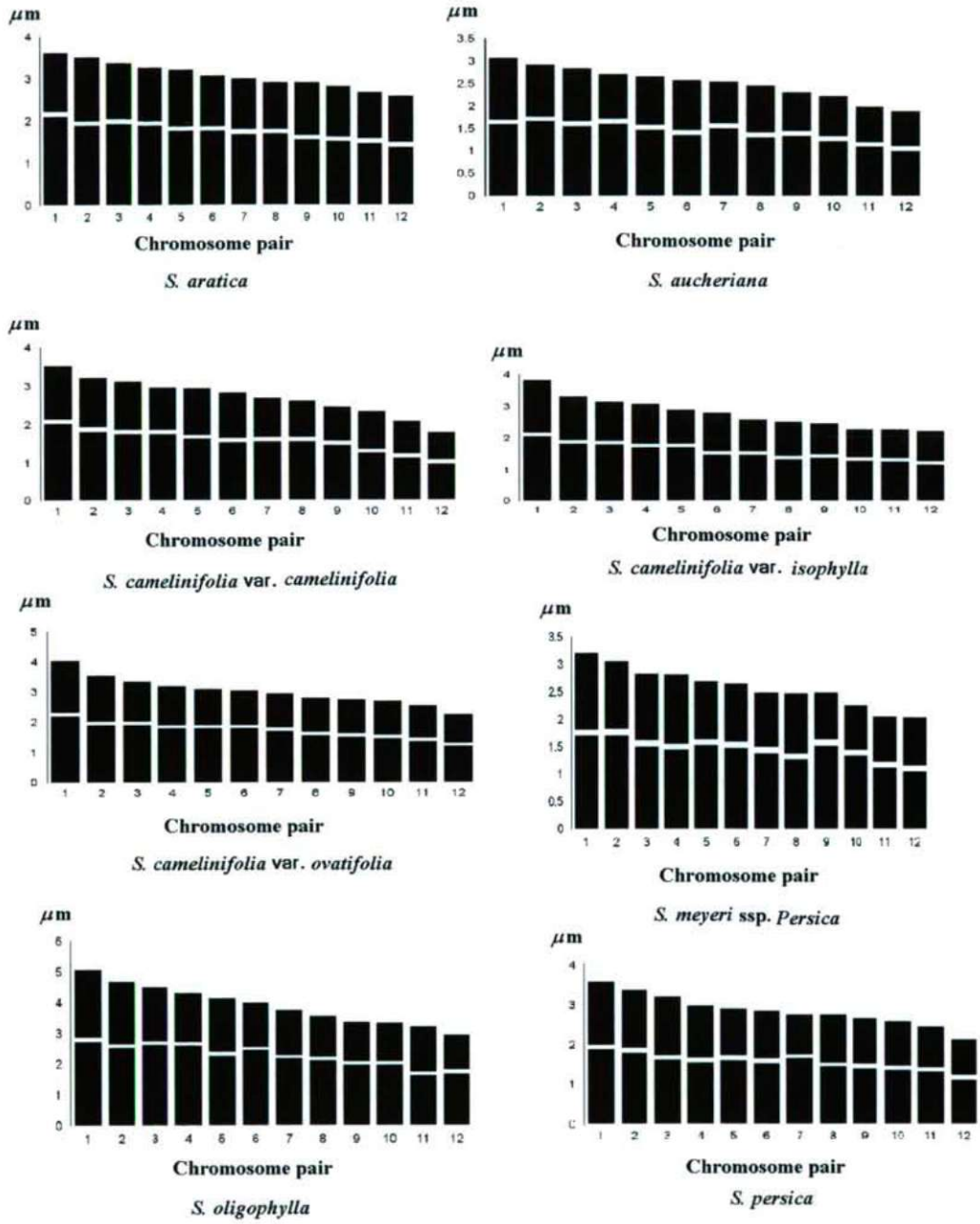

and *S. oligophylla* to 45.5 in *S. rhynchocarpa* and *S. meyeri* ssp. *persica*, a higher value of TF% indicates the presence of relatively more symmetrical karyotype. The species studied also differ in their karyotype formula.

The *Silene* species were placed in 1A and 1B classes of Stebbins 1971 karyotype classification which are considered relatively primitive in this system. Ahvan population of *S. commelinifolia* var. *commelinifolia* shows the highest asymmetric karyotype among the species studied as it stands in 1B class of Stebbins classification. Among the species placed in 1A class, Damavand population of *S. aucheriana* shows a higher value of Romero-Zarco A1 index (0.33) and has relatively a more asymmetrical karyotype.

Different clustering methods and PCO ordination of the *Silene* species based on karyotypic data produced similar results (Figs. 2 and 3). UPGMA dendrogram showed the highest cophenetic correlation (r>0.80). In general two major clusters were formed; the first major cluster is comprised of

Figure 3. UPGMA clustering of *Silene* species based on karyotypic data. Species code: com1-5 = *S. commelinifolia* Ahvan population, Shahrood population, Solok population, Touchal population and Darake population respectively, auch1-4 = Shahrood population, Neor population, Damavand population and Anguran population of *S. aucheriana* respectively, mpers = *S. meyeri* ssp. *persica*, rhyn = *S. rhynchocarpa*, nizvan = *S. nizvana*, oligo = S. *oligophylla*, persica = *S. persica*, ara = *S. araratica*.

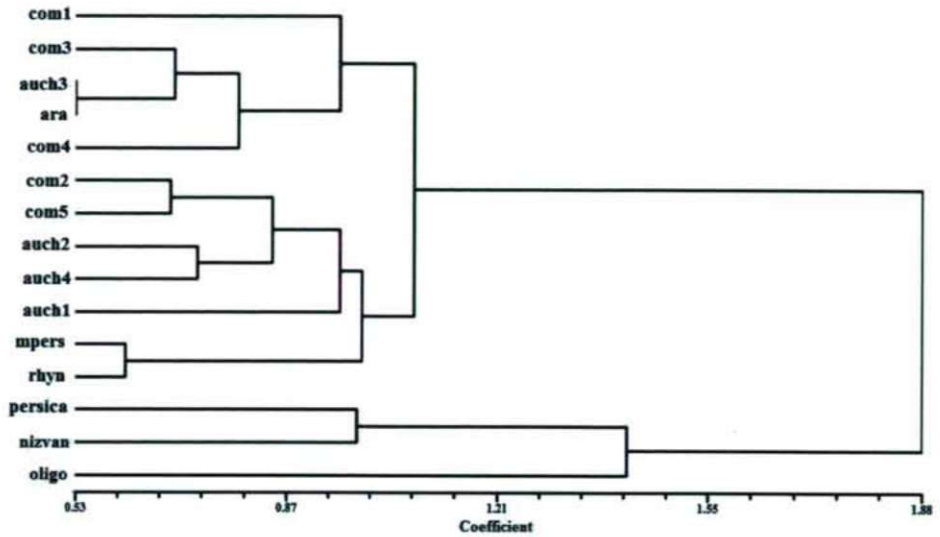

Figure 4. PCA plot of *Silene* species based on karyotypic data. Species code as in Fig. 2.

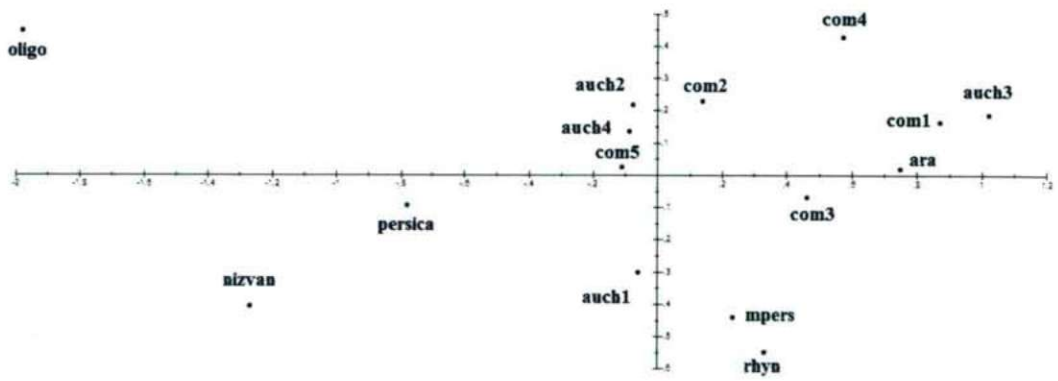

two sub-clusters. Three populations of *S. commelinifolia* var. *commelinifolia* (com1, com3 and com4 in Fig. 2), show more similarity and are grouped together in the first sub-cluster, while populations of *S. commelinifolia* var. *isophylla* and *S. commelinifolia* var. *ovatifolia* (com2 & com5 in Fig. 2) are placed in the second sub-cluster. Similarly three populations of *S. aucheriana* (auch 1, auch 2 & auch 4 in Fig. 2) show more similarity and are placed together, while Damavand population of *S. aucheriana* (auch3 in Fig. 2) differs in its karyotype features and is placed in another sub-cluster.

S. persica, S. nizvana and *S. oligophylla* form the second major cluster showing more differences from the other species studied. PCA and PCO ordination (Fig. 3) support the clustering results.

Discussion

The results obtained support the earlier report on *S. araratica* (Nersesian and Goukasian 1995), while the chromosome numbers of *S. commelinifolia* var. *isophylla, S. commelinifoilia* var. *ovatifolia, S. meyeri* ssp. *persica, S. aucheriana, S. nizvana, S. oligophylla, S. persica*, S. *rhynchocarpa, S. pseudoaucheriana, S. gynodioica, S. erysimifolia, S. guntensis, S. goniocaula, S. lucida, S. microphylla* and *S. hirticalyx* are new to science. *S. aucheriana* showed both 2n = 2x = 24 and 2n = 4x = 48 chromosome numbers.

Polyploidy is of limited occurrence in the genus *Silene* reported in some of arctic and subarctic species and in some species endemic to North America (Oxelman et al. 2000;

Popp and Oxelman 2007). The present study shows that about 30% of the species in the section *Auriculatae* growing in Iran are polyploid.

ANOVA and LSD tests showed significant differences ($p < 0.01$) for total size of the chromosomes, size of the short arms and the long arms among the species; subspecies and varieties studied, indicating the role of quantitative genomic changes in the *Silene* species diversification.

Pearson correlation determined among the karyotypic features showed a positive significant correlation between the mean chromosomes length and the size of the short and long arms of the chromosomes ($r > 0.70$, $p < 0.01$). Therefore the significant quantitative change in the chromosomes has been occurred in the size of both chromosomes arms during the species diversification.

Difference of the species in TF%, karyotype formulae and symmetry of karyotype indicate the occurrence of structural changes in their chromosomes which is also supported by PCA analysis given bellow.

PCA analysis (data not given) showed that the first 3 components comprise about 81% of the total variation. In the first component with about 66% of total variance, the mean chromosome length, size of the short arms and long arms as well as total length of the chromosomes are the most variable characters ($r > 0.80$), supporting the results of ANOVA stated earlier.

In the second factor with about 9% of total variance, the ratio of the long arm to the short arm of the chromosomes pair number 4, 7, 8 and 9 are most variable characters ($r > 0.65$), supporting our earlier suggestion about the role of qualitative changes in the *Silene* species diversification. In the third factor with about 5% of total variance, the ratio of the long arm to the short arm of the chromosomes pair numbers 1, 11 and 12 are most variable characters ($r > 0.60$). Clustering and PCO ordination of the *Silene* species indicate karyotypic distinctness of the *Silene* species studied.

Morphological studies performed on the section, supports karyotype analysis (Sheidaei et al. 2010). Separation of the *S. oligophylla*, *S. persica* and *S. nizvana* from the other species studied are supported by morphological analysis. Close affinity of *S. oligophylla* and *S. nizvana* has also been shown by both karyotype and morphological analyses. Close affinity between *S. araratica* and *S. commelinifolia* var. *commelinifolia* and *S. commelinifolia* var. *ovatifolia* due to shared morphological characters like reticulate calyx veins, large conspicuous auricle, claw placed in calyx, is also observed in both karyotype and morphological analyses. Therefore, karyotype features can be used in both species delimitation and illustrating species relationships in the genus *Silene*.

References

Bari EA (1973) Cytological studies in the genus *Silene* L. New Phytol 72:833-838.

Burleigh JG, Holtsford TP (2003) Molecular systematics of the eastern North American Silene (Caryophylaceae): Evidence from nuclear ITS and chloroplast trnL intron sequences. Rhodora 105:76-90.

Chowdhuri PK (1957) Studies in the genus *Silene*. Notes from the Royal Bot. Garden Edinb 22:221-278.

Levan A, Fredga K, Sandberg A (1964) Nomenclature for centromeric position on chromosomes. Hereditas 52:201-220.

Gholipour A, Sheidai M (2010) Karyotype analysis and new chromosome number reports in *Silene* L. species (Sect. *Auriculatae*, Caryophyllaceae). Biologia 65:23-27.

Greuter W (1995) *Silene* (Caryophylaceae) in Greece: A subgeneric and sectional classification. Taxon 44:543-581.

Heaslip MB (1951) Some cytological aspects in the evolution of certain species of the plant genus *Silene*. Ohio J Sci 51:62-70.

Markova M, Martina L, Zluvova J, Janousek B, Vyskot B (2006) Karyological analysis of an interspecific hybrid between the diocious Silene latifolia and the hermaphroditic *Silene viscosa*. Genome 42:373-379.

Melzheimer V (1978) Notes on cytology of several species of the genus *Silene* (Caryophyllaceae) from central Greece and from Crete. Plant Sys Evol 130:203-207.

Melzheimer V (1988) *Caryophyllaceae*. In KH Rechinger, ed., Flora Iranica, No.163. pp. 353-508. Akademische Druck-U, Verlagsanstalt, Graz, Austria.

Nersesian AA, Goukasian AG (1995) On the karyology of the representatives of the genus *Silene* L. s. l. (Caryophylaceae) from southern Transcaucasia. Thaiszia 5:13-19.

Oxelman B, Lidén M (1995) Generic boundaries in the tribe Sileneae (Caryophyllaceae) as inferred from nuclear rDNA sequences. Taxon 44:525-542.

Oxelman B, Berglund D (1997) Chloroplast rps16 intron phylogeny of the tribe Sileneae (Caryophyllaceae). Plant Sys Evol 206:411-420.

Oxelman B, Lidén M, Rabeler RK, Popp M (2001) A revised generic classification of the tribe Sileneae (Caryophylaceae). Nordic J Bot 20:743-748.

Popp M, Oxelman B (2007) Origin and evolution of North American polyploidy *Silene* (Caryophyllaceae), Amer J Bot 94:330-349.

Romero-Zarco C (1986) A new method for estimating karyotype asymmetry. Taxon 35:526-530.

Sheidai M, Gholipour A, Noormohammadi Z (2010) Species relationships in the genus *Silene* L. Section *Auriculatae* (Caryophyllaceae) based on morphology and RAPD analyses. Acta Biol Szeged 54:25-31.

Sheidai M, Jalilian N (2008) Karyotypic studies in some species and populations of the genus *Lotus* L. in Iran. Acta Bot Croat 67:45-52.

Sheidai M, Nikoo M, Gholipour A (2009) Cytogenetic variability and new chromosome number reports in *Silene* L. species (Sect. *Lasiostemones*, Caryophylaceae). Acta Biol Szeged 52:313-319.

Sheidai M, Rashid S (2007) Cytogenetic study of some *Hordeum* L. species in Iran. Acta Biol Szeged 51:107-112.

Stebbins GL (1971) Chromosomal Evolution in Higher Plants. Edward Arnold, London.

Swank GR (1932) The Ethnobotany of the Acoma and Laguna Indians. MA Thesis, University of New Mexico.

Volume 54(2):117-125, 2010
Acta Biologica Szegediensis
http://www.sci.u-szeged.hu/ABS

ARTICLE

Micromorphological studies on leaf, fruit and pollen of four species from *Typhaceae* (*Typha laxmannii, T. azerbaijanensis, T. minima* and *T. lugdunensis*) from Iran, and their thematic significance

S. M. M. Hamdi[1]*, M. Assadi[2], A. R. Iranbakhsh[3]

[1]Department of Biology, Islamic Azad University, Garmsar branch, Garmsar, Iran, [2]Research Institute of Forest & Rangelands, Tehran, Iran, [3]Department of Biology, Islamic Azad University, Aliabad-katoul branch, Aliabad, Iran

ABSTRACT Previous research has made it clear that the intrinsic taxonomy encountered difficulties in identifying species in the genus *Typha*. Therefore, in the present study we have tried to investigate the micromorphological characteristics of pollens, achenes and leaves as well as their systematic utility. Four *Typha* species identified from the Iranian flora *i.e. Typha minima* Funk in Hoppe, *Typha lugdunensis* Chab., *Typha azerbaijanensis* Hamdi & Assadi and *Typha laxmannii* Lepechin were taken into consideration. Three of them are easily distinguishable with their closest relative *i.e. T. laxmannii* Lepechin. Scanning electron microscopy was used to examine pollens, achenes and leaves of the four taxa of the proposed *Typha* from Iran. A part of these micromorphological studies attempted to investigate achenes, pollens and leaf characteristics of these species under SEM. Interestingly, *Typha martini* Jordan is also considered as a synonym of *T. lugdunensis*. The study does not only discuss relationships between close species but it also clarifies their geographical patterns. Finally, a diagnostic key is provided for the distribution of the four *Typha* species in Iran. The results show that the ornamentation characters of pollens, achenes and leaf cells prove to be very helpful. Ornamentation of pollens and achenes could be used to distinguish between the four morphological types. Micromorphological studies on achenes, pollens and leaves of *Typha* were found useful with respect to taxa differentiation, hence it provides a key to make distinctions between species or groups of species.
Acta Biol Szeged 54(2):117-125 (2010)

KEY WORDS

achene
Iran
leaf
pollen
SEM
Typha

Typha, a monotypic genus, is distributed widely throughout the world, the Mediterranean region is considered to be the most diversified center. *Typha* is a genus with approximately 24 species, 50% of which are present in Iran. Twelve *Typha* species were recorded by Hamdi and Assadi (2003), after the floristic contributions of others (Kronfeld 1888; Komarov 1934; Townsend and Guest 1968; Riedl 1970; Hegi 1981; Davis 1984; Nassir 1987; Fedorov 2001; Takhtajan 2001; Mavrodiev 2002; and Changkyun et al. 2003). The genus *Typha* is divided into *Typha* and *Bracteolate* sections. In the section *Typha*, there are no bracteolate female flowers like in *T. laxmannii* and *T. azerbaijanensis*. The section *Beracteatae* consists of bracteolate female flowers, such as in *T. minima* and *T. lugdunensis*. Some previous research has shown difficulties in identifying species belonging to the genus *Typhaceae*. Among these, we can name the palinology carried out by Moore et al. (1991); Moar (1993), and the biomolecular studies by Kuehn-Marcinko and White (1999). However, the intrinsic taxonomic difficulties of the genus *Typhaceae* are increased further because important differential characters are observed only with difficulty and not at all on dried specimens. With regard to pollens and achenes, several studies have been carried out, each analyzing different aspect with scanning electron microscopy (SEM; e.g. Panich-pat et al. 2005). Interestingly, SEM allows observing structures that could be observed with difficult by other means. Some authors have highlighted the importance of this technique while studying achene coat, leaf surface and pollen ornamentation, especially for those families whose identification is complicated, particularly Typhaceae for hybridizing between species (Smith 1967; Kuehn-Marcinko et al. 1999), where morphological features of pollens, achenes and leaves were used widely in order to distinguish between different taxa or to find similarities between them. As mentioned earlier, the aim of the present study is to illustrate the role of pollens, achenes and leaf features to identify four species of *Typhaceae* in Iran as well as to help relate those characters to a systematic group. The present paper discusses four species *i.e. T. minima*, *T. lugdunensis*, *T. azerbaijanensis* and *T. laxmannii*. Here, *T. laxmannni* and

Accepted Aug 2, 2010
*Corresponding author. E-mail: mhamdi@iau-garmsar.ac.ir

Table 1. Macromorphological characteristic features of four species representing Iranian *Typha*.

	T. azerbaijanensis	*T. laxmannii*	*T. lugdunensis*	*T. minima*
Vouchers	Hamdi 81266 TARI	Mozaffarian 47032 TARI	Mozaffarian & al. 58975 TARI	Hamdi 80846 TARI
Rhizome (mm)	3	2-4	3-4	2-3
Stem (cm)	75-90	80-140	50-130	45-65
Largest of leaf long (cm)	75	80	110	25
Largest of leaf wide	8-9	6-9	2-4	2-3
Male inflorescence (cm)	9-15	10-32	4.5-7	1.5-5
Female inflorescence (cm)	7-10	4-11	2-4.5	2.5-4.5
Female inflorescence color	reddish- brown	brown	brown-light brown	brown
Rate of female inflorescence to male inflorescence	0.7	0.7	0.7	1
Gap of female inflorescence to male inflorescence (mm)	15-50	5-30	5-25	2-8
Scale of female flower (mm)	_	_	2.5-6	5-6
Number of hairs in female flower	35-40	25-35	10-15	12-25
Gynophores (mm)	3-7	4-5	1.5-4	3.5-4.5
Female flower (mm)	9-9.5	7-10	5-6	5.5-6
Stamen stalk (mm)	0.5-0.7	0.5-1	0.4-0.8	0.5
Stamen anther (mm)	1.5	1-2	1-1.5	1.2-1.7
Stamen number in male flowers	1-2	1-2	1	1-2

Table 2. Micromorphological features of pollen grains, achene and leaf in four species representing Iranian *Typha*.

	T. azerbaijanensis	*T. laxmannii*	*T. lugdunensis*	*T. minima*
Vouchers	Hamdi 81266 TARI	Mozaffarian 47032 TARI	Mozaffarian & al. 58975 TARI	Hamdi 80846 TARI
Shape of leaf testa cells	tetragonal	tetragonal & pentagonal	tetragonal & pentagonal	Pentagonal
Size of leaf testa cells	15-30×10-14	16-20×10-12	20-25×12-15	30-40×10-15
Shape of achene testa cell	pantagonal	pantagonal	Tetragonal	tetragonal & pentagona
Size of achene testa cells (μm)	100-125×12-15	80-110×12-15	10-12×6-8	35-55×10-15
Lumina (μm)	0.1-0.2	0.5-1.1	0.4-1.0	0.3-0.8
Length of large muri (μm) Distal face	1.9-2.1	3.5-4.0	1.0-1.8	0.8-1.0
Width of large muri (μm) Distal face	0.3-0.6	0.6-0.9	0.2-0.4	0.3-0.4
E (μm)	26-27	28-30	25-27	20-22
P(μm)	19-21	26-28	14-16	18-20
P/E ratio	0.73-0.77	0.92-0.93	0.56-0.59	0.90-0.91

T. minima are considered to be the most widespread species, extending throughout the temperate Northern Hemisphere (Smith 2000). *T. lugdunensis* is found in the Middle Eastern and Central Asian region (Riedl 1970) and *T. azerbaijanensis*, is restricted to northwestern Iran (Hamdi and Assadi 2003). At the same time, the scanning electron microscopic studies of leaves, achenes and pollens can be considered useful in separating those species. During studying the above-mentioned four species, botanists have been considerably attentive so far as the pollen morphology of *Typha* is concerned as well as the terminology for pollen ornamentation. The present study has followed Moore et al. (1991), Punt et al. (1999, 2007) and Panich-Pat et al. (2005) in order to test their results.

Materials and Methods

Pollen, capsule and leaf micromorphology was studied in four taxa of the *Typha* L. genus from Iran, using a scanning electron microscope. For every taxon, samples were collected from the populations within the study area. Mainly specimens from TARI (acronyms according to Holmgren et al. 1990) were used, although some of the samples acquired from a collection of Iranian fields that, however, proved problematic in finding pollens, achenes and leaves for the analysis. The collectors of samples and their localities are shown in the Appendix. The data represent the measurements done on 30-40 pollens, 10-15 achenes and selection of apex of middle

leaves per taxon, by means of direct visual observation under optical microscopy. For scanning electron microscopy, the pollen samples were examined and photographed using a LEO-440I scanning electron microscope. However, dry pollens, achenes and leaves were mounted directly on stubs using dual-sided adhesive tape and were coated with gold/palladium in a sputter coater. Morphological observations were made using a TESCAN microscope from the Electronic Microscopy Service of Razi Institute of Tehran. To describe the pollen ornamentation, the current study has followed the terminologies used by Moore et al. (1991) and Punt et al. (1999, 2007) and achene ornamentation used by Steam (1993) and acronyms of the herbariums follow Holmgren et al. (1990).

Results

Scanning electron microscopic observations indicated that two basic types of pollens could be found in Iranian *Typha* species. These are related to pollen dispersal in *Typha* which can be as tetragonal tetrads (Fig. 1) or monads (Fig. 2), (according to Punt et al. 1999, 2007). As a matter of fact, while tetrad pollens are found in two Iranian species: *T. lugdunensis and T. minima*, whereas monad pollens are found in two others: *T. azerbaijanensis and T. laxmannii* as listed in Table 2. The scanning electron microscopic observation could indicate three pollen types of Typha. Type 1: reticulate, Type 2: vermiculate, Type 3: perforate. Table 2 summarizes the main features of the investigated pollens. The study shows that the exine sculpturing provided valuable characteristics for separating species, sometimes even for closely related ones, and delimitation of natural groups within the genus. The exine of genus *Typha*, in most cases, is reticulated upon tectum. It seems that the structure of the muri is solid, which is very important in recognizing natural groups within the genus. With regard to the exine sculpture in proximal face, three basic types of pollen grains can be distinguished: perforate, reticulate, and vermiculate (Table 2). The pollen grains are partly medium in size. [Range: From 20-22_18-20 µm in *T. minima* to 28-30_26-28 µm in *T. laxmanii* P/E ratio ranges from 1-1.2. The aperture is simple, distal-polar (ana-sulcate), elongated, and reaches the proximal side of the pollen with rounded or acute ends (Figs. 1 and 2). The exine is perforated or rarely tectate-columellate upon tectum. The muri are solid or compound, simpli-, dupli- or pluricolumellate (according to Punt et al. 1999). Among the studied species, tectal perforations vary from 0.2 to 2.0 µm in diameter. Three main pollen types recognized on the basis of the exine sculpturing at proximal face are described below.

Type 1: Reticulate; this type occurs in *T. laxmannii* (Fig. 2). The largest pollen of all the species is classified under this type and occurs in *T. laxmannii* [26-28_28-30 µm in size].

Type 2: Vermiculate; occurs in two species: *T. minima* and *T. lugdunensis* (Fig. 1). The smallest pollen grains are found in *T. minima* [18-20_20-22 µm in size] and the largest in *T. lugdunensis* [18-20-_25-27 µm in size].

Type 3: Perforate; occurs in species *T. azerbaijanensis* (Fig. 1).

The basic palynomorphological characters of *Typha* are due to a shallow sulcus, a reticulate, microreticulate, vermiculate and perforate exine with solid or compound columellate muri. The taxonomy of the genus *Typha* is difficult due to emergence of several problems. Moreover, there are very controversial views with respect to subgeneric grouping within the genus. In the most recent published works, pollen morphological characters provide valuable characteristics for delimitation of the species in Typhaceae. This point of view has also been confirmed by the present study. Some of these groups are in congruence with the formerly supposed grouping within the genus. Of the micromorphological characteristics, the current paper examines achenes, pollens and leaf characters of species under SEM. Interestingly, here *Typha martini* Jordan is considered as a synonym of *T. lugdunensis*. The study discusses not only the relationship between close /nearest species rather gives their geographical patterns, too. Finally, a diagnostic key is provided to four *Typha* species distribution in Iran.

Table 1 indicates morphological differences between four taxa studied during the present research. Despite their overall close morphology, the four taxa could be distinguished from each other by a number of morphological traits. An identification key to these taxa has been provided. These species differ from *T. laxmannii* with respect to their female inflorescence long, gap between male and female inflorescence, male inflorescence long, female flower long, shape and size of leaf and achene (Figs. 3, 4, Table 1 and 2).

Discussion

Morphological differentiation between four taxa of *Typha*

Tables 1 and 2 present morphological differences among the four taxa studied above. Despite the overall close morphology, these taxa can be distinguished from each other by a number of morphological traits. These species differ from *others* in having long female and male inflorescences, a gap between the male and female inflorescences, female flowers are long, scale of female, number of hairs in female flower, shape and size of leaves, pollens and achenes (Figs. 1, 2, 3 and 4). Detailed pollen morphological characteristics are given for these species. Among the studied species, the newly described *T. lugdunensis, and T. minima* possess the tetrad pollen grains (Moar 1993) also, *T. laxmannii* and *T. azerbaijanensis* are monad pollen grain (Hamdi and Assadi 2003). The study shows that the sculpturing of pollen exine provides valuable characteristics for separating the species (Moore et al. 1991; Punt et al. 1999, 2007), sometimes even for closely related ones, and delimitation of natural groups within the genus. Re-

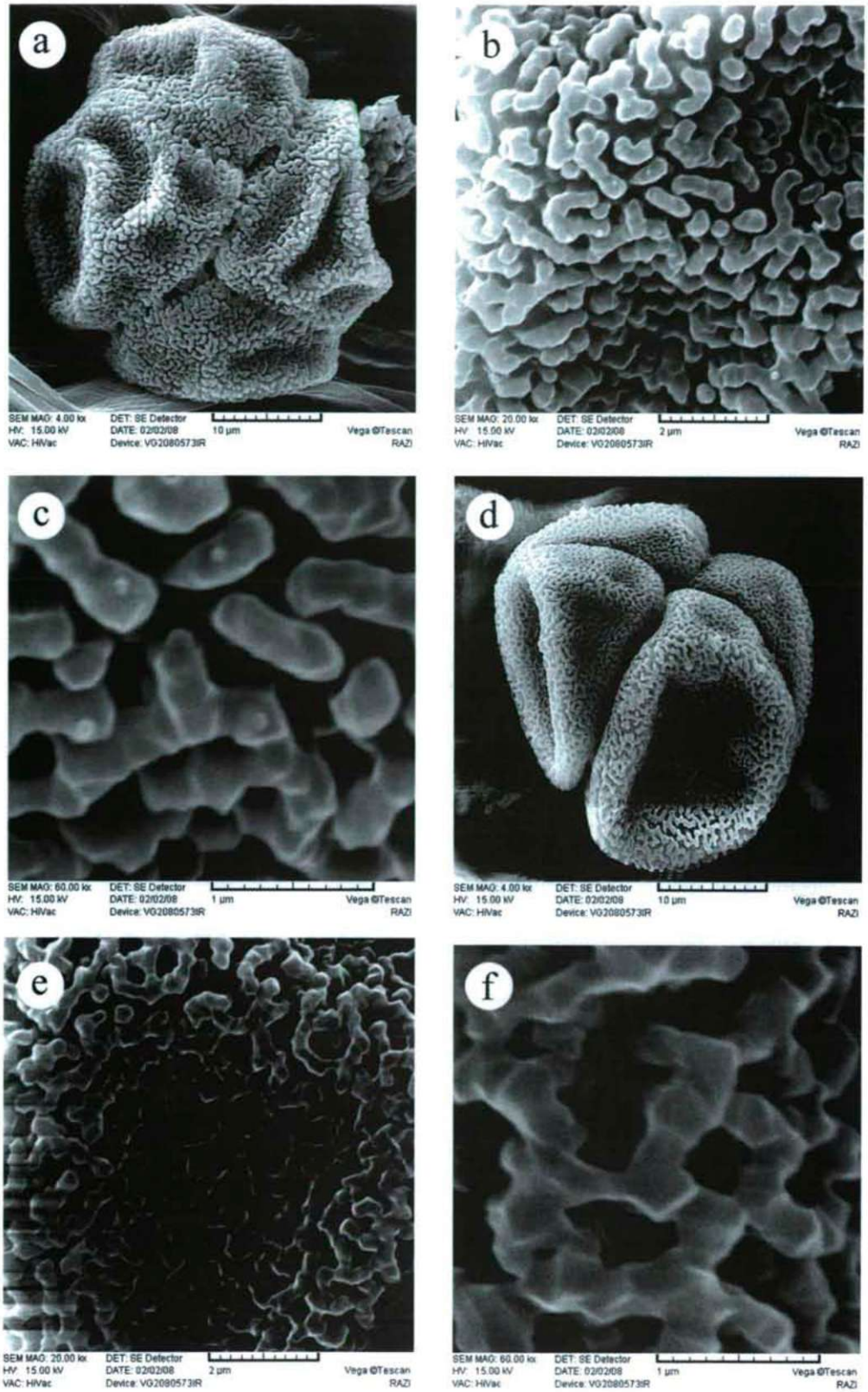

Figure 1. Micrographs of pollen grains in *Typha* (Typhaceae). Fig. a-c, vermiculate tectum at the proximal face in *T. minima* pollen with vermiculate muri. Fig. e-f, vermiculate tectum at proximal face of pollen of *T. lugdunensis* with vermiculate muri. Scale bar = 1 µm; Figs c and f, scale bar = 2 µm; Figs b and e, scale bar = 10 µm; Fig. a and d.

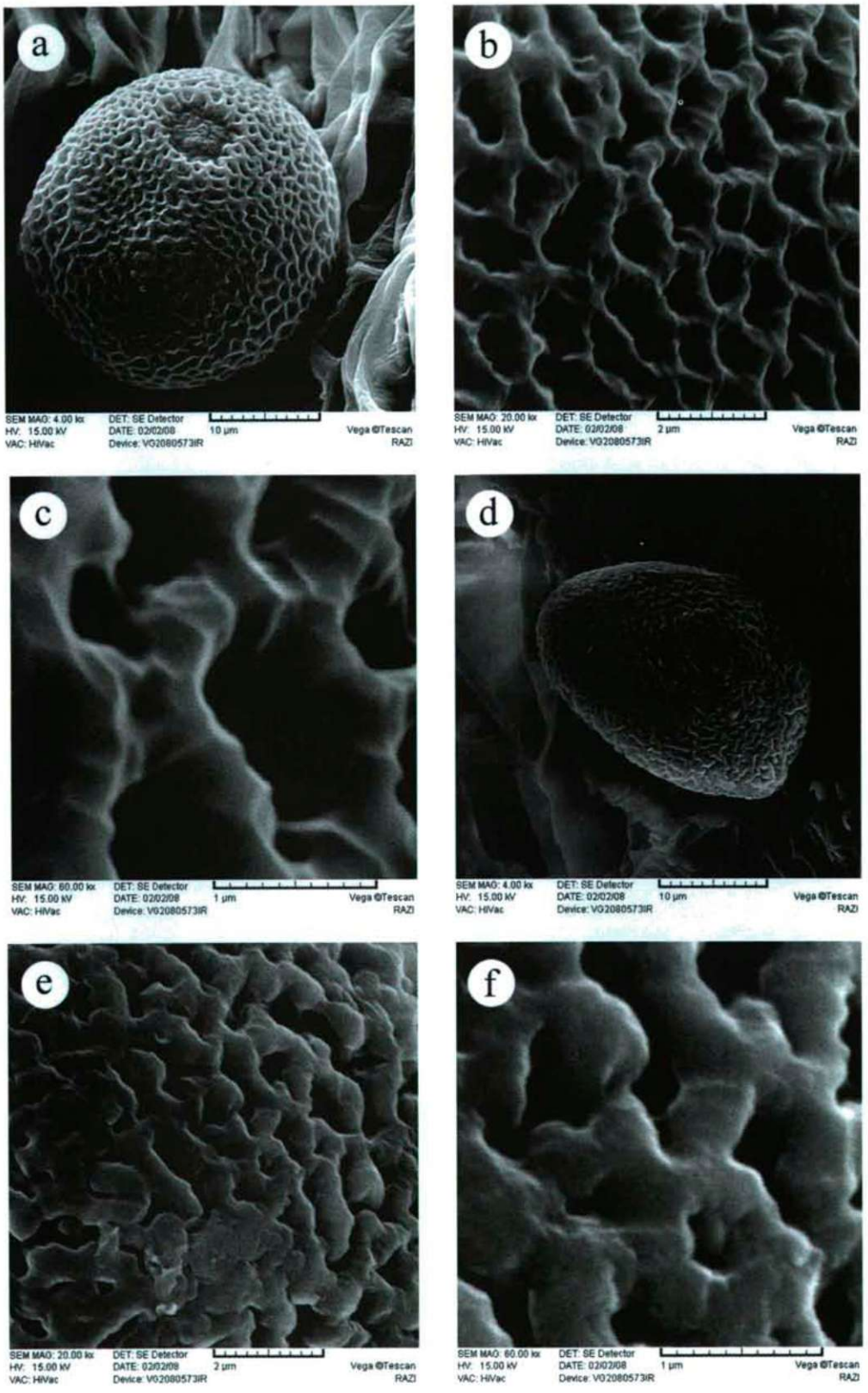

Figure 2. Micrographs of pollen grains in *Typha* (Typhaceae). Fig. a-c, Reticulate tectum at the proximal face in *T. laxmanii* pollen with perforate muri. Fig e-f, perforate tectum at proximal face of pollen of *T. azerbaijanensis* with perforate muri. Scale bar = 1 µm; Figs c and f, scale bar = 2 µm; Figs b and e, scale bar = 10 µm; Fig. a and d.

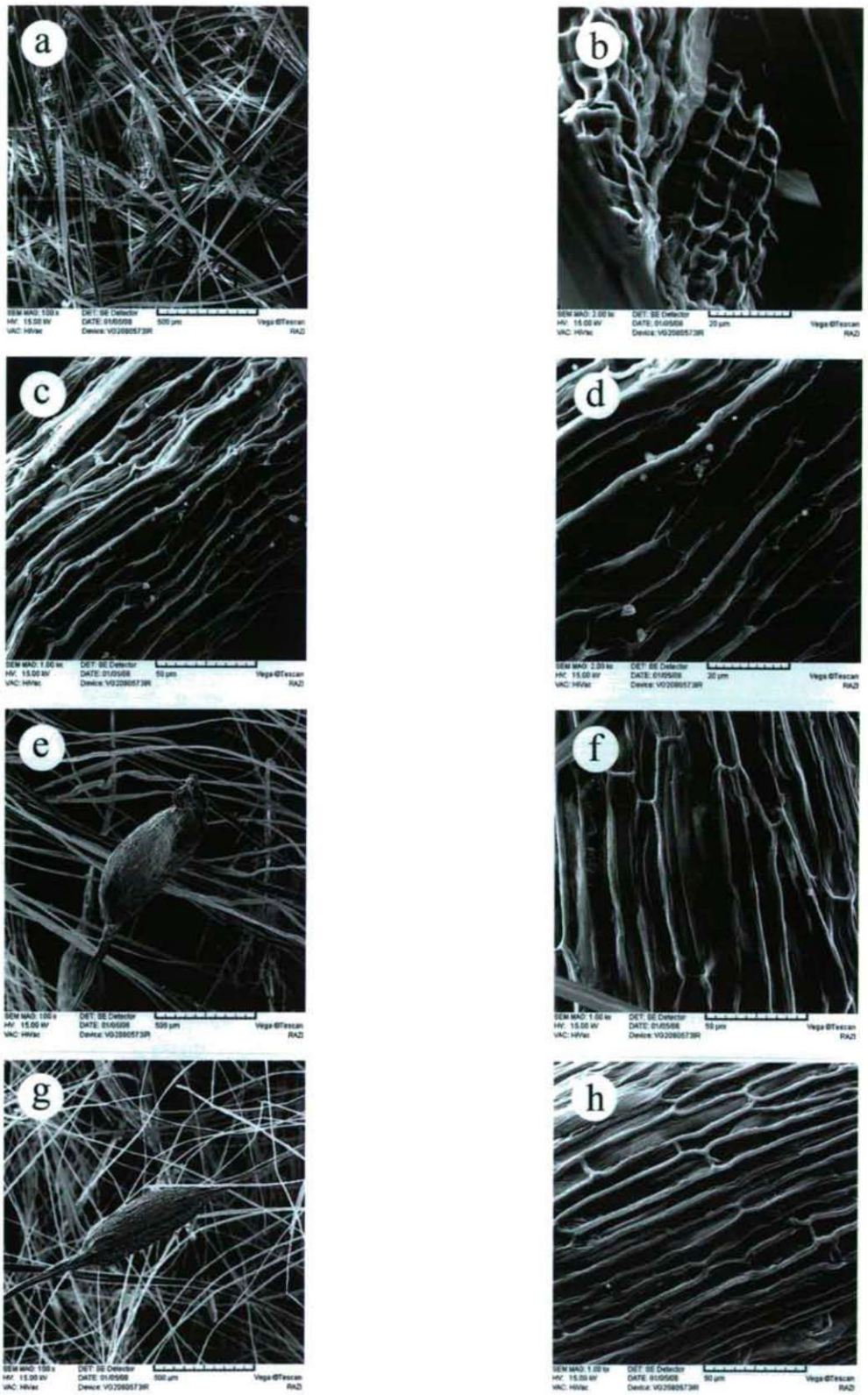

Figure 3. Scanning electron micrographs of *Typha* (Typhaceae) - a-b: *T. lugdunensis* from 58975 Mozaffarian and Abouhamze (TARI), overview of capsule (a) testa cells of capsule (b); -c-d: *T. minima* from 80846 Hamdi (TARI), testa cells of capsule (c, d); e-f: *T. azerbaijanensis* from 81266 Hamdi (TARI), overview of capsule (e) testa cells of capsule (f); - g-h: T. laxmannii from 61619 Assadi and Akhani (TARI), overview of capsule (g) testa cells of capsule (h); - Scale bars: a = 500 µm, b = 20 µm, c = 50 µm, d = 20 µm, e = 500 µm, f = 50 µm, g = 500 µm, h = 50 µm.

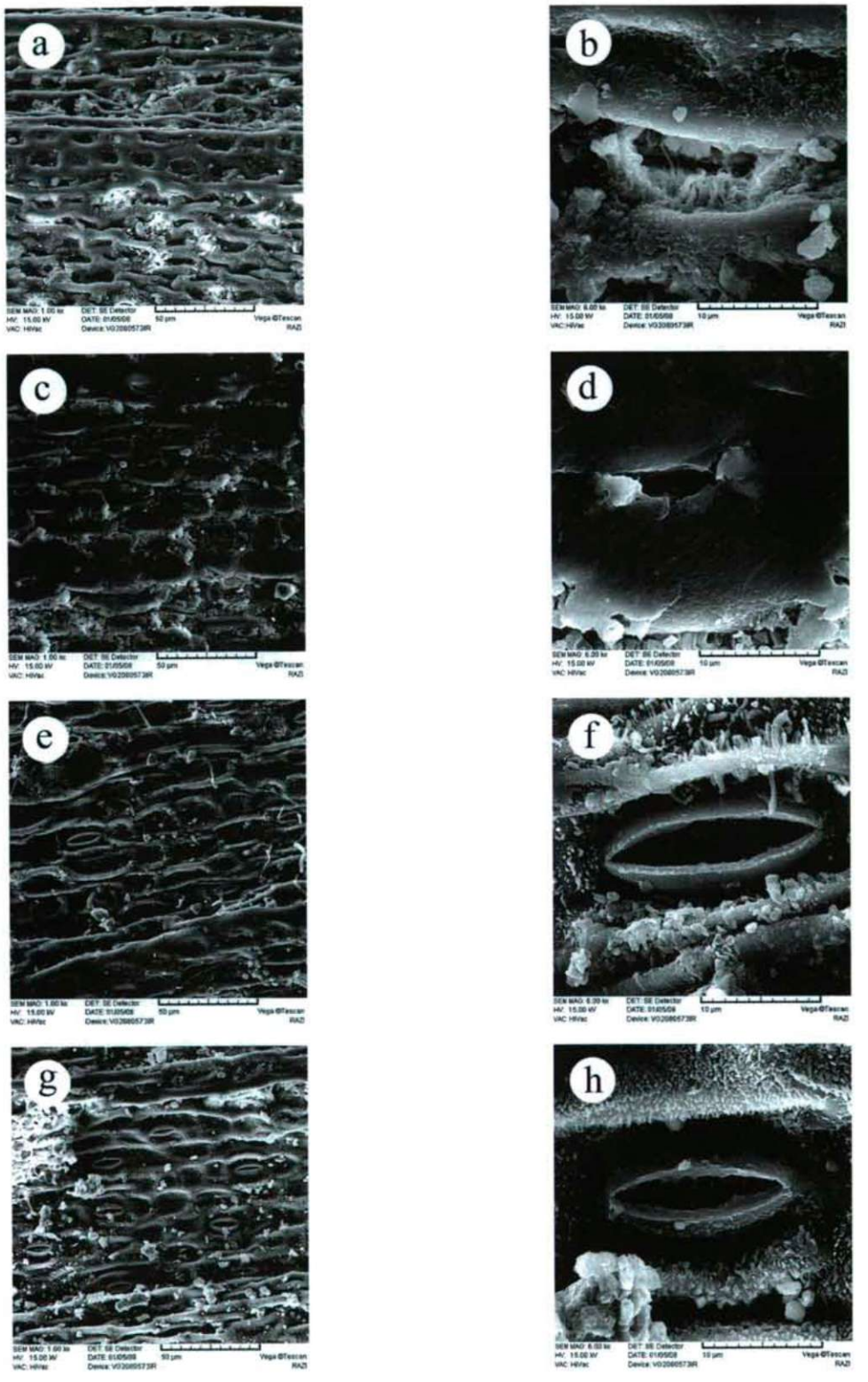

Figure 4. Scanning electron micrographs of *Typha* (Typhaceae) - a-b: *T. lugdunensis* from 58975 Mozaffarian and Abouhamze (TARI), testa cells of leaf (a), stomata ornamentation surface (b); -c-d: *T. minima* from 80846 Hamdi (TARI), testa cells of leaf (e) stomata ornamentation surface (d); e-f: *T. azerbaijanensis* from 81266 Hamdi (TARI), testa cells of leaf (e) stomata ornamentation surface (f); - g-h: *T. laxmannii* from 18559 Wendelboo and Assadi (TARI), testa cells of leaf (g) stomata ornamentation surface (h); - Scale bars: a = 50 µm, b = 10 µm, c = 50 µm, d = 10 µm, e = 50 µm, f = 10 µm, g = 50 µm, h = 50 µm.

garding exine sculpturing in proximal face, three basic types of pollen grains can be distinguished: perforate, vermiculate and reticulate. Perforate type occurs in: *T. azerbaijanensis* (Figs. 2, 3 and 4) *T. azerbaijanensis* with lumina 0.1-0.2 µm, length and width of large muri distal face 1.9-2.1×0.6-0.9 µm, E 26-27 µm, P 19-21 µm, P/E ratio 0.73-0.77. Reticulate type occurs in *T. laxmannii,* with lumina 0.5-1.1 µm length and width of large muri distal face 3.5-4.0 × 0.6-0.9 µm, E 28-30 µm, P 26-28 µm, P/E ratio 0.92-0.93. (Fig. 2). Vermiculate type occurs in *T. minima* and *T. lugdunensis* (Fig. 1). *T. minima,* with lumina 0.3-0.8 µm length and width of large muri distal face 0.8-1×0.3-0.4 µm, E 20-22 µm, P 18-20 µm, P/E ratio 0.90-0.91 and *T.lugdunensis* with lumina 0.4-1 µm, length and width of large muri distal face 1.0-1.8-0.2-0.4 µm, E 25-27 µm, P 14-16 µm, P/E ratio 0.56-0.59 (Table 2). Table 2 presents micromorphological achene character differences between the four taxa. These differ in size, shape of testa cells and size of testa cells. The acquired results confirm the usefulness of pollen, achene and leaf surface characters for identifying most of the studied species, and highlight their division into three (*i.e.* reticulate, vermiculate and perforate), as has been traditionally recognized (Komarov 1934; Davis 1984; Hamdi and Assadi 2003). The results of this studies show that SEM can be considered useful in making separation between the aforementioned species of this genus.

Acknowledgements

We express our gratitude for the proposed research at by Research Council of Islamic Azad University, Garmsar branch, as well as Dr. Shahrookh Ranjbar Bahadori for his partial support for the project (No. 108). We would also like to thank the Electron Microscopy Unit of Razi Institute in Tehran especially Mr. Rahmani for his valuable contribution. Last but not the least is Dr. Massoumi from National Botanic Garden of Iran.

Appendix

Localities of collections studied

Typha lugdunensis Chab. IRAN. Azerbaijan province; Aras Lake, between Pol-Dasht, 730 m, Izadpanah and Taheri (TARI 68417). Khorasan province; Kalat, Archangan, 950 m, Hamdi (TARI 80898); Kalat, 25 km to Kalat, near Soltan Abad village, Assadi and Massoumi (TARI 55806). Tehran province; Taleghan, Karaj, Sikaroud, 185 m, Amin and Bazargan (TARI 18580); Firouzkouh, margin of Nemroud, Mozaffarian and Abouhamzeh (TARI 58975).

Typha minima Funk in Hoppe. IRAN. Gorgan province; Kourdkoy, protected area Jahan nema, 1800-2000 m, Massoumi (TARI 55059). Azerbaijan province, Parsabad, 5 km to Aslandouz, Hamdi (TARI 80879). Tehran province, Tehran toward Firouzkouh, Harandeh village, margin of river of Nomroud, Hamdi (TARI 80846).

Typha azerbaijanensis Hamdi and Assadi. IRAN. Azerbaijan province; Khoy, 5 km to Marand, margin of road, 1100 m, Hamdi (TARI 81266).

Typha laxmannii Lepechin. IRAN. Gorgan; 15 km west of Gorgan, Ilka Coconen (TARI 7790); Kourdkoy, 5 km to Bandare-Tourkemn, margin of road, Hamdi (TARI 80854). Mazandaran province; Pole-Sefid; 150 m, Akhani (TARI 65315). Guilan province; Bandare-Anzali, 25 m, Mozaffarian (TARI 66213); Rasht, 3 km to Bandare-Anzali, margin of road, Hamdi (TARI 80867). Azerbaijan province; Ardebil, 30 km to Naier, Yamchi Sofla village, Hamdi (TARI 80881); Parsabad, toward Aslandouz village, 5 km of Pirevatloo village, Hamdi (TARI 80875). Fars province; Stahbanat, south of Bash mointain, 1700- 2200 m, Mozaffarian (TARI 47032).

References

Changkyun K, Hyunchur S, Hong-Keun C (2003) A phenetic analysis of *Typha* in Korea and Far East Russia. Aquatic Botany75(1):33-43.

Davis PH (1984) Typhaceae in Flora of Turkey and East Aegean Islands, Vol. 8. Edinburg University Press, Edinburg, p. 632.

Fedorov AA (2001) Typh-aceae. In Flora of Russia. Vol. 4, pp. 472-478.

Hamdi SMM, Assadi M (2003) Typhaceae. In Hamdi SMM, Assadi M, eds., Flora of Iran 42 Verlag Paul Parey, Berlin and Hamburg, 299-317.

Hegi G (1981) Typhaceae in Illustrierte Flora von Mittel-Europa Band II Teil 1. Verlag Paul Parey Berlin and Hamburg Auschriften, 299-317.

Holmgren PK, Holmgren NH, Barnett LC (1990) Index Herbariorum. Part I. The herbaria of the world, 8th ed., Regnum vegetabile. International Association for Plant Taxonomy by New York Botanical Garden, p. 693.

Komarov V (1934) Typhaceae. In Flora U. S. S. R. Vol. 1, p. 167, Moskva-Leningrad.

Kronfeld M (1888) Monographie der Gattung Typha Tourn Typhinae Agde., (Typhaceae Schur-Engl.): Vorgelegt in der Versammlung am Verhandlungen der Zoologisch-Botanischen Gesellschaft Wien 39:89-192 (1889).

Kuehn-Marcinko M, Minor JE, White BN (1999) An examination of hybridization between the cattail species *Typha latifolia* and *Typha angustifolia* using random amplified polymorphic DNA and chloroplast DNA markers. Molecular Ecology 8(12):1981-1990.

Kuehn-Marcinko M, White BN (1999) Morphological analysis of genetically identified cattails *Typha latifolia*, *Typha angustifolia* and *Typha xglauca.* Canadian J. Botany 77:906-912.

Mavrodiev EV (2002) Two new species of *Typha* L. (Typhaceae Juss from the Far East of Russia and from Mongolia. Feddes Reportorium 113(3-4):281-288.

Moar NT (1993) Pollen grains of New Zealand dicotyledonous plants. Maanaki Whenua Press, Lincoln, Canterbury, New Zealand, p. 200.

Moore PD, Webb JA, Collinson ME (1991) Pollen analysis. Blackwell, London, p. 216.

Nassir E (1987) Typhaceae in Flora of Pakistan, No. 177:1-8.

Panich-pat T, Srinives P, Kruatrachue M, Pokethitiyook P, Upatham S, Lanza GR (2005) Electron microscopic studies on localization of lead in organ of *Typha angustifolia* grown on contaminated soil. ScienceAsia 31:49-53.

Punt W, Blackmore S, Nilsson S, Thomas, A (1999, 2007) Glossary of Pollen and Spore Terminology. LPP Foundation, Utrecht, http:// www.bio.uu.nl/_palaeo/glossary/glos-tin.htm

Riedl I (1970) Typhaceae. In Rechinger KH. ed., Flora Iranica. No. 71, Graz, pp. 1-8.

Smith SG (1967) Experimental and natural hybrids in North American *Typha* (Typhaceae). American Midland Naturalist 78:257-287.

Smith SG (2000) Typhaceae Jussieau. In Flora of North America north of

Mexico. Vol. 22, Oxford University Press, USA, pp. 278-285.
Steam WT (1993) Botanical Latin. History, grammar, syntax, terminology and vocabulary. 4th ed. David and Charles Timber Press, Newton Abbot, Devon, 546 pp.
Takhtajan AL (2001) Typhaceae. In Flora Armenii. Vol. 10. Ruggel, Liechtenstein, pp. 581-582.
Townsend CC, Guest E (1968) Typhaceae. In Flora of Iraq Vol. 7. Ministry of Agriculture of the Republic of Iraq, pp. 153-156.

Volume 54(2):127-129, 2010
Acta Biologica Szegediensis
http://www.sci.u-szeged.hu/ABS

ARTICLE

In vivo NAD(P)H fluorescence from the epidermal cells of onion (*Allium cepa*) bulb scale leaves

Csilla Slezak, Eva Herrhofer, Gabor Laskay*

Department of Plant Biology, University of Szeged, Szeged, Hungary

ABSTRACT *In vivo* fluorescence measurements were carried out on intact layers of onion (Allium cepa) bulb scale leaf epidermal cells in order to study if the blue autofluorescence can be used for monitoring the redox satate of NAD(P)H in these plant leaf cells and/or mitochondria *in vivo*. When recording the fluorescence spectra (excited at 340 nm) of the intact cell layers, a well-resolvable shoulder was always present at around 465-469 nm. An empirical formula $((F_{467}-F_{500})/F_{500})$ was derived to normalize the differential fluorescence intensity of the shoulder at 467 nm $(F_{467}-F_{500})$ to that at 500 nm (F_{500}). Treatment of the cell layers with 1 mM KCN, an inhibitor of the mitochondrial electron transport chain at Complex IV led to an increase in the $(F_{467}-F_{500})/F_{500}$ fluorescence emission ratio, leaving the fluorescence intensity of the untreated cell layers unchanged. Qualitatively similar results were obtained using 1 mM rotenone, an inhibitor of Complex I (NADH-oxidase) of the mitochondrial electron transport chain. These findings imply that the fluorescence at 467 nm derives dominantly from mitochondrial NADH in the epidermal cells of onion scale leaves. Moreover, it is concluded that the $(F_{467}-F_{500})/F_{500}$ fluorescence emission ratio can be used to observe changes in the redox state of the NAD pool in these cells.
Acta Biol Szeged 54(2):127-129 (2010)

KEY WORDS

epidermal cells
in vivo fluorescence
NAD(P)H
Allium cepa

Pyridine nucleotides (NAD^+, $NADP^+$) are the main H-carriers in both plant and animal cells and play therefore important roles in cellular bioenergetic processes. They serve as co-enzymes for various enzymatic reactions and at the same time they constitute one of the key determinants of cellular redox regulation and provide reducing equivalents for various biosynthetic processes. In addition, the roles of pyridine nucleotides in various signaling processes (Berger et al. 2004) and their connection to stress tolerance (Noctor et al. 2006) have been receiving renewed attention. Being essential determinants of cellular redox reactions, there have been various attempts to quantify the absolute or relative amounts of the oxidized or reduced forms of the various pyridine nucleotides in living cells (Eggers et al. 1982; Eng et al. 1989; Leskovac et al. 1995; Queval and Noctor 2007). Although these methods are considered accurate *in vitro*, they suffer from the major drawback of having to disrupt the cells during the extraction procedure leading to the inevitable loss of cell viability. NAD(P)H fluorescence, however, may offer an easily conducible yet reliable means to monitor the status of these redox compounds *in vivo*. Both NADH and NADPH absorb ultraviolet light with a maximum at 340 nm and emit a blue fluorescence centered at 465-470 nm while their oxidised counterparts NAD^+ and $NADP^+$ neither absorb nor fluoresce significantly at these wavelengths (Chance 1954; Galeotti et al. 1970). Monitoring the fluorescence of individual cells or tissue slices at these wavelengths therefore offers a convenient and reliable way to assess the redox state of the cells and/or the metabolic state of the mitochondria *in vivo*. This method has been successfully used in a wide range of studies with animal cells, tissues and organs (Balaban and Blum 1982; Mayevsky and Rogatsky 2007).

Epidermal cells of onion bulb scale leaves form natural mono- or bicellular layers on both sides of every scale leaf. They are valuable experimental objects as they are easy to obtain and work with. In addition, they are devoid of chloroplasts and therefore offer a convenient and appropriate experimental means with which to study the interconnection between mitochondrial functions and the redox state of the cells. The objective of this communication is to report on the successful application of NAD(P)H fluorescence in epidermal cells of onion bulb scale leaves *in vivo*.

Materials and Methods

Plant material and treatment

Brown onion (*Allium cepa* L.) bulbs were obtained from a local supplier. The same batch of onions were used throughout the experiments. Before the measurements the outer brown leaf scales of the onions were removed and the upper epidermal layer from the inner (concave) surface of the tissue between the 4th and 5th fleshy subleaves was excised care-

Accepted Dec 9, 2010
*Corresponding author. E-mail: glaskay@bio.u-szeged.hu

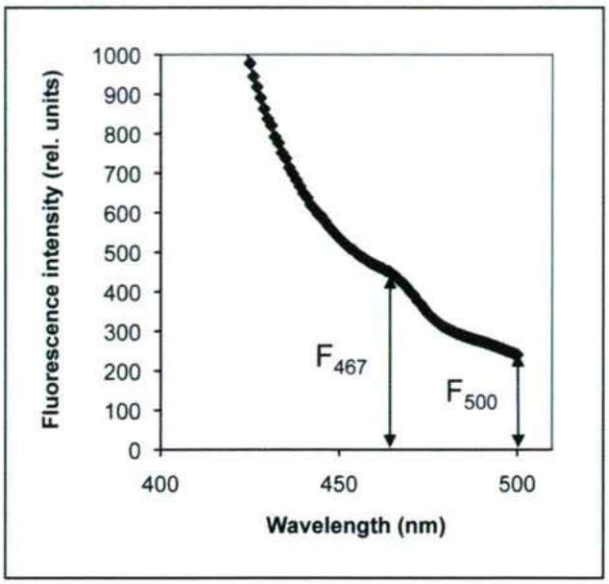

Figure 1. Representative fluorescence spectrum of an intact onion bulb epidermal cell layer excited at 340 nm. Fluorescence intensities at 467 and 500 nm (F_{467} and F_{500}, respectively) are indicated by arrows.

fully using a pair of forceps and placed immediately into an incubation solution containing 0.1 mM KCl, 0.05 mM $CaCl_2$, 5 mM HEPES, pH 6.5. Typically, a section of approximately 10-15 mm x 10-15 mm was prepared for analysis using a combination of razor and scalpel blades. The control and treated samples were examined in parallel experiments carried out on the same day, using leaf cell layers from the same bulb for each experiment. The experiments were repeated at least 3 times on the same day using different bulbs of the same batch for different parallel experiments. The samples were placed in the incubation solution in the presence or absence of 1 mM KCN, an inhibitor of Complex I (Cooper and Brown 2008) or rotenone, an inhibitor of Complex I (Soole and Menz 1995) of the mitochondrial electron transport chain.

Fluorescence measurements

For fluorescence measurements the cell layers were applied to a manually shaped plastic plate of 0.8 x 0.3 cm, which was then carefully immersed diagonally in a 1-cm quartz glass cuvette containing the incubation solution. The cuvette was placed in the sample holder of a Hitachi F-2500 recording spectrofluorimeter. The plate was oriented at 45° with respect to the excitation light beam and so the perpendicularly emitted fluorescence was directed towards the detector. All experiments were carried out at room temperature.

Data analysis and statistical treatments

For the quantitation of the fluorescence intensities at 467 and 500 nm, fluorescence spectra were recorded of the cell layers. Every registered spectrum was converted into an Excel file from which the fluorescence intensities were recorded. All experiments were repeated 9 times (3 parallel experiments on 3 different days) and the values are expressed as the mean fluorescence intensity ± SD (n=number of experiments). Statistically significant differences ($p<0.005$) were assessed by the use of Student's *t*-test.

Results and Discussion

A representative fluorescence spectrum (excited at 340 nm) of an intact onion bulb scale leaf epidermal layer *in vivo* is shown in Figure 1. A shoulder at 465-469 nm can be resolved in the spectrum. This shoulder lies exactly in the range of the NAD(P)H fluorescence emission maximum measured both *in vitro* and *in vivo* (Chance 1954; Galeotti et al. 1970). An

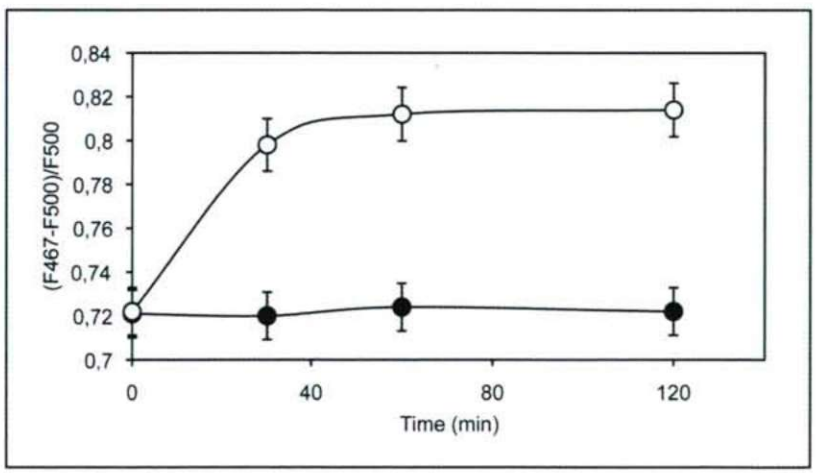

Figure 2. Effect of 1 mM KCN (open circles) on the $(F_{467}-F_{500})/F_{500}$ fluorescence emission ratio in the epidermal cells of onion bulb scale leaves in the function of time. Each point represents the mean ± S.D. from 9 independent experiments.

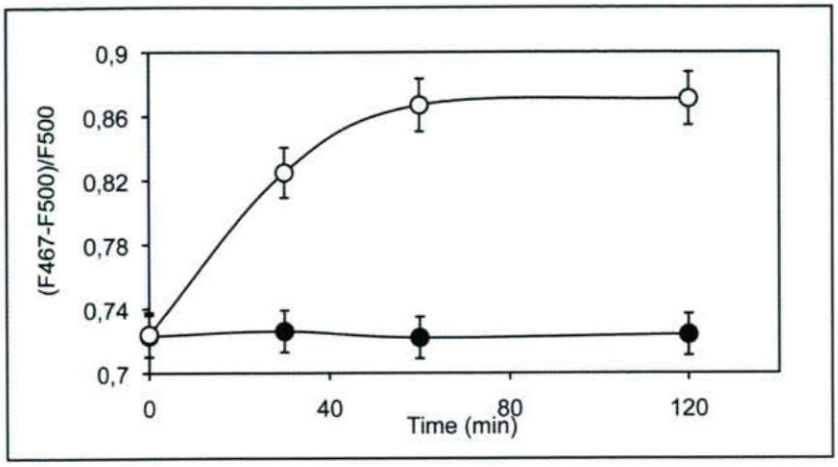

Figure 3. Effect of 1 mM rotenone (open circles) on the $(F_{467}-F_{500})/F_{500}$ fluorescence emission ratio in the epidermal cells of onion bulb scale leaves in the function of time. Each point represents the mean ± S.D. from 9 independent experiments.

empirical formula $(F_{467}-F_{500})/F_{500}$ was derived to normalize the differential fluorescence intensity at 467 nm $(F_{467}-F_{500})$ to that of 500 nm (Fig. 1).

KCN, a commonly used inhibitor of the mitochondrial electron transport chain at Complex IV (cytochrome c oxidase, Cooper and Brown 2008) was used at 1 mM concentration to study if the observed fluorescence at 467 nm was sensitive to the inhibition of the mitochondrial electron transport. Treatment of epidermal cells of onion bulb scale leaves with 1 mM KCN induced significant elevation in the fluorescence intensity at 467 nm during the examination period (0 to 2 hours), leaving the fluorescence intensity of the untreated samples unchanged (Fig. 2). This finding indicates that the *in vivo* fluorescence at 467 nm reflects the inability of the mitochondrial electron transport to reoxidise NADH and therefore it indicates that the fluorescence at 467 nm originates mainly from the NADH in the mitochondria in the epidermal cells of onion scale leaves.

Plant mitochondria exhibit an alternative electron transport route mediated by the alternative oxidase bypassing the KCN site (Maxwell et al. 1999). Therefore, the direct inhibition of NADH oxidation was also studied using 1 mM rotenone, a specific inhibitor of Complex I (NADH oxidase) of the mitochondria (Soole and Menz 1995). Rotenone treatment produced qualitatively similar results to those obtained by the use of KCN, it induced significant elevation in the fluorescence intensity at 467 nm during the examination period (0 to 2 hours) leaving the fluorescence intensity of the untreated samples unchanged (Fig. 2). This finding gives further support that the 467-nm fluorescence originates mainly from the NADH in the mitochondria in the epidermal cells of onion scale leaves. Moreover, it is concluded that monitoring the fluorescence intensity at 467 nm can be used to study the redox state of the NAD pool *in vivo*.

References

Balaban RS, Blum JJ (1982) Hormone-induced changes in NADH fluorescence and O_2-consumption of rat hepatocytes. American J. Physiol. - Cell Physiology 242:C172-C177.

Berger F, Ramírez-Hernández MH, Ziegler M (2004) The new life of a centenarian: signalling functions of NAD(P). Trends Biochem Sci 29:111-118.

Chance B (1954) Spectrophotometry of intracellular respiratory pigments. Science 120:767-775.

Cooper CE, Brown GC (2008) The inhibition of mitochondrial cytochrome oxidase by the gases carbon monoxide, nitric oxide, hydrogen cyanide and hydrogen sulfide: chemical mechanism and physiological significance. J Bioenerg Biomembr 40:533-539.

Eng J, Lynch RM, Balaban RS (1989) Nicotinamide adenine dinucleotide fluorescence spectroscopy and imaging of isolated cardiac myocytes. Biophys J 55:621-630.

Eggers HM, Halsall HB, Heineman WR (1982) Enzyme immunoassay with flow-amperometric detection of NADH. Clin Chem 28:1848-1851.

Galeotti T, van Rossum GDV, Mayer DH, and Chance B (1970) On the fluorescence of NAD(P)H in whole-cell preparations of tumours and normal tissues. Eur J Biochem 17:485-496.

Leskovac V, Trivić S, Anderson BN (1995) A novel spectrophotometric method for the enzymatic determination of NAD^+ and NADH. Acta Physiol Hung. 83:243-248.

Maxwell DP, Wang Y, McIntosh L (1999) The alternative oxidase lowers mitochondrial reactive oxygen production in plant cells. Proc. Natl. Acad. Sci. USA 96:8271-8276.

Mayevsky A, Rogatsky GG (2007) Mitochondrial function in vivo evaluated by NADH fluorescence: from animal models to human studies. Am J Physiol Cell Physiol 292: C615-C640.

Noctor G, Queval G, Gakière B (2006) NAD(P) synthesis and pyridine nucleotide cycling in plants and their potential importance in stress conditions. J Exp Bot 57:1603-1620.

Queval G, Noctor G (2007) A plate reader method for the measurement of NAD, NADP, glutathione, and ascorbate in tissue extracts: Application to redox profiling during Arabidopsis rosette development. Anal Biochem 363:58-69.

Soole KL, Menz RI (1995) Functional molecular aspects of the NADH dehydrogenases of plant mitochondria. J Bioenerg Biomembr 27:397-406.

Tabata M, Totani M, Murachi T (1990) A chemiluminometric method for NADPH and NADH using a two-enzyme bioreactor and its application to the determination of magnesium in serum. Biomed Chromatogr 4:123-127.

Volume 54(2):131-134, 2010
Acta Biologica Szegediensis
http://www.sci.u-szeged.hu/ABS

ARTICLE

Antimicrobial effects of commercial herbs, spices and essential oils in minced pork

Judit Krisch[1]*, Zsuzsanna Pardi[1], Rentsenkhand Tserennadmid[2], Tamás Papp[3], Csaba Vágvölgyi[3]

[1]Institute of Food Engineering, Faculty of Engineering, University of Szeged, Szeged, Hungary, [2]Institute of Biology, Mongolian Academy of Sciences, Ulaanbaatar, Mongolia, [3]Department of Microbiology, Faculty of Science and Informatics, University of Szeged, Szeged, Hungary

ABSTRACT Effect of fresh and dried garlic, onion, thyme and oregano on the bacterial germ count of minced pork stored at 5°C was evaluated. All spices were added in 1% concentration. Furthermore, MIC (Minimal Inhibitory Concentration) values of marjoram and thyme essential oils on *Escherichia coli* were determined *in vitro*, and their antibacterial effect was tested in minced pork inoculated with *E. coli*. In general, fresh spices showed weak or no inhibition on the total cell count of minced pork, or even caused increased microbe count. On the contrary, dried garlic and thyme decreased total cell count with 1 or two orders of magnitude. MIC values for marjoram and thyme essential oils were 0.5 µl/ml and 2 µl/ml, respectively. The essential oils decreased *E. coli* cell number in minced pork with 1 log cfu after 24 h storage at 5°C.

Acta Biol Szeged 54(2):131-134 (2010)

KEY WORDS

antibacterial effect
essential oils
herbs
minced pork
spices

Herbs and spices are used for flavoring foods but also, since ancient times, as medicines against a variety of diseases. Garlic (*Allium sativum*) and onion (*Allium cepa*) possess many biological activities including antimicrobial, antioxidant, anticarcinogenic, immunomodulatory and prebiotic action. The biological and medical effects of garlic and onion are mainly due to their high content of organo-sulphur compounds, such as alliin and allicin and their breakdown products. Flavonoids, abundant in onion but practically absent in garlic, are also responsible for a great part of the health benefits of both vegetables (Corzo-Martinez et al. 2007). *In vitro* and *in vivo* studies have shown a great effectiveness of garlic and onion against a broad spectrum of fungi and yeasts, including certain *Candida, Torulopsis, Cryptococcus* and *Aspergillus* species. Garlic has been proven to inhibit the growth of gram positive and gram-negative bacteria including strains of, e.g. *Pseudomonas, Proteus, Escherichia,, Staphylococcus, Salmonella* (Iwalokun et al. 2004; Uhart et al. 2006). Onion, however, unlike garlic, was not effective against gram-negative bacteria (Corzo-Martinez et al. 2007).

Essential oils in aromatic plants are among the most important active constituents of herbs and spices. Their efficiency against a wide range of microorganisms is well documented. *Thymus* species are used as medicinal and aromatic plants, as well as in cosmetics and perfumery. The essential oil of *Thymus vulgaris* contains various levels of thymol and/or carvacrol, phenolic derivatives with strong and wide-spectrum antimicrobial activity (Nevas et al. 2004).

Accepted Oct 21, 2010
*Corresponding author. E-mail: krisch@mk.u-szeged.hu

Origanum vulgare has been applied in traditional medicine, as well as in agriculture, pharmaceutical and cosmetic industry. Antimicrobial activity of *Origanum vulgare* essential oil (with carvacrol as the main compound) against bacteria and fungi has been reported (Nevas et al. 2004; Carvo et al. 2008). *Origanum majorana* also possesses substantial antimicrobial effects (Tserennadmid et al. 2010).

There is a growing interest in using natural compounds in food protection instead of chemical preservatives (Burt 2004; Abdel-Hammiad et al. 2009). Minced meat is one of the most perishable foods. Several strategies have been investigated to extend the shelf life of fresh meat products; one is the use of natural antioxidants and antibacterials of plant origin, alone or in combination with other preservation techniques (Busatta et al. 2008; Del Nobile et al. 2009).

We studied the germ count reducing effect of fresh and dried garlic, onion, thyme and oregano in 1% concentration in minced pork stored at 5°C. We supposed that fresh spices contain bioactive ingredients in higher concentrations than dried ones, which probably lose part of the drug during drying. Antibacterial effect of thyme and marjoram essential oils against *E. coli* in inoculated minced pork was also evaluated.

Materials and Methods

Bacterium and growth conditions

Escherichia coli SZMC 0582 (Szeged Microbiological Collection) was grown on Luria-Bertani medium (LB; 1% tryptone, 0.5% yeast extract, 1% NaCl) and was incubated at 37°C.

Table 1. Effect of onion and garlic on the MPN of minced pork stored at 5°C. (Onion was added in 2% and garlic in 1%.).

Time (h)	Onion			Garlic		
	Control	Dried	Fresh	Control	Dried	Fresh
0	2.3×10^2	2.3×10^2	2.3×10^2	2.3×10^2	2.3×10^2	2.3×10^2
24	2.4×10^3	2.4×10^3	6.6×10^4	6.6×10^3	6.6×10^3	6.6×10^4
48	2.4×10^4	6.6×10^4	2.4×10^5	2.4×10^5	6.6×10^4	2.4×10^5
72	1×10^6	2.4×10^4	2.4×10^5	7×10^4	7×10^4	2.4×10^5

Table 2. Effect of thyme and oregano on the MPN of minced pork stored at 5°C. (The herbs were added in 1%.).

Time (h)	Thyme			Oregano		
	Control	Dried	Fresh	Control	Dried	Fresh
0	6.2×10^1	6.2×10^1	6.2×10^1	2.4×10^2	2.4×10^2	2.4×10^2
24	2.4×10^4	6.6×10^3	2.4×10^5	2.4×10^2	2.4×10^2	2.4×10^2
48	2.4×10^3	2.4×10^3	2.4×10^4	2.4×10^3	6.2×10^2	2.4×10^4
72	2.3×10^4	1.3×10^5	6.2×10^4	2.4×10^3	2.4×10^4	2.4×10^4

Table 3. Combined effect of onion or garlic and 1% salt on the MPN of minced pork stored at 5°C. (Onion was added in 2% and garlic in 1%.)

Time (h)	Onion + salt			Garlic + salt		
	Control	Dried	Fresh	Control	Dried	Fresh
0	2.4×10^2	2.4×10^2	2.4×10^2	6.2×10^1	6.2×10^1	6.2×10^1
24	2.4×10^4	6.6×10^4	6.6×10^3	2.4×10^2	6.1×10^1	2.4×10^2
48	5×10^3	2.4×10^3	6.1×10^3	2.4×10^3	2.4×10^2	6.6×10^3
72	2.3×10^4	6.1×10^3	6.1×10^4	2.4×10^5	2.4×10^3	2.4×10^5

Herbs, spices and essential oils

All investigated materials were purchased in local shops in Szeged (Hungary). The essential oils were purchased from Aromax Natural Products (Budapest, Hungary).

The bulbs of *Allium sativum* (garlic) and *Allium cepa* (onion) were peeled and crushed before use. The aerial parts of *Thymus vulgaris* (thyme) and *Origanum vulgare* (oregano) were washed, rinsed with sterile distilled water, and chopped just before addition to the meat. All spices and essential oils were stored at room temperature.

In vitro tests of antibacterial activity

Agar hole diffusion test was used to investigate the antibacterial activity of the fresh and dried spices on *E. coli*. Solid culture media were overlaid with a suspension of 10^5 cells in 1 ml of distilled water and were dried. One gram of the crushed or chopped fresh herbs was mixed with 5 ml sterile distilled water. After 30 min, samples were centrifuged and the supernatant was used in the tests. Dried spices were extracted with hot water (5 ml for 1 g), centrifuged and the supernatants were used. Aliquots (100 µl) of the supernatants were filled into wells of 8 mm diameter; and sterile water was used as negative control. The diameter of the inhibition zones was measured after incubation at 37°C for 24 h. The experiments were repeated three times.

Evaluation of MIC values for essential oils

The MIC values of the essential oils were determined by macrodilution assays. The thyme and marjoram oils were added directly to LB medium resulting in final concentrations of from 0.0625 µl/ml to 2 µl/ml in twofold increments. The tubes were inoculated with 10^5 CFU/ml *E. coli* and then incubated at 37°C for 24 h. MICs were taken as the lowest concentration at which no visible growth occurred.

Antibacterial activity in minced pork: Fresh and dried herbs/spices alone or in combination, with and without 1% salt, were mixed in 1% concentration to minced pork (100 g). The meat was stored at 5°C. Every day, total and coliform MPN (Most Probably Number) was determined (Roberts and Greenwood 2003) for 72 h. Essential oils of thyme and marjoram were added to the minced pork, previously inoculated with 2×10^5 *E. coli*, in a concentration range from 0,125 to 1%

Table 4. Combined effect of thyme or oregano with 1% salt on the MPN of minced pork stored at 5°C. (The herbs were added in 1%.)

Time (h)	Thyme + salt			Oregano + salt		
	Control	Dried	Fresh	Control	Dried	Fresh
0	<10	<10	<10	6.2×10^1	6.2×10^1	6.2×10^1
24	2.4×10^2	2.4×10^2	2.4×10^3	2.4×10^3	2.4×10^3	6.6×10^3
48	2.4×10^4	2.4×10^3	6.1×10^4	6.6×10^3	6.2×10^4	2.4×10^4
72	2.4×10^5	2.4×10^5	7×10^5	2.4×10^5	2.3×10^4	6.2×10^4

Table 5. Effect of mixed spices and salt on the germ count of minced pork after 72 h incubation at 5°C.

Onion + thyme + salt			Onion + garlic + salt			Onion + oregano + salt		
Control	Dried	Fresh	Control	Dried	Fresh	Control	Dried	Fresh
2.4×10^3	2.4×10^4	1.3×10^4	2.3×10^4	7×10^5	6.6×10^5	6.6×10^2	2.4×10^3	2.4×10^2

Table 6. Effect of spices and herbs on the MPN of coliforms in minced pork after 72 h storage at 5°C.

Spice/herb	Control	Dried	Fresh
Onion	6.6×10^2	6.6×10^2	2.4×10^3
Onion + salt	6.2×10^2	<10	<10
Garlic	2.4×10^3	2.4×10^2	6.2×10^2
Garlic +salt	6.2×10^1	2.2×10^1	6.2×10^2
Thyme	6.0×10^1	2.3×10^2	1.3×10^3
Thyme + salt	2.3×10^1	2.3×10^1	<10
Oregano	2.3×10^1	2.4×10^2	2.3×10^1
Oregano + salt	2.3×10^1	<10	<10

Table 7. *E. coli* CFU count of minced pork treated with different concentrations of essential oils. (Size of inoculum: 4×10^5 CFU/ml).

Concentration (% w/w)	0	0.125	0.25	0.5	1.0
Thyme	7.5×10^5	7.5×10^5	4.1×10^5	2.2×10^5	1.3×10^5
Marjoram	6.5×10^5	6.5×10^5	4.0×10^5	3.0×10^5	7.5×10^4

(w/w). After 24 h incubation *E. coli* CFU (Colony Forming Unit) was determined on VRBG agar (Merck).

Results and Discussion

Inhibition zones for water extracts of dried and fresh garlic were 16.5 ± 2.32 mm and 18.82 ± 1.84 mm, respectively. No inhibition zone was detected with the other herbs and spices. Iwalokun et al. (2004) found an inhibition zone of 23.7 ± 2.4 mm of aqueous garlic extract for *E. coli.* In their study, garlic also exerted an excellent antibacterial and antifungal effect against various multidrug-resistant bacterial isolates and certain *Candida* species. In general, fresh and dried spices showed weak or no inhibition on the total cell count of minced pork (Table 1 and 2). Furthermore, in some cases, the microbe number increased. Supplementation with 1% salt resulted in germ count reduction by dried onion and garlic, and dried and fresh oregano (Table 3 and 4). The combination of onion with the other spices plus salt had no reducing effect on the germ count, MPN was the same or even greater than that of the control (Table 5). These spices exerted more considerable antimicrobial effect on coliform bacteria when salt was added (Table 6). In general, it can be said, that the spices mostly failed to exert considerable growth reducing effect in fresh or in dried form. The number of germs was influenced by the initial number of germs in minced meat. Our results agreed well with the results of Uhart and coworkers (2004) who found that spices (garlic, ginger and turmaric) inhibited *Salmonella* Typhimurium DT 104 when they were in direct contact. However, when the spices were added to a complex food system such as ground beef, the inhibitory activity was considerably decreased.

The MIC values of thyme and marjoram essential oils were 0.5 and 2 µl/ml in LB medium. We were not able to determine MIC values in minced pork, only the highest concentration (1%) of marjoram oil reduced the *E. coli* CFU/ml with 1 log (Table 7). In the study by Busatta et al (2008), MIC of marjoram essential oil against *E. coli* was 0.92 mg/ml. They applied marjoram oil in fresh sausage inoculated with *E. coli*, and after 25 days of incubation the MPN was reduced by approximately 1 log. The main component in marjoram EO having antibacterial activity is terpinene-4-ol, causing changes in membrane permeability. The main component of thyme essential oil, thymol was effective on coliforms and Enterobacteriaceae in minced beef patties (Del Nobile et al. 2009). Thyme, oregano and savory essential oils showed the broadest antibacterial activity in the study of Nevas et

al. (2004). In our experiments, thyme EO had only a slight CFU reduction effect which might be due to differences in its composition.

Herbs, spices and essential oils in minced pork had variable and moderate antibacterial effect in our study. Best candidates for prolonging minced pork shelf life are garlic and marjoram essential oil. Further experiments are needed to evaluate the antibacterial effect of these substances combined with other hurdle techniques.

Acknowledgments

This work was supported in part by the grant NKTH TéT MN-1/2009.

References

Abdel Hammiad AA, Nassar AG, El-Badry N (2009) Investigation on antioxidant and antimicrobial activities of some natural extracts. World J Dairy Food Sci 4:01-07.

Burt S (2004) Essential oils: antibacterial application and potential applications in foods - a review. Int J Food Microbiol 94:223-253.

Busatta C, Vidal RS, Popiolski AS, Mossi AJ, Dariva C, Rodrigues MRA, Corazza FC, Corazza M, Oliviera JV, Cansian RL (2008) Application of *Origanum majorana* L. essential oil as an antimicrobial agent in sausage. Food Microbiol 25:207-211.

Carvo ES, de Oliveira Lima E, de Souza E (2008) The potential of *Origanum vulgare* L (Lamiaceae) essential oil in inhibiting the growth of some food-related *Aspergillus* species. Braz J Microbiol 39:362-367.

Corzo-Martinez M, Corzo N, Villamiel M (2007) Biological properties of onions and garlic. Trends Food Sci Technol 18:609-615.

de Souza EL, Montenegro Stamford TL, de Oliveira Lima E, Trajano VN, Barbosa Filho JM (2005) Antimicrobial effectiveness of spices: an approach for use in food conservation systems. Braz Arch Biol Technol 48:549-558.

del Nobile MA, Conte A, Cannarsi M, Sinigaglia M (2007) Strategies for prolonging the shelf life of minced beef patties. J Food Safe 29:14-25.

Iwalokun BA, Ogunledun A, Ogbolu DO, Bamiro SB, Jimi-Omojola J (2004) In vitro antimicrobial properties of aqueous garlic extract against multidrug-resistant bacteria and *Candida* species from Nigeria. J Med Food 7:327-333.

Nevas M, Korhonen A-R, Lindström M, Turkki P, Korkeala H (2004) Antibacterial efficiency of Finnish spice essential oils against pathogenic and spoilage bacteria. J Food Prot 67:199-202.

Roberts D, Greenwood M (2003) Practical Food Microbiology. Blackwell Publishing, Oxford, pp. 118-122.

Tserennadmid R, Takó M, Galgóczy L, Papp T, Vágvölgyi Cs, Gerő L, Krisch J (2010) Antibacterial effect of essential oils and interaction with food components. Cent Eur J Biol 5:641-648.

Uhart M, Maks N, Ravishankar S (2006) Effect of spices on growth and survival of *Salmonella* Typhimurium DT 104 in ground beef stored at 4 and 8°C. J Food Safety 26:115-125.

Volume 54(2):135-141, 2010
Acta Biologica Szegediensis
http://www.sci.u-szeged.hu/ABS

ARTICLE

Statistical optimization of conditions for protease production from *Bacillus* sp.

Rajshree Saxena[1], Rajni Singh[2]*

[1]Amity Institute of Biotechnology, Amity University, Sector-125, Noida, Uttar Pradesh, India, [2]Amity Institute of Microbial Biotechnology, Amity University, Sector-125, Noida, Uttar Pradesh, India

ABSTRACT Response surface methodology was employed for the optimization of different nutritional and physical parameters for the production of protease by a soil isolated *Bacillus* strain in submerged fermentation. Initial screening of production parameters as carbon (glucose) and nitrogen source (soybean) were optimized together with four variables K_2HPO_4, NaCl, $MgSO_4.7H_2O$, $CaCl_2.2H_2O$ and four physical parameters including agitation, inoculum size, pH and time was performed using Plackett Burman design and the variables with statistically significant effect on the protease production identified. These variables were selected for further optimization studies using central composite design in RSM. The protease activity under unoptimized conditions was 330 U/ml. Under the final optimized conditions, the predicted response for protease production was 449 U/ml, and the observed validated experimental value was 577 U/ml. The statistical optimization by response surface methodology resulted in about two fold increase in the production of the enzyme by the selected bacterial strain

Acta Biol Szeged 54(2):135-141 (2010)

KEY WORDS

central composite design protease optimization
Placket Burman design
production media
response surface methodology

Proteases, also known as peptidyl-peptide hydrolases (EC 3.4.21-24 and 99) are industrially useful enzymes which catalyze the hydrolysis of a peptide bond in a protein molecule. Microbial proteases, especially from *Bacillus* sp. have traditionally held the predominant share of the industrial enzyme market of the worldwide enzyme sales with major application in food and feed, leather, detergent, pharmaceutical, silk, and recovery of silver from photographic films (Anisworth 1994; Outtrup et al. 1995; Inhs et al. 1999).

Protease production by microorganism is highly influenced by media components as carbon, nitrogen ratio, presence of some easily metabolizable sugars such as glucose (Gupta et al. 2002; Beg et al. 2002; Ferrero et al. 1996) and metal ions (Varela et al. 1996). Besides this several other factors such as aeration, inoculums, density, pH, temperature and incubation time also affect the amount of protease produced (Nehete et al. 1985; Hameed et al. 1999). Process optimization is a topic of central importance in industrial production processes with particular regard to biotechnology (Reddy et al. 2008). Optimization of medium by the classical method involves changing one independent variable while maintaining all others at a fixed level is extremely time consuming and expensive when a large number of variables are evaluated. To overcome this difficulty, experimental factorial design and response surface methodology can be employed to optimize the medium components.

Accepted Nov 2, 2010
*Corresponding author. E-mail: rsingh3@amity.edu
rajni_vishal@yahoo.com

The Plackett–Burman factorial designs allow for the screening of main factors from a large number of process variables, and these designs are thus quite useful in preliminary studies in which the principal objective is to select variables that can be fixed or eliminated in further optimization processes as response surface methodology (RSM). RSM is a collection of statistical and mathematical techniques useful for the modeling and analysis of problems in which a response of interest is influenced by several variables, with the objective being to optimize this response (Montgomery, 2001). Response surface methodology has eliminated the drawbacks of classical methods and has proved to be powerful and useful for the optimization of the target metabolites production (Deepak et al. 2008; Liu and Wang 2007; Sayyad et al. 2007). Second-order models like Central Composite Box–Behnken and Doehlert designs are widely used in RSM as they can take on a wide variety of functional forms, and this flexibility allows them to more closely approximate the true response surface (Srinivas et al. 1994; Carvalho et al. 1997; Adinarayan and Elliah 2002; Rahman and Gomes 2003; Li et al. 2007; Xiao et al. 2007). Moreover, it is easy to estimate the parameters in a second-order model using the method of least squares. RSM has been recently used for the modelling and optimization of several bioprocesses, including fermentations (Sen 1997) enzymatic reactions (Ferreira et al. 1998) product recovery (Annadurai et al. 1996) and enzyme immobilization techniques (Zhao et al. 2007; Chang et al. 2007). The application of experimental design and response surface methodology in fermentations process can result in improved

Table 1. Design Placket Burman.

Std Run	Factor 1 A: Glucose %	Factor 2 B: Soybean %	Factor 3 C: K_2HPO_4 %	Factor 4 D: $MgSO_4$ %	Factor 5 E: NaCl %	Factor 6 F: $CaCl_2$ %	Factor 7 G: Agitation RPM	Factor 8 H: Inoculum %	Factor 9 J: pH	Factor 10 K: Time h	Response 1 Protease Activity U/ml
1	2	5	0.05	0.5	0.5	0.2	120	1	8	48	187.6
2	1	5	0.5	0.01	0.5	0.2	180	1	8	24	218.4
3	2	2	0.5	0.5	0.05	0.2	180	3	8	24	228.2
4	1	5	0.05	0.5	0.5	0.01	180	3	10	24	234.4
5	1	2	0.5	0.01	0.5	0.2	120	3	10	48	200.2
6	1	2	0.05	0.5	0.05	0.2	180	1	10	48	238
7	2	2	0.05	0.01	0.5	0.01	180	3	8	48	330.2
8	2	5	0.05	0.01	0.05	0.2	120	3	10	24	166.6
9	2	5	0.5	0.01	0.05	0.01	180	1	10	48	231.2
10	1	5	0.5	0.5	0.05	0.01	120	3	8	48	240.8
11	2	2	0.5	0.5	0.5	0.01	120	1	10	24	35.2
12	1	2	0.05	0.01	0.05	0.01	120	1	8	24	134.2

product yields, reduced process variability and development time and over all costs (Rao et al. 2000).

This paper aims to optimize the composition of the production medium and the cultivation parameters of the bioprocess for obtaining protease by *Bacillus* strain using the response surface methodology

Materials and Methods

Isolation and screening of protease producing strain

About 45 strains were isolated from soil collected from various sites. Primary screening of the isolates for protease production was done by milk agar plate method. The strain exhibiting largest zone of hydrolysis was selected for further experimentation. Stock culture of the organism was maintained at -20°C in 50% glycerol.

Protease production

Enzyme production was studied in media containing (g/l) glucose 10.0, soybean 10.0, K_2HPO_4 5.0, $MgSO_4$.$7H_2O$ 0.5, NaCl 0.5 and $CaCl_2$ 0.5. Batch mode shake flask experiments were conducted at 37°C and 120 rpm for 24 h in100-ml Erlenmeyer flasks containing 50 ml of the media. The production media was inoculated with 1% of inoculums and incubated in a shaking incubator. The fermentation broth was then centrifuged at 10,000 g for 10 min in a centrifuge, and the total protease activity in the cell-free supernatant was determined.

Enzyme assay

Protease activity was measured using casein as substrate. The enzyme extract suitably diluted, was mixed with 50 mM glycine–NaOH buffer (pH 8) to make 1 ml volume. 1ml of 1% casein was added and incubated for 10 min at 60°C. The reaction was stopped by addition of 0.5 ml TCA (20%, w/v). The mixture was allowed to stand at room temperature for 30 min to 1 h and then filtered to remove the precipitate. 1 ml of the filtrate was mixed with 5 ml of 0.5 M Na_2CO_3 solution. 0.5 ml of Folin Ciocalteu's (phenol reagent) reagent was added and the mixture was incubated in dark to develop the blue colour. The blue coloured solution was then was estimated spectrophotometrically at 660 nm. One unit of protease activity was defined as the amount of enzyme required to liberate 1 µg tyrosine per millilitre in 1 min under the experimental conditions used. The experiments were carried out in triplicates and standard error was calculated.

Optimization of media

The optimization of media for enzyme production was carried out using statistical design of experiments in two steps. In the first step the screening of variables which was done by Plackett- Burman design. The second step involved the optimization of significant variables by RSM employing the central composite design. Design Expert® 8.0.2.0 (Stat-Ease, Inc., Minneapolis, MN, USA) was used to design and analyze both the experiments.

Selection of significant variables by Plackett–Burman design

Plackett–Burman design is an effective method for screening for significant medium components that influence enzyme production. It allows the evaluation of N variables in the N+1 experiments; each variable is examined at two levels: -1 for a low level and +1 for a high level (Plackett and Burman 1946; Rama et al. 1999; Ghanem et al. 2000). In this part, the selected carbon (glucose) and nitrogen source (soybean) were optimized together with four variables: K_2HPO_4, NaCl, $MgSO_4$.$7H_2O$, $CaCl_2$ $2H_2O$ and four physical parameters including agitation, inoculum size, pH and time. These vari-

Table 2 a. Ranking of the variables investigated in the Plackett–Burman design.

Variable	Component	M_i^+–	M_i^-	$E(x_i)$	Absolute $E(x_i)$	Ranking
A	Glucose	1179	1266	-14.5	14.5	8
B	Soyabean	1279	1166	18.8333	18.8333	7
C	K_2HPO_4	1154	1291	-22.833	22.833	5
D	$MgSO_4$	1164.2	1280.8	-19.433	19.433	6
E	NaCl	1206	1239	-5.5	5.5	9
F	$CaCl_2$	1239	1206	5.5	5.5	10
G	Agitation	1480.4	964.6	85.9667	85.9667	1
H	Inoculum	1400.4	1044.6	59.3	59.3	4
I	pH	905.4	1339.4	-72.333	72.333	2
J	Time	1428	1017	68.5	68.5	3

Table 2 b. ANOVA for Placket Burman.

Source	Sum of Squares	df	Mean Square	F Value	p-value Prob > F	
Model	55925.61	10	5592.561	373.751	0.0402	significant
A-Glucose	630.75	1	630.75	42.15304	0.0973	
B-Soybean	1064.083	1	1064.083	71.11272	0.0751	
C-K_2HPO_4	1564.083	1	1564.083	104.5277	0.0621	
D-$MgSO_4$	1132.963	1	1132.963	75.71597	0.0728	
E-NaCl	90.75	1	90.75	6.064825	0.2456	
F-$CaCl_2$	90.75	1	90.75	6.064825	0.2456	
G-Agitation	22170.8	1	22170.8	1481.675	0.0165	
H-Inoculum	10549.47	1	10549.47	705.0214	0.0240	
J-pH	4555.203	1	4555.203	304.4244	0.0364	
K-Time	14076.75	1	14076.75	940.7496	0.0207	
Residual	14.96333	1	14.96333			
Cor Total	55940.57	11				

Std. Dev: 3.87; R-Squared: 0.9997; Adj R-Squared: 0.9971, Pred R-Squared: 0.9615; PRESS: 2154.72; Adeq Precision: 79.653.

ables screened with a twelve-run Plackett–Burman design are shown in Table 1. The effect of each variable was determined by the following equation: $E(x_i) = 2(\sum M_i^+ - M_i^-) / N$ (1) where $E(x_i)$ is the concentration effect of the tested variable, M_i^+ and M_i^- are the total production from the trials where the measured variable (x_i) was present at high and low concentrations, respectively; and N is the number of trials.

Central composite design

The next step in the optimization was to determine the optimum levels of significant variables screened by Placket Burman design. For this purpose, RSM, using a central composite design (CCD) was adopted. The CCD is a statistical experimental design where each numeric factor is varied over 5 levels- alpha points (-1.682, +1.682), 1 factor (-1, +1) and one centre point resulting in a total of 20 experiments. Three significant variables (glucose, soybean K_2HPO_4,) were chosen for the experiment. The 20 experiments were conducted in duplicates. The design is shown in Table 3 (a and b).

Statistical analysis and Modelling

The statistical analysis of the data obtained from RSM for protease production was subjected to analysis of variance (ANOVA). A second order polynomial equation (1) can be used to represent the function in the range of interest.

$$Y = \beta o + \beta_1 X_1 + \beta_2 X_2 + \beta_3 X_3 + \beta_{11} X_1^2 + \beta_{22} X_2^2 + \beta_{33} X_3^2 + \beta_{12} X_1 X_2 + \beta_{13} X_1 X_3 + \beta_{23} X_2 X_3$$

Where Y is the measured response, β_0 is the intercept term, β_1, β_2, β_3 are linear coefficient, β_{11}, β_{22}, β_{33} are quadratic coefficient, β_{12}, β_{13}, β_{23} are interaction coefficient and X_1, X_2 X_3 are coded independent variables.

Results and Discussion

The selected isolate was a *Bacillus* strain as identified on the basis of microscopic and biochemical analysis.

Table 3 a. Design Summary CCD.

Study Type			Response Surface			Runs			20	
Design Type			Central Composite			Blocks			No Blocks	
Design Model			Quadratic			Build Time (ms)			4.67898	
Factor	Name	Units	Type	Subtype	Minimum	Maximum	-1 Actual	+1 Actual	Mean	Std. Dev.
A	Glucose	%	Numeric	Continu-ous	0.659104	2.340896	1	2	1.5	0.413171
B	Soybean	%	Numeric	Continu-ous	0.977311	6.022689	2	5	3.5	1.239514
C	K_2HPO_4	%	Numeric	Continu-ous	-0.20681	1.306807	0.1	1	0.55	0.371854
Response Name	Units	Obs	Analysis	Mini-mum	Maxi-mum	Mean	Std. Dev.	Ratio	Trans	Model
Protease Activity	U/ml	20	Polyno-mial	199.65	456.64	358.8005	92.7528	2.287203	None	Quadratic

Table 3 b. Central composite design matrix for the experimental design and predicted responses for protease activity.

Std Run	Factor 1	Factor 2	Factor 3	Response 1 Protease Activity (U/ml)			
	A:Glucose %	B:Soybean %	C:K_2HPO_4 %	Actual Value	Predicted Value	Residual value	Validation Value
1	1	2	0.1	214.9	218.8342	-3.93	291.06
2	2	2	0.1	199.65	195.1977	4.452	148.5
3	1	5	0.1	309.17	306.0927	3.077	380.16
4	2	5	0.1	288.75	296.2112	-7.46	249.99
5	1	2	1	356.4	350.9927	5.407	406.89
6	2	2	1	298.65	303.7812	-5.13	317.81
7	1	5	1	440.87	447.3762	-6.51	482.24
8	2	5	1	415.8	413.9197	1.88	449.4
9	0.66	3.5	0.55	372.9	372.7273	0.173	420.76
10	2.34	3.5	0.55	327.45	324.718	2.732	361.12
11	1.5	0.98	0.55	216.98	218.4424	-1.46	252.66
12	1.5	6.02	0.55	388.8	384.4329	4.367	337.24
13	1.5	3.5	-0.21	218.6	217.2916	1.308	233.89
14	1.5	3.5	1.31	429	427.4038	1.596	500.48
15	1.5	3.5	0.55	448.45	449.7647	-1.31	577.67
16	1.5	3.5	0.55	456.64	449.7647	6.875	577.67
17	1.5	3.5	0.55	448.23	449.7647	-1.53	577.67
18	1.5	3.5	0.55	449.64	449.7647	-0.12	577.67
19	1.5	3.5	0.55	442.68	449.7647	-7.08	577.67
20	1.5	3.5	0.55	452.45	449.7647	2.685	577.67

Screening of significant variables using Plackett–Burman design

A total of ten variables were analyzed with regard to their effects on protease production using a Plackett–Burman design. The design matrix selected for the screening of significant variables for protease production and the corresponding responses are shown in Table 1. Table 2a represents the $E(x_i)$ value and ranking of the variables investigated in the Plackett–Burman design. A large $E(x_i)$ coefficient, either positive or negative, indicates a large impact on response; while a coefficient close to zero indicates little or no effect. Agitation, inoculum size and time along with chemical factors soybean and $CaCl_2$ had a positive effect on the production, while pH, glucose, K_2HPO_4, $MgSO_4$ and NaCl negatively affected the production. The adequacy of the model was calculated, and the variables evidencing statistically significant effects were screened via Student's t-test for ANOVA (Table 2b). The Model F-value of 373.75 implies the model is significant. There is only a 4.02% chance that a Model F-Value this large could occur due to noise. Values of Prob > F less than 0.0500 indicated that the model terms are significant. In this case factors G, H, J and K are significant model terms. The Predicted R-Squared of 0.9615 is in reasonable agreement with the Adjusted R-Squared of 0.9971. Adequate Precision measures

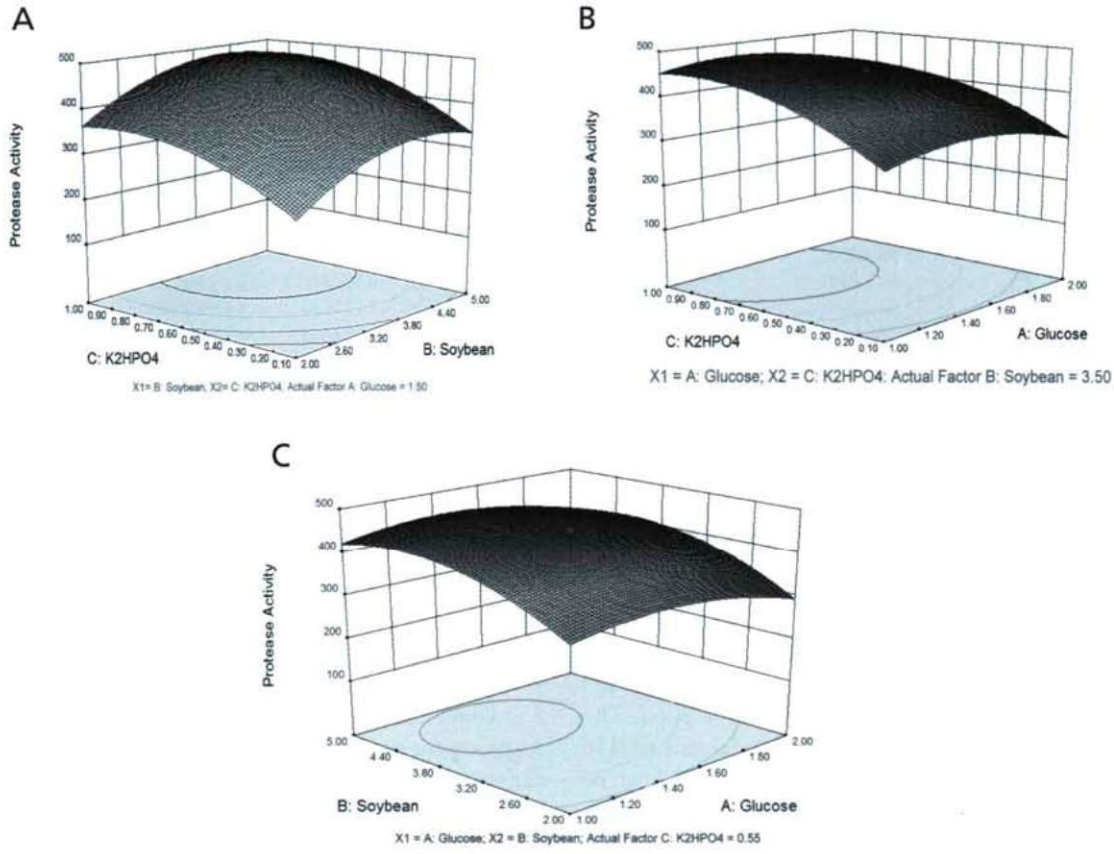

Figure 1. Contour plots of enzyme activity as a function of the interactions of two variables by keeping the other at centre level: interactions of soybean and K_2HPO_4 with glucose at 1.5% (a), interactions of glucose and K_2HPO_4 with soybean at 3.5% (b), and interactions of glucose and soybean with K_2HPO_4 at 0.55% (c).

the signal to noise ratio. A ratio greater than 4 is desirable. In our model the ratio of 79.653 indicates an adequate signal. This model can be used to navigate the design space.

Optimization of significant variables using response surface methodology

A quadratic model consisting of twenty trials experiments was designed (Table 3a). The design matrix and the corresponding results of RSM experiments to determine the effects of three independent variables (glucose, soybean and K_2HPO_4), along with the mean predicted values and the residual value are shown in Table 3b.

The ANOVA analysis of the optimization study is given in table 4. The Model F-value of 527.45 implies the model is significant. There is only a 0.01% chance that a "Model F-Value" this large could occur due to noise. The model was found to be highly significant and sufficient to represent the actual relationship between the response and the significant variables as indicated by the small model P-value (<0.0001), large lack-of-fit P-value (0.2089). The "Lack of Fit F-value" of 2.16 implies that it is non significant relative to the pure error. Non-significant lack of fit is good.

Values of "Prob > F" less than 0.0500 indicate model terms are significant.In this case A, B, C, AC, A^2, B^2, C^2 are significant model terms.

The regression equation coefficients were calculated and the data was fitted to a second-order polynomial equation. Thus the response (Y), (in terms of coded factors) protease production by the selected *Bacillus* sp. can be expressed in terms of the following regression equation:

$$\text{Protease Activity} = +449.76 - 14.27A + 49.35B + 62.47C + 3.44AB - 5.89AC + 2.28BC - 35.72A^2 - 52.44B^2 - 45.05C^2$$

Where A is glucose, B is soybean and C is K_2HPO_4.

The regression equation obtained from the ANOVA showed that the R^2 (multiple correlation coefficient) was 0.9979 (a value >0.75 indicates fitness of the model). This is an estimate of the fraction of overall variation in the data accounted by the model, indicating that the model is capable of explaining 99.79% of the variation in response. The adjusted R^2 is 0.9960. The pred R^2 of 0.9864 is in reasonable agreement with the ad-

Table 4. Analysis of variance table (ANOVA for Response Surface Quadratic Model - CCD).

Source	Sum of Squares	Df	Mean Square	F Value	p-value Prob > F	
Model	163114.9	9	18123.88	527.4532	< 0.0001	significant
A-Glucose	2782.246	1	2782.246	80.97074	< 0.0001	
B-Soybean	33259.21	1	33259.21	967.9314	< 0.0001	
C-K_2HPO_4	53290.33	1	53290.33	1550.89	< 0.0001	
AB	94.60001	1	94.60001	2.753112	0.1281	
AC	277.8903	1	277.8903	8.087346	0.0174	
BC	41.63281	1	41.63281	1.211625	0.2968	
A^2	18391.5	1	18391.5	535.2416	< 0.0001	
B^2	39632.7	1	39632.7	1153.417	< 0.0001	
C^2	29246.1	1	29246.1	851.1393	< 0.0001	
Residual	343.6112	10	34.36 112			
Lack of Fit	234.8798	5	46.97595	2.160182	0.2089	not significant
Pure Error	108.7315	5	21.7463			
Cor Total	163458.6	19				

Std. Dev: 5.86; R-Squared: 0.9979; Adj R-Squared: 0.9960; Pred R-Squared: 0.9864; Adeq Precision: 61.416.

justed R^2 of 0.9960. For a good statistical model, the R^2 value should be in the range of 0–1.0, and the values as obtained in the data analysis indicates that the model is good. The 'adequate precision value' of the present model was 61.416 which indicates an adequate signal and that the model can be used to navigate the design space.

The optimal levels of each variable for maximum protease production were determined by the three-dimensional response surface plots which were constructed by plotting the response (protease production) on the Z-axis against any two independent variables, while maintaining other variables at their optimal levels. As is shown in Fig. 1 A, a increase in protease production was observed when the concentrations of soybean and K_2HPO_4 increased initially but a concomitant decline was observed when concentration of both the components were further increased at a constant level of glucose. Similar results was observed when concentrations of glucose and K_2HPO_4 (Fig. 1B) and glucose and soybean (Fig.1C) were increased at a single concentration of soybean and K_2HPO_4 respectively. All the three figures show a fairly strong degree of curvature of 3D surface where the optimum can easily be determined.

Thus the maximum protease production was 452 U/ml after 48h when the levels of glucose, soybean and K_2HPO_4 were at their central value of 1.5, 3.5 and 0.55 % respectively

Validation of the model equation in shake flask culture

The validation of the statistically optimized condition for the production of protease by the selected Bacillus strain was verified by carrying out shake flask fermentation at bench scale in the laboratory. The model was verified for the three variables within the design space. 15 production combinations were prepared and tested for the protease production (Table 7). The protease activity under unoptimized conditions was 330 U/ml. Under the final optimized conditions, the predicted response for protease production was 449U/ml, and the observed validated experimental value was 577U/ml. These results confirmed the validity of the model, and the experimental were found to be quite close to the predicted values. The optimization of the media led to a two fold increase in the production value.

Conclusion

The use of Plackett–Burman design and Central Composite Design in Response Surface Methodolgy for determination of optimal medium composition for protease production is demonstrated in the present study. The optimization resulted in about two fold increase in the production of the enzyme by the selected bacterial strain. The results show the effect of various factors on the enzyme production. The results of ANOVA and regression of the second-order model showed that the effects of glucose, soybean and K_2HPO_4 and the interactive effects of all variables are more significant for protease production.

References

Adinarayana K, Ellaiah P (2002). Response surface optimization of the critical medium components for the production of alkaline proteases by a newly isolated *Bacillus* sp. J Pharm Pharmaceut Sci 5(3):272-278.

Annadurai G, Raju V, Chellapandian M, Krishnan MRV (1996) Citric acid production. Bioprocess Eng 16:13-5.

Anisworth SJ (1994) Soap and Detergents. Chem Engineering news 72:34-59.

Beg QK, Saxena RK, Gupta R, (2002) De- repression and subsequent induction of protease synthesis by *Bacillus mojevenesis* under fed- batch operations. Process Biochem 37:1103-1109

Carvalho CML, Serralheiro MLM, Cabral JMS, Airebarros MR (1997) Application of factorial design to the study of transesterification reactions using cutinase in AOT-reversed micelles. Enzyme Microb Technol 21:117-123.

Chang SF, Chang SW, Yen YH, Shieh CJ (2007) Optimum immobilization of *Candida rugosa* lipase on celite by RSM. Appl Clay Sci 37:67-73.

Deepak V, Kalishwaralal K, Ramkumarpandian S, Babu, SV, Senthilkumar SR, Sangiliyandi G (2008). Optimization of media composition for Nattokinase production by *Bacillus subtilis* using response surface methodology. Biores Technol 99:8170-8174.

Ferrero MA, Cartro GR, Abate CM, Baigori MD, Sineriz F, (1996) Thermostable alkaline protease of *Bacillus licheniformis* MIR 29: isolation production and characterizaion. Appl Micrbiol Biotechnol 45:327-332.

Ferreira-Dias S, Duarte CS, Falaschi V, Marques SR, Gusmao JH, da Fonseca MMR. In Stability and Stabilization of Biocatalysts. Ballesteros A, Plou FJ, Iborra JL, Halling P, eds., Elsevier; Amsterdam, The Netherlands, 1998.

Greasham RL (1983) Biotechnology. In Rehm, H.J., Read, G., Puhler, A., Stagler P eds., Bioprocessing. VCH Publishers, New York USA pp. 128-139.

Gupta R, Beg QK, Khan S, Chandan B (2002) An overview on fermentation, downstream processing and properties of microbial alkaline protease, Appl Micrbiol Biotechnol 60:381-395.

Hameed A, Keshavarz T, Evans CS (1999) Effect of dissolved oxygen tension and pH on the production of extracellular protease from a new isolate of *Bacillus subtilis* K2, for use in leather processing. J Chem Technol Biotechnol 74:5-8

Inhs DA, Schimdt W, Ritcher FR (1999) Proteaolytic enzyme cleaner,US. Patent Number 5961366.

Kole MM, Draper I, Gerson DF (1988) Production of protease by *Bacillus subtilis* using simultaneous control of glucose and ammonium concentrations. J Chem Technol Biotechnol 41:197-206.

Li J, Ma C, Ma Y, Li Y, Zhou W, Xu P (2007) Medium optimization by combination of response surface methodology and desirability function: an application in glutamine production. Appl Microbiol Biotechnol 74:563-571.

Liu, GQ, Wang XL (2007) Optimization of critical medium components using response surface methodology for biomass and extracellular polysaccharide production by *Agaricus blazei*. Appl Microbiol Biotechnol 74:78-83.

Montgomery DC (2001) Design and analysis of experiments. New York, John Wiley & Sons.

Nehete PN, Shah VD, Kothari RM (1985) Profiles of alkaline protease production as a function of composition of the state of culture Biotechnol Lett 7:413-418.

Outtrup H, Dambmann C, Christiansen M, Aaslyng DA (1995) *Bacillus* sp.JP 395, Method of making and detergent composition.US patent Number, 5466594.

Rahman A, Gomes DJ (2003) Optimization of medium ingredients for α-mannanase production by *Aspergillus* sp. isolated from commercial guar gum. Dhaka Univ J Biol Sci 12(2):153-164.

Rao K, Jagannadha KIM, Chul-Ho, RHEE Sang-Ki (2000). Statistical optimization of medium for the production of recombinant hirudin from *Saccharomyces cerevisiae* using response surface methodology. Process Biochem 35(7):639-647.

Reddy LVA, Wee Y-J, Yun J-S, Ryu H-W (2008) Optimization of alkaline protease production by batch culture of *Bacillus* sp. RKY3 through Plackett–Burman and response surface methodological approaches. Biores Technol 99:2242-2249.

Sayyad SA, Panda BP, Javed S, Ali M (2007) Optimization of nutrient parameters for lovastatin production by *Monascus purpureus* MTCC 369 under submerged fermentation using response surface methodology. Appl Microbiol Biotechnol 73:1054-1058.

Sen R (1997) Response surface optimization of the critical media components for the production of surfactin. J Chem Tech Biotechnol 68:263-70.

Srinivas MRS, Chand N, Lonsane BK (1994) Use of Plackett– Burman design for rapid screening of several nitrogen sources, growth product promoters, minerals and enzyme inducers for the production of alpha-galactosidase by *Aspergillus niger* solid state fermentation system. Bioprocess Eng 10:139-144.

Varela H, Ferrari MD, Belobradjie L, Weyruch R, Loperena ML (1996) Effect of medium composition on the production by a new *Bacillus subtilis* isolate of protease with promising unhairing activity. World J Microbiol 12:643- 645.

Wolff AM, Showell MS, Venegas MG, Barnett BL, Wertz WC (1993) Laundry performance of subtilisin proteases. In Bolt R, Betzel eds., Subtilisin enzymes: practical protein engineering. New York, Plenum Press pp. 113-120.

Xiao ZJ, Liu PH, Qin JY, Xu P (2007) Statistical optimization of medium components for enhanced acetoin production from molasses and soybean meal hydrolyzate. Appl Microbiol Biotechnol 74:61-68.

Zhao S, Zixia Z, Xia Q, Jiadong H, Haibin S, Baoyan WU (2007) Highly sensitive choline biosensor based on carbon nanotube-modified Pt electrode combined with sol–gel immobilization. Front Chem China 2:146-150.

Volume 54(2):143-148, 2010
Acta Biologica Szegediensis
http://www.sci.u-szeged.hu/ABS

ARTICLE

Characterization of petite mutants of the basidiomycetes *Phaffia rhodozyma* CBS 5905

Ilona Pfeiffer[1], Csaba Vágvölgyi[1], Tadashi Hirano[2], Judit Kucsera[1]*

[1]Department of Microbiology, Faculty of Science and Informatics, University of Szeged, Szeged, Hungary, [2]Jikei University, School of Medicine, Minatoku, Tokyo, Japan

ABSTRACT Small, "petite" colonies appeared with almost 1% frequency among the normally growing colonies in the astaxanthin-producing *Phaffia rhodozyma (Xanthophyllomyces dendrorhous)* CBS 5905 strain. These colonies fermented glucose in the presence of oxygen, were not able to grow on nonfermentable carbon sources and did not respond to inhibitors of respiration. Besides spontaneous occurrence, petite mutation proved to be inducible almost to 100% by low levels of ethidium bromide treatment. Cell hybridization experiments revealed that both the spontaneous and induced mutation was mitochondrially inherited. The RFLP pattern of the mtDNAs isolated from purified mitochondria of the grand and petite strains were similar. Consequently, unlike to the mtDNA of *Saccharomyces cerevisiae,* not large deletions were the reason for petite mutant induction. The size of mtDNA in the grand cells was calculated by restriction enzyme analysis and proved approximately 17.6 kb. In teleomorphic strains of *P. rhodozyma* (*Xanthophyllomyces dendrorhous*) spontaneous petite mutants did not arise and the phenotype could not be induced either by ethidium bromide treatment. According to our results, *Phaffia rhodozyma* is the only known petite-positive basidiomycetous yeast.
Acta Biol Szeged 54(2):143-148 (2010)

KEY WORDS

basidiomycetous yeast
petite positive
mitochondrial DNA
Phaffia rhodozyma

Phaffia rhodozyma is an asexual, psychrophylic, fermentative yeast species which is represented by the single isolate, strain CBS 5905. Its relation to basidiomycetous yeasts was verified via cell wall ultrastructure, the mode of bud formation and diazonium B test (Miller et al. 1976). The teleomorphic form was described as *Xanthophyllomyces dendrorhous* by Golubev in 1995, although comparison of sequences of rDNA on the IGS and ITS regions, suggested that *P. rhodozyma* CBS 5905 may be a distinct species from the other examined strains (Fell and Blatt 1999). Additional results from the analysis of viral RNAs (Pfeiffer et al. 1996), electrophoretic karyotyping (Nagy et al. 1994), RAPD analysis (Palágyi et al. 2004) and the detection of DNA plasmids in the mitochodria of *Xanthophyllomyces* strains (Wilber and Proffitt 1987; Kucsera et al. 2000; Santopietro and Kula 2001) reinforced this further. The hypothesis that *P. rhodozyma* and *X. dendrorhous* may represent the same species is favoured again (Fell et al. 2007; Libkind et al. 2007). The microorganism is biotechnologically important, as the cells produce high amount of astaxanthin. The well-functioning respiratory system is an important requirement both for biomass production and high amount of astaxanthin production. Low aeration slows growth, consequently reduces the yield of yeast cells and markedly reduces the red pigment yield (Lewis 1990). In this paper we report, that respiratory-deficient petite mutants occurred spontaneously, or could be induced by ethidium bromide (EtBr) treatment in the strain *Phaffia rhodozyma* CBS 5905. Such mutant could not be isolated either spontaneously or induced by EtBr treatment in *Xanthophyllomyces dendrorhous*. RFLP pattern of mtDNA from the wild-type and petite strains were compared in strain CBS 5905. The size of the wild type mtDNA calculated on the bases of restriction enzyme analysis proved about 17.6 kb, what is quite small genome size in yeast (Wolf and Del Giudice 1988; Pramateftaki et al. 2006). According to our results *Phaffia rhodozyma* CBS 5905 is a member of the petite positive yeast group (Bulder 1964), which is the only known case among the basidiomycetous yeasts.

Materials and Methods

Strains, media and growth conditions

The yeast strains used in this study are listed in Table 1. The media used were 2xYPD: 1% yeast extract, 2% peptone, 2% glucose; YPEt: 0.05% yeast extract, 0.05% peptone, 2% ethanol; for plating media contained 2% agar. Yeast cells were grown under continuous shaking at 20°C.

Determination of spontaneous petite frequency

Yeast cells were grown in YPEt medium for 48 hr, then diluted and plated onto 2xYPD plates. After 5 days of incubation at

Accepted Oct 22, 2010
*Corresponding author. E-mail: kucsera@bio.u-szeged.hu

Table 1. Yeast strains used in this experiment.

Strains	Markers		Origin
	Nuclear	Mitochondrial	
Ph. rhodozyma			
CBS 5905	prototrophic	ρ^+	Kindly provided by BioColours Ltd
CBS 5905 *pet1/1*	prototrophic	ρ^-	Spontaneously arising petite isolates from CBS 5905
arg ben^{R}2	arg$^-$, benomyl resistant	ρ^+	Isolated after repeated mutagenesis from CBS 5905
arg ben^{R}2 ρ^-10	arg$^-$, benomyl resistant	ρ^-	Ethidium bromide induced petite mutant of *arg ben^{R}2*
X. dendrorhous			
CBS 5908			Kindly provided by BioColours Ltd
CBS 6938			Kindly provided by BioColours Ltd
ATCC 24203			Kindly provided by BioColours Ltd
ATCC 24229			Kindly provided by BioColours Ltd
ATCC 24261			Kindly provided by BioColours Ltd

Table 2. Frequencies of petite mutants after 10 µg/ml ethidium bromide treatment.

Time of treatment (hour)	Frequencies of petite colonies (%)
0	0.5
12	9.2
24	40.7
48	74.3

20°C, the small colonies were scored and tested for ability to grow on YPEt.

Isolation of respiratory deficient mutants

The isolation of respiratory deficient mutants using ethidium bromide has been described by Rickwood et al. (1988).

Respiration measurements

All respiration measurements were made using Clark type oxygen electrode, at 20°C, according to the method published by Rickwood et al. (1988).

Colony assay for cytochrome c oxidase activity

Five-day-old colonies were stained by tetramethyl-*p*-phenylenediamine (TMPD) according to the method published by McEwen et al. (1985).

Electron microscopy

Yeast cells from the stationary growth phase were fixed at 4°C for 24 h in 2% glutaraldehyde in 0.1 M phosphate buffer (pH 7.4). After fixation, the cells were washed four times in phosphate buffer, postfixed in 2% $KMnO_4$ for 2 h, dehydrated in a graded series of ethanol, and embedded in Spurr resin. Sections were cut with a Reichert-Jung ultramicrotome, and stained with uranylacetate. Ultrathin sections were examined under a JEM 1200EX electron microscope at 60 kV (Bozzola and Russel 1992).

Determination of extrachromosomal inheritance in strain pet1/1

For hybridization of strain *pet1/1* the protoplast fusion method was used. Protoplasts were prepared from exponentially growing cultures of *arg ben^{R}2*, *arg ben^{R}2 ρ^-10* and *pet1/1* essentially according to the method described by Maráz et al. (1978) with the following modifications: cells of the fusion partners were precultivated in 2xYPD liquid medium; after pretreatment in 1% 2-mercaptoethanol, the cell wall was digested with 1.5% snail enzyme and 0.1% NovoZym in 0.8 M KCl for 2 hours. Partners in protoplast fusion were: *pet1/1* x *argben^{R}2 ρ^-10* and *pet1/1* x *argben^{R}2*; for hybrid selection minimal medium supplemented with 1µg/ml benomyl and 0.8 M KCl was used.

Separation of nuclear and mitochondrial DNA

A modification of the procedure previously described for *Saccharomyces cerevisiae* was applied. Protoplasts were formed from cells of stationary phase (10^7 cells/ml). After two hours incubation in the lysing enzyme the crude lysate of $5x10^9$ protoplasts were applied to separate DNAs on isopycnic CsCl/ bisbenzimide (Hoechst 33258) gradient according to Williamson and Fennel (1974), in Sorvall Pro80 Ultraspeed Centrifuge.

Isolation of mitochondria

Protoplasts from about 10^9 cells were broken by French press at 4°C at 3000ψ. Mitochondria were isolated on sucrose gradient according to Rickwood et al. (1988).

Restriction endonuclease digestion and electrophoresis

Restriction endonucleases were obtained from Fermentas (Vilnius, Lithuania) and the reactions were carried out ac-

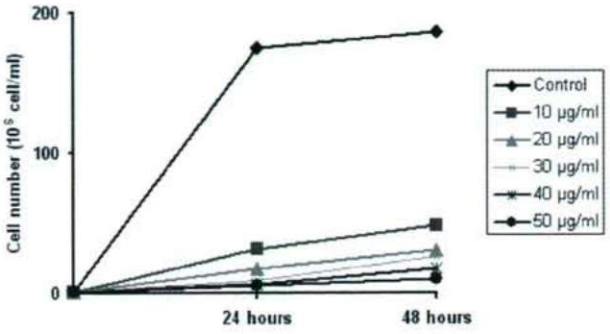

Figure 1. Effect of different concentration of ethidium bromide on cell growth.

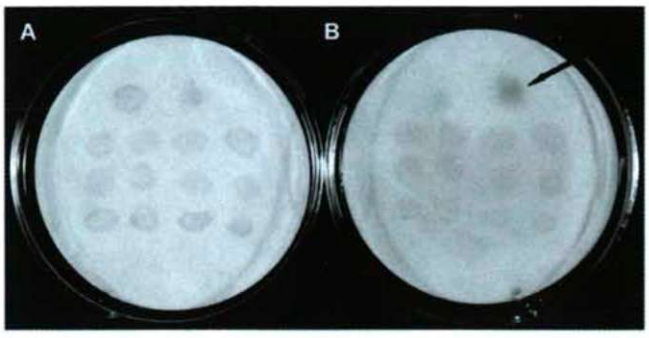

Figure 2. TMPD staining of *Phaffia rhodozyma* wild type and petite mutant colonies. A: colonies without TMPD, B: colonies with TMPD, arrows show the respiratory competent wild type colonies.

cording to the supplier's directions.

Pulsed field gel electrophoresis (PFGE)

DNA samples from *P. rhodozyma* protoplasts were prepared in agarose blocks and separated in a 1.0% (w/v) agarose gel using a CHEF-DRTM II System (BIORAD) with switching time 60s. All separations were performed in 0.5x TBE buffer (45 mM Tris-borate, 1 mM EDTA pH 8.0) at 12°C for 14 hours.

Results and Discussion

The occurrence of spontaneous petite mutation in *Phaffia rhodozyma*

During our preliminary study on *P. rhodozyma* CBS 5905 strain the occurrence of small colonies was revealed with about 1% frequency on complete media (Kucsera et al. 1995). Replicating colonies onto media containing nonfermentable carbon source (ethanol) the small ones failed to grow. One of these spontaneous petite mutant strains (*pet1/1*) was isolated for further experiments. No such mutants were found in the *X. dendrorhous* strains when 10^4 cells were plated for colonies.

Detection of the respiration rate in isolated grand and petite mitochondria

The O_2 consumption of isolated mitochondria of the grand and the petite strains was measured by 'Clark-type' oxygen electrode. The grand mitochondria respired at a rate of 25 µM O_2/min/mg protein in the presence of succinate as substrate and the respiration was almost totally blocked with Antimycin *A*. Some residual respiration which can be due to the activity of an alternative oxidase enzyme system was also detected (An and Johnson 1990). The mitochondria of petite cells neither respired nor responded to the addition of Antimycin *A* in the presence of the substrate.

Specific induction of petite mutation by ethidium bromide

Ethidium bromide (EtBr) inhibits *de novo* synthesis of mtDNA as well as stimulates destruction of the pre-existing mtDNA molecules resulting in almost 100% conversion of *S. cerevisiae* culture into a respiratory-deficient one. Cells of *P. rhodozyma* were exposed to various concentrations of EtBr for various periods of time in complete liquid medium and the changes in the growth rate and survival rate were determined. The inhibition of cell growth is illustrated on Figure 1. Although the growth rate was gradually inhibited at concentrations higher than 10 µg/ml, the yeast cells still grew reasonable well in the presence of EtBr. Even at higher concentration they remained viable (data not shown). This behaviour of *P. rhodozyma* mtDNA suits the well-known sensitivity of fungal mtDNAs to low levels of EtBr. The conversion of cells to petite phenotype by EtBr treatment (10 µg/ml) as a function of time was also determined (Table 2). Petite mutants could be isolated almost in 80% after 48 hours treatment. These results are also similar to those of *S. cerevisiae*, where low concentration of EtBr could cause a 99% of petite induction (Dujon 1981). Treatment with EtBr did not resulted in petite mutation of the *X. dendrorhous* strains: 2500 surviving colonies of each strain were tested after 10-25-50 µg/ml EtBr treatments of 48 hours and respiratory deficient isolates could not be found.

Screening of cytochrome c oxidase activity in ethidium bromide induced petite isolates

The activity of the respiratory-chain enzymes was checked by cytochrome *c* oxidase test, in more than 100 isolates of the ethidium bromide induced mutants. Grand type colonies showed purple coloration within two minutes due to intensive oxidation while all of the petites remained pink when stained by TMPD (Fig. 2). The result proved that cytochrome c oxidase enzyme did not function, however other enzymatic

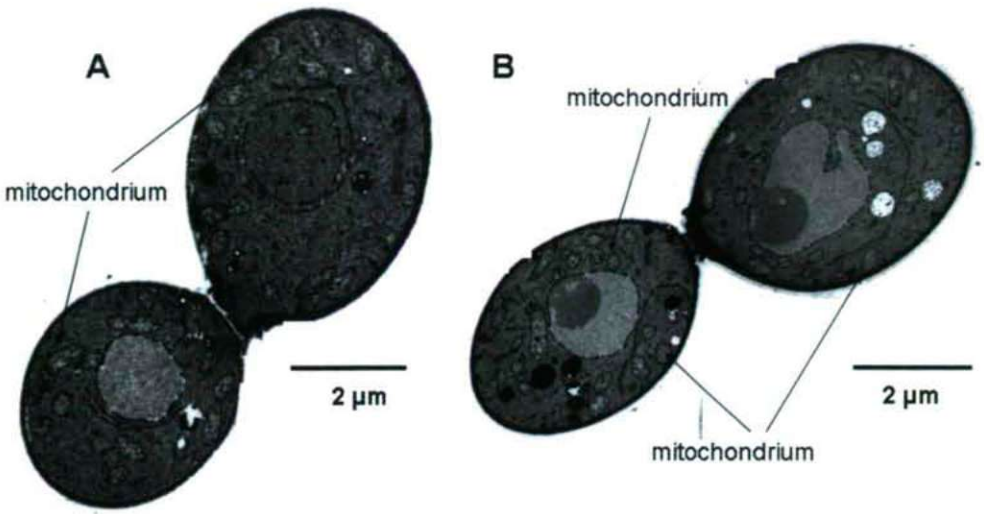

Figure 3. Ultrathin section from *Phaffia rhodozyma* wild type (A) and *pet1/1* petite cells (B).

(e. g. cytochrome b) deficiency prior to cytochrome c oxidase could not be excluded.

Electron microscopic structure of the grand and petite cells

Studies on the morphology of mitochondria in grand cells and cytoplasmic petite mutants of *S. cerevisiae* revealed that in the later they are often smaller and spherical. The major alteration is the loss of normal cristae, and very often the mitochondria tend to aggregate in some cytoplasmic regions (Stevens 1981).

In *P. rhodozyma* the wild-type cells had very well structured grand mitochondria with developed internal lamelles (Fig. 3a). The mutant cells also contained recognizable mitochondria (Fig. 3b). Its structure appeared normal we could observe neither distinct morphological alteration nor irregular distribution of the organelles in the cytoplasm.

Characterization of the mtDNA

Mitochondrial DNA of *P. rhodozyma* CBS 5905 migrates as a "smear" during PFGE what is peculiar for circular mitochondrial genomes. Separation of nuclear and mtDNA in isopycnic CsCl gradient showed that the buoyant density of DNA deriving from whole cell lysates was the same. Accordingly, for further experiments the mtDNA was isolated from purified mitochondria and analysed by restriction endonucleases.

Enzymes having six-base recognition site gave partial digestion, therefore endonucleases with four-base recognition sites were used to determine the size of the mitochondrial DNA (Fig. 4.). The estimated molecular weight was 17.6 kb, however, this result can alter after refining the number of the comigrated fragments. The mtDNA contained relatively high number of restriction sites recognized by enzyme which specifically cut in GC clusters. This is similar to the published

Figure 4. RFLP patterns of mtDNA of *P. rhodozyma* CBS 5905 strain. Lane M: λ-pUC Mix as molecular weight marker (Fermentas). Lanes 1-3: *Rsa*I-, *Msp*I-, and *Hae*III-digested mtDNA, respectively.

results by Piskur et al. (1996, 1998) in the *Saccharomyces sensu stricto* complex where the members of the species group showed variable RFLP pattern, when such enzymes were used, although there were only slight differences when enzymes specifically cutting in the coding regions were applied.

Characterization of the mtDNA of petite mutants

The cytoplasmically inherited petite mutation in *S. cerevisiae* is due to smaller or larger deletions in mitochondrial DNA (Dujon 1981). The deleted segments may derive from any part and length of the mitochondrial genome or in extreme cases the mtDNA may be completely lost (ρ° mutant). The non-deleted sequences may be amplified, and its amphimeric organization is thought to be general (Rayko and Goursot 1996a, b). In *P. rhodozyma* petite strain either induced by EtBr or arised spontaneously the restriction enzyme pattern of the mtDNA generated by *Hae*III and *Rsa*I was the same as in the wild type mtDNA. The mutants possibly arose by point mutation or may be due to only very small deletions which could not be detected by using these enzymes.

Inheritance of respiratory deficient mutation in strain pet1/1

As RFLP pattern of the mtDNA in spontaneous petite and in the grand strain was similar, we were wondering about the origin of the mutation (viz. mitochondrial or nuclear). As *P. rhodozyma* is not capable for sexual processes, unlike its teleomorph form *Xanthophyllomyces dendrorhous* (Kucsera et al. 1998), the protoplast fusion method was applied for hybridization. The idea was, if the mutation of the spontaneous petite strain 1/1 is on nuclear DNA, hybrid cells obtained from a fusion to *arg ben*^{R}*2* ρ$^-$ ethidium bromide induced petite should have a grand phenotype. The reason is the presence of a normal complement of nuclear genes in strain *arg ben*^{R}*2* ρ$^-$ (since EtBr has no effect on nuclear DNA) and of mitochondrion (in strain 1/1). On the other hand, if the mutation is on mtDNA, the hybrid progeny resulting from the fusion will exhibit the mutant phenotype, since the petite parent (strain 1/1), having no functional mtDNA cannot supply the wild-type copy of the mutated gene. In fusion experiment *A* the 1/1 petite was fused to *arg ben*^{R}*2*. After selection on minimal medium containing benomyl, all of the twelve isolated colonies were grand. In fusion experiment *B*, the strain 1/1 was fused to *arg ben*^{R}*2* ρ$^-$ EtBr induced petite. After selection ten fusion colonies were isolated and all of them were petites. According to this result, the spontaneous petite mutation was mitochondrially inherited in strain 1/1.

In conclusion the occurrence of small colonies during the cultivation of *Phaffia rhodozyma* and the fact that they are not able to use nonfermentable carbon sources revealed that *Phaffia rhodozyma* is a petite-positive basidiomycetous species. This was confirmed by the following results: i. the difference between the O_2 consumption of the grand and the petite cells and their mitochondria suggested that the petite cells do not contained functioning mitochondria; ii. ethidium bromide proved to be an effective petite inducer; iii. the petite mutants might arise by point mutation or small deletion even after ethidium bromide treatment as their RFLP profile generated by *Hae*III or *Rsa*I digestion proved the same as the RFLP pattern of the wild type.

References

An GH, Johnson EA (1990) Influence of light on growth and pigmentation of the yeast *Phaffia rhodozyma*. Antonie van Leeuwenhoek 57:191-203.

Bozzola JJ, Russel LD (1992) Electron Microscopy; Principle and Techniques for Biologists. Jones and Bartlett Publisher. Inc., Boston.

Bulder CJEA (1964) Induction of petite mutation and inhibition of synthesis of respiratory enzymes in various yeasts. Antonie van Leeuwenhoek 30:1-9.

Dujon B (1981) Mitochondrial genetics and functions. In Strathern, J. N., Jones, E. W. and Broach, J. R. (Eds), The Molecular Biology of the Yeast Saccharomyces, Life Cycle and Inheritance, Cold Spring Harbour Laboratory, pp. 505-635.

Fell JW, Blatt GM (1999) Separation of strains of the yeasts *Xanthophyllomyces dendrorhous* and *Phaffia rhodozyma* based on rDNA IGS and ITS sequence analysis. Ind Microbiol Biotechnol 23:677-681.

Fell JW, Scorzetti G, Statzell-Tallman A, Boundy-Mills K (2007) Molecular diversity and intragenomic variability in the yeast genus *Xanthophyllomyces*: the origin of *Phaffia rhodozyma*? FEMS Yeast Research 7:1399-1408.

Golubev WI (1995) Perfect state of *Rhodomyces dendrorhous* (*Phaffia rhodozyma*). Yeast 11:101-110.

Jadeyel DM (1986) Variation in the organization and structure of the mitochondrial DNA of species *Aspergillus. Ph.D. Thesis*, University of Birmingham, Birmingham, UK

Kucsera J, Pfeiffer I, Ferenczy L (1995) Occurrence of petite mutation in *Phaffia rhodozyma.* Acta Microbiol Immunol Hung 42:134-135.

Kucsera J, Pfeiffer I, Ferenczy L (1998) Homothallic life cycle in the diploid red yeast *Xanthophyllomyces dendrorhous* (*Phaffia rhodozyma*). Antonie van Leeuwenhoek 73:163-168.

Kucsera J, Pfeiffer I, Takeo K (2000) Biology of the red yeast *Xanthophyllomyces dendrorhous* (*Phaffia rhodozyma*). Mycoscience 41:195-201.

Lewis MJ (1990) *Phaffia rhodozyma:* A red yeast with potential as an animal feed. In Lyons, T. P. (ed) Biotechnology in the Feed Industry, Proceedings of Alltech's Sixth Annual Symposium, pp. 391-403.

Libkind D, Ruffini A, Broock MJ, Alves L, Sampaio JP (2007) Biogeography, host specificity, and molecular phylogeny of the basidiomycetous yeast *Phaffia rhodozyma* and its sexual form *Xanthophyllomyces dendrorhous.* Appl Environ Microbiol 73:1120-1125.

Maráz A, Kiss M, Ferenczy L (1978) Protoplast fusion in *Saccharomyces cerevisiae* strains of identical and opposite mating types. FEMS Letters 3:319-322.

McEwen JE, Cameron VL, Poyton O (1985) Rapid method for isolation and screening of cytochrome *c* oxidase-deficient mutants of *Saccharomyces cerevisiae*. J Bacteriol 161:831-835.

Miller M, Yoneyama WM, Soneda M (1976) *Phaffia*, a new yeast genus in the Deuteromycotina (Blastomyces). Int J Syst Bacteriol 26:286-291.

Nagy Á, Garamszegi N, Vágvölgyi Cs, Ferenczy L (1994) Electrophoretic karyotypes of *Phaffia rhodozyma* strains. FEMS Microbiol Letters 123:315-318.

Palágyi Zs, Papp T, Takó M, Nagy Á, Pesti M, Vágvölgyi Cs (2004) Genetic variability of astaxanthin-producing yeasts: random amplified polymorphic DNA (RAPD) analysis of *Phaffia rhodozyma* and *Xanthopyllomyces dendrorhous.* Acta Biol Szeged 48:35-38.

Pfeiffer I, Kucsera J, Varga J, Párducz Á, Ferenczy L (1996) Variability and inheritance of double-stranded RNA viruses in *Phaffia rhodozyma*. Curr Genet 30:294-297.

Piskur J, Smole-Mozina S, Stenderup J, Pedersen MB (1996) A mitochondrial marker, *ori-rep-tra*, for differentiation of yeast species. Appl Environ Microbiol 51:2780-2782.

Piskur J, Smole S, Groth C, Petersen RF, Pedersen MB (1998) Structure and genetic stability of mitochondrial genomes vary among yeasts of the genus *Saccharomyces*. Int J Syst Bacteriol 48:1015-24.

Pramateftaki PV, Kouvelis VN, Lanaridis P, Typas MA (2006) The mitochondrial genome of the wine yeast *Hanseniaspora uvarum*: a unique genome organization among yeast/fungal counterparts. FEMS Yeast Res 6:77-90.

Rayko E, Goursot R (1996a) Amphimeric mitochondrial genomes of petite mutants of yeast. I. Flip-flop amphimers make up the mitochondrial genomes of "palindromic" petite mutants of yeast. Curr Genet 30:126-134.

Rayko E, Goursot R (1996b) Amphimeric mitochondrial genomes of petite mutants of yeast. II. A model for the amplification of amphimeric mitochondrial petite DNA. Curr Genet 30:135-144.

Rickwood D, Dujon B, Darley-Usmar VM (1988) Yeast mitochondria. In Campbell I and Duffus JH eds., Yeast - a practical approach. IRL Press, pp. 185-254.

Santopietro LM, Kula MR (2001) Cloning and nucleotide sequence of a linear DNA plasmid from *Xanthophyllomyces dendrorhous* (*Phaffia rhodozyma*). Folia Microbiol (Praha) 46:277-88.

Stevens B (1981) Mitochondrial structure. In Strathern JN, Jones EW and Broach JR eds., *The Molecular Biology of the Saccharomyces, Life Cycle and Inheritance*, Cold Spring Harbour Laboratory, pp. 471-504.

Wilber KA, Proffitt JH (1987) Detection of linear plasmids in *Phaffia rhodozyma*. UCLA Yeast Symp. p. 106.

Williamson DH, Fennell DJ (1974) Apparent dispersive replication of yeast mitochondrial DNA as revealed by density labelling experiments. Mol Gen Genet 131:193-207.

Wolf K, Del Guidice L (1988) The variable mitochondrial genome of Ascomycetes: organization, mutational alteration, and expression. Adv Genet 25:185-308.

Volume 54(2):149-154, 2010
Acta Biologica Szegediensis
http://www.sci.u-szeged.hu/ABS

ARTICLE

Aging photosynthetic bacteria monitored by absorption and fluorescence changes

Emese Asztalos, Mariann Kis, Péter Maróti*

Department of Medical Physics, University of Szeged, Hungary

ABSTRACT Production and arrangement of photosynthetic pigments into protein complexes were monitored by steady state and kinetic absorption and fluorescence methods in different phases of growth curve of photosynthetic purple bacterium *Rhodobacter sphaeroides*. The increase of the number of pigments (B800, B850 and B875) followed that of the cells and could be described by the modified Gompertz equation. The newly synthesized chromophores were imbedded immediately into the proteinous scaffold independently on the age of the cell (no free pigments were observed). The assembly, however, showed age-dependent changes manifested by slight (~5 nm) blue-shift of the absorption peak of B875 in LH1, by small increase (~10%) of the variable fluorescence and by increased duration of the electrochromic shift detected at 525 nm. The observed changes of the organization of the bacteriochlorophylls in the photosynthetic units upon aging the cell correspond to the tendency of more efficient capture and utilization of light energy.

Acta Biol Szeged 54(2):149-154 (2010)

KEY WORDS

growth curves
photosynthetic pigments
light harvesting systems
absorption spectra
fluorescence induction

The photosynthetic purple bacteria are among of the most ancient and primitive organisms whose bioenergetics has been thoroughly studied and serves as model of more complex energy converting biological systems (Asztalos and Maróti 2009). The antenna pigment proteins in the intracytoplasmic cell membrane (ICM) absorb solar light and transport the energy to the bacterial reaction center (RC), where the light energy is converted into chemical energy directly utilized by the organism (Fig. 1). These antenna molecules are referred to as light harvesting complex 1 (LH1) and light harvesting complex 2 (LH2; Jungas et al. 1999). The LH1 core antenna, a closely coupled pigment system, surrounds the bacterial RC (Jamieson et al. 2002; Roszak et al. 2003). LH1 is, in many types of bacteria, connected to a peripheral antenna, LH2 (Sundstrom et al. 1999). The elementary building block of both LH1 and LH2 is a coupled pair of helical transmembrane polypeptides, the so-called α/β dimer. Both helices bind a bacteriochlorophyll *a* (BChl a) at a conserved histidine position (Olsen et al. 1997, 2008), in the case of LH2 the β polypeptide also binds a second Bchl *a* (Waltz et al. 1998). The α/β dimers are arranged in ring like structures. In the case of the LH1 complex of *Rhodobacter (Rba.) sphaeroides* the BChls form two interconnected open rings of 28 dimers in total, with each dimer proposed to have a gate for quinone exchange formed by the PufX protein (Siebert et al. 2004; Qian et al. 2008). In the case of LH2, there is a circular arrangement of 9 dimers binding two concentric rings of 18 B850 BChls and 9 B800 BChls, structurally and energetically connected by carotenoid molecules. While the major interactions that stabilize LH1 are within the α/β subunits, in LH2 the interactions of neighboring amino acids between α/β–pairs are essential. These rings are named according to their absorption maxima, B875 (LH1), B850 (LH2) and B800 (LH2). The LH1 and LH2 have strong internal dipole coupling, exhibit fast transfer between the elements of the ring (a biphasic equilibration of exciton states with lifetimes of ~100 fs and ~400 fs is generally reported), have a big absorption cross section and high structural stability. These properties of the light harvesting system make good candidate to follow structural and functional changes during the cell cycle of the photosynthetic bacteria.

The facultative photoheterotroph purple bacterium *Rhodobacter (Rba.) sphaeroides* is a member of the α-3 subclass of the *Proteobacteria* (Imhoff 1995) that provides an excellent experimental system to study membrane biogenesis and assembly (Koblizek et al. 2005). When grown under anaerobic conditions in the light, *Rba. sphaeroides* forms a system of intracytoplasmic membranes that house the photosynthetic apparatus. It was shown that the photosynthetic units were assembled in a sequential manner, where the appearance of the LH1-RC cores was followed by the activation of functional electron transfer, and finally by the accumulation of the LH2 complexes. The ICM formation is repressed in the presence of oxygen. The invagination of the cytoplasmic membrane (CM) and the synthesis and assembly of light-harvesting and RC complexes are under the control of a global two-component oxygen sensing, signal transduction system and

Accepted Oct 25, 2010
*Corresponding author. E-mail: pmaroti@sol.cc.u-szeged.hu

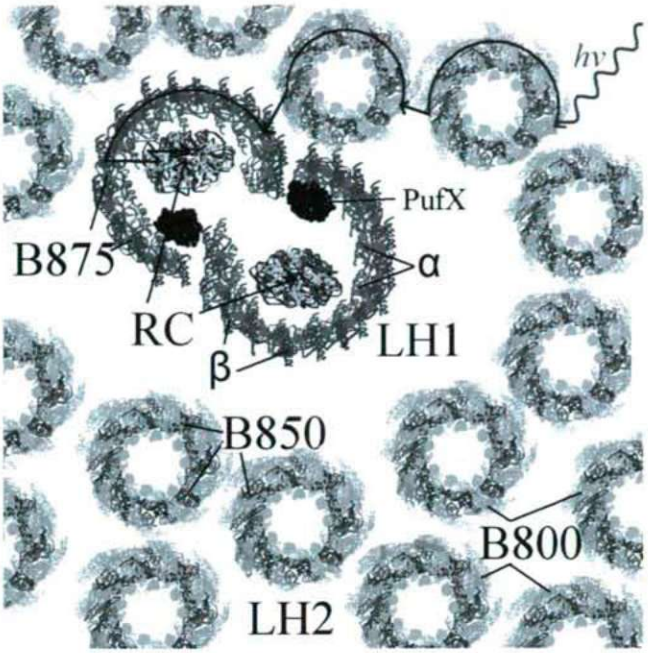

Figure 1. Artistic visualization of the photosynthetic light harvesting apparatus of *Rba. sphaeroides* 2.4.1. and migration and capture of the excitation photon hν by the reaction center RC. LH1: light harvesting complex 1, PufX: PufX protein, α and β: bacteriochlorophyll binding proteins, B875, B850 and B800: bacteriochlorophylls of absorption maxima at 875, 850 and 800 nm bound to α/β dimers, respectively, LH2: light harvesting complex 2.

additional regulatory components (Takemoto and Lascelles 1973; Masuda et al. 2002).

Based on the time evaluation of the concentration of the bacterial cells in the culture, the growth curve of *Rba. sphaeroides* under constant illumination can be divided into lag, exponential, intermediate and stationary phases (De Klerk et al. 1969). We can pose the following simple but not yet properly answered questions: 1) What is the rate of production of the pigments and 2) how do they assemble to functional units (e.g. to light harvesting system) in the different phases of the growth? More frankly, are there any differences between young and old cells in composition and arrangement of the pigments in the light harvesting complexes? We will demonstrate in this paper, that the conventional steady-state absorption spectra of the intact cells at room temperature can hardly answer these questions. The fluorescence characteristics of the pigments, however, will shed some light to and reveal the complexity of this problem.

Methodologically, we can add some novelties to the generally used instrumentation of similar types of physiological studies. Despite the overwhelming use of different chlorophyll fluorometers in functional studies of plants and cyanobacteria (Papageorgiou and Govindjee 2004), the induction of BChl fluorescence of photosynthetic bacteria has gained interestingly very restricted application (Maróti 2008; Bina et al. 2009; Kocsis et al. 2010). The Kautsky-effect was used to monitor the marine ecosystem (Hohmann-Marriott and Blankenship 2007), the development of the functional photosynthetic units during the growth (aging) of the bacterium cells (De Klerk et al. 1969; Koblizek et al. 2005) and the influence of heavy metal contamination of cultures of photosynthetic bacteria (Asztalos et al. 2010). Here, we display the applicability of variable BChl *a* fluorescence transients for elucidating the assemble/dissemble processes of the photosynthetic unit during aging of the bacteria. Beside the conventional absorption techniques, the fluorescence kinetics of intact cells opens new possibilities to reveal up to now hidden aspects of aging.

Materials and Methods

Cells of purple non-sulfur photosynthetic bacterium *Rhodobacter* (*Rba.*) *sphaeroides* strain 2.4.1 were obtained from the German Collection of Microorganisms and Cell Cultures (DSM n. 160) and were cultivated anaerobically in Siström medium (Siström 1962) under stirring in 1 liter screw top flasks at 33°C. The cultures of the bacteria were deoxygenated by bubbling N_2 gas for 15 minutes. Tungsten lamps (40 W) whose spectrum is rich in red components, provided continuous and homogeneous illumination of 13 $W \cdot m^{-2}$ irradiance at the surface of the vessel. The volume of the sample ($\approx$ 1.5 ml) taken regularly was negligible compared to the total volume of the culture and therefore did not modify the growing conditions. The concentration of the cells in the culture was determined by visual counting the number of the sample cells with calibrated Bürker chamber under light microscope.

The steady state spectra of absorption and fluorescence of the cells were measured by Helios γ spectrophotometer (Thermo Electron Corporation) and spectrofluorometer (Perkin Elmer MPF 4) with home-made red-extension of the photodetection by replacing the photomultiplier (Hamamatsu R-446F) by pin photodiode (10DI, UDT Sensors Inc), respectively. The kinetics of light-induced absorption- and fluorescence changes of the whole cells were detected by home-constructed spectrophotometer (Maróti and Wraight 1988) and bacteriochlorophyll fluorometers (Maróti 2008; Maróti and Wraight 2008; Kocsis et al. 2010), respectively.

Results

Steady state absorption and fluorescence spectra

Even at room temperature, three bands with center wavelengths of about 800 nm (LH2), 850 nm (LH2) and 875 nm (LH1) can be recognized in the red part of the absorption spectrum of the cells (Fig. 2). After approximation of the baseline originating from intense light scattering by hyperbolic function and subtraction from the measured spectrum,

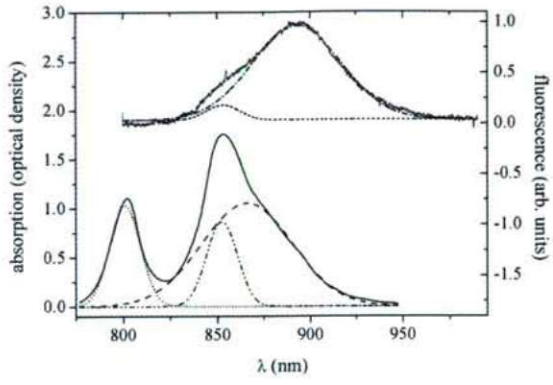

Figure 2. Steady state absorption and fluorescence spectra of intact cells of *Rba. sphaeroides*. The absorption spectrum is decomposed into three Gaussian components of peaks at 800 (· · ·), 850 (– · · –) and 875 nm (– – –) and the fluorescence spectrum into two Gaussian components of peaks at 850 nm (· · · · · ·) and 895 nm (– · – · ·). The blue part of the fluorescence spectrum is cut by a red filter (RG-850).

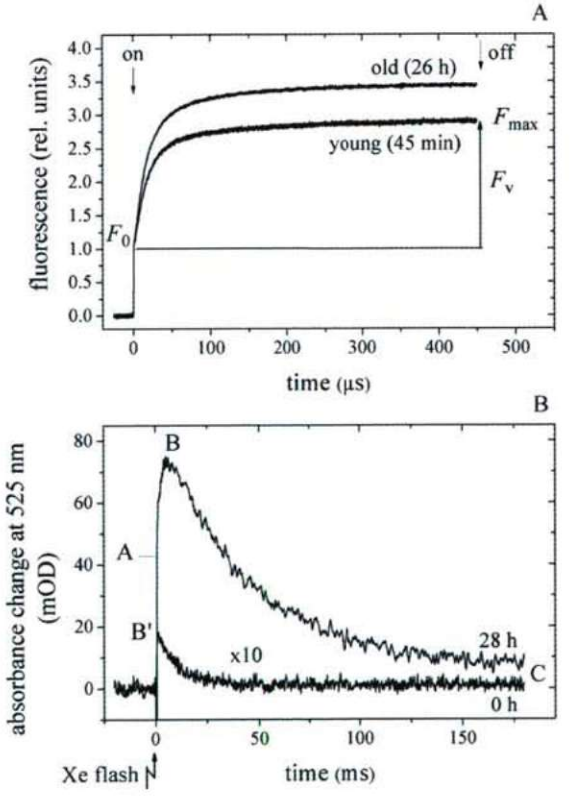

Figure 3. Fluorescence induction (A) and kinetics of flash-induced absorption changes (B) of young and old cells of *Rba. sphaeroides* 2.4.1. Panel A: Fluorescence induction kinetics upon stepwise dark-light transition. F_0, F_v and F_{max} are the dark, the variable and the maximum levels of fluorescence, respectively. The variable fluorescence in young cells is smaller than in old cells. Panel B: Electrochromic signals at 525 nm. (The trace taken at 0 hrs is multiplied by 10.) While the young cells have fast decay kinetics after the small abrupt increase, the old cells have a second and slower increase followed by a slow decay. (For details see Table1.)

the difference curve was decomposed into the sum of three Gaussian components:

$$(1) \quad y = \sum_{i=1}^{3} \frac{A_i}{w_i \sqrt{\pi/2}} \cdot \exp\left[-\frac{2 \cdot (\lambda - \lambda_{c,i})^2}{w_i^2}\right]$$

where A_i, w_i and $\lambda_{c,i}$ are the area, the bandwidth and the central wavelength of the i-th component (i =1,2 and 3). The Gaussian peeling reveals the dominant role of the core complex (LH1) which cannot be expected from the visual inspection of the spectrum (a shoulder is appearing at the descending part of the spectrum). As the oscillator strength of the component is proportional to the area of the band, this parameter was used to characterize the (absolute and relative) changes of the absorption bands during aging of the bacteria.

The steady-state fluorescence spectrum of the intact cells displays a main band at 895 nm and a satellite band centered at 850 nm that can be also quantified by Gaussian decomposition of the observed spectrum according to Eq. (1).

Flash induced absorption and fluorescence kinetics

Relatively large absorption change can be detected at 525 nm upon flash illumination in intact cells (Fig. 3). Similar effects were reported in chromatophores of bacteria (Wraight et al. 1978) and utilized widely in algal photosynthesis (Bailleul et al. 2010). The observed changes were attributed to electrochromic shift of marker molecules (e.g. carotenoids) in the membrane. The rise of the signal is due to the energetization of the membrane and the decay is characteristics of discharge of the membrane capacitor. Table 1 includes the major kinetic parameters of the electrochromic signals in young and old cells. Note the deceleration of dissipation of the electric field across the membrane upon aging the cells (10 ms → 42 ms).

The fluorescence of the cells was obtained by rectangular shape of laser excitation (at 808 nm) and showed typical transient as it increased from F_0 level to F_{max} level (Fig. 3). As the variable fluorescence ($F_v = F_{max} - F_0$) indicates the photochemical trapping of the excitons in the pigment bed, its ratio to the maximum fluorescence, F_v/F_{max} characterizes the capability of the bacterium to utilize the excitation (Bina

Table 1. (Bi)exponential fit of the flash induced electrochromic kinetics of young and old cells (Fig.3, panel B).

age of the cells (hrs)	abrupt (OB' or OA)	rise slow (AB)		decay (B'C or BC)	
	amplitude (mOD)	amplitude (mOD)	time (ms)	amplitude (mOD)	time (ms)
young (0)	1.8	–	–	1.8	10
old (28)	27	54	2.3	81	42

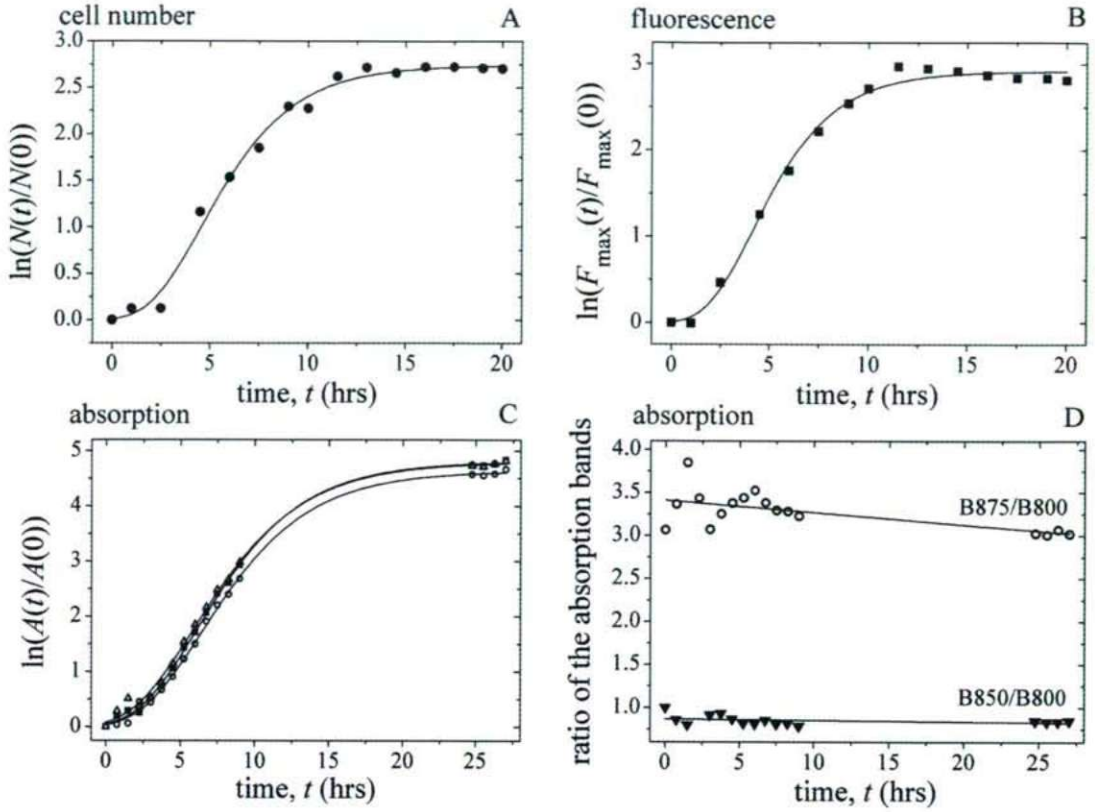

Figure 4. Growth curves calculated from cell number (Panel A, ●), from maximum fluorescence level (F_{max}) of the induction (Panel B, ■) and from areas of the Gaussian components (B800 (□), B850 (●) and B875 (▲)) of the absorption spectrum (Panel C) and fitted with the modified Gompertz equation (Eq. (2)). The best fit values are shown in Table 2. Panel D: The ratios of the absorption bands, B875/B800 (○) and B850/B800 (▼) are indicative of the changes of the LH1:LH2 distribution and of the share of the two BChl rings (B850 and B800) within the LH2 complex, respectively.

Table 2. Parameters of the growth curves (Fig. 4, panels A-C) fitted by the Gompertz equation (Eq. (2)) using N_0, N and N_{max} as initial, actual and asympthotic values of the investigated physical quantity (cell number, fluorescence, absorption or electrochromism), respectively, μ_{max} as maximum rate of doubling and Δt_0 as lag time. The cultures used in rows 1 and 2 were different from that used in rows 3 and 4.

physical quantities	initial value	fitting parameters: asymptothotic value	fitting parameters: maximum rate of doubling μ_{max} (h^{-1})	Δt_0 (h)
cell number	$5.5 \cdot 10^8$ cells/ml	$8.2 \cdot 10^9$ cells/ml	0.4	1.9
fluorescence, F_{max} (rel. units)	1.5	24	0.5	1.8
absorption (area, relative units)	0.18	23	0.44	2.2
B800	0.18	19	0.42	2.4
B850	0.55	68	0.43	1.8
B875				
electrochromism	1.8 mOD	81 mOD	0.7	2.9

et al. 2009; Kocsis et al. 2010). The larger is this ratio (the closer it is to 1), the more effective is the capture of excitation for photochemical purposes.

Growth curves

The growth curves were obtained by plotting the natural logarithm of the relative increase of the population, ln ($N(t)/N_0$), against the time, t elapsed from the inoculation of the cells in the culture medium (Fig. 4). The maximum of growth rate (μ_{max}), the lag phase duration (Δt_0) and the asymptotic population size (N_{max}) were determined by fitting the modified Gompertz equation to the growth curves (Zwietering et al. 1990):

$$(2) \quad \ln\frac{N(t)}{N_0} = N_{max} \cdot \exp\left\{-\exp\left[\frac{e \cdot \mu_{max}}{N_{max}}(\Delta t_0 - t) + 1\right]\right\}$$

where $N(t)$ is the cell concentration at the time t, N_0 is the initial cell concentration and e (the Euler's number) is the base of the natural logarithm. Similar fitting procedures were carried out for the oscillatory strengths of the dipoles (the

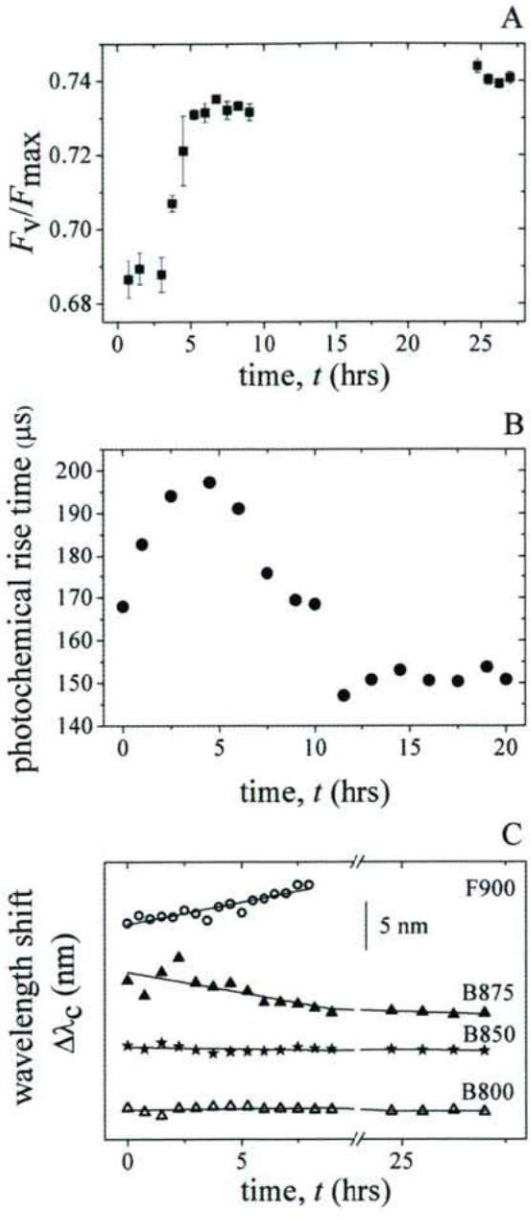

Figure 5. Fluorescence induction (A and B) and spectral changes (C) during cultivation of *Rba. sphaeroides* 2.4.1. Panel A: The F_v/F_{max} ratio shows abrupt rise upon cell division (■) and remains constant even in old cells. Panel B: The photochemical rise time (●) increases in younger cells, then levels off and decreases finally to the initial level in older cells. Panel C: Wavelength shifts of the peaks of characteristic bands during the growth of the bacterial culture. The main fluorescence band F900 shows red shift, the absorption band B875 of LH1 has blue shift and the B800 and B850 bands of LH2 have no changes during the exponential phase of the growth.

band area) of the antenna pigments B800, B850 and B875, for the maximum fluorescence levels after induction F_{max} and for the magnitude of the electrochromic changes. The fitting parameters are included in Table 2.

Discussion

The absorption and fluorescence properties of intact bacteria were measured in different phases of the growth to reveal what pigments and at what rate they are produced in the biochemical factories of the organism and how they are assembled into functional units essential to harvest the light and to energize the membrane.

After inoculation of the cells in the culture, the bacteria accommodate to the new conditions (large supply of light and nutrients). All of the investigated parameters show a lag phase of duration about 2 hours. After this transient, the cells divide with high rate (exponential phase, the doubling time is 3 hrs) and the population consists of young (mother and daughter) cells. Upon graduate exhaustion of the food supply, however, the rate of division progressively decreases (intermediate phase) and finally gets zero, *i.e.* no (net) cell division takes place (late stationary phase). These cells can be aged and we call them as old cells. The primary purpose of this study is the comparison of the young and old cells based on spectroscopic characteristics to get easily accessible marks for aging the cells.

Principally, the activity of pigment production and incorporation into protein complexes were in full accordance with the rate of cell division (Fig. 4). We observed slight but definite deviations from this general tendency in some cases only (Fig. 5). 1) The dominance of the core light harvesting complex LH1 compared to the peripheral complex LH2 was stronger in old cells, than in young cells. 2) The fluorescence maximum of the old cells showed red shift of about 5 nm and similar size but blue spectral shift was observed for the B875 pigment. 3) The variable fluorescence was larger by 10% in old bacteria than in young bacteria and the photochemical rise time showed also slight variation indicating moderate changes of the size or connectivity of the antenna system during aging. 4) The old cells performed more stable membrane potential after flash excitation than the younger cells (Fig. 3). As the kinetics of establishment and breakdown of the membrane potential depends on movement of electric charges (electrons, ions and protons) and the dielectric properties (sealing) of the photosynthetic membrane (Bailleul et al. 2010), one can conclude for more sophisticated (finely tuned) dielectrics in old cells than in young cells.

These observations indicate that roughly the same pigments are produced and incorporated into the same protein complexes throughout the growth and no large deviations from this tendency were experienced. That would shed some light of critics on recent conclusions of sequential assembly of photosynthetic units in *Rhodobacter sphaeroides* (Koblizek et al. 2005). If the assembly was sequential i.e. the appearance of LH1 was followed by the creation of LH2, then one would expect large changes in the photochemical rate and/or variable fluorescence. As we did not observe the predicted changes in neither phases of the growth curve, the model of parallel pro-

duction and assemble of complexes would be more adequate to our observations. We expect more straightforward proof of the parallel model by performing similar experiments not on asynchronous (as in this study) but on synchronous culture of bacteria under which conditions all cells are brought to the same physiological state.

Acknowledgements

We are indebted to Dr Tamás Herczeg for the valuable discussions and to Ms Diana Nyúli for preparation of Figure 1. The support of NKTH-OTKA (K-67850), COST Action on "*Molecular machineries for ion translocation across biomembranes*" (CM0902) and MTA-CNR Bilateral agreement on "*Bacterial photosynthesis: artificial photosystems and bioremediation*" is acknowledged.

References

Asztalos E. Maróti P (2009) Export or recombination of charges in reaction centers in intact cells of photosynthetic bacteria. Biochim Biophys Acta 1787:1444–1450.

Asztalos E, Italiano F, Milano F, Maróti P, Trotta M (2010) Early detection of mercury contamination by fluorescence induction of photosynthetic bacteria. Photochem Photobiol Sci 9:1218-1223.

Bailleul B, Cardol P, Breyton C, Finazzi G (2010) Electrochromism: a useful probe to study algal photosynthesis. Photosynth Res 106:179-189.

Bina D, Litvin R, Vácha F (2009) Kinetics of in vivo bacteriochlorophyll fluorescence yield and the state of photosynthetic apparatus of purple bacteria. Photosynth Res 99:115–125.

De Klerk H, Govindjee, Kamen MD, Lavorel J (1969) Age and Fluorescence Characteristics in some Species of *Athiorhodaceae*. Proc Nat Acad Sci 62:972-978.

Imhoff JF (1995) Taxonomy and Physiology of Phototrophic Purple Bacteria and Green Sulfur Bacteria, In: Anoxygenic Photosynthetic Bacteria (Eds. Blankenship RE, Madigan MT and Bauer CE), Kluwer Academic Publishers, Dordrecht, The Netherlands, pp.1-15.

Jamieson SJ, Wang P, Qian P, Kirkland KY, Conroy MJ, Hunter CN, Bullough PA (2002) Projection structure of the photosynthetic reaction centre antenna complex of *Rhodospirillum rubrum* at 8.5 Å resolution. EMBO Journal, 21(15):3927-3935.

Jungas C, Ranck J, Rigaud J, Jolliot P, Verméglio A. (1999) Supramolecular organization of the photosynthetic apparatus of *Rhodobacter sphaeroides*. EMBO Journal 18(3):534-542.

Hohmann-Marriott MF, Blankenship RE (2007) Variable fluorescence in green sulfur bacteria. Biochim Biophys Acta 1767:106–113.

Koblizek M, Shih JD, Breitbart SI, Ratcliffe EC, Kolber, ZS, Hunter CN, Niederman RA (2005) Sequential assembly of photosynthetic units in *Rhodobacter sphaeroides* as revealed by fast repetition rate analysis of variable bacteriochlorophyll a fluorescence. Biochim Biophys Acta 1706: 220–231.

Kocsis P, Asztalos E, Gingl Z, Maróti P (2010) Kinetic bacteriochlorophyll fluorometer. Photosynth Res 105:73-82.

Maróti P (2008) Kinetics and yields of bacteriochlorophyll fluorescence: redox and conformation changes in reaction center of *Rhodobacter sphaeroides*. Eur Biophys J 37:1175–1184.

Maróti P, Wraight CA (1988) Flash-induced H^+ binding by bacterial photosynthetic reaction centers: comparison of spectrometric and conductometric methods. Biochim Biophys Acta 934:314–328.

Maróti P, Wraight CA (2008) The redox midpoint potential of the primary quinone of reaction centers in chromatophores of *Rhodobacter sphaeroides* is pH independent. Eur Biophys J 37:1207–1217.

Masuda S, Bauer CE (2002) AppA is a blue light photoreceptor that antipresses photosynthesis gene expression in *Rhodobacter sphaeroides*. Cell 110:613-623.

Olsen JD, Sturgis JN, Westerhuis WH, Fowler GJS, Hunter CN, Robert B. (1997) Site-directed modification of the ligands to the bacteriochlorophylls of the light-harvesting LH1 and LH2 complexes of *Rhodobacter sphaeroides*. Biochemistry 36(41):12625-12632.

Olsen JD, Tucker JD, Timney JA, Qian P, Vassilev C, Hunter CN (2008) The Organization of LH2 Complexes in Membranes from *Rhodobacter sphaeroides*. J Biol Chem 283(45):30772–30779.

Papageorgiou G, Govindjee (eds) (2004) Chlorophyll a fluorescence: a signature of photosynthesis. Advances in photosynthesis and respiration. Springer, Dordrecht, The Netherlands.

Qian P, Bullough PA, Hunter CN (2008) Three-dimensional reconstruction of a membrane-bending complex - The RC-LH1-PufX core dimer of *Rhodobacter sphaeroides*. Journal of Biological Chemistry 283(20):14002-14011.

Roszak AW, Howard TD, Southall J, Gardiner AT, Law CJ, Isaacs NW, Cogdell RJ (2003) Crystal structure of the RC-LH1 core complex from *Rhodopseudomonas palustris*. Science 302(5652):1969-1972.

Siebert CA, Qian P, Fotiadis D, Engel A, Hunter CN, Bullough PA (2004) Molecular architecture of photosynthetic membranes in *Rhodobacter sphaeroides*: the role of PufX. EMBO Journal 23(4):690-700.

Sistrom WR (1962) The Kinetics of the Synthesis of Photopigments in *Rhodopseudomonas sphaeroides*. *J Gen Microbiol* 28:607–616.

Sundstrom V, Pullerits T, van Grondelle R (1999) Photosynthetic light harvesting: Reconciling dynamics and structure of purple bacterial LH2 reveals function of photosynthetic unit. J Phys Chem B 103(13):2327-2346.

Takemoto J, Lascelles J (1973) Coupling between bacteriochlorophyll and membrane protein synthesis in *Rhodopseudomonas sphaeroides*, Proc Natl Acad Sci USA 70: 799-803.

Walz T, Jamieson SJ, Bowers CM, Bullough PA, Hunter CN (1998) Projection structures of three photosynthetic complexes from *Rhodobacter sphaeroides:* LH2 at 6 Å, LH1 and RC-LH1 at 25 Å. J Mol Biol 282(4):833-845.

Wraight CA, Cogdell RJ, Chance B (1978) Ion Transport and Electrochemical Gradients in Photosynthetic Bacteria. In: The Photosynthetic Bacteria (Eds. Clayton RK, Sistrom WR) Plenum Publishing Corporation 471-511.

Zwietering MH, Jongenburger I, Rombouts FM, van't Riet K (1990) Modeling of the Bacterial Growth Curve. Appl Environ Microbiol 56:1875–1881.

Volume 54(2):155-160, 2010
Acta Biologica Szegediensis
http://www.sci.u-szeged.hu/ABS

ARTICLE

Electrochemical responses of carbon fiber microelectrodes to dopamine *in vitro* and *in vivo*

Dénes Budai[1,2]*, István Hernádi[3], Beatrix Mészáros[2], Zsolt K. Bali[3], Károly Gulya[1]

[1]Department of Cell Biology and Molecular Medicine, University of Szeged, Szeged, Hungary, [2]Kation Europe Bt., Szeged, Hungary, [3]Department of Experimental Zoology and Neurobiology, University of Pécs, Pécs, Hungary

ABSTRACT Cylindrical, 7 µm in diameter carbon fiber (CF) microelectrodes were constructed and tested for their responses to dopamine in constant potential amperometry or fast scan cyclic voltammetry (FSCV). Amperometry was carried out in a miniature perfusion chamber whereas background subtracted FSCV was performed both *in vitro* and *in vivo*. For calibration performance of the microelectrodes, peak oxidation currents were determined using unmodified carbon tips of varying lengths and plotted against the tip lengths. A very close linear correlation ($r = 0.997$) was found between the two variables for tip lengths ranging from 25 to 300 µm. Also, a very close linear correlation was found between the oxidation current at a given carbon tip length in response to increasing dopamine concentrations measured by either amperometry or FSCV. *In vivo* experiments were carried out in the visual cortex of the anaesthetized rat to detect dopamine release in response to visual stimulation. Indeed, background subtracted cyclic voltammograms showed an increase in the current at 0.65 V which is the typical dopamine oxidation potential.

Acta Biol Szeged 54(2):155-160 (2010)

KEY WORDS

carbon fiber
microelectrode
extracellular recording
amperometry
cyclic voltammetry

Carbon fiber (CF) microelectrodes have been used to extracellularly record neuronal action potentials (Armstrong-James and Millar 1979) and to detect electrochemical signals *in vitro* and *in vivo* (Ponchon et al. 1979). They have been demonstrated to be very suitable for detection of catecholamines such as dopamine or norepinephrine and other oxidizable biological species including nitric oxide (Malinski and Taha 1992). Since the early times in CF applications for biorecording, a variety of enzyme-modified CF microbiosensors has been introduced for the *in situ* determination of biologically important compounds. Recently, the immobilization of DNA molecules or carbon nanotubes onto CF microelectrodes allowed the construction microsensors for a great variety of analytes. Another novel use of CF microelectrodes is sensing tissue oxigen levels at a micrometer scale. For review, see (Budai 2010).

The CF microelectrodes are graphite monofilaments and are about 7 µm in diameter. A basic CF microelectrode is an elementary carbon filament built in a mechanically supportive and electrically insulating borosilicate glass or plastic sheathing. The uninsulated carbon tip protruding from the sheathing by 10 µm to a few 100 µm provides an electroactive surface for picking up spikes from the near vicinity of neurons and/or surface for electron transfer in electrochemical measurements and microbiosensor applications. The chemically relatively inert CF has outstanding mechanical and electrical properties and provides an excellent base electrode for electrophysiological, electrochemical and biosensor applications on a micrometer or perhaps even on a submicrometer scale.

Miniaturization, however, has its own limitations. At a given current density, for example, an overly small electroactive surface may greatly diminish the electrode performance and shows a poor signal-to-noise ratio. When the electrochemical measurement is combined with single-unit recording a shorter tip of 20 to 30 µm is required, as longer carbon lengths give rise to multiple-unit recording (Stamford et al. 1993). For these reasons, and as longer carbon tip represents a greater active surface, we studied the electrochemical responses of CF microelectrodes as a function of the exposed carbon tip length. Experiments were performed using constant potential amperometry in a miniature perfusion chamber or employing fast scan cyclic voltammetry (FSCV) *in vitro* or *in vivo*.

Materials and Methods

Manufacturing CF microelectrodes

Single-barrel CF microelectrodes were made from borosilicate glass capillary tubing (1.50 mm O.D., 0.84 mm I.D., WPI, Sarasota, FL) containing a 7 µm in diameter carbon fiber monofilament as previously described in details (Budai and Molnár 2001). After pulling the blank, the excess length of the CF protruding from the tip of the glass was cut with a fine pair of scissors to about 5 mm. The exposed CF was finally trimmed to lengths of 25, 50, 75, 100, 200 or 300 µm using high voltage spark etching under a light microscope.

Accepted Dec 20, 2010
*Corresponding author. E-mail: kations@aol.com

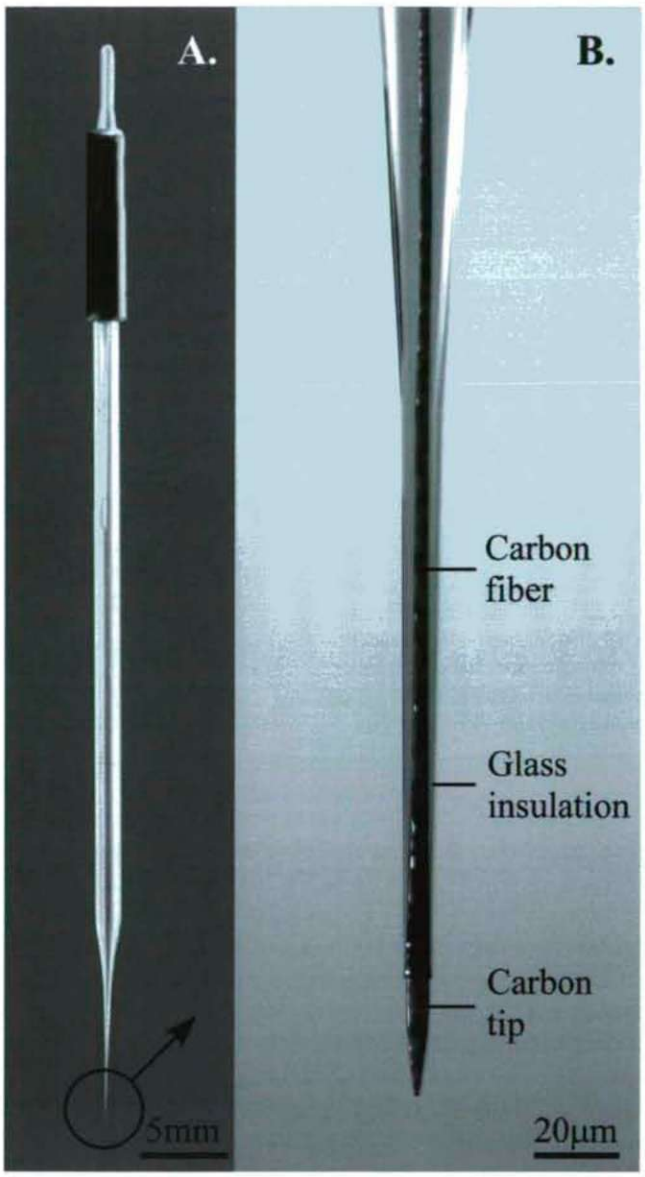

Figure 1. A: View of a carbon carbon fiber microelectrode. The gold-plated connector is galvanically connected to the 7 µm in diameter carbon monofilament that provides the lead element in the borosilicate glass micropipette. B: Light microscopic stucture of the tip. The carbon fiber protrudes from the electrically insulating glass support and ends in a sharp, conical tip. The length of the exposed carbon tip were selected between 25 µm (shown) and 300 µm in the present experiments.

The completed microelectrode is shown in Figure 1.

Electrochemical measurements

Constant potential amperometric experiments were carried out at room temperature (25°C) using a 'Micro C' carbon fiber potentiostat (WPI, Sarasota, FL). The oxidization currents were measured using various lengths of the carbon tip as working electrodes that were kept at 0.65 V against a Ag/AgCl half cell in a miniature, 1 ml perfusion chamber. Physiological saline was continuously perfused at a rate of 2 ml/min from one of the syringes of a two-syringe infusion pump. The other syringe contained dopamine hydrochloride (Sigma, Saint Louis, MO) dissolved in saline at various concentrations and switchings between the two syringes were made using 3-port manifold. Data acquisition was performed using a NI PCI6221 multifunction data acquisition board placed in a desktop computer and programmed in LabView (National Instruments, Austin, TX). Fast scan cyclic voltammetry (FSCV) were performed using a custom-built analogue triangle waveform generator hardware (System Kellényi, BioPot V4, 2009) controlled by a LabVIEW driver developed in-house and the resulting signals were acquired by a PCI-6025E data acqisition card (National Instruments, Austin, TX). A CED 1401Plus data acquisition system (CED, Cambridge, UK) was also used to synchronize waveform application, data acquisition, and light stimulation delivery for *in vivo* experiments. A scan rate of 300 V/s was applied with a resting potential of -0.2 to -0.4 V. For reference Ag/AgCl electrode was used. In individual scans, the anodic limit was set to 1.0 V, and the measurements were typically repeated at 200 ms intervals. The collected raw data signal was on line background subtracted, signal averaged, and digitally filtered with a custom-built control software in a LabView environment. Dopamine solutions of various concentrations were measured to plot the calibration curves of CF microelectrodes. Dopamine was dissolved in 100 mmol/l phosphate buffer solution (pH= 7.4). Voltammograms obtained in phosphate buffer solution were subtracted from the curves of dopamine solutions to eliminate the background current (Howell et al. 1986). Maximum oxidation currents were plotted against the concentration of dopamine to find correlation between the two variables.

In vivo recordings

FSCV recordings were taken using 100 µm-long, unmodified CF microelectrodes in various areas of the visual neocortex of anesthetized rats to test the involvement of V1/V2ML cortical neurons in stimulation paradigm using light flash stimuli to induce related activity. Experiments were carried out in male Wistar rats (Charles River Laboratories, Gödöllő, Hungary) with the approval of the Animal Care Committee of the University of Pécs, Hungary and in compliance with international standards. Anaesthesia was induced with a single intraperitoneal injection of ketamine (100 mg/kg, SBH, Budapest, Hungary) and maintained with 20% of the initial dose administered in approximately every 45 min thereafter for a maximum of three times. Stereotaxic coordinates for the targeted regions were selected according to the atlas of Paxinos and Watson (1986) and were as follows: AP (from bregma): -5.5 to -6.5 mm; L: 2 to 3 mm; V (from brain surface): 0.5 to 3.0 mm.

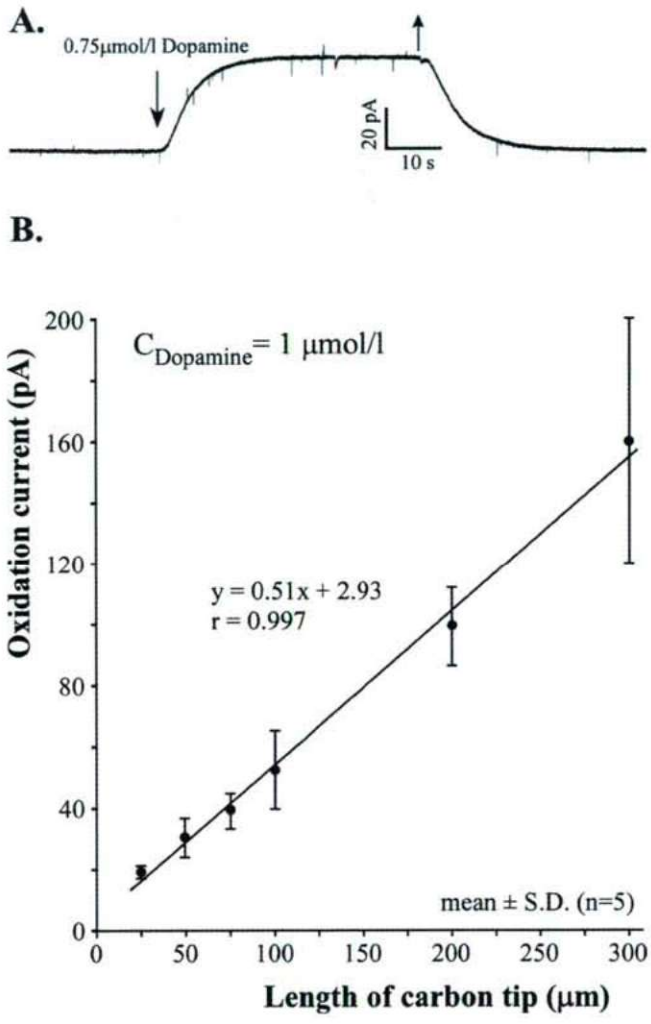

Figure 2. A: A representative constant potential amperometric response of a 100 µm long carbon tip to 0.75 µmol/l dopamine at 0.65 V in a miniature perfusion chamber. B: Linear relationship between the length of the carbon tip and the oxidation current at 0.65 V in response to 1.0 µmol/l dopamine. Data represent the mean ± SD of 5 experiments.

Visual stimulation were performed using two bright green LEDs (one on each side) served as whole field visual stimuli and were lit for 200 to 500 ms from a distance of 7 cm to the eyes of the subject. The frequency of visual stimulation was set between 0.2 and 0.5 Hz and a typical block of trials contained 20 to 50 trials to enable averaging of the electrochemical data. Extracellular multiple unit activity and micro-EEG was recorded through the carbon fiber of the microelectrode to ensure that the cortical area in the vicinity of the electrode was responding to visual stimulation. Neuronal signal was passed through a biological amplifier (BioAmp, Supertech Ltd, Pécs, Hungary) and an analogue-digital converter interface (Power 1401, CED, Cambridge, UK) and saved in a desktop computer.

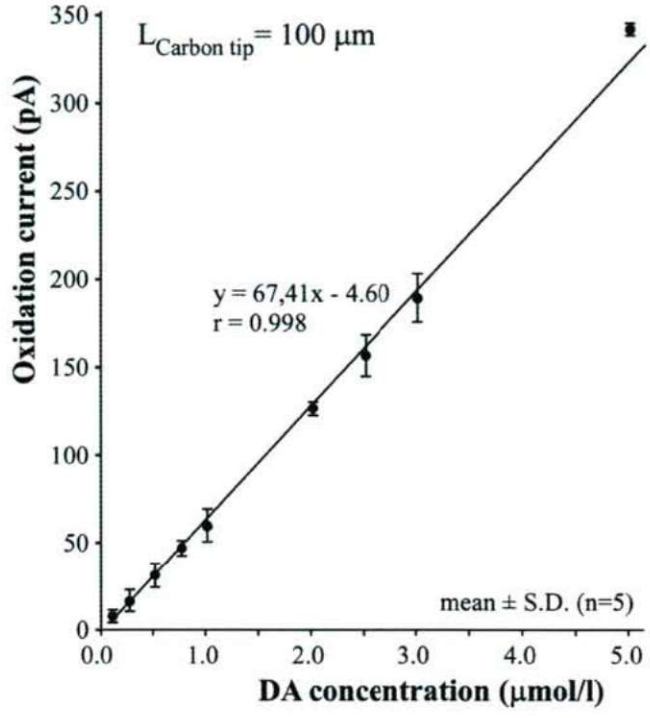

Figure 3. Linear correlation between dopamine (DA) concentration and the resulting oxidation current at a 100 µm-long carbon tip kept at 0.65 V. Data represent the mean ± S.D. of 5 experiments.

Results and Discussion

Constant potential amperometry

In amperometric measurements, the CF microelectrode is held at a constant potential (e.g., 0.65 V for catecholamines) exceeding the redox potential of the substance of interest. When molecules such as epinephrine or dopamine hit the carbon surface, electrons are transferred and a current can be measured. For reviews, see (Kawagoe et al. 1993; Wightman 2006). Constant potential amperometry offers the best temporal resolution among the available techniques, however, it suffers from poor selectivity: any molecule that can be oxidized or reduced at the potential of the electrode is detected, so there is no way to differentiate between molecules. As expected, the surface area available for electron transfer will significantly influence the sensitivity and, hence, the signal-to-noise ratio in such electrochemical recordings (Kawagoe et al. 1991; Armatore et al. 2009). In case of the 7 µm in diameter CF microelectrodes the smallest possible electroactive area is formed when a glass-encased carbon monofilament is beveled to 90° or to other angles for studying dopamine release from single cells (Armatore et al. 2009; Adams et al. 2011). On the other end, up to 250 µm of the exposed carbon tip is usually left protruding from the sheathing when *in vivo* electrochemical recordings are taken from the brain (Fig. 1B) (Dugast et al. 2002; Clark et al. 2010). These larger cylindri-

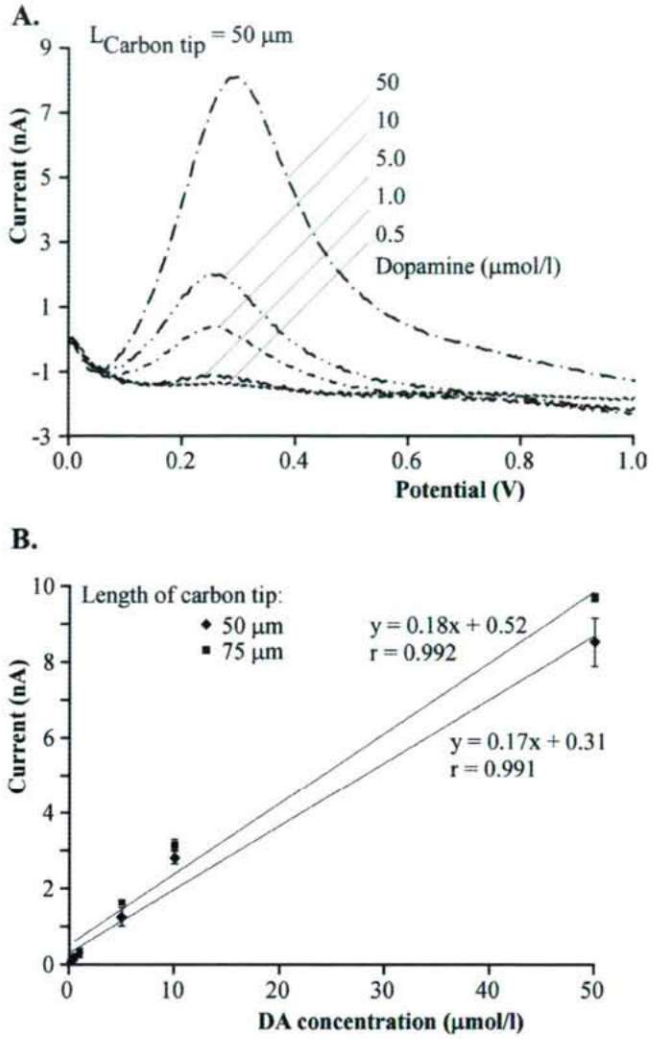

Figure 4. Fast scan cyclic voltammetry of dopamine (DA) in 0.1 mol/l phosphate buffer (pH= 7.4) using CF microelectrodes. A: Background subtracted voltammograms of dopamine plotted against the electrode potential. Measurements were performed using a 50 µm-long CF microelectrode. Only the oxidative phases of cycles are shown for clarity. B: Linear correlation between peak oxidation currents shown in panel A and the dopamine concentrations for CF microelectrodes having 50 µm or 75 µm tip lengths. Data represent the mean ± SD of 3 experiments.

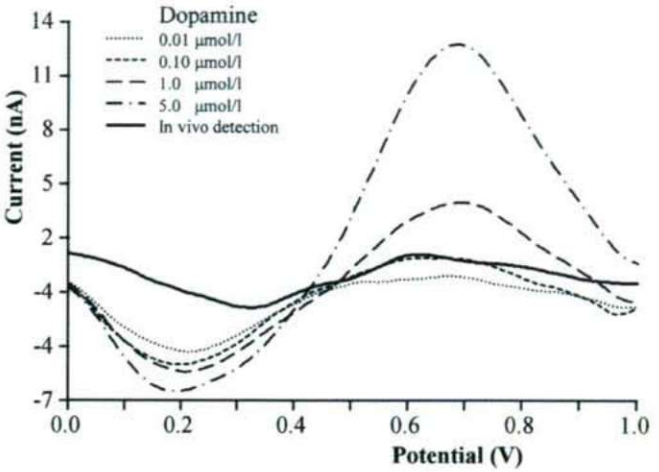

Figure 5. Fast scan cyclic voltammetry in the V2ML region of the visual cortex of rat brain using CF microelectrodes. Comparison of the background subtracted cyclic voltammograms obtained in dopamine solutions and in the V2ML region of the visual cortex in rat brain during light stimulation. Each curve is the average of 10 scans. The background signals to be subtracted were recorded in phosphate buffer solutions (for *in vitro* experiments) or in the V2ML without stimulation (for *in vivo* experiment). Oxidation peak currents for *in vivo* experiments appeared at the same electrode potential as in typical measurements of dopamine solutions *in vitro*.

cal microelectrodes are advantageous because the secreted molecules come from multiple terminals near the electrode, and the greater electroactive area leads to a larger signal that emerges from the Johnson noise of the current amplifier (Kovach et al. 1984). However, when the electrochemical measurement is combined with single-unit recording a shorter tip of 20 to 30 µm is required, as longer carbon lengths give rise to multiple-unit recording (Stamford et al. 1993).

In the present set of experiments, we studied the constant potential amperometric responses of cylindrical CF microelectrodes in a miniature perfusion cell to dopamine while the electrode potential was kept at 0.65 V (Fig. 2A). These electrodes were `pristine`, that is untreated and unmodified with any procedure, and their selected lengths were 25, 50, 75, 100, 200 or 300 µm. We found a linear relationship between the exposed carbon tip length and the dopamine oxidation current as shown in Figure 2B. For example, a 100 µm-long carbon tip produced about 50 pA oxidation current under these conditions. The linear regression analysis based on 5 measurements for each data point resulted in the equation of $y = 0.51x + 2.93$ with a correlation coefficient of $r = 0.997$. Also, a very close linear correlation was found between the oxidation currents measured at a 100 µm-long carbon tip in response to increasing dopamine concentrations (Fig. 3). The relationship between the two variables was $y = 67.41x - 4.60$ with a correlation coefficient of $r = 0.998$, based on 5 measurements for each data point.

Our primary goal was to find an exact relationship between dopamine oxidation current and the length of untreated carbon tip or dopamine concentration. It should be noted, however, that electrochemical pretreatment of the carbon tip or modifying the electroactive surface with Nafion (Kuhr and Wightman 1986, Brazell et al. 1987; Hashemi et al. 2009), 4-sulfobenzene (Hermans et al. 2006) or modified with an over-oxidized polypyrrole film (Zhang et al. 1996) can greatly enhance the selectivity and sensitivity of these CF microelectrodes. For review, see (Troyer et al. 2002).

Fast scan cyclic voltammetry

Fast scan cyclic voltammetry (FSCV) is performed by holding the microelectrode at a constant potential versus a reference electrode, followed by a rapid increase in potential and an immediate return back to the holding potential. The voltage limits are chosen so that the reduction and oxidation of the analyte of interest lies within this potential window. FSCV provides good chemical selectivity while retaining subsecond temporal resolution. Each measurement consists of a cyclic voltammogram that serves as a chemical identifier to provide chemical selectivity. It has been shown to be very useful for the detection of catecholamine fluctuations *in vivo* because of the high sensitivity and selectivity (Robinson et al. 2003, 2008).

CF microelectrodes are well-suited for use in FSCV measurements for the detection of monoamines (Baur et al. 1988). In the present experiments, 7 µm in diameter and 50 or 75 µm-long CF microelectrodes were used to measure dopamine oxidation currents in FSCV carried out in 100 mmol/l phosphate buffer (pH 7.4) at 300 V/s scan speed. As shown in Figure 4A, increasing dopamine concentrations led to increasing oxidation currents at a 50 µm-long CF microelectrode. When the background subtracted peak currents were plotted *versus* concentrations of dopamine, a close correlation between the two variables was revealed (Fig. 4B). The linear regression analyses based on 3 measurements for each data point resulted in the respective equations of $y = 0.17x + 0.31$ ($r = 0.991$) and $y = 0.18x + 0.52$ ($r = 0.992$) for 50 and 75 µm-long carbon tips.

In vivo measurements

Because fast scan cyclic voltammograms can be repeated every 100 ms, changes in dopamine concentration can be monitored with good chemical selectivity on the subsecond time scale. These characteristics make FSCV well suited for detecting phasic dopamine changes in the brain even in the freely moving animal (Robinson et al. 2003, 2008). By locating the potentials at which the maximum cathodic and anodic currents occur, one can distinguish many different neurotransmitters.

In our present study, FSCV was carried out in visual cortex of the rat to detect dopamine release in response to visual stimulation. Indeed, background subtracted cyclic voltammograms showed an increase in the current at 0.65 V which is the typical dopamine oxidation potential (Fig. 5). The background to be subtracted was recorded in the absence of light stimulation so the raise in oxidation current was clearly due to the visual stimulation afterward. It should also be noted, however, that there may be other electroactive substances which show oxidation peak at the potential similar to that of the dopamin. Hence, the measured oxidation peak can represent not only dopamine but other monoamines or dopamine metabolites. Through electrical stimulation of midbrain areas containing dopaminergic neurons (such as VTA) or local administration of dopamine can further justify the measured electrochemical signal (Phillips and Wightman 2003).

Acknowledgments

This work was financially supported by the Hungarian Ministry of Economy and Transport (GVOP-3.3.1-05/1.-2005-05-0141/3.0) and the National Office for Research and Technology (INNO_08-6-2009-0024).

References

Adams KL, Jena BK, Percival SJ, Zhang B (2011) Highly sensitive detection of exocytotic dopamine release. Anal Chem In Press.

Amatore C, Arbault S, Bouret Y, Guille M, Lemaitre F Verchier Y (2009) Invariance of exocytotic events detected by amperometry as a function of the carbon fiber microelectrode diameter. Anal Chem 81:3087-3093.

Armstrong-James M, Millar J. (1979) Carbon fibre microelectrodes. J Neurosci Methods 1:279-287.

Baur JE, Kristensen EW, May LJ, Wiedemann DJ, Wightman RM (1988) Fast-scan voltammetry of biogenic amines. Anal Chem 60:1268-1272.

Brazell MP, Kasser RJ, Renner KJ, Feng J, Moghaddam B, Adams RN (1987) Electrocoating carbon fiber microelectrodes with Nafion improves selectivity for electroactive neurotransmitters. J Neurosci Methods 22:167-72.

Budai D (2010) Carbon Fiber-based Microelectrodes and Microbiosensors. In Somerset VS ed., Intelligent and Biosensors. INTECH, Vukovar, Croatia 269-288.

Budai D, Molnár Z (2001) Novel carbon fiber electrodes for extracellular electrophysiology. Acta Biol Szeged 45:65-73.

Clark JJ, Sandberg SG, Wanat MJ, Gan JO, Horne EA, Hart AS, Akers CA, Parker JG, Willuhn I, Martinez V, Evans SB, Stella N, Phillips PEM (2010) Chronic microsensors for longitudinal, subsecond dopamine detection in behaving animals. Nature Methods 7:126-129.

Dugast C, Cespuglio R, Suaud-Chagny MF (2002) In vivo monitoring of evoked noradrenaline release in the rat anteroventral thalamic nucleus by continuous amperometry. J Neurochem 82: 529-537.

Hashemi P, Dankoski EC, Petrovic J, Keithley RB, Wightman RM (2009) Voltammetric detection of 5-hydroxytryptamine release in the rat brain. Anal Chem 81:9462–9471.

Hermans A, Seipel AT, Miller CE, Wightman RM (2006) Carbon-fiber microelectrodes modified with 4-sulfobenzene have increased sensitivity and selectivity for catecholamines. Langmuir 22:1964–1969.

Howell JO, Kuhr WG, Ensman RE, Wightman MR (1986) Background subtraction for rapid scan voltammetry. J Electroanal Chem Interfac Electrochem 209:77-90.

Kawagoe KT, Jankowski JA, Wightman RM (1991) Etched carbon-fiber electrodes as amperometric detectors of catecholamine secretion from isolated biological cells. Anal Chem 63:1589-1594.

Kawagoe KT, Zimmerman JB, Wightman RM (1993) Principles of voltammetry and microelectrode surface states. J Neurosci Methods 48:225-240.

Kovach PM, Ewing AG, Robert L. Wilson RL, Wightman RM (1984) In vitro comparison of the selectivity of electrodes for in vivo electrochemistry. J Neurosci Methods 10:215-227.

Kuhr WG, Wightman RM (1986) Real-time measurement of dopamine release in rat brain. Brain Res 381:168-171.

Malinski T, Taha Z (1992) Nitric oxide release from a single cell measured in situ by a porphyrinic-based microsensor. Nature 358:676-678.

Paxinos G, Watson C (1986) The rat brain in stereotaxic coordinates. Burlington, MA: Elsevier.

Phillips PEM, Wightman MR (2003) Critical guidelines for validation of the selectivity of in-vivo chemical microsensors, Trends in Anal Chem 22:509-514.

Ponchon JL, Cespuglio R, Gonon F, Jouvet M, Pujol JF (1979) Normal pulse polarography with carbon fiber electrodes for in vitro and in vivo determination of catecholamines. Anal Chem 51:1483-1486.

Robinson DL, Venton BJ, Heien ML, Wightman RM (2003) Detecting subsecond dopamine release with fast-scan cyclic voltammetry in vivo. Clin Chem 49:1763-1773.

Robinson DL, Hermans A, Seipel AT, Wightman RM (2008) Monitoring rapid chemical communication in the brain. Chem Rev 108:2554-84.

Stamford JA, Palij P, Davidson C, Jorm CM, Millar J (1993) Simultaneous "real-time" electrochemical and electrophysiological recording in brain slices with a single carbon-fibre microelectrode. J Neurosci Methods 50:279-290.

Troyer KP, Heien ML, Venton BJ, Wightman RM (2002) Neurochemistry and electroanalytical probes. Curr Opin Chem Biol. 6:696-703.

Wightman RM (2006) Probing cellular chemistry in biological systems with microelectrodes. Science 311:1570-1574.

Zhang X, Ogorevc B, Tavcar G, Svegl IG (1996) Over-oxidized polypyrrole-modif ied carbon fibre ultramicroelectrode with an integrated silver/silver chloride reference electrode for the selective voltammetric measurement of dopamine in extremely small sample volumes. Analyst 121:1817-1822.

Volume 54(2):161-164, 2010
Acta Biologica Szegediensis
http://www.sci.u-szeged.hu/ABS

ARTICLE

Spreading depression and evoked potentials recorded in the somatosensory cortex of the rat

Gáspár Oláh[1], Dávid Nagy[1], Máté Marosi[1], Tamás Farkas[1], Zsolt Kis[1], Árpád Párdutz[2], János Tajti[2], László Vécsei[2], József Toldi[1]*

[1]Department of Physiology, Anatomy and Neuroscience, University of Szeged, Szeged, Hungary, [2]Department of Neurology, University of Szeged, Szeged, Hungary

ABSTRACT Cortical spreading depression (CSD) is associated with changes in the caliber of surface blood vessels; others have described it as a phenomenon which arises spontaneously and repetitively following acute cortical injury in animals, including both focal ischemia and trauma, while yet other researchers consider it to be an electrophysiological substrate of migraine aura, which may trigger headache. Our group is involved in research into both migraine and ischemia-induced pathophysiological states. It therefore appeared reasonable to include the study of CSD in the methodological repertoire utilized in our laboratory. We introduced two models of CSD induction: CSD evoked during continuous topical KCl application and CSD induced through a single KCl microinjection into the cortical tissue. This paper describes details of these two methods and of basic parameters of CSDs. **Acta Biol Szeged 54(2):161-164 (2010)**

KEY WORDS

cortical spreading depression,
migraine,
aura,
ischemia,
ischemic brain tissue

Cortical spreading depression (CSD), discovered by Leao in 1944, is a transient negative direct current (DC) potential shift that slowly propagates throughout the cortex irrespective of functional or vascular territories. The main event during the generation and propagation of CSD is the depolarization of a critical mass of brain tissue associated with a massive increase in extracellular K^+ and neurotransmitters, water influx into the cells and shrinkage of the extracellular space volume (Kraig and Nicholson 1978; Gardner-Medwin 1981; Somjen 2001).

Under experimental circumstances, various stimuli or functional states can trigger CSD, e.g. electrical stimulation, cortical trauma, high concentrations of excitatory amino acids or K^+. Different experimental models have been introduced, such as the recording of CSDs evoked during continuous topical KCl application (Ayata et al. 2006; Kudo et al. 2008), or the microinjection of KCl into the brain tissue (Richter et al. 2008, 2010).

In humans, CSD was for a long time mostly associated with the pathogenesis of migraine aura (Lauritzen 1994; Pietrobon and Striessnig 2003). Human imaging data have revealed the occurrence of a CSD-like event during a migraine attack (Woods et al. 1994; Hadjukhani et al. 2001). Recent research, however, demonstrated the occurrence of CSD with prolonged depression periods in the ECoG in patients with brain injury, brain hemorrhage and ischemia (Dohmen et al. 2008; Hartings et al. 2009).

Accepted Nov 30, 2010
*Corresponding author. E-mail: toldi@bio.u-szeged.hu

In *in vitro* studies, it has been shown that oxygen and glucose deprivation, for example, cause an anoxic depolarization similar to CSD (Jarvis et al. 2001). The question arises as to whether ischemia-related CSDs occur in the adult brain, and whether this is a relevant pathological mechanism via which to link hypoxia with a neuronal dysfunction.

During recent years, we have worked on the fields of both migraine and ischemia-induced pathophysiological states and the possibilities of neuroprotection (Robotka et al. 2008; Sas et al. 2008, 2010; Vamos et al. 2010). It seemed reasonable to introduce the study of CSD into the methodological repertoire used in our laboratory for the investigation of the pathomechanism of migraine and brain ischemia, and protection procedures.

We introduced two models of CSD induction: i) CSD evoked during continuous topical KCl application, ii) CSD induction through a KCl microinjection into the cortical tissue. The aim of this study was to adopt these methods and a) to quantify the basic parameters of the CSDs (the mean amplitude and the duration of half the amplitude), b) to determine the average CSD frequencies during continuous topical KCl application, and c) to study the relation between the evoked potentials (EPs) and CSDs.

Materials and methods

Animals

The experimental procedure used in this study adhered to the protocol for animal care approved by the Hungarian Health Committee (1998) and the European Communities Council

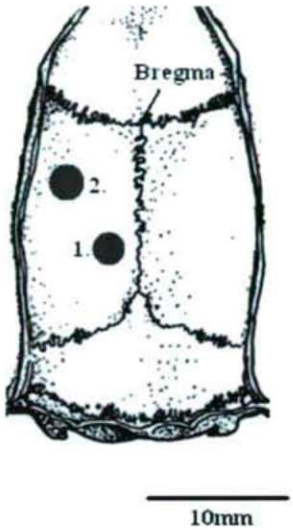

Figure 1. Schematic drawing showing the configuration of the experiment. 1: A hole above the occipital cortrex (-5;2 mm from the bregma) for the administration of KCl. 2: An exposed area in the parietal part of the skull beyond the somatosensory cortex (-3;5 mm fom the bregma) for the recording of the CSDs and SEPs.

Directives (86/609/EEC). Male Wistar rats (230-250 g) were used in the experiments. Every effort was made to minimize the number of animals used and their suffering. The animals were kept under 12-h light and 12-h dark conditions, with lights on at 6 a.m., and were raised with free access to water and food pellets. The room temperature was 22 ± 1°C.

Surgical procedures

All surgical procedures were carried out under deep anesthesia. During the experiments, the animals were anesthetized with an intraperitoneal injection of urethane (1.3 g/kg, i.p.), and their heads were then fixed in a stereotaxic head-holder (David Kopf. Instr.). On the left side, above the occipital cortex, a hole (diameter 1-2 mm) was made with a mini-drill. On the parietal part of the skull (just above the primary somatosensory area), the cortex was also exposed via another hole (diameter also 1-2 mm), with the same mini-drill (Fig. 1). The exposures were made under saline cooling. The dura mater and the underlying archnoidea were removed. After surgical preparation, the cortex was allowed to recover for 30 min under saline irrigation.

Recording of DC and evoked potentials

Ag/AgCl reference electrodes were fixed onto the skin of the neck. Intracortical DC potentials were recorded through use of a glass micropipette filled with 150 mM NaCl. This microelectrode was inserted into the primary somatosensory cortex to a depth of 1000-1200 μm corresponding to cortical layer V. In parallel with the DC potentials, EPs induced by whisker pad stimulation (4-6 V, 0.2 ms, 0.1 Hz), were recorded from the cortical surface with a ball-tipped silver electrode. The details relating to the stimulation and cortical recordings of EPs were published earlier (Farkas et al. 1999; Nagy et al. 2010). The distance between the intracortical (DC) and cortical surface electrodes was less than 1 mm. To elicit CSD, either continuous KCl application was carried out or 1 μl of KCl (3 M) was injected with a microinjector (CMA/100) into the cortex. For continuous KCl application, a cotton ball (2 mm in diameter) soaked with 3 M KCl was placed on the pial surface and kept moist by the addition of 5 μl of KCl solution every 15 min. The number of KCl-induced CSDs was counted for 2 h.

Data acquisition and evaluation

The amplified responses were fed into a computer via an interface. All data were recorded on a PC by using custom signal acquisition programs (Neurosys, Experimetria). As concerns the EPs, each point in Figure 2B represents a single somatosensory EP (SEP).

Results

In some experiments (6 rats), CSD was induced by a single microinjection of KCl (3 M, 1 μl) into the frontal pole of the occipital cortex (Fig. 1). This single injection induced 1-3 CSD waves, which were recorded in the primary somatosensory cortex, 3.6 mm apart from the site of the injection. The parameters of the CSD waves: the onset latency of the first wave: 66 ±12 s (n=6); maximum amplitude: 20±8 mV (n=13); and duration at half-maximum amplitude: 39±15 s (n=13) (Fig. 2A).

In parallel with the CSD, SEPs were recorded from the pial surface of the primary somatosensory cortex. Whisker pad stimulation evoked cortical responses with about 450-500 μV. The amplitudes of the evoked responses were stable for a long period, except during the CSD waves. When a CSD wave arrived, the amplitude of the SEP gradually decreased and in parallel the amplitude of the CSD wave increased. When a CSD wave was at its maximum, the amplitude of the SEP was close to zero μV, and it virtually disappeared. As the CSD amplitude decreased, the SEP amplitude increased in parallel. Between two CSD waves, the SEPs were fully recovered (Fig. 2A, B).

In another series of experiments, the continuous topical application of 3 M KCl evoked repetitive CSD in all the animals studied (n=3). Under the given experimental circumstances, the average CSD frequency was 36±3 CSD waves/2 h (Fig. 3).

Discussion

Although CSD was discovered more than 60 years ago (Leao 1944), our knowledge of its mechanism, and particularly its

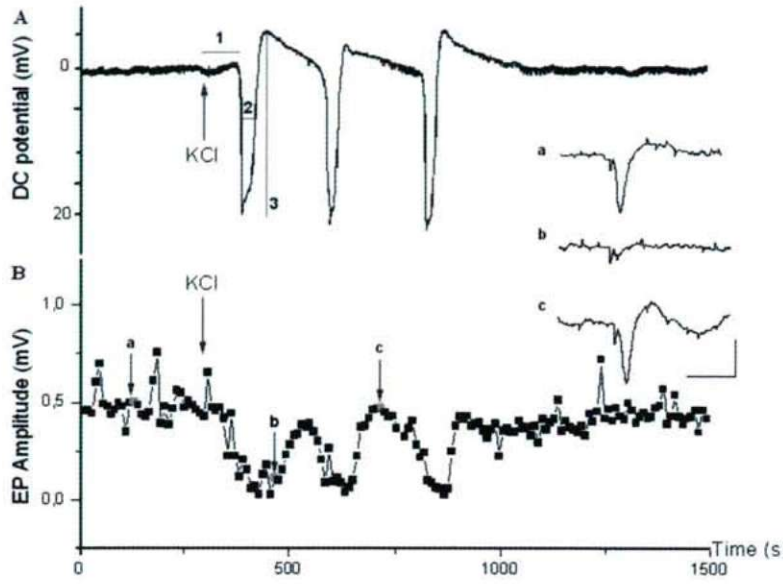

Figure 2. Cortical spreading depression (CSD) waves and somatosensory evoked potentials (SEPs) were recorded in parallel in the primary somatosensory cortex. A: CSD waves were induced with a single injection of KCl. The three characteristic parameters of the presented CSDs: (1): the onset latency of the first CSD wave: 76 s, (2): the duration at half maximum amplitude of the CSD: 33 s, (3): the maximum amplitude of the CSDs: 25 mV. B: Evoked potentials were recorded in parallel with the CSD waves. Each square in this graph represents single potentials. a, b, c: SEPs before, during and between CSD waves, respectively. Calibration in insert: 50 ms, 250 μV.

relation to the different pathological conditions such as migraine and ischemia, is rather limited. It is generally accepted that a migraine aura reflects the migration of CSD over the cortex. It has also been suggested that CSD may participate in the generation of head pain in migraine (Moskowitz et al. 1993).

A short-lasting interruption of the cerebral blood supply (up to 1 min) is known to cause a cessation of EEG activity, but this is usually not accompanied by a CSD wave. A prolonged interruption of the blood supply, however, causes a long-lasting negative DC shift in the cerebral cortex, which undergoes recovery only after release of the arterial occlusion. This phenomenon has been demonstrated both in the cortex (Leao 1947) and in the brainstem (Richter et al. 2010).

The precise molecular mechanisms of CSD are not known, but two pathological states, migraine aura and an ischemic condition of the brain, seem to be related to this phenomenon. Brain ischemia induces glutamate release from neurons and astrocytes (Rossi et al. 2000). In CSD, glutamate is thought to depolarize remote neurons and thereby cause propagation of the depolarizing wave (Somjen 2001). However, glutamate receptor blockers do not inhibit the onset and propagation of anoxic depolarization (Jarvis et al. 2001). At the same time, it has been suggested that the brainstem CSD induced by KCl administration can be explained by glutamatergic mechanisms (Richter et al. 2008).

These literature findings clearly demonstrate that CSD is somehow involved in such pathological conditions of the CNS as anoxic ischemia and migraine. During recent years, our research activity has focused on the pathomechanisms of migraine and ischemia-induced processes in the CNS, and mainly on the possibilities of neuroprotection in these conditions (Knyihár-Csillik et al. 2007, 2008; Robotka et al. 2008; Sas et al. 2008; Vámos et al. 2009, 2010). Although the symptoms, the progression and the outcome of stroke and migraine differ, there are some common pathophysiological mechanisms relating mainly to mitochondrial malfunctions (Sas et al. 2010).

Our recent studies on migraine and on ischemia-induced changes in the CNS increasingly require methodology involving excess glutamate, mass depolarization and glutamate

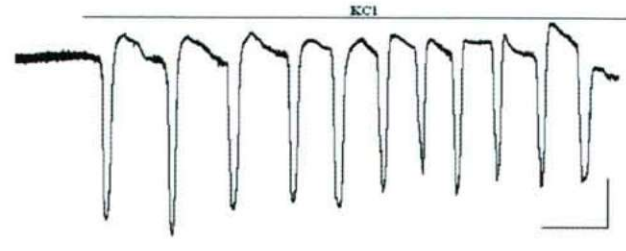

Figure 3. Representative 45 min DC potential recording from the primary somatosensory cortex during 2 h topical KCl application to the frontal part of the occipital cortex. Calibration scales indicate 5 min and 5 mV.

excitotoxiticy. CSD measurement appears to be the most appropriate such method.

In the course of these experiments, we introduced a method of recording CSD and characterized the main parameters of CSD waves (frequency, amplitude and duration). An extra feature of our approach is that the CSD waves are recorded in parallel with the evoked potentials.

In the near future, this combined method will be applied in our research on the pathomechanisms of migraine and glutamate excitotoxicity, and in the development of new neuroprotective kynurenic acid analogs.

Acknowledgement

This work was supported by grants ETT 026-04 and OTKA (K75628 and K67563). The authors declare no conflicts of interest.

References

Ayata C, Jin H, Kudo C, Dalkara T, Moskowitz MA (2006) Suppression of cortical spreading depression in migraine prophylaxis. Ann Neurol 59:652-661.

Dohmen C, Sakowitz OW, Fabricius M, Bosche B, Reithmeier T, Ernestus RI, Brinker G, Dreier JP, Woitzik J, Strong AJ, Graf R (2008) Spreading depolarizations occur in human ischemic stroke with high incidence. Ann Neurol 63:720-728.

Farkas T, Kis Z, Toldi J, Wolff JR (1999) Activation of the primary motor cortex by somatosensory stimulation in adult rats is mediated mainly by associational connections from the somatosensory cortex. Neuroscience 90:353-361.

Gardner-Medwin AR (1981) Possible roles of vertebrate neuroglia in potassium dynamics, spreading depression and migraine. J Exp Biol 95:111-127.

Hadjikhani N, Sanchez Del Rio M, Wu O, Schwartz D, Bakker D, Fischl B, Kwong KK, Cutrer FM, Rosen BR, Tootell RB, Sorensen AG, Moskowitz MA (2001) Mechanisms of migraine aura revealed by functional MRI in human visual cortex. Proc Natl Acad Sci USA 98:4687-4692.

Hartings JA, Strong AJ, Fabricius M, Manning A, Bhatia R, Dreier JP, Mazzeo AT, Tortella FC, Bullock MR (2009) Spreading depolarizations and late secondary insults after traumatic brain injury. J Neurotrauma 26:1857-1866.

Jarvis CR, Anderson TR, Andrew RD (2001) Anoxic depolarization mediates acute damage independent of glutamate in neocortical brain slices. Cereb Cortex 11:249-259.

Knyihar-Csillik E, Mihaly A, Krisztin-Peva B, Robotka H, Szatmari I, Fulop F, Toldi J, Csillik B, Vecsei L (2008) The kynurenate analog SZR-72 prevents the nitroglycerol-induced increase of c-fos immunoreactivity in the rat caudal trigeminal nucleus: comparative studies of the effects of SZR-72 and kynurenic acid. Neurosci Res 61:429-432.

Knyihar-Csillik E, Toldi J, Mihaly A, Krisztin-Peva B, Chadaide Z, Nemeth H, Fenyo R, Vecsei L (2007). Kynurenine in combination with probenecid mitigates the stimulation-induced increase of c-fos immunoreactivity of the rat caudal trigeminal nucleus in an experimental migraine model. J Neural Transm 114:417-421.

Kraig RP, Nicholson C (1978) Extracellular ionic variations during spreading depression. Neuroscience 3:1045-1059.

Kudo C, Nozari A, Moskowitz MA, Ayata C (2008) The impact of anesthetics and hyperoxia on cortical spreading depression. Exp Neurol 212:201-206.

Lauritzen M (1994) Pathophysiology of the migraine aura. The spreading depression theory. Brain 117 (Pt 1):199-210.

Leao AA (1944) Spreading depression of activity in the cerebral cortex. J. Neurophysiol 7:359-390

Leao AA (1947) Further observations on the spreading depression of activity in the cerebral cortex. J Neurophysiol 10:409-414.

Moskowitz MA, Nozaki K, Kraig RP (1993) Neocortical spreading depression provokes the expression of c-fos protein-like immunoreactivity within trigeminal nucleus caudalis via trigeminovascular mechanisms. J Neurosci 13:1167-1177.

Nagy D, Knapp L, Marosi M, Farkas T, Kis Z, Vecsei L, Teichberg VI, Toldi J (2010) Effects of blood glutamate scavenging on cortical evoked potentials. Cell Mol Neurobiol 30:1101-1106.

Pietrobon D, Striessnig J (2003) Neurobiology of migraine. Nat Rev Neurosci 4:386-398.

Richter F, Bauer R, Lehmenkuhler A, Schaible HG (2008) Spreading depression in the brainstem of the adult rat: electrophysiological parameters and influences on regional brainstem blood flow. J Cereb Blood Flow Metab 28:984-994.

Richter F, Bauer R, Lehmenkuhler A, Schaible HG (2010) The relationship between sudden severe hypoxia and ischemia-associated spreading depolarization in adult rat brainstem in vivo. Exp Neurol 224:146-154.

Robotka H, Sas K, Agoston M, Rozsa E, Szenasi G, Gigler G, Vecsei L, Toldi J (2008) Neuroprotection achieved in the ischaemic rat cortex with L-kynurenine sulphate. Life Sci 82:915-919.

Rossi DJ, Oshima T, Attwell D (2000) Glutamate release in severe brain ischaemia is mainly by reversed uptake. Nature 403:316-321.

Sas K, Pardutz A, Toldi J, Vecsei L (2010) Dementia, stroke and migraine - Some common pathological mechanisms. J Neurol Sci [Epub ahead of print] PMID:20828765

Sas K, Robotka H, Rozsa E, Agoston M, Szenasi G, Gigler G, Marosi M, Kis Z, Farkas T, Vecsei L, Toldi J (2008) Kynurenine diminishes the ischemia-induced histological and electrophysiological deficits in the rat hippocampus. Neurobiol Dis 32:302-308.

Somjen GG (2001) Mechanisms of spreading depression and hypoxic spreading depression-like depolarization. Physiol Rev 81:1065-1096.

Vamos E, Fejes A, Koch J, Tajti J, Fulop F, Toldi J, Pardutz A, Vecsei L (2010) Kynurenate derivative attenuates the nitroglycerin-induced CamKIIalpha and CGRP expression changes. Headache 50:834-843.

Vamos E, Pardutz A, Varga H, Bohar Z, Tajti J, Fulop F, Toldi J, Vecsei L (2009) l-kynurenine combined with probenecid and the novel synthetic kynurenic acid derivative attenuate nitroglycerin-induced nNOS in the rat caudal trigeminal nucleus. Neuropharmacology 57:425-429.

Woods RP, Iacoboni M, Mazziotta JC (1994) Brief report: bilateral spreading cerebral hypoperfusion during spontaneous migraine headache. N Engl J Med 331:1689-1692.

Volume 54(2):165-170, 2010
Acta Biologica Szegediensis
http://www.sci.u-szeged.hu/ABS

ARTICLE

Subacute exposure of rats by metal oxide nanoparticles through the airways: general toxicity and neuro-functional effects

Gábor Oszlánczi[1], Edina Horváth[1], Andrea Szabó[1], Endre Horváth[2], András Sápi[2], Gábor Kozma[2], Zoltán Kónya[2], Edit Paulik[1], László Nagymajtényi[1], András Papp[1]*

[1]Department of Public Health, Faculty of Medicine, University of Szeged, Szeged, Hungary, [2]Department of Applied and Environmental Chemistry, Faculty of Science and Informatics, University of Szeged, Szeged, Hungary

ABSTRACT In order to create an animal model of human inhalational exposure by industrial metal fumes, nanoparticulate metal oxides (MnO_2, CdO_2, PbO) were synthesized and instilled into the trachea of rats 5 times a week for 6 weeks (metal doses per kg b.w.: 2.63 and 5.26 mg Mn; 0.04 and 0.4 mg Cd; 2 and 4 mg Pb). At the end, the rats' body weight gain during the treatment was determined, the animals had an open field session to investigate their spontaneous motility, and finally spontaneous and stimulus-evoked cortical activity was recorded in urethane anaesthesia. Mn caused decrease of open field ambulation and rearing, Cd had no effect, whereas Pb caused decreased rearing and increased ambulation. Spontaneous cortical activity was shifted to higher frequencies with each metal. Cortical evoked potentials had lengthened latency, mainly with Mn and Cd; and increased frequency dependence with Cd and Pb but hardly with Mn. The effects proved indirectly that the metal content of the nanoparticles had access from the airways to the CNS. Our method seems suitable for modelling human nervous system damage due to inhaled nanoparticles.
Acta Biol Szeged 54(2):165-170 (2010)

KEY WORDS

nanoparticle
neurotoxicity
manganese
cadmium
lead
rat

The nervous system is a target for various environmental xenobiotics including the heavy metals manganese, lead and cadmium (ATSDR, 1999a, 1999b, 2000). These metals, as well as their alloys and compounds, have a number of applications including a lot of industrial procedures which emit metal, metal oxide etc. particles. Inhalation of airborne metal dusts or fumes is a major way of occupational exposure, causing acute and chronic diseases such as metal fume fever and COPD. In inhalational exposure situations, the size of the particles is crucial, whereby the importance of submicroscopic particles – also called nanoparticles (NPs) – has been recognized only recently. Particles of <100 nm diameter, found typically in metal fumes, have a huge surface area relative to their mass, and can penetrate across tissue boundaries such as the alveolar wall and the blood-brain barrier, which possibly results in direct access to the CNS (Obedörster et al. 2005; Oszlánczi et al. 2010).

Manganese-containing fumes are generated in welding and other high-temperature industrial operations. Inhalation of Mn fumes can cause manganism (a chronic neurological syndrome resembling Parkinson's disease: Bowler et al. 2006) and other neurological manifestations. Deposition of Mn following chronic exposure in the human brain (Yamada et al. 1986) and the resulting damages to the dopaminergic system (Shinotoh et al. 1997) have been reported.

Occupational exposure by cadmium metal fumes resulted in reduced visuomotor performance, and difficulties of concentration and postural balance (Viaene et al. 2000). Exposed children showed straight relationship between hair Cd levels and altered sensory evoked potential parameters (Thatcher et al. 1984).

Lead processing and recycling, and the use of leaded petrol in the past (but in certain countries also at present) have been the main sources of airborne exposure by lead. Whatever the physicochemical form of the absorbed lead is, it is deposited in the central nervous system, first of all in the cortex and hippocampus (Grandjean 1978). In lead-exposed workers, sensory evoked potentials and nerve conduction velocity were affected (Araki et al. 2000). There exists a well-known relationship between blood or dental lead level and IQ loss or behavioural abnormalities in exposed children (Fergusson et al. 1997; – whereby it is noteworthy that children's lead exposure also can come from scaling-off old lead paint in the home environment: ATSDR, 1999b).

In this study, exposure by airborne NPs was modelled by intratracheal instillation of a nanosuspension of MnO_2, CdO_2 or PbO to rats, and the resulting behavioural and electrophysiological alterations were investigated.

Accepted Oct 25, 2010
*Corresponding author. E-mail: ppp@puhe.szote.u-szeged.hu

Table 1. Treatment groups and doses of the metal oxide nanoparticles.

Group	Code	Substance	Dose (mg metal / kg b.w.)
Untreated control	Con	--	--
Vehicle control	W	Distilled water	--
Manganese low dose	LD-Mn	MnO_2 nanosuspension	2.63
Manganese high dose	HD-Mn		5.26
Cadmium low dose	LD-Cd	CdO_2 nanosuspension	0.04
Cadmium high dose	HD-Cd		0.4
Lead low dose	LD-Pb	PbO nanosuspension	2
Lead high dose	HD-Pb		4

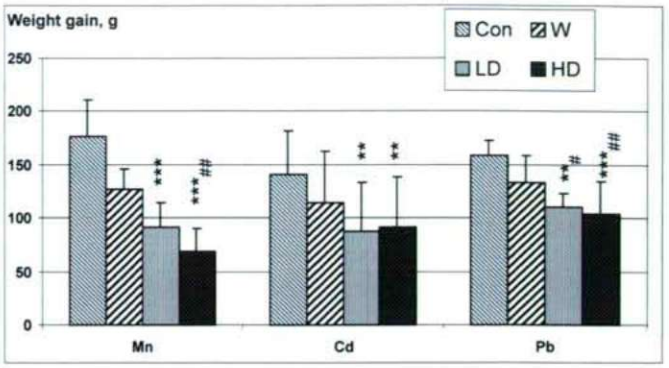

Figure 1. Weight gain of the control and treated rats during the 6 weeks treatment period. The data (mean + SD, n=10) represent the difference in the rats' body weight measured on week 0 and week 6. The metals and treatment groups are indicated on the abscissa and in the insert, respectively (see Table 1 for explanation). **, ***: $p<0.01$, 0.001 vs. Con; ##: $p<0.01$ vs. W.

Materials and Methods

Adult male Wistar rats (300-350 g body weight) were used. The experiments with the three metal oxide NPs were carried out separately. In each of them, there was an untreated control group (Con), a vehicle control group (W), and a low dose (LD) and a high dose (HD) group; with 10 rats each. For doses and group coding, see Table 1. The rats were kept under normal conditions in a GLP-certified animal house. They were weighed weekly, and the weight gain during the 6 weeks was calculated.

The nanoparticulate metal oxides (mean diameter: MnO_2, 23.2±3.3 nm; CdO_2, 20.1±5.7; PbO, 19.5±3.6 nm – determined by X-ray diffraction) were synthesized at the Department of Applied Chemistry, University of Szeged. The NPs were made up in distilled water to a dilute suspension, which was sonicated to prevent aggregation and was instilled into the rats' trachea 5 days a week for 6 weeks under brief ether anesthesia, using a syringe and 1.2 mm OD plastic tubing, inserted between the vocal chords (for details, see Sárközi et al. 2009).

One or two days after the last instillation, the animals had a 10 min session in an open field (OF) box to investigate spontaneous motility. The box was equipped with two arrays of infrared beam gates at floor level and at 12 cm height (Conducta 1.0 System, Experimetria Ltd., Budapest), for automatic detection of the beam interruptions caused by the moving animal during the 10 min session. The software of the system computed these to data of counts, time and run length of the basic activity forms (ambulation, local activity, rearing, immobility).

The rats were finally anesthetized with urethane ip. (1000 mg/kg b.w. ip.), and the left hemisphere was exposed by removing the most of the left parietal bone and the above lying soft tissues. For recording cortical electrical activity, silver electrodes were placed over the primary somatosensory (SS), visual (VIS) and auditory (AUD) area, and electrocorticogram (ECoG) was recorded for 6 min. From the records, the relative spectral power of the frequency bands (delta, theta, alpha, beta1, beta2, gamma; standard human EEG bands as described in Kandel and Schwartz 1985) was calculated. After recording ECoG, sensory stimulation was applied and the cortical evoked potentials (EPs) were recorded from the same points. The SS stimuli were square electric pulses (3-4 V, 0.05 ms) delivered to the contralateral whisker pad of the rat by means of a pair of needle electrodes at 1, 2 and 10 Hz frequency. The contralateral eye (for VIS EPs) was stimulated by flashes of a white LED, and the ear with clicks from a mini-speaker, at 1 Hz. After averaging the EPs, onset latency was measured manually. All electrophysiological recording and analysis was done by means of the Neurosys 1.11 software (Experimetria Ltd, Budapest, Hungary).

From the individual data, group means were calculated and compared by means of one-way ANOVA using the SPSS 17.0 software. During the whole study, the principles of the Ethical Committee for the Protection of Animals in Research of the University were strictly followed.

Results

The rats' body weight gain during the 6 weeks of treatment (Fig. 1) showed some difference between the untreated (Con) and vehicle-treated (W) groups. This effect was, however, mild and did not obscure the weight gain reducing effect of the instilled NPs, indicating substantial general toxicity of the instilled NPs.

The results of the OF tests demonstrated in contrast that on the investigated central nervous functions the treatment procedure itself (ether anesthesia and instillation of distilled water) had no major effect. Figure 2 shows the time (in seconds) spent by the rats in the various forms of motor activity during the 600 s of the OF session. High dose Mn caused significantly decreased ambulation and rearing. In the HD-Pb group, increased ambulation and local activity

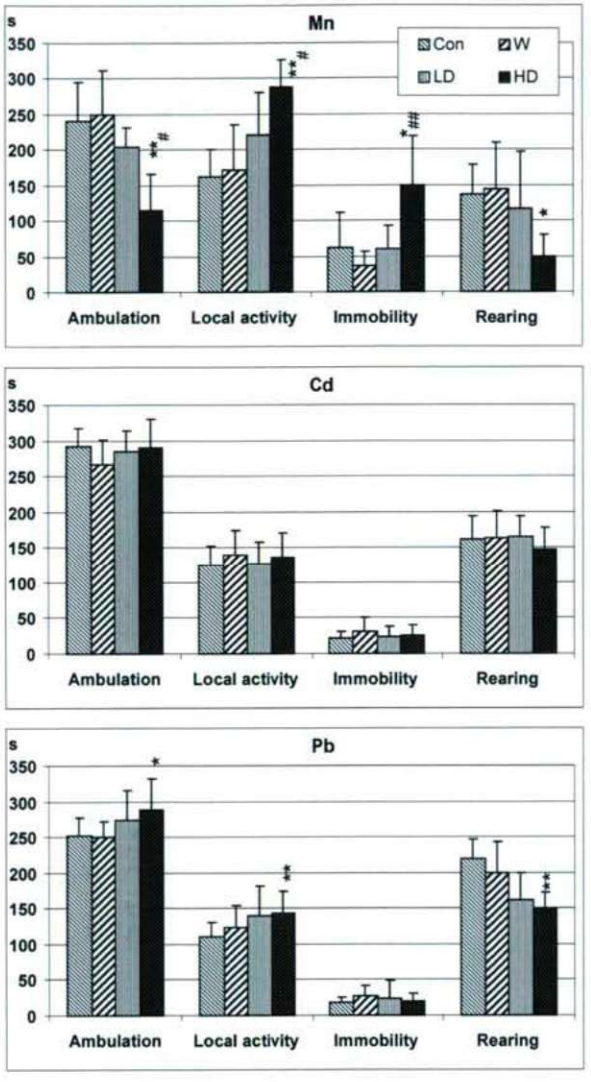

Figure 2. Open field activity after 6 weeks treatment with Mn, Cd and Pb containing nanoparticles (top, middle and bottom panel, respectively). The data (mean + SD, n=10) represent the time spent with the activity forms given on the abscissa. For control and treated groups, see insert in the top panel. *, **: p<0.05, 0.01 vs. Con; #, ##: p<0.05, 0.01 vs. W.

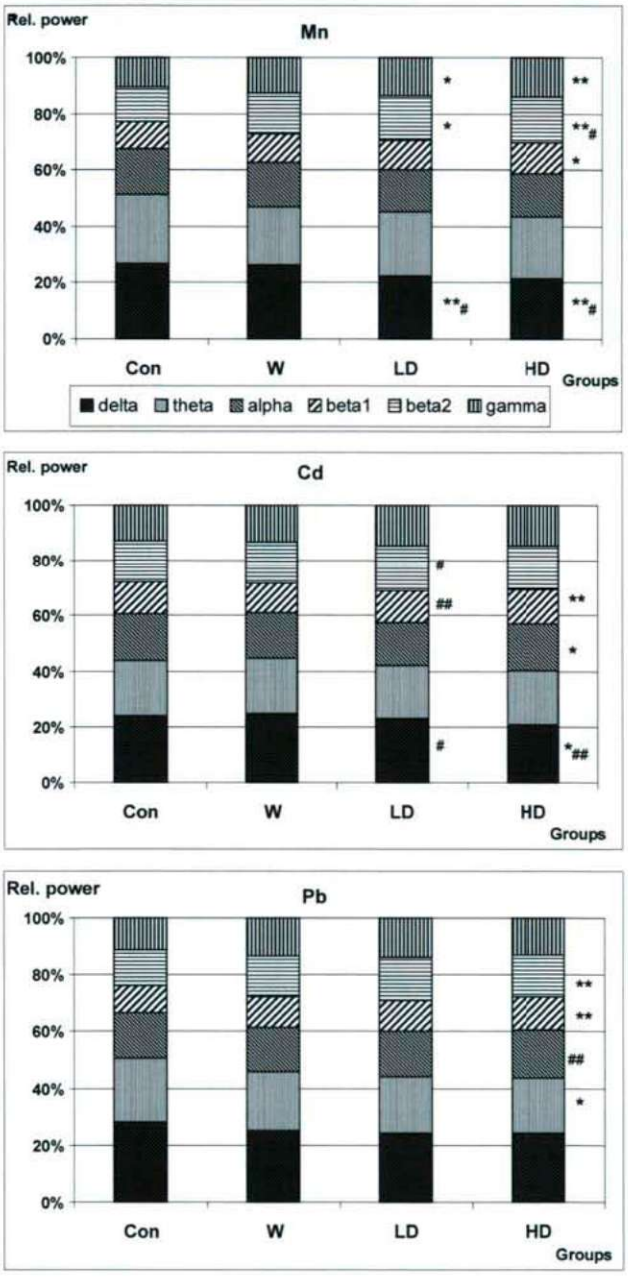

Figure 3. Band spectrum of the electrocorticogram recorded from the somatosensory cortex of the rats after 6 weeks treatment with Mn, Cd and Pb (top, middle and bottom panel, respectively). Abscissa: groups. Ordinate: relative power of the ECoG bands (for the bar filling pattern of the bands, see insert in the top panel). *, **: p<0.05, 0.01 vs. Con; #, ##: p<0.05, 0.01 vs. W, always between identical bands.

was seen, while the applied doses of Cd had no noteworthy effect.

The spontaneous cortical electrical activity, recorded in urethane anaesthesia, was shifted to higher frequencies by all three metal oxides. There was no qualitative difference between the changes seen in the three cortical areas; hence, only the activity spectra from the SS area are shown in Figure 3. The change was, similarly to that of the open field activity, apparently dose-dependent; and the difference between the Con and W groups was also here minimal.

The most typical change in the cortical EPs was latency lengthening. The SS EPs had significantly longer latency in the HD groups than in Con or W with each metal (Fig. 4). With Mn, the effect of the low dose was also significant. The dependence of latency on the frequency of stimulation was also more pronounced in the treated rats, but the extra increase of latency at faster (2 and 10 Hz) stimulation vs. 1 Hz was

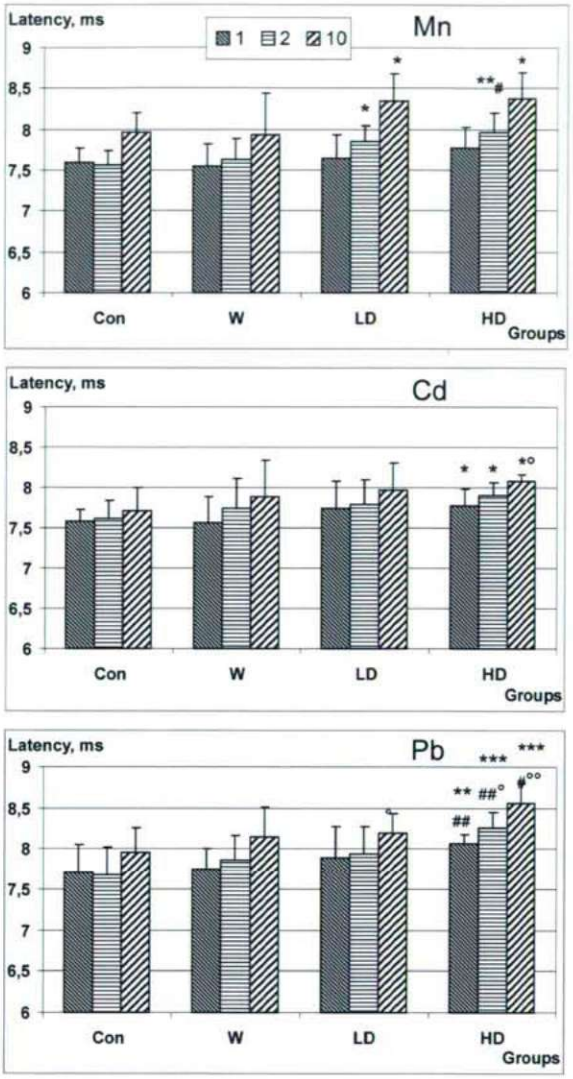

Figure 4. Latency of the somatosensory evoked potentials obtained with stimulation frequency of 1, 2 and 10 Hz (see insert in the top panel) in Mn, Cd and Pb treated rats. Ordinate: treatment groups. Mean + SD, n=10. *, **, ***: p<0.05, 0.01, 0.001 vs. Con; #, ##: p<0.05, 0.01 vs. W; °: p<0.05 vs. 1 Hz stimulation within the same group.

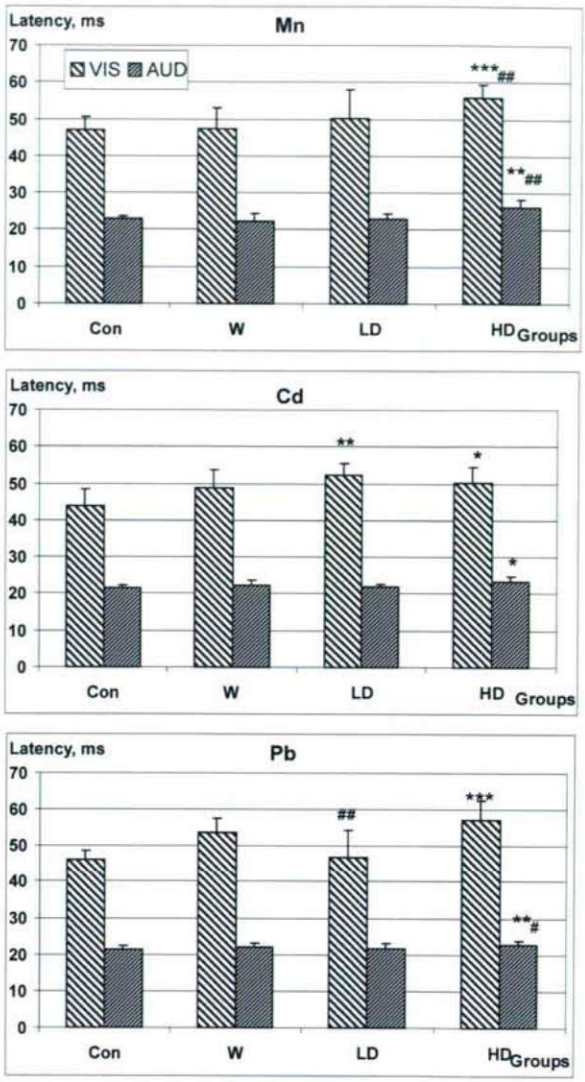

Figure 5. Latency of the visual and auditory evoked potentials (see insert in the top panel) in Mn, Cd and Pb treated rats. Ordinate: treatment groups. Mean + SD, n=10. *, **, ***: p<0.05, 0.01, 0.001 vs. Con; #, ##: p<0.05, 0.01 vs. W.

significant only with Pb and Cd. The increase of latency of the VIS and AUD EPs was also significant in all HD groups (Fig. 5) The VIS EP latency was significantly longer also in LD-Cd and LD-Pb.

Discussion

The similarity of the three metals' effects suggested some common mechanism, oxidative stress being a likely candidate (Mn: McNeilly et al. 2004; Cd: Zhang et al. 2007; Pb: Adonaylo and Oteiza, 1999). The reduced body weight gain observed in the treated animals also might be due to this, more exactly to the metabolic disturbance caused by the presence of free radicals (Merry 2002). Systemic oxidative stress is present also in the brain (Mn: Zhang et al. 2009; Cd: Kumar et al. 1996; Pb: Patra et al. 2001) resulting in membrane lipid peroxidation (Mn: Ávila et al. 2008; Cd and Pb: Zanchi et al. 2010; Pb: Ahamed and Siddiqui 2007). This in turn results in altered neuronal membrane functions, and in a disturbance in a number of events depending on that, including all receptor-bound phenomena such as synaptic transmission.

In ionic form, each of the studied metals is known to affect Ca homeostasis (Büsselberg 1995). Considering the role of Ca influx in presynaptic transmitter release, interference by the metals (Mn: Takeda 2003; Cd: Soliakov and Wonnacott 1996; Pb: Sandhir and Gill 1993) can explain the lengthening of EP latency (together with the membrane damage mentioned above). Whether the applied metal was in fact present in the

rats' brain after the 6 weeks of intratracheal NP exposure, has been proven by us in case of Mn only (Oszlánczi et al. 2010) and that analysis did not discriminate among forms of Mn. It may be generally true, however, that the surface of the NPs, consisting of a normally water-insoluble metal oxide, releases free metal ions in the acidic environment of the phagolysosomes of alveolar macrophages (Lundborg et al. 1985) which then escape and reach the brain via the bloodstream. Alternatively, complete NPs can be transported to the CNS (Elder et al. 2006; Wang et al. 2008) and can themselves act on the neurons or can be phagocyted by the microglia and release metals in a process mentioned above.

The increase of high-frequency cortical spontaneous activity was probably due to increased reticular ascending cholinergic activation in case of Cd and Pb (Carageorgiou et al. 2004; Suszkiw et al. 1984). In case of Mn, effects on the cholinergic system are also known (Finkelstein et al. 2007) but decreased inactivation of glutamate (inhibition of astrocytic glutamin synthetase by Mn: Normandin and Hazell 2002) probably contributed to the more intense input into the reticular ascending fibres.

The changes in the OF motor behaviour of the treated rats are not sufficiently explained by the possible effects of the metal NPs mentioned so far. Here, damages to the dopaminergic influence on the cortex exerted by mid-brain structures like the ventral tegmental area may be of importance. Mn is well-known to damage dopaminergic structures in the brain (Verity 1999; Takeda 2003), and the decreased motility of rats can be set in analogy to the symptoms observed in Mn-exposed welders. Decrease of dopaminergic cortical receptors and hypermotility in rats was reported also after Pb exposure in rats (Ma et al. 1999). In this case an analogy may exist between the hypermotility seen in rats and the "attention deficit hyperactivity disease" found to be more frequent among children with elevated blood Pb (Needleman and Gatsonis 1990).

Our results showed that metal oxide nanoparticles can cause significant alterations in certain indicators of the CNS activity in the treated rats. The changes of the electrophysiological phenomena were similar to our earlier results obtained by oral application of Mn, Cd and Pb in water-soluble form (Nagymajtényi et al. 1997; Papp et al. 2003; Vezér et al. 2005) which indicated that the metal content of the instilled nanoparticles most probably had access to the brain. Experiments of the type presented here may constitute a suitable model of the nervous system effects of nanoparticle inhalation.

References

Adonaylo VN, Oteiza PI (1999) Pb^{2+} promotes lipid oxidation and alterations in membrane physical properties. Toxicology 132:19-32.

Ávila DS, Gubert P, Fachinetto R, Wagner C, Aschner M, Rocha JBT, Soares FAA (2008) Involvement of striatal lipid peroxidation and inhibition of calcium influx into brain slices in neurobehavioral alterations in a rat model of short-term oral exposure to manganese. NeuroToxicol 29:1062-1068

Ahamed M, Siddiqui MKJ (2007) Low level lead exposure and oxidative stress: Current opinions Clinica Chimica Acta 383:57-64

Araki S, Sato H, Yokoyama K, Murata K (2000) Subclinical neurophysiological effects of lead: A review on peripheral, central, and autonomic nervous system effects in lead workers. Am J Ind Med 37:193-204.

ATSDR (1999a) Toxicological Profile for Cadmium. US Department of Health and Human Services, Atlanta.

ATSDR (1999b) Toxicological Profile for Lead. US Department of Health and Human Services, Atlanta

ATSDR (2000) Toxicological Profile for Manganese. US Department of Health and Human Services, Atlanta

Bowler R, Koller W, Schultz PE (2006) Parkinsonism due to manganism in a welder: Neurological and neuropsychological sequelae. NeuroToxicol 27:327-332.

Büsselberg D (1995) Calcium channels as target sites of heavy metals. Toxicol Lett 82:255-261.

Carageorgiu H, Tzotzes V, Pantos C, Mourouzis C, Zarros A, Tsakiris S (2004) In vivo and in vitro effects of cadmium on adult rat brain total antioxidant status, acetylcholinesterase, (Na^+,K^+)-ATPase and Mg^{2+}-ATPase activities: protection by L-cysteine. Bas Clin Pharmacol Toxicol 94:112-118.

Elder A, Gelein R, Silva V, Feikert T, Opanashuk L, Carter J, Potter R, Maynard A, Ito Y, Finkelstein J, Oberdörster G (2006) Translocation of ultrafine manganese oxide particles to the central nervous system. Environ Health Persp 114:1172-1178.

Fergusson DM, Horwood J, Lynskey MT (1997) Early dentine lead levels and educational outcomes at 18 years. J Child Psychol Psychiatr 38:471-478.

Finkelstein Y, Milatovic D, Aschner M (2007) Modulation of cholinergic systems by manganese. NeuroToxicol 28:1003-1014.

Grandjean P (1978) Regional distribution of lead in human brains. Toxicology 2:65-69.

Kandel ER, Schwartz JH (1985) Principles of Neural Science. Elsevier, New York, pp. 643-644.

Kumar R, Agarwal AK, Seth PK (1996) Oxidative stress-mediated neurotoxicity of cadmium Toxicol Lett 89:65-69.

Lundborg M, Eklund A, Lind DB et al (1985) Dissolution of metals by human and rabbit alveolar macrophages. Brit J Ind Med 42:642-645.

Ma T, Chen H, Ho I (1999) Effects of chronic lead (Pb) exposure on neurobehavioral function and dopaminergic neurotransmitter receptors in rats. Toxicol Lett 105:111-121.

McNeilly JD, Heal MR, Beverland IJ et al (2004) Soluble transition metals cause the pro-inflammatory effects of weiding fumes ion vitro. Toxicol Appl Pharmacol 196:95-107.

Merry BJ (2002) Molecular mechanisms linking calorie restriction and longevity. Intern J Biochem Cell Biol 34:1340-1354.

Nagymajtényi L, Schulz H, Papp A, Dési I (1997) Behavioural and electrophysiological changes caused by subchronic lead exposure in rats. Centr Eur J Occup Environ Med 3:195-209.

Needleman HL, Gatsonis CA (1990) Low-level lead exposure and the IQ of children. JAMA 263:673-678.

Normandin L, Hazell AS (2001) Manganese neurotoxicity: an update of pathophysiologic mechanisms. Metab Brain Dis 17:375-387.

Oberdörster G, Oberdörster E, Oberdörster J (2005) Nanotoxicology: An Emerging discipline evolving from studies of ultrafine particles. Environ Health Persp 7:823-839.

Oszlánczi G, Vezér T, Sárközi L, Horváth E, Kónya Z, Papp A (2010) Functional neurotoxicity of Mn-containing nanoparticles in rats. Ecotox Environ Saf 73:2004-2009.

Papp A, Nagymajtényi L, Dési I (2003) A study on electrophysiological effects of subchronic cadmium treatment in rats. Env Toxicol Pharmacol 13:181-186.

Patra RC, Swarup D, Dwidedi SK (2001) Antioxidant effects of α-tocopherol, ascorbic acid and L-methionine on lead-induced oxidative stress of the liver, kidney and brain in rats. Toxicology 162:81-8.

Sandhir R, Gill KD (1993) Alterations in calcium homeostasis on lead exposure in rat synaptosomes. Mol Cell Biochem 131:25-33.

Sárközi L, Horváth E, Kónya Z, Kiricsi I, Szalay B, Vezér T, Papp A (2009) Subacute intratracheal exposure of rats to manganese nanoparticles: Behavioral, electrophysiological and general toxicological effects. Inhal Toxicol 21(S1):83-91.

Shinotoh H, Snow BJ, Chu NS, Huang CC, Lu CS, Lee C, Takahashi H, Calne DB (1997) MRI and PET studies of manganese intoxicated monkeys. Neurology 45:1199-1204.

Soliakov L, Wonnacott S (1996) Voltage-sensitive Ca^{2+} channels involved in nicotinic receptor-mediated [3H]dopamine release from rat striatal synaptosomes. J Neurochemistry 67:163-170.

Suszkiw J, Tóth G, Murawsky M, Cooper GP (1984) Effects of Pb^{2+} and Cd^{2+} on acetylcholine release and Ca^{2+} movements in synaptosomes and subcellular fractions from rat brain and torpedo electric organ. Brain Res 323:31-46.

Takeda A (2003) Manganese action in brain function. Brain Res Rev 41:79-89.

Thatcher RW, McAlaster R, Lester ML (1984) Evoked potentials related to hair cadmium and lead in children. Ann NY Acad Sci 425:384-390.

Verity MA (1999) Manganese neurotoxicity: a mechanistic hypothesis. NeuroToxicol 20:489-498.

Vezér T, Papp A, Hoyk Z, Varga C, Náray M, Nagymajtényi L (2005) Behavioral and neurotoxicological effects of subchronic manganese exposure in rats. Environ Toxicol Pharmacol 19:797-810.

Viaene MK, Masschelein R, Leenders J, De Groof M, Swerts LJ, Roels HA (2000) Neurobehavioural effects of occupational exposure to cadmium: a cross sectional epidemiological study. Occup Environ Med 57:19-27.

Wang J, Liu Y, Jiao F, La o F, Li W, Guc Y, Li Y, Ge C, Zhoua Q, Li B, Zhao Y, Chai Z, Chen C (2008) Time-dependent translocation and potential impairment on central nervous system by intranasally instilled TiO_2 nanoparticles. Toxicology 254:82-90.

Yamada M, Ohno S, Okayasu I, Okeda R, Hatakeyama S, Watanabene H, Ushio K, Tsukagoshi H (1986) Chronic manganese poisoning: a neuropathological study with determination of manganese distribution. Acta Neuropathol 70:273-278.

Zanchi ACT, Fagundes LS, Barbosa F Jr, Bernardi R, Rhoden CR, Saldiva PHN, do Valle AC (2010) Pre and post-natal exposure to ambient level of air pollution impairs memory of rats: the role of oxidative stress. Inhal Toxicol 22:910-918.

Zhang P, Wong TA, Lokuta KM, Turner DE, Vujisic K, Liu B (2009) Microglia enhance manganese chloride-induced dopaminergic neurodegeneration: Role of free radical generation .Exp Neurol 217:219-230.

Zhang Y, Chen W, Zhang J et al (2007) In vitro and in vivo toxicity of CdTe nanoparticles. J Nanosci Nanotechnol 7:497-503.

Instructions to Authors

Submission of manuscripts

Submission of a manuscript to Acta Biologica Szegediensis automatically involves the assurance that it has not been published and will not be published elsewhere in the same form. Manuscripts should be written in English. Since poorly-written material will not be considered for publication, authors are encouraged to have their manuscripts corrected for language and usage by a trusted expert.

There are no explicit length limitations: a normal research article will occupy 4-6 printed pages; reviews might be considerably longer. Authors should submit three sets of the complete manuscript and illustrations, together with a computer disk containing an electronic version of their manuscript. The elctronic file is considered the final material. Both Macintosh and PC versions will be accepted. The disk should be labeled with the date, the first author's name, the file name of the manuscript and the software, disk format and hardware used. Acta Biologica Szegediensis will not return copies of submitted manuscripts and figures. Requests to return original figures will be honored as a courtesy, but cannot be guaranteed. If instructions are not followed, authors will be asked to retype their manuscripts.

Manuscript format

Only good-quality laser printouts will be accepted. All pages should be printed with full double spacing, 2.5 cm margins, and a nonjustified right margin. A standard 12 point typeface (e.g. Times, Helvetica or Courier) should be used throughout the manuscript, with symbol font for Greek letters. Boldface, italics or underlined text should not be used anywhere in the manuscript. Footnotes are not permitted. Each page should be numbered at the bottom as follows:

Page 1. Title page: Complete title, first name, middle initial, last name of each author; where the work was done (authors' initials in parentheses if necessary); mailing address, phone, fax, and e-mail of the corresponding author; a running title of no more than 48 characters and spaces.

Page 2. Abstract: no more than 200 words, followed by 4-6 key words.

Beginning on page 3: Introduction, Materials and Methods, Results, Discussion, Acknowledgments, References, Figure Legends, Tables. Each section should be begun on a new page.

The manufacturer's name and location should be given in parentheses for reagents and instruments. Sources for all antibodies and nucleotide sequences should be indicated. Customary abbreviations in common use need not be defined in the text (e.g. DNA or ATP). Other abbreviations should be defined the first time that they are used. Quantitative results must be presented as graphs or tables and supported by appropriate experimental design and statistical tests. Only SI units may be used. For studies that involve animals or human subjects, the institutional, national or international guidelines that were followed should be indicated.

References

Only work that has been published or is in the press may be referred to. Personal communications should be acknowledged in the text and accompanied by written permission. In the text, references should be cited by name and year, e.g. Bloom (1983) or (Schwarz-Sommer et al. 1990) or (Maxam and Gilbert 1977). In the References, references should be listed alphabetically by first authors (including all co-authors) and chronologically for a given author (beginning with the most recent date of publication). Where the same author has more than one publication in a year, lower case letters should be used (e.g. 1999a, 1999b, etc.). Periods should not be used after authors' initials or abbreviated journal titles (e.g. Acta Biologica Szegediensis should be cited as Acta Biol Szeged). Inclusive page numbers should be used. Examples:

Bloom FE (1983) The endorphins: a growing family of pharmacologically pertinent peptides. Annu Rev Pharmacol Toxicol 23:151-170.

Coons AH (1978) Fluorescent antibody methods. In Danielli JF, ed., General Cytochemical Methods. Academic Press, New York, 399-422.

Maxam AM, Gilbert WA (1977) A new method for sequencing DNA. Proc Natl Acad Sci USA 74:560-564.

Monod J, Changeux J-P, Jacob F (1963) Allosteric proteins and cellular control systems. J Mol Biol 6:306-329.

Schwarz-Sommer Z, Huijser P, Nacken W, Saedler H, Sommer H (1990) Genetic control of flower development by homeotic genes in Antirrhinum majus. Science 250:931-936.

Illustrations

Three complete sets, including a high-quality "original" for publication, must be submitted with the manuscript. The back of each figure or composite plate should be labeled in soft lead pencil, indicating the orientation, the figure number, and the first author's name. The back of the best set should be marked "use for reproduction" or "original". Authors are encouraged to submit digital images of photographs, line drawings or graphs for printing. Most major image editing and drawing/illustrator computer software files (both Macintosh and PC) in TIFF or EPS formats are acceptable. It is particularly important that adequate resolution (at least 300 dpi, preferably 600 dpi) is used in making the original image.

Figure legends

Figures should be numbered consecutively with Arabic numerals. Material in the text should not be duplicated and methods should not be described. The size of scale bars should be indicated when appropriate. The first figure in the text should be referred to as Fig. 1, and so on.

Tables

Tables should be numbered consecutively with Arabic numerals. A brief title should be included above the table. Each table should be printed double spaced, without vertical or horizontal lines, and on a separate sheet. Material in text should not be duplicated and methods should not be described. The first table in the text should be referred to as Table 1, and so on.